AEROTHERM
FINAL REPORT NO. 69-51

A STUDY OF THE BOUNDARY FLOW IN A ROCKET COMBUSTION CHAMBER

PART II

DATA ANALYSIS, CORRELATION, AND THEORETICAL PREDICTION

by

R. D. Grose
M. R. Wool
C. J. Deblaye

AEROTHERM CORPORATION

ADVANCES IN AEROTHERMOCHEMISTRY

AEROTHERM
FINAL REPORT NO. 69-51

A STUDY OF THE BOUNDARY FLOW IN A ROCKET COMBUSTION CHAMBER

PART II

DATA ANALYSIS, CORRELATION, AND THEORETICAL PREDICTION

by

R. D. Grose
M. R. Wool
C. J. Deblaye

AEROTHERM FINAL REPORT NO. 69-51

September 22, 1969

Aerotherm Project 7009

A STUDY OF THE BOUNDARY FLOW IN A ROCKET COMBUSTION CHAMBER

PART II

DATA ANALYSIS, CORRELATION, AND THEORETICAL PREDICTION

by

R. D. Grose
M. R. Wool
C. J. Deblaye

Prepared for

Jet Propulsion Laboratory
Pasadena, California

Contract No. NAS7-463

JPL Technical Monitor - D. L. Bond

TABLE OF CONTENTS

TABLE OF CONTENTS (concluded)

LIST OF FIGURES

LIST OF FIGURES (continued)

LIST OF SYMBOLS

C	carbon
F	fuel (flow rate); atoms of fuel/unit volume
H_2O	water
H	hydrogen atom
HO	hydrogen oxide
HN	hydrogen nitride
H_2	hydrogen
$\mathcal{m}$	molecular weight
N	nitrogen atom
N_2	nitrogen
NH_3	ammonia
N_2H_4	hydrazine
N_2O_4	nitrogen tetroxide
NO	nitrous oxide
O	oxygen atom; oxidizer (flow rate); atoms of oxidizer/unit volume
O/F	oxidizer to fuel ratio
O_2	oxygen
P	pressure

Q	source/sink intensity
R	radius of separation surface (defined by Eq. (6), pp. 73)
$\overline{R}$	gas constant
T	temperature
V	specific volume
e	experimental
f	fuel
m	mass ($\dot{m}$ mass flow rate)
o	oxidizer
t	theoretical
u	velocity
x	Cartessian coordinate (parallel with chamber axis); element mass fraction
y	Cartessian coordinate (normal to wall)
z	Cartessian coordinate
α	gram atom fraction
β	element mass fraction
γ	molor flow rate
δ	

LIST OF SYMBOLS (concluded)

δ	boundary layer height
ζ	width of integration strip (sketch, pp. 73)
η	transformed boundary layer coordinate
λ	curvalinear coordinate
μ	viscosity
ξ	transformed boundary layer coordinate
Π	function defined by Eq. (9), pp. 74
ρ	density
τ	time
ϕ	angular position relative to injector (see Fig. 2)
χ	mole fraction of species

SUBSCRIPTS

o	oxidizer
f	fuel
i,j	indices
e	edge
s	sample

SECTION 1

INTRODUCTION

The analysis described in this report treats the data obtained from a rocket combustion chamber buring nitrogen tetroxide and hydrazine at a nominal mixture ratio of 1.3 and at a nominal chamber pressure of 150 psi. A description of the apparatus and experimental technique are presented in Part IV and the data and data reduction procedure are presented in both Parts III and IV. In addititon to the analysis, the details of the injector design and construction are presented here since they are necessary to an understanding of certain of the correlations.

Most of the analyses were performed using operational computer codes as computational tools. These computer codes were developed at Aerotherm Corporation under other contracts over a period of years and represent a high degree of sophistication in the treatment of both the boundary flow and chemical events which occur in the boundary flow.

This report then is concerned with describing the way in which these computational tools were used, the preparation of input, the assumptions implicit in the input and computations, and the interpretation of the results from the computer codes. It was not possible to discuss in more than the most general terms the underlying theory and computational technique employed in the computer codes and instead reference is made to supporting documentation.

SECTION 2

OBJECTIVES OF STUDY

In an experimental program it is generally desired to enhance the experimental results by performing certain analysis which may verify the results, explain certain trends and increase understanding of the physical processes at work through correlations etc. Wherever possible it is also desirable to compare the results with existing data. Such is the intent of the work reported here. To the extent that practical limitations of time and funding permitted this objective was achieved although significant areas for future exploration remain.

One of the principle objectives of the program is to increase the understanding of the relationship between events occurring in the boundary flow and certain injector design features. In this study the two principle boundary flow events of interest are the chemical composition of the boundary flow and the heat flux to the chamber wall. These two are intimately inter-related and together directly affect specific impulse performance and survivability of the materials forming the chamber and nozzle. It is the purpose of this report to describe the results of the correlations of the injector design features and the boundary flow characteristics and where possible to rationalize and explain the characteristics and trends found in the experimental data.

SECTION 3

CORRELATION OF BOUNDARY FLOW CHEMISTRY AND HEAT FLUX WITH INJECTOR PARAMETERS

The quantitative relationship between the plethara of injector design parameters and events which occur in the combustion chamber are to this day largely a mystery even though these events are vital to the satisfactory performance of the rocket motor. This lack of understanding is a measure not so much of a lack of analytical effort but of the complexity of the subject. It was hoped at the outset of this program that a detailed experimental study of some of the boundary flow parameters in the chamber would be helpful to the understanding of these relationships. As will be seen in the following data correlation, the experimental data show very significant trends (albeit unexpected) which are probably *really not* characteristic of a properly functioning injector. Aside from the dramatic trends the correlation of boundary flow composition and heat flux is found to not bear a strong relationship to the injector spray pattern. This may possibly be a fault of inconsistent data. On the other hand preliminary predictions of composition by Aerotherm, unreported in the literature, demonstrate that the interplay between the injector elements is very significant and that as a consequence an accurate description of the dependence of the boundary flow parameters requires a more closely spaced data acquisition than that used in this program.

3.1 INJECTOR DESIGN FEATURES

The combustion chamber injector used in this program was one of a series of high pressure drop injector designs developed in the Advanced Liquid Propulsion System program at the Jet Propulsion Laboratory (JPL). A discussion and description of these injectors may be found in References 1 and 2. The injector for this program is one of two having the same design which were tested at the Edwards California facility of JPL with ablative chambers and nozzles. The first injector

demonstrated the most uniform and lowest ablation of the nozzle of the four injector types tested. Readers interested in reviewing this data are directed to Reference 2. Curiously the second injector and the one used in this program, while identical in design to the first injector, demonstrated poor ablation response (data not reported in the open literature – Reference 3). Because of the first injector's good performance, this anomalous severe erosion of the nozzle material was initially attributed to a defect in the material itself and not the injector. The results of this program show the poor ablation performance was indeed most probably a consequence of the injector although the differences between the two injectors which could cause this anomalous behavior remain, at present, a mystery. This ablation behavior is discussed further in Section 6.

3.1.1 Construction Details

The stainless steel injector is made up of two flanges which hold twenty tubes forming the ten doublets. The flanges serve to form the fuel and oxidizer manifolds as well. The stainless steel centerless ground tubes have an inside diameter of somewhat less than .020 inches and a length to diameter ratio of 100. The orifices were carefully aligned during the manufacturing process to produce accurate impingement and care was taken that the orifice lips was sharp and burr-free. Post testing 20-power stereo microscopic examination of the injector showed this initial manufactured condition still prevailed although some surface roughness on the inside surface of the tubes could be seen. One oxidizer orifice was seen to be blunted (number 3 in Figure 1) but this is not in the area where injector anomalies are found. The pressure drop at rated flow conditions is about 400 psi. This pressure drop and the fact that fully developed pipe flow exists in the tube, makes the flow pattern and impingement pattern very reproducible. The oxidizer and fuel tubes are inclined one to another to form a 60° included (impingement) angle for all doublets. At a mixture ratio of 1.2 this produces a net momentum vector (of the impinged jets) which is parallel with the chamber axis. Since the tests in this program were run at a slightly higher O/F ratio (O/F $\cong$ 1.3), there was a corresponding inclination of the spray towards the chamber axis. The calculated

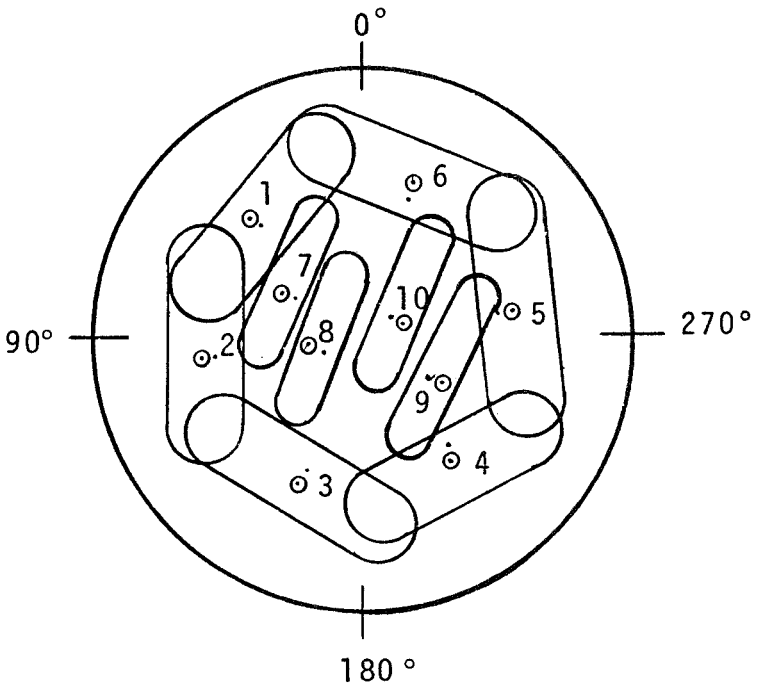

a. Doublet Non-Reactive Spray Pattern

A-2135

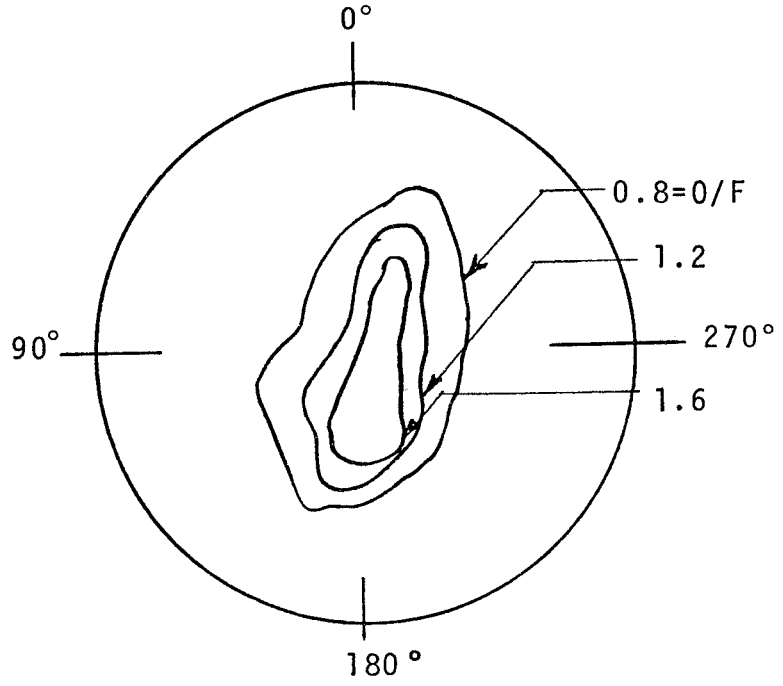

b. Mixture Ratio Distribution

Figure 1. Injector Non-Reactive Spray Pattern and Mixture Ratio Distribution

distance between the orifice and the point of impingement is 0.08 inches (from Reference 2).

3.1.2 Doublet Flow Pattern

The spray pattern from an impinging doublet has been found experimentally to be elliptical in cross section (for nonreacting fluids at least). Considerable work has been done at JPL in studying the impingement of both reacting and nonreacting jets. For the latter, a mass and mixture ratio variation (in the elliptical fan) has been measured using specially constructed spray booths.*[4] The mass distribution has been found to have a hyperbolic decay, with the centerline mass flux having a square power law decay from the point of impingement.[4,5] The mixture ratio variation has a modified error function type of profile on the minor axis of the ellipse (which contains the orifices) and is relatively constant in planes parallel to the major axis. The O/F varies from about 4:1 to about 1:2 and shows significant penetration. That is, the spray is oxidizer rich on the fuel orifice side of the doublet and vice-versa.

Some interesting recent studies show that the penetration phenomena demonstrated by nonreactive fluids may not model the reactive jet situation especially for hyperbolic propellants such as N_2O_4 and N_2H_4. Such phenomena has been termed reactive flow separation (or blow apart) and results in a reversal of the mixture characteristics described above. For the present injector design this means that the boundary flow would be oxidizer rich instead of fuel rich were the blow apart effect to prevail.

*Numbers in parenthesis refer to items in reference section.

3.1.3 Spray Booth Non-Reactive Data

Because the injector used in this program has ten doublets, the flow field in the chamber is necessarily a composite of the flow field produced by all of the doublets, each of which have the characteristics described in the preceding section. A representation of this superposition is shown in Figure 1 (reproduced from Reference 2).* Even in this simple representation it is evident that the composite flow field is a complex interaction of the ten element flow fields.

Currently the most frequently used method for obtaining a "feel" for the composite flow field is to gather non-reactive distribution data from a shower booth using simulated propellants. Flow field data for the injector of interest is shown in Figure 1-b. Such data can only show the most general features of the flow field. For example, the data in Figure 1-b shows that the injector does not produce the symmetrical flow field one might expect from the layout of the injector elements although a directional bias due to the orientation of the central elements is evident.**

3.2 CHEMISTRY CORRELATIONS

This section of the report presents the correlation of the boundary flow chemical composition data with the injector angle orientation (Figure 1). This data was obtained from the basic mass spectrometer determinations of the atomic composition in the sample bottles which is presented in Part III. This data has been cast in mass frame of reference by multiplying the oxygen to hydrogen atomic ratio by the molecular weight ratio of the oxidizer and fuel respectively.

$$O/F = \frac{O}{H} \quad \frac{\mathcal{M}_O}{\mathcal{M}_f} \tag{1}$$

---

*Figures 1-a and b reproduced from Reference 2 have been modified slightly to account for the different angular relationship of the subject injector.

**Such irregularities are typically attributed to manufacturing tolerances which are very critical for small orifices.

This technique is based on the premise that each atom of oxygen represents one molecule of oxidizer and similarly for one atom of fuel. Multiplying by the molecular weight provides a convenient way of comparing non-reactive and reactive data on a mass flow basis.

The circumferential distribution of the oxidizer to fuel ratio is presented first in cartesian coordinates (Section 3.2.1) for a particular station (or bottle number). Later the data is presented in polar coordinates (Section 3.2.2). There are six sampling stations located at about 3/4-inch increments down the chamber. The axial locations are shown in the sketch of Figure 2-a. Note that the last station is located in the converging section approximately midway between the constant diameter chamber and the throat. The circumferential position, ϕ, is measured from the zero mark on the injector in a counter clockwise direction (viewed upstream) corresponding to the injector angles shown in Figure 2-b.

3.2.1 O/F Position Dependence

The spatial variation of the boundary flow composition is best visualized in cartesian coordinates and this is done in a series of figures, one for each sampling station (Figure 3), beginning near the injector end of the chamber. While these figures show the O/F dependence, the reader is cautioned that this alone does not specify the boundary flow composition because, as shown elsewhere in this report and throughout the data in Part III, unequal diffusion and perhaps other events not understood at present cause the flow to demonstrate nitrogen rich characteristics which dilution modifies the enthalpy potential of the boundary flow among other parameters of significance. Such complications are not treated in the correlations presented here.

The figures in this set show that the boundary flow is predominantly fuel rich as desired--becoming less fuel rich as the flow proceeds down the chamber to the exit. However in one region, specifically between 220 and 280 degrees in Figure 3-a (but in similar regions for all figures) the boundary flow has a very high oxidizer to fuel ratio characteristic; which for the last stations is as high as the highest

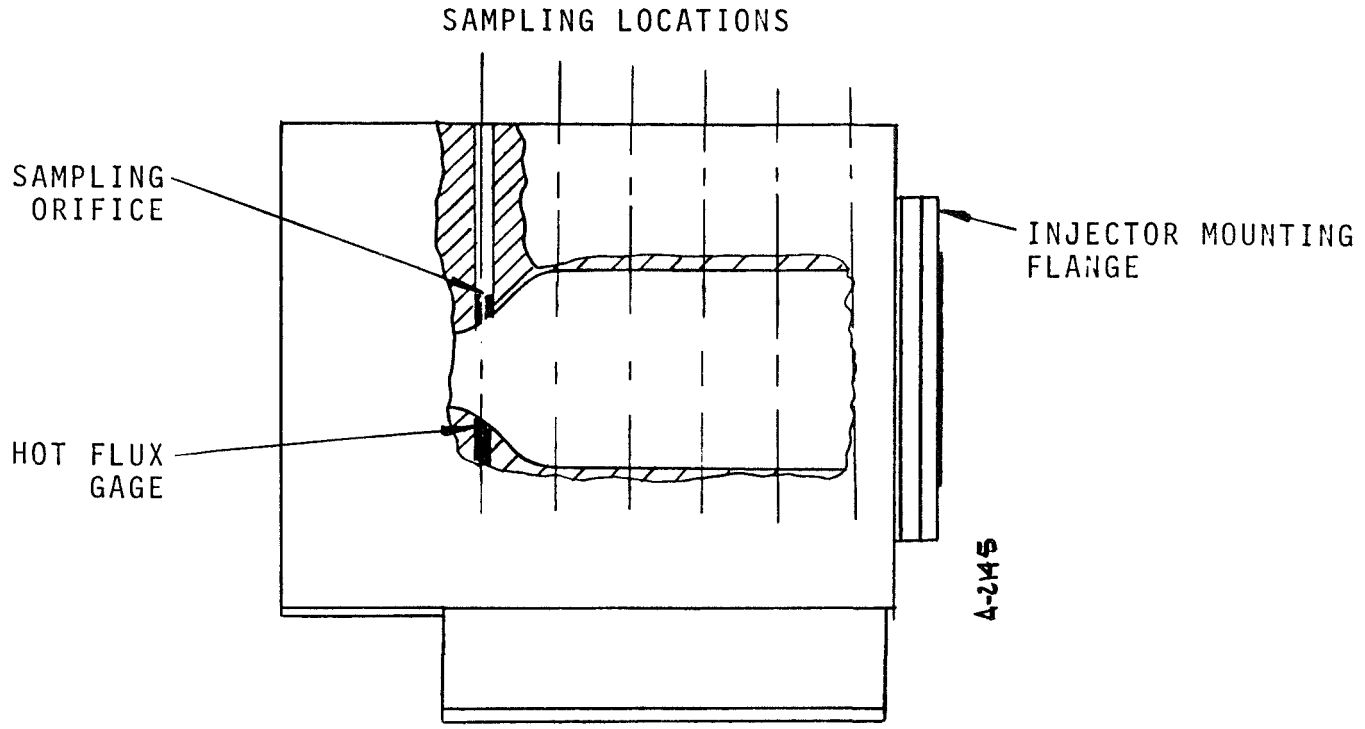

b. Combustion Chamber

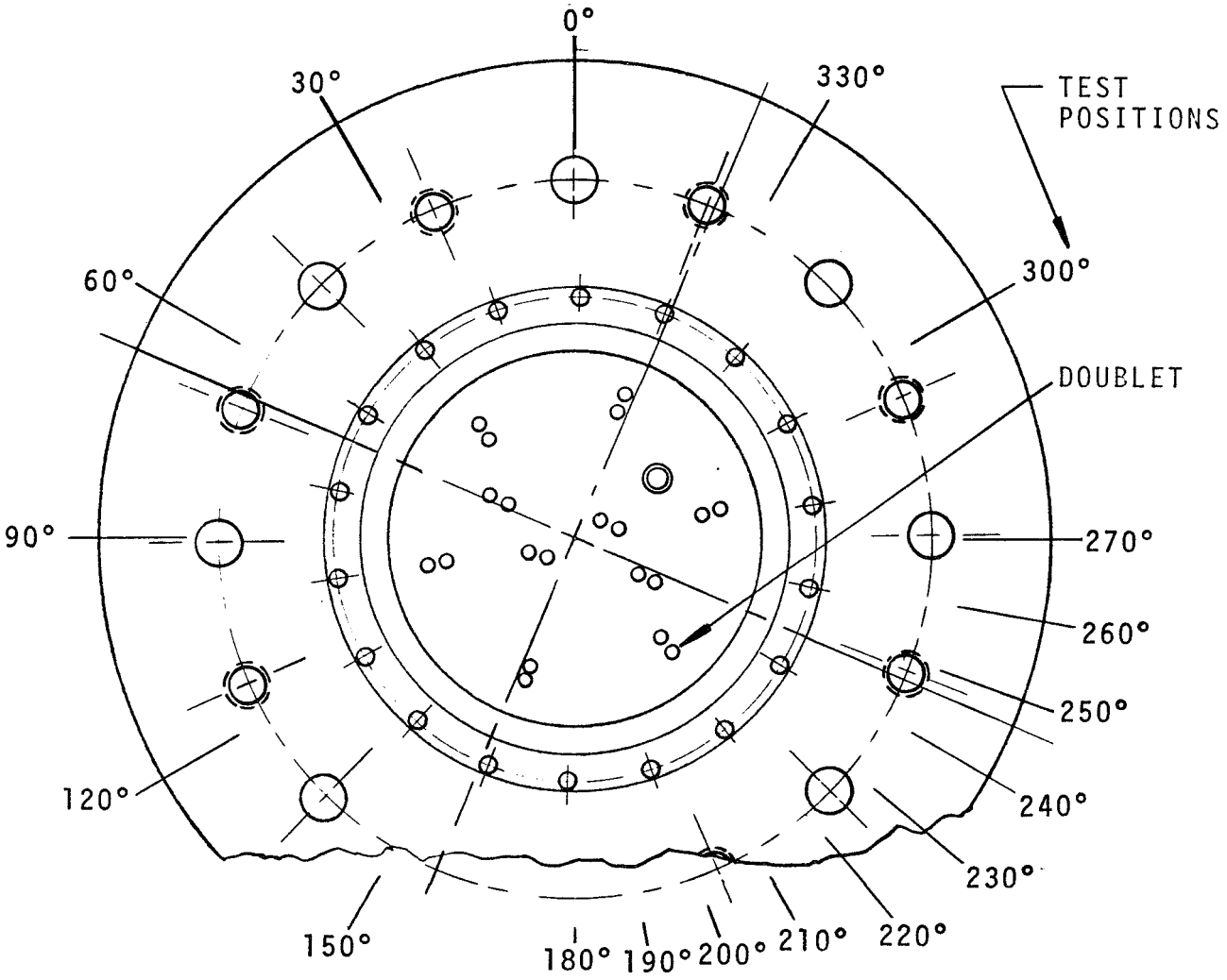

a. Injector

Figure 2. Sampling and Heat Flux Determining Locations

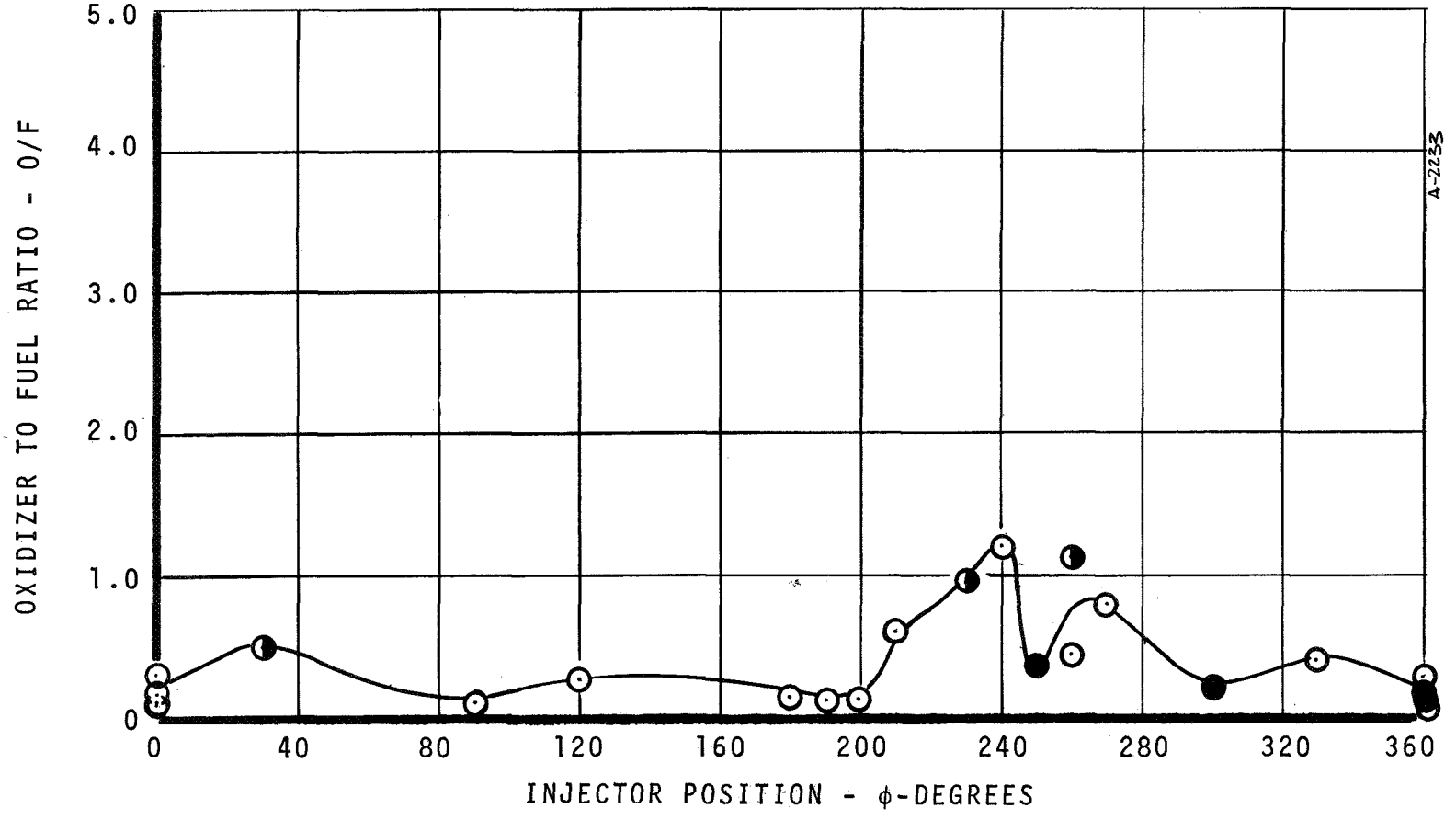

Figure 3. Oxidizer to Fuel Ratio Spatial Dependence
a. x = 1.03 INCHES

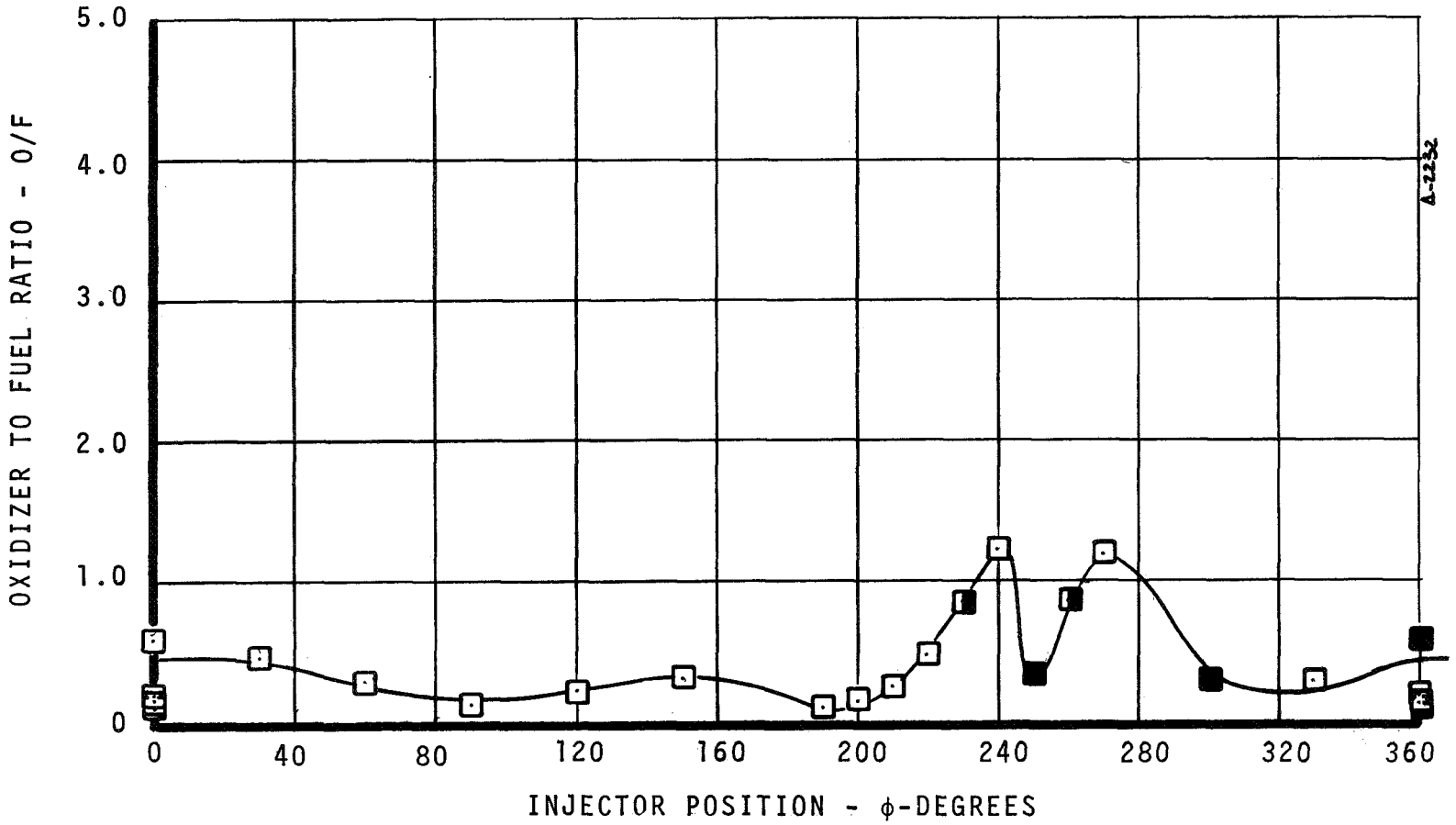

Figure 3. Continued

b. x = 1.78 Inches

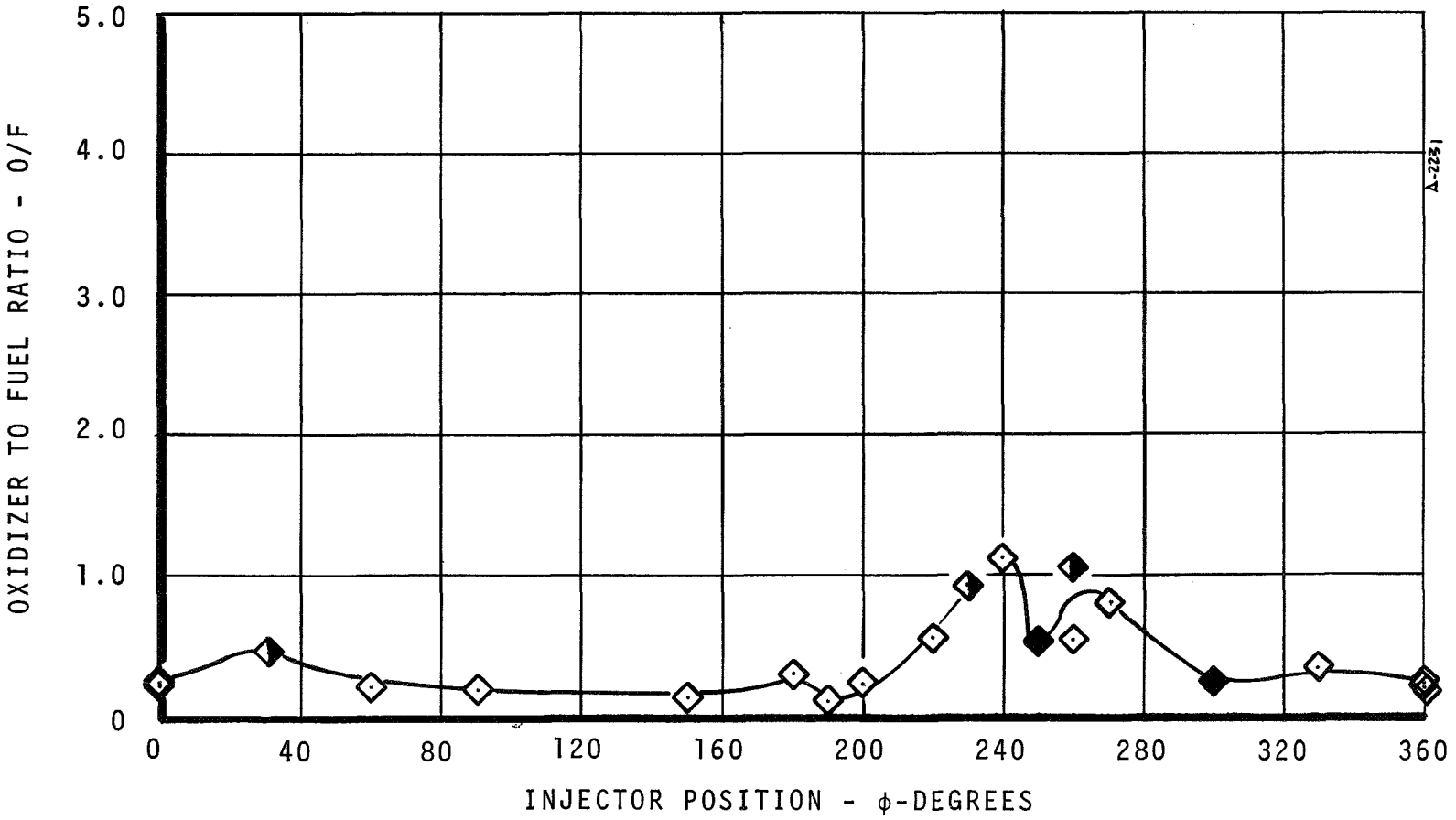

Figure 3. Continued

c. X = 2.53 Inches

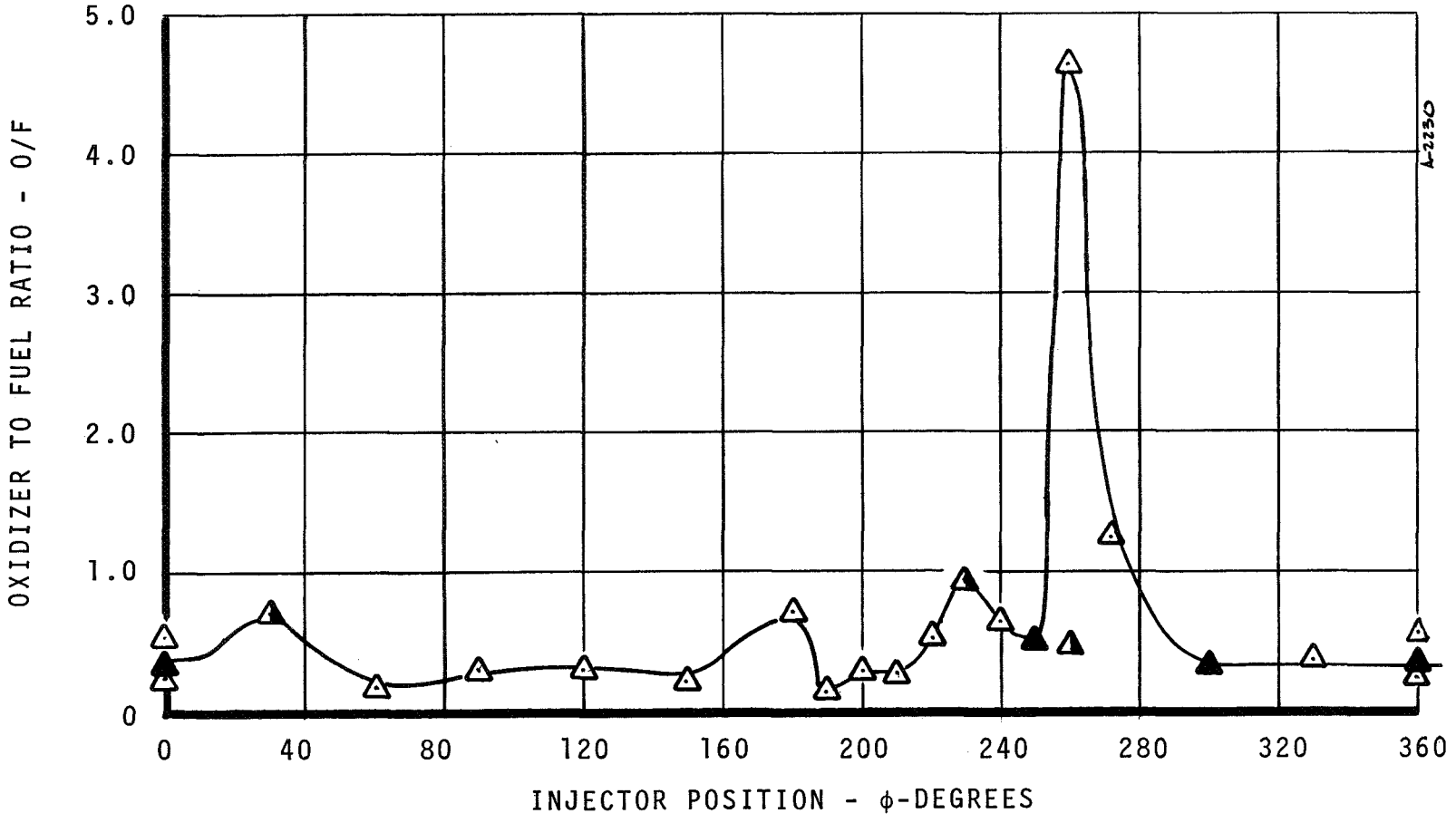

Figure 3. Continued

d. x = 3.28 Inches

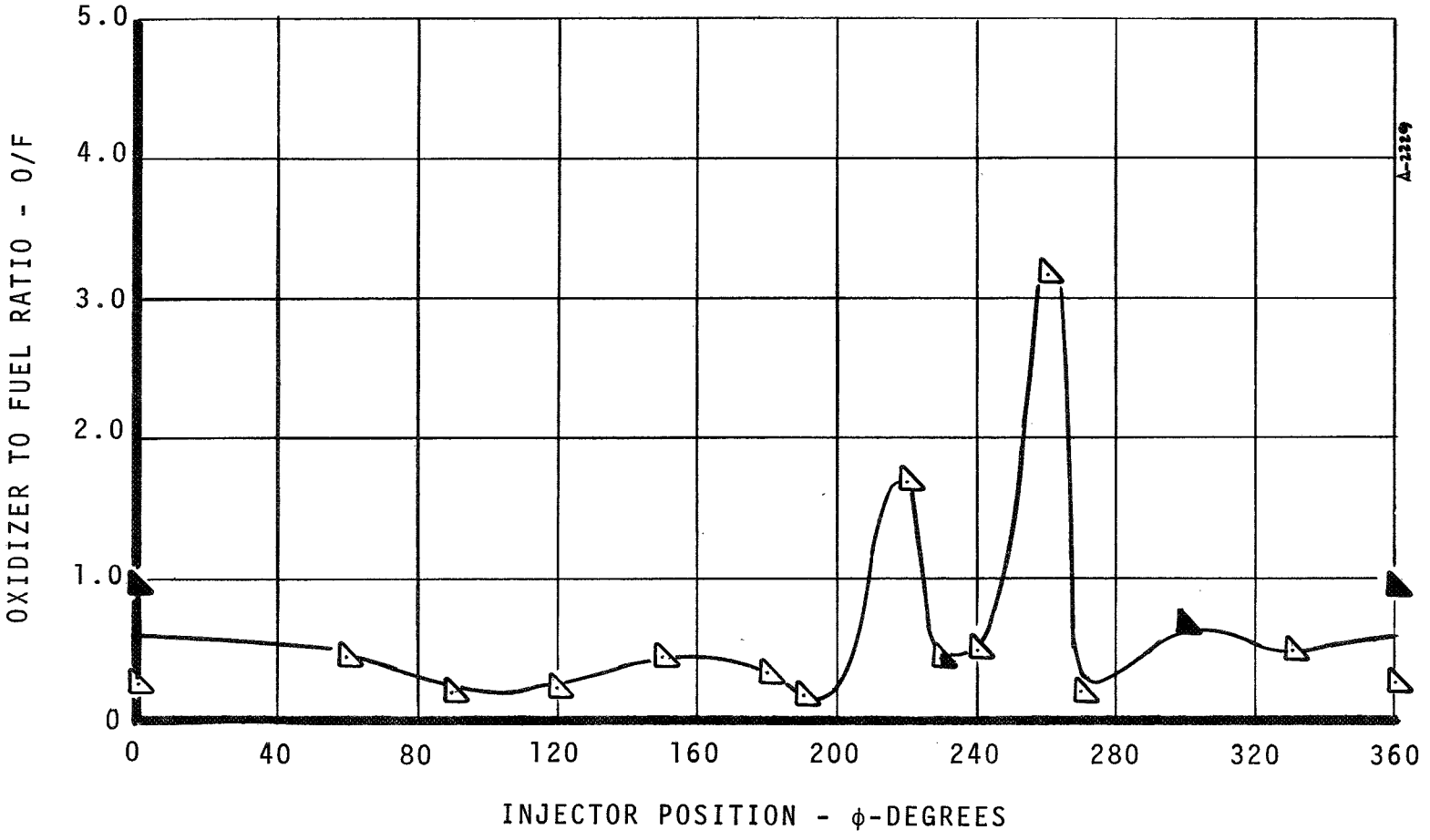

Figure 3. Continued

e. x = 4.03 Inches

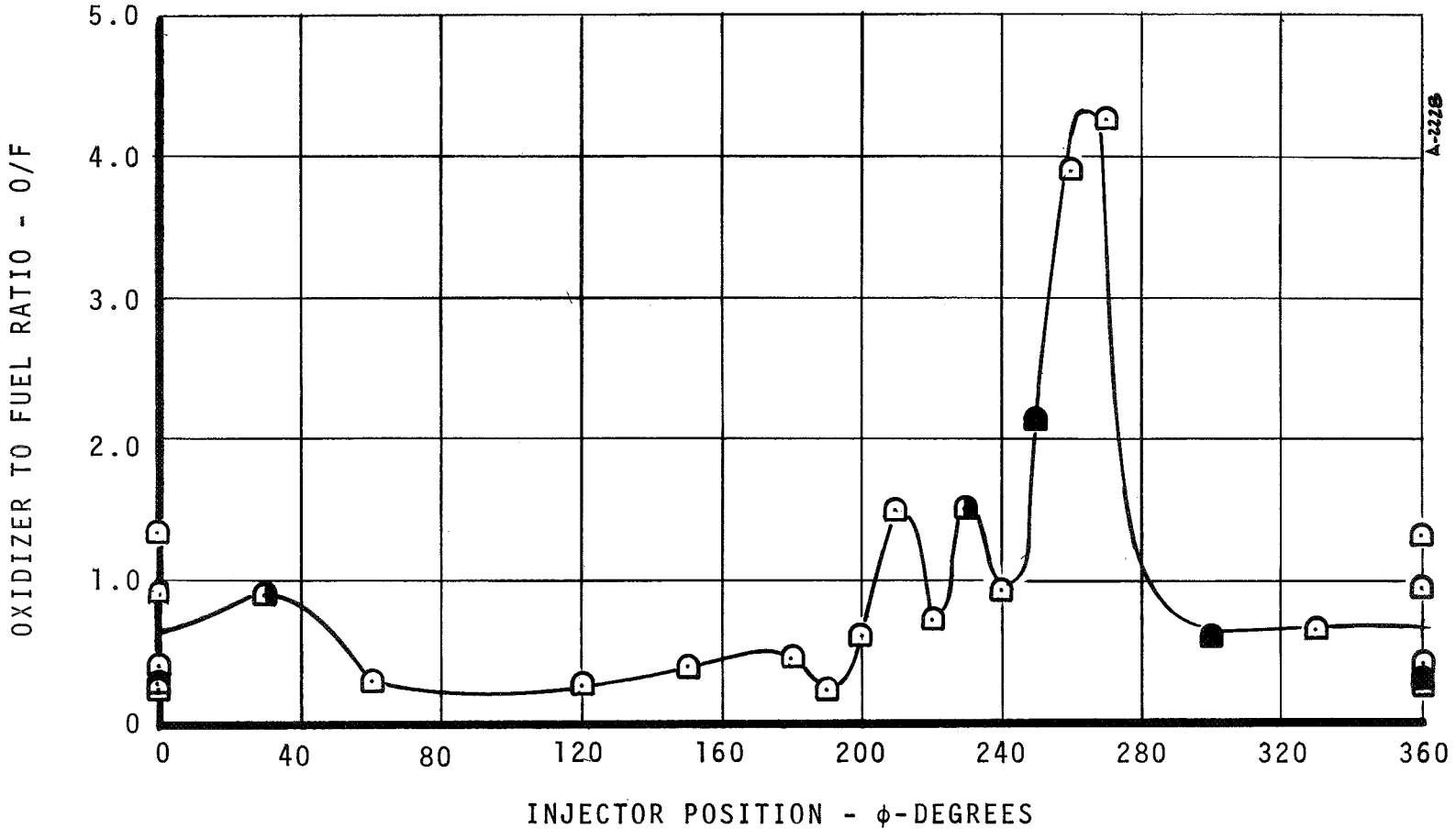

Figure 3. Concluded

f. x = 4.78 Inches

determined in the tests of the individual element in non-reactive tests--(i.e., O/F = 4:1) mentioned in the preceding section. Note also in the fuel rich regions the O/F values are lower than the non-reactive data from the individual elements (O/F < 1:2).

While the data does show higher O/F ratios in the 270° quadrant as expected from the shower booth data (though not to the extent displayed in the data here) the high ratios expected at the 75° sector do not appear although a slight rise is seen for the 30° position for most of the stations.

3.2.2 Spray Pattern Correlation

Although more difficult to assimalate, the most practical way to correlate the foregoing variations in boundary flow mixture ratio with the injector element orientation is to compare it with the doublet locations in polar coordinates. This is done in Figures 4a through 4f (again for the six axial locations). The doublets are numbered from one to ten as they are encountered in rotating counterclockwise. In the following discussion it will be necessary to visualize the interaction of the spray patterns bearing in mind the elliptical pattern (probably oxidizer rich) on the fuel orifice side (denoted by the letter f) and vice-versa for the oxidizer side (denoted by the letter o). Also bear in mind the mixture ratio is probably relatively constant in planes parallel to the ellipse major axis (the long line) of the spray pattern.

In Figure 4-a it is quite apparent that the boundary flow is oxidizer rich in the neighborhood of the number 4 and 5 doublets. As will be seen in the remaining figures of this series this is a consistent trend. Doublets 2, 6, 7, and 8 appear to be running very fuel rich. Some preliminary insight into the complicated interaction of the spray can be inferred from these data. For example note how the oxidizer rich spray from 3 penetrating the oxidizer rich spray from 4 produces a low O/F at 180°. Conversely, the oxidizer rich side of doublet 2 could produce the slight hump in O/F at 30° as it penetrates the fuel rich spray from 1. Similar interactions can be visualized for 2 and 3; 1 and 6 etc. One is tempted to conclude that except for 4 and 5 the variations noted in O/F distributions are due to these

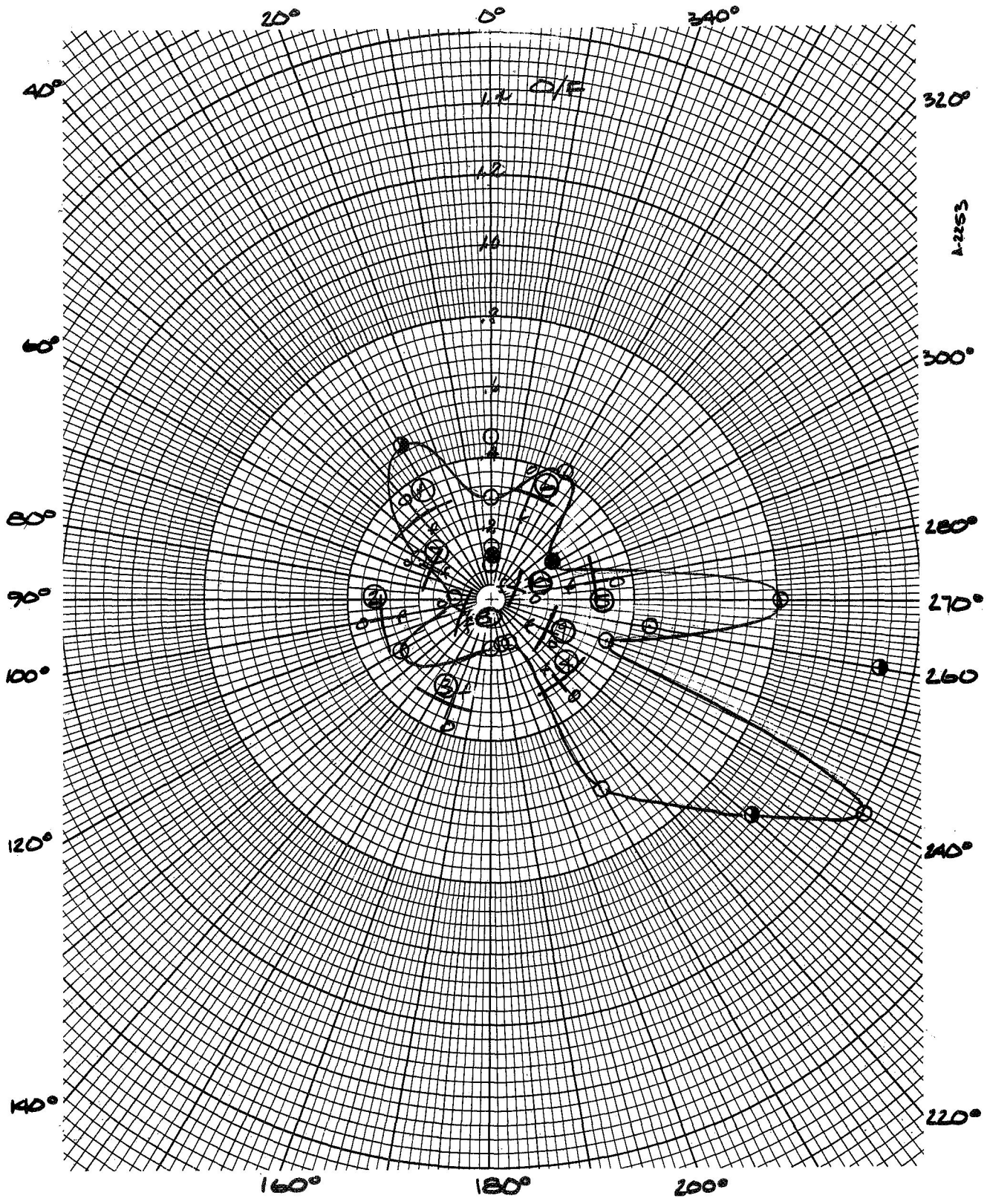

Figure 4. Correlation of Oxidizer to Fuel Ratio Spatial Dependence with Injector Doublet Location

a. x = 1.03 Inches

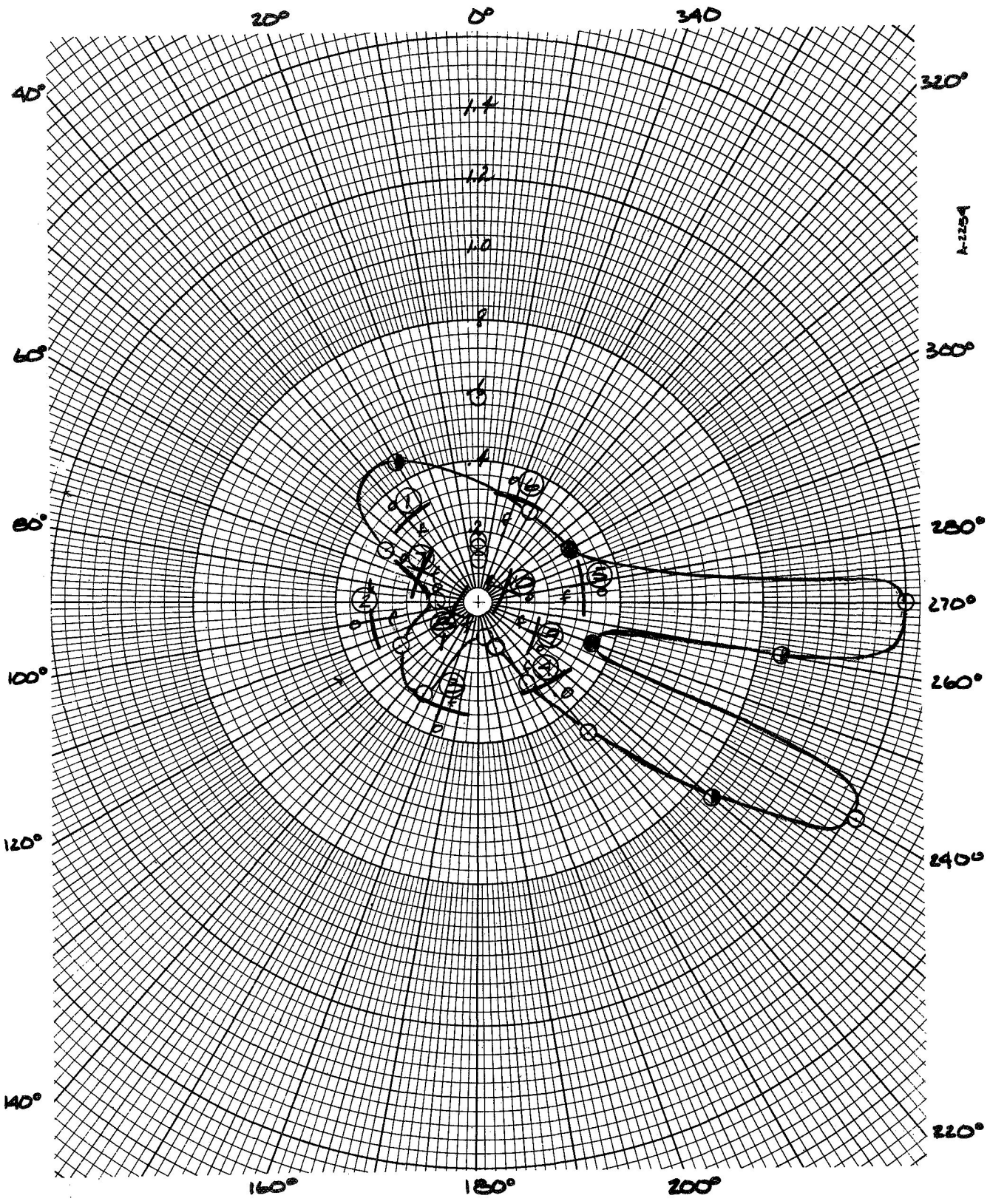

Figure 4. Continued

b. x = 1.78

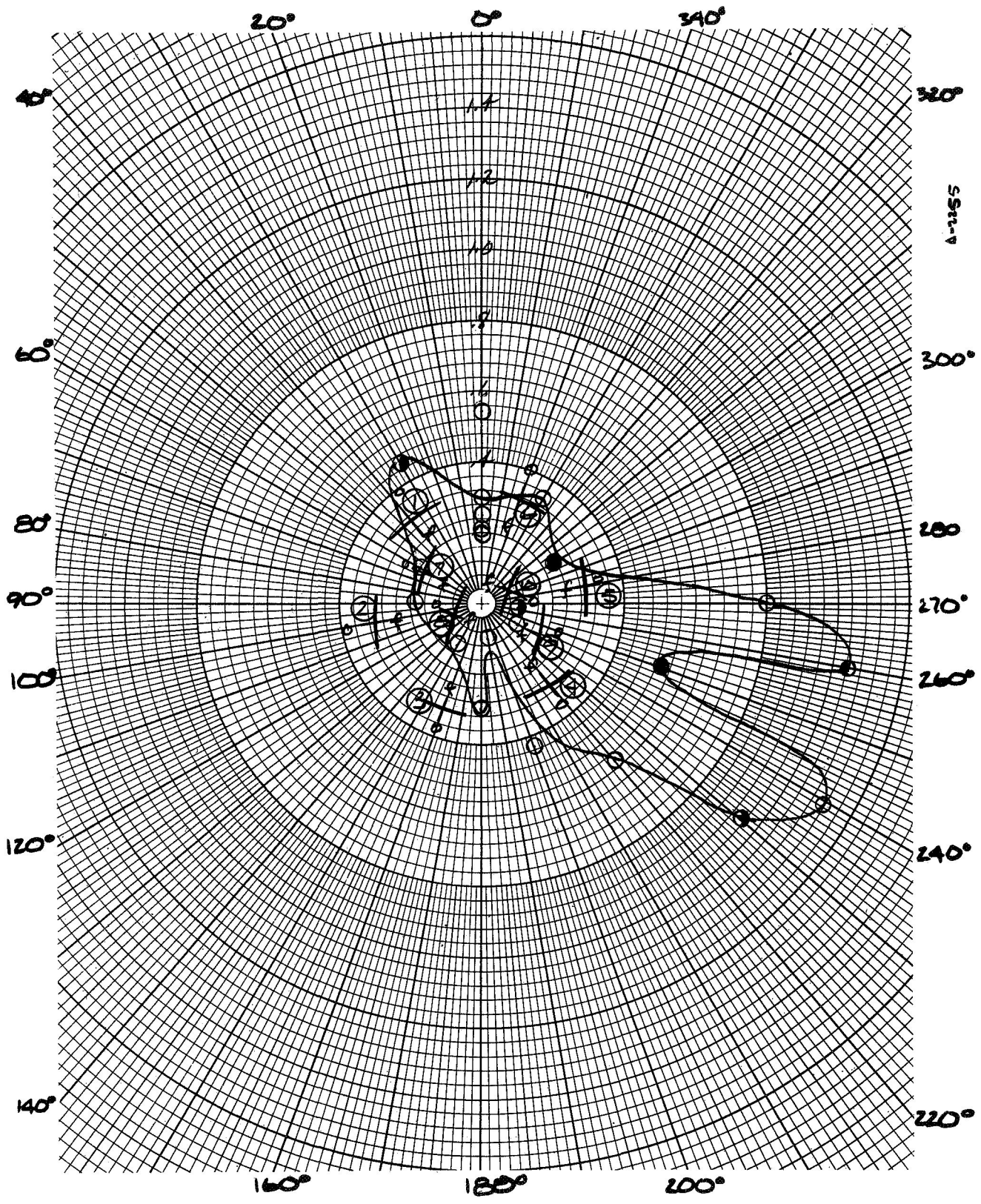

Figure 4. Continued

c. x = 2.53

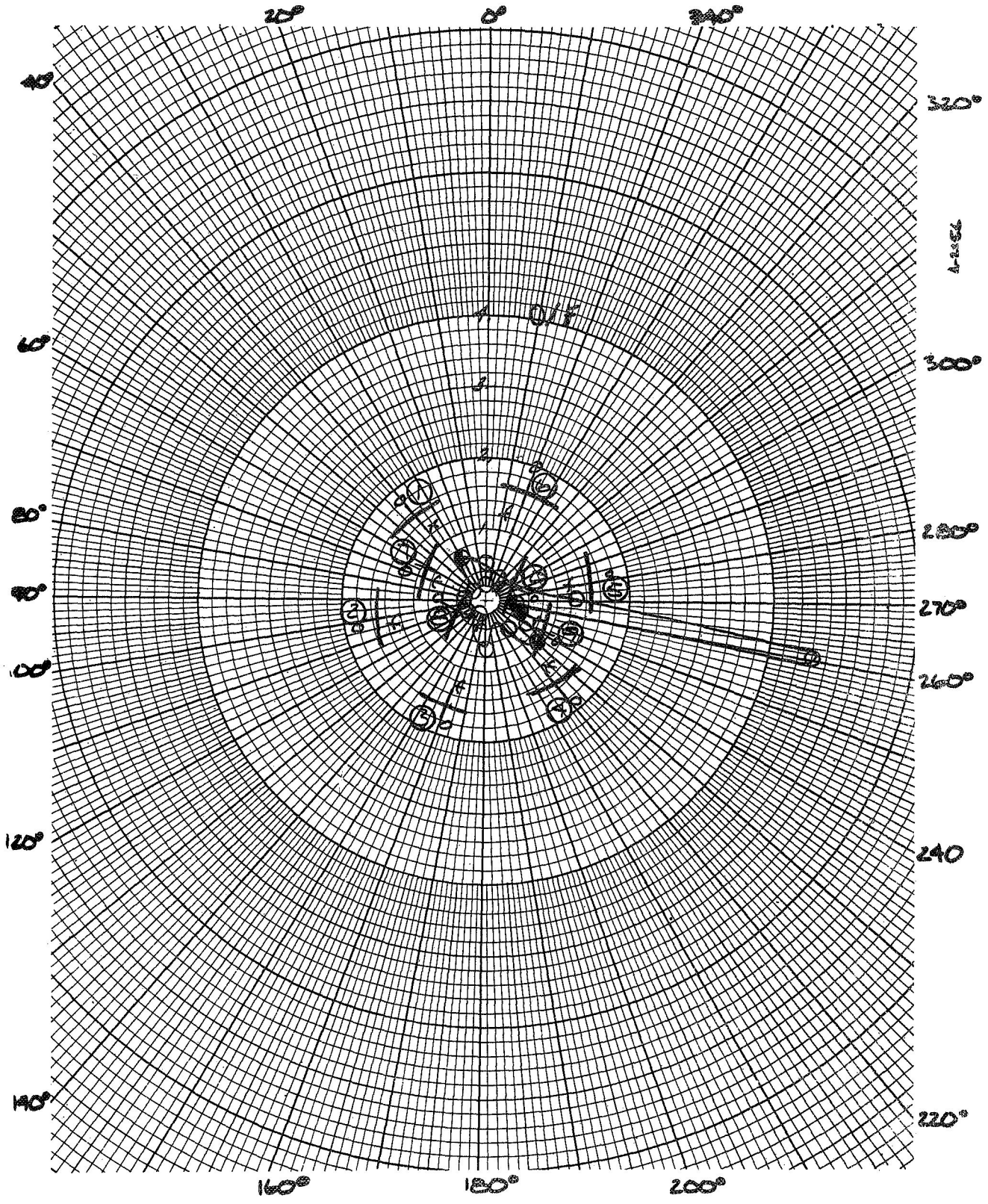

Figure 4. Continued

d. x = 3.28

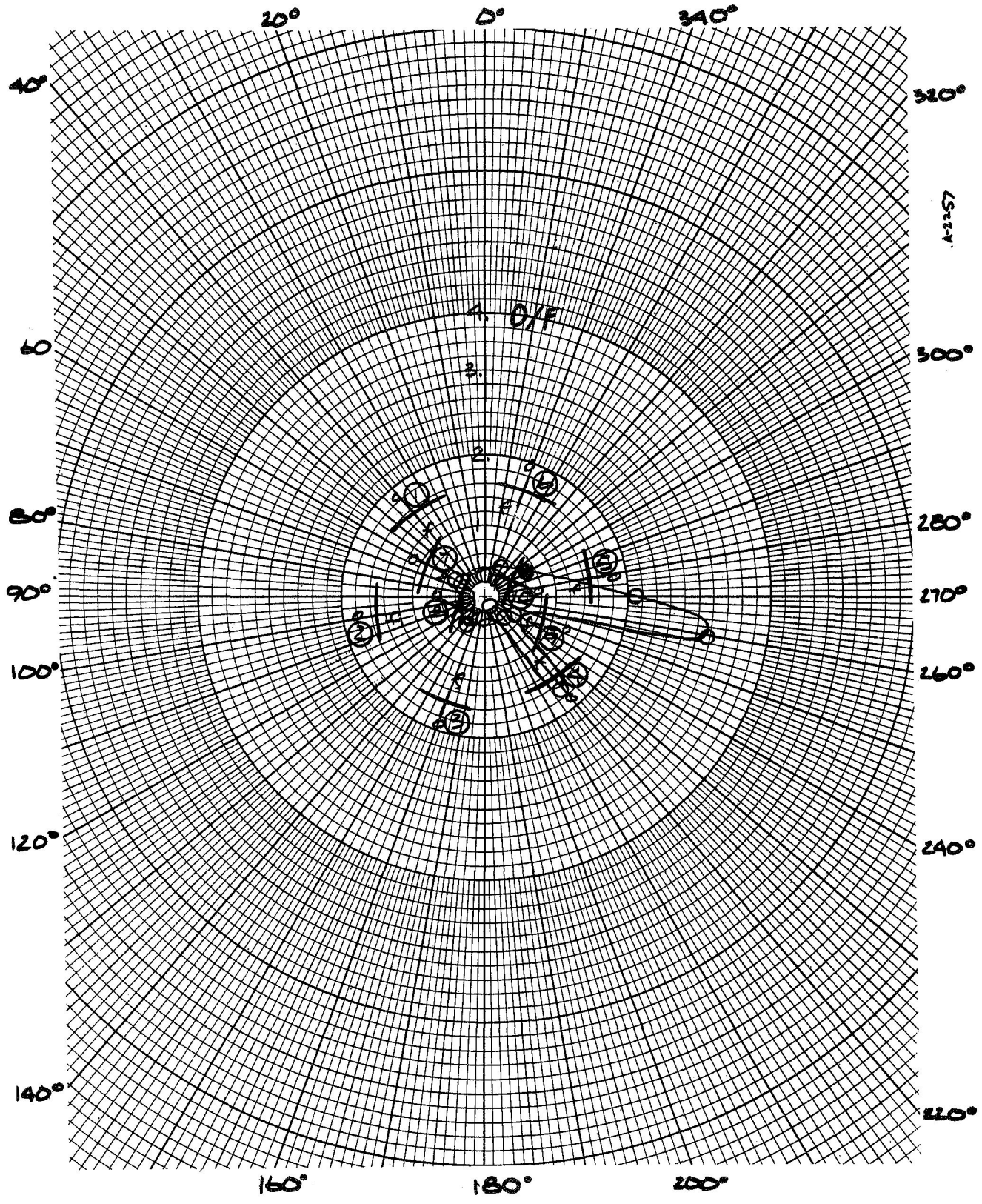

Figure 4. Continued

e. x = 4.03

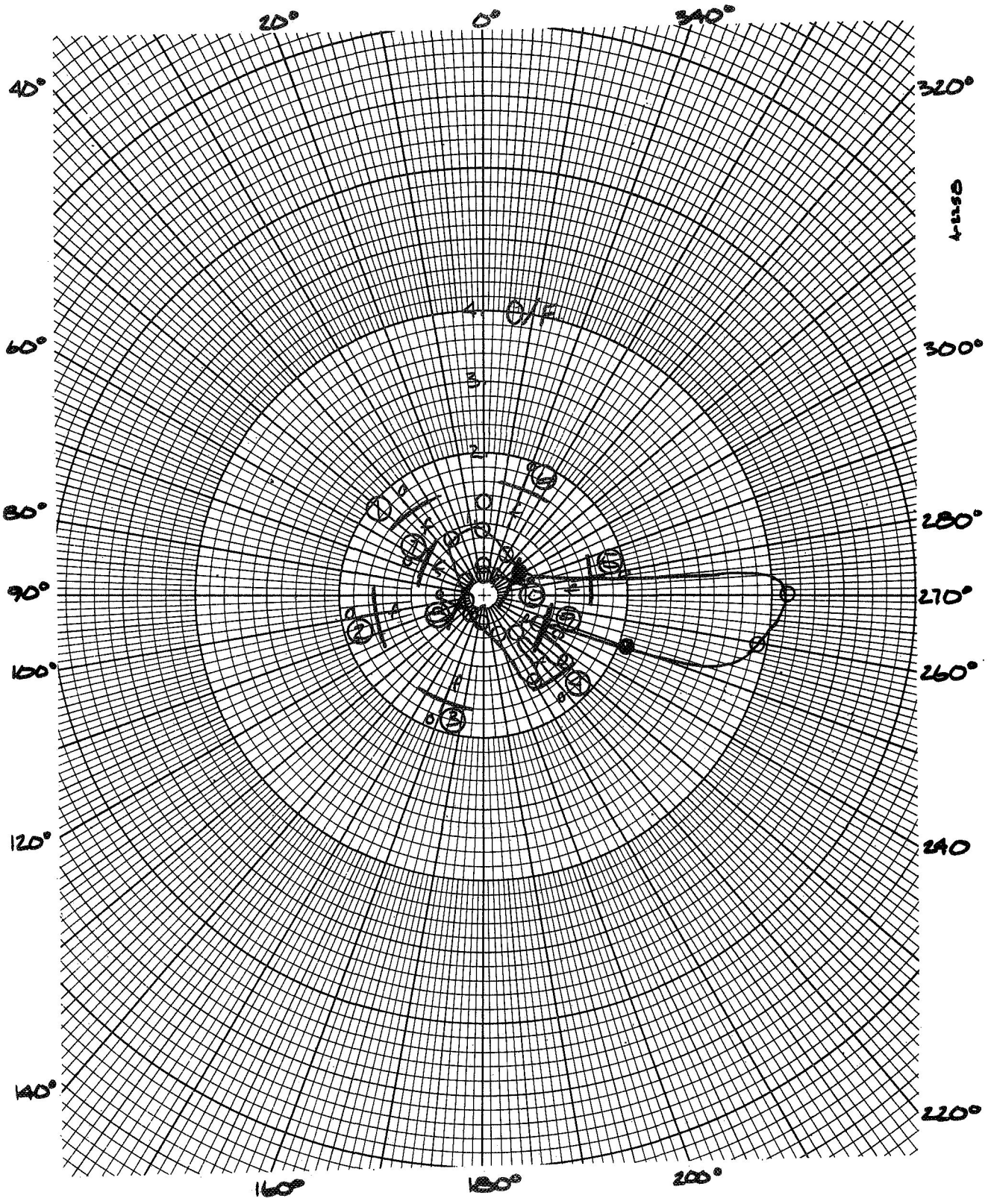

Figure 4. Concluded

f. x = 4.78

interactions. Unfortunately the very real possibility of doublet variation due to manufacturing tolerances (as evidenced by 4 and 5) clouds the issue. Anything more than qualitative correlations such as these must explain the details of predicting spray interaction.

The effects or trends noted in Figure 4-a are reported in 4-b with some exaggeration. The disappearance of the hump at 330° is the major difference. The exaggeration of the oxidizer rich region increases with axial distance from the injector face as can be seen by examining subsequent figures (note the scale change in Figures 4-d through 4-f). The other strong feature which is repeatedly evident in the figures is the region around 30° where the boundary flow tends to be near a mixture ratio of unity.

It is also apparent in these figures that a definite correlation between the O/F spatial characteristics and the location of the injector doublets does not exist. That is, for instance, the peaks in O/F do not line up with the doublet location as might be expected. As a matter of fact, a slight swirling of O/F pattern in the clockwise direction can be noted. It should also be pointed out that only in the quadrant between 180° and 270° were data points obtained in sufficient intervals to accurately define the O/F profile. There exists the possibility that a "finer" mesh of data points would define a stronger correlation between the O/F profile and the doublet locations.

3.3 HEAT FLUX CORRELATION

The best of the heat flux data obtained in the program (all of which is presented in Part III) is presented in Figure 5 which both conveniently summarizes the data and compares it with the spatial composition trends. It is seen for the positions near the injector that there is a fair degree of correlation between the change in heat flux magnitude and changes in oxidizer to fuel ratio, although the extreme changes in the oxidizer rich region does not seem to have a heat flux counterpart. The relationship between the two becomes more tenuous for the other axial locations and near the throat there seems to be little if any relationship. It can be noted that the phenomenon causing the significant changes in heat flux appears to be represented in all three gage responses. In particular, attention is drawn to the

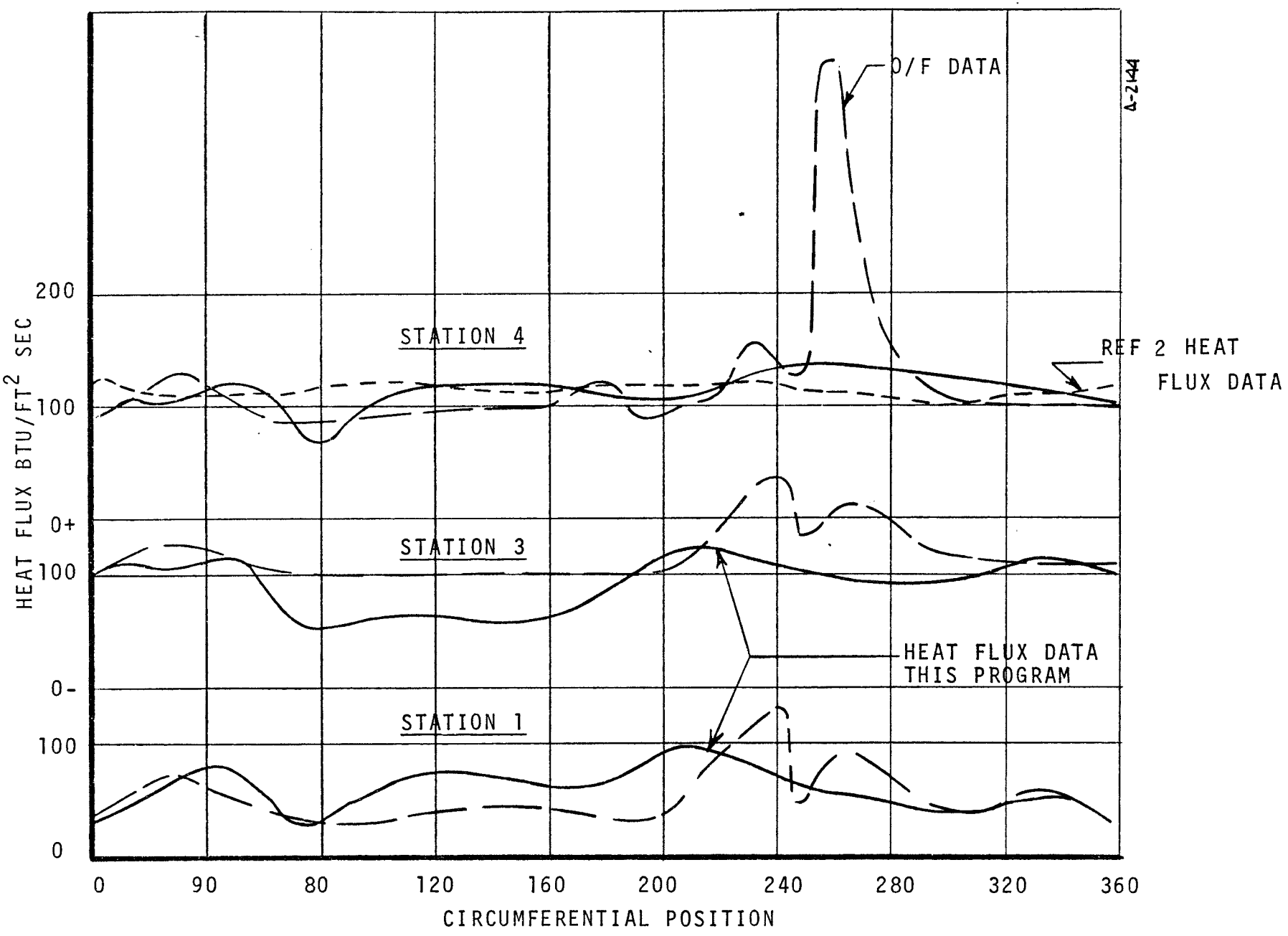

Figure 5. Comparison of Mixture Ratio and Heat Flux Dependence

the rise in heat flux to the 60° position and the sudden drop at about 80°. A general rising trend to the oxidizer rich region followed by a drop back down to the 0° position values can be seen. The data from Reference 1 taken from an identical injector in a steel chamber at a slightly higher wall temperature displays a completely different spatial characteristic since the data are much more constant. The calorimeters of Reference 1 were constructed on a different principle and a different analytical technique for calculating heat flux was employed. These differences may or may not account for the different characteristics between the two data sets.

SECTION 4

ANALYSIS AND PREDICTION OF BOUNDARY FLOW CHEMICAL COMPOSITION

The analysis and prediction of the boundary flow composition was performed in two ways. First the samples were compared with equilibrium chemistry theory and secondly the boundary flow and sampling event were theoretically modeled using a recently developed turbulent boundary layer code. In addition equilibrium analysis were made of the propellants at various mixture ratios and of the decomposition products of the individual propellants as function of temperature. These efforts were extremely limited in view of the great amount of data which was generated in this program but which was not compared with theory in this way. Though preliminary in nature, the results are so satisfactory that the analysis of all the data should be completed using and expanding upon the techniques demonstrated here.

First the general equilibrium results will be discussed to set the stage for the detailed analysis. Next, the analysis of some of the samples taken in the program will be presented, and finally, the boundary layer treatment will be described.

4.1 CHEMICAL EQUILIBRIUM STUDIES

The chemical composition in the combustion chamber is not uniform even away from the boundary flow because of the substantial composition variation in each doublet spray. This should be especially pronounced near the injector while for regions near the throat the global composition should be more uniform due to turbulent mixing and because of intersection of the spray patterns. Chemical equilibrium analysis can demonstrate the effect that such composition variations have on thermodynamic properties such as local enthalpy and theoretical flame temperature. Because knowledge is lacking on the details of the global composition variations in the chamber there is no way at present to relate such equilibrium calculations to events happening near the wall. This lack of knowledge poses a significant barrier to the analysis of the physical situation since such global variations certainly exert

a strong influence on such measurable quantities as heat transfer to the wall. To make the situation even more formidable it must be recognized that even if such relationships were to be developed, equilibrium analysis would be additionally limited by unequal diffusion and reaction kinetics which occur in the real flow situation. Despite these limitations, the equilibrium analysis can be useful in providing a feeling for the gross situation in the chamber and how the global composition variations could possibly produce the data obtained in this program.

4.1.1 Average Chamber Composition Dependence on O/F

The Aerotherm Chemical Equilibrium (ACE) computer code was exercized for O/F ratios varying from 0.1 to 5.0. The results of these theoretical calculations are presented in Figure 6-a and 6-b. In Figure 6-a the propellant enthalpy input to the ACE program is shown along with the theoretical flame temperature. Observe that the experimental firings which were conducted at mixture ratios of about 1.3 yield the maximum equilibrium temperature. This value is also close to that for maximum specific impulse. In the plot of equilibrium mole fraction of the species considered in these calculations (Figure 6-b) a maximum for both water and nitrogen is found near this same mixture ratio value. More importantly, it is seen that at low O/F values the principle species are nitrogen and hydrogen. This contrasts with the experimental findings presented in Part III which, for low O/F, show ammonia to be a significant species (see Section 4.3.3 of this report). Ammonia is not present at all in the theoretical compositions and this is because of the high temperature of reaction found even for O/F = 0.5. This is a direct consequence of the exothermic nature of hydrazine decomposition (note the enthalpy curve in Figure 6-a).

On the oxidizer rich end of the spectrum a significant fraction of free oxygen is found, a characteristic which, this time, <u>is</u> borne out by the experimental compositions in oxidizer rich regions.

These findings suggested that a study of the hydrazine decomposition by itself might provide some illumination on the type of experimental data that was obtained since the equilibrium chamber results are

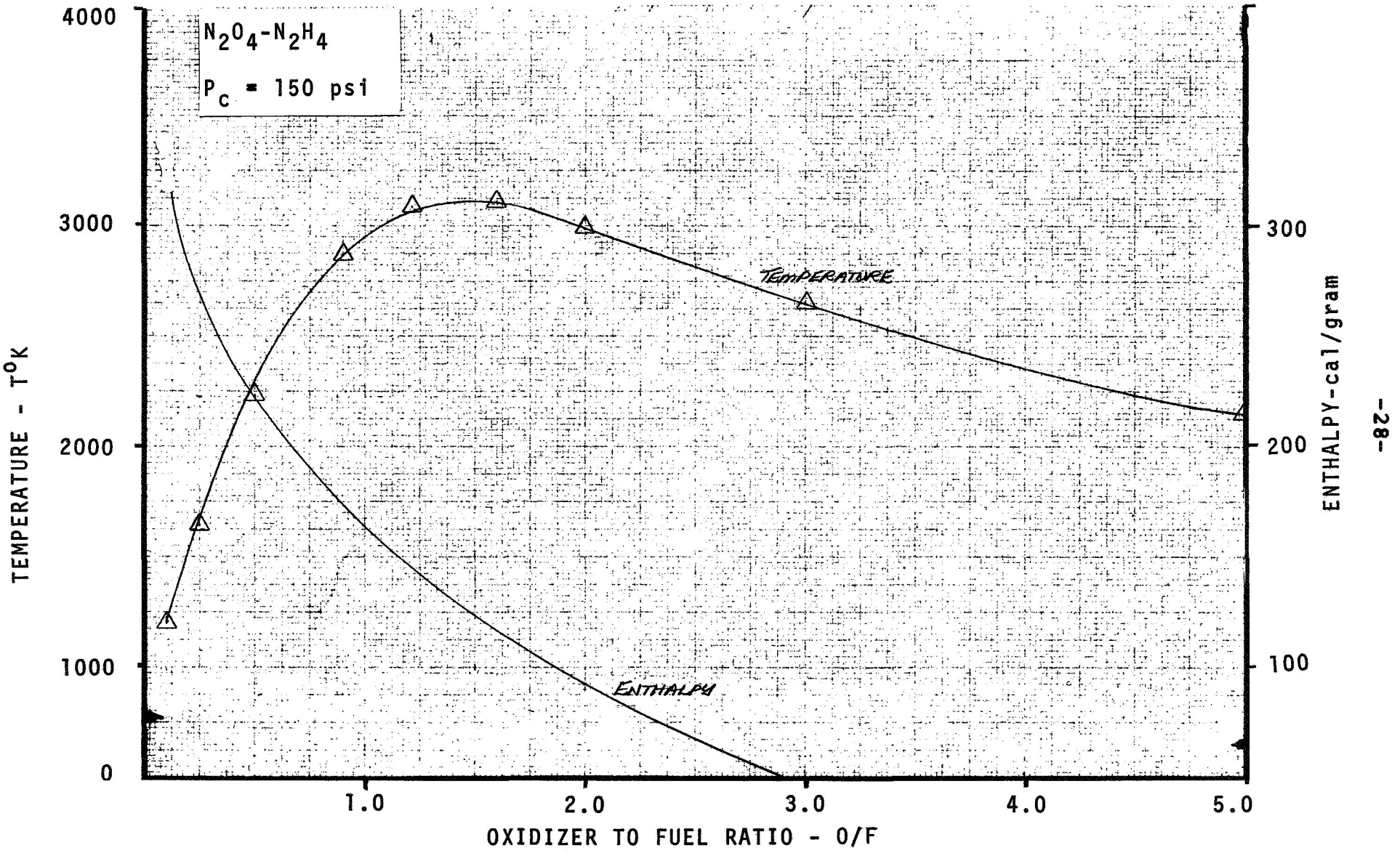

Figure 6. Chamber Equilibrium Properties
a. Temperature and Enthalpy

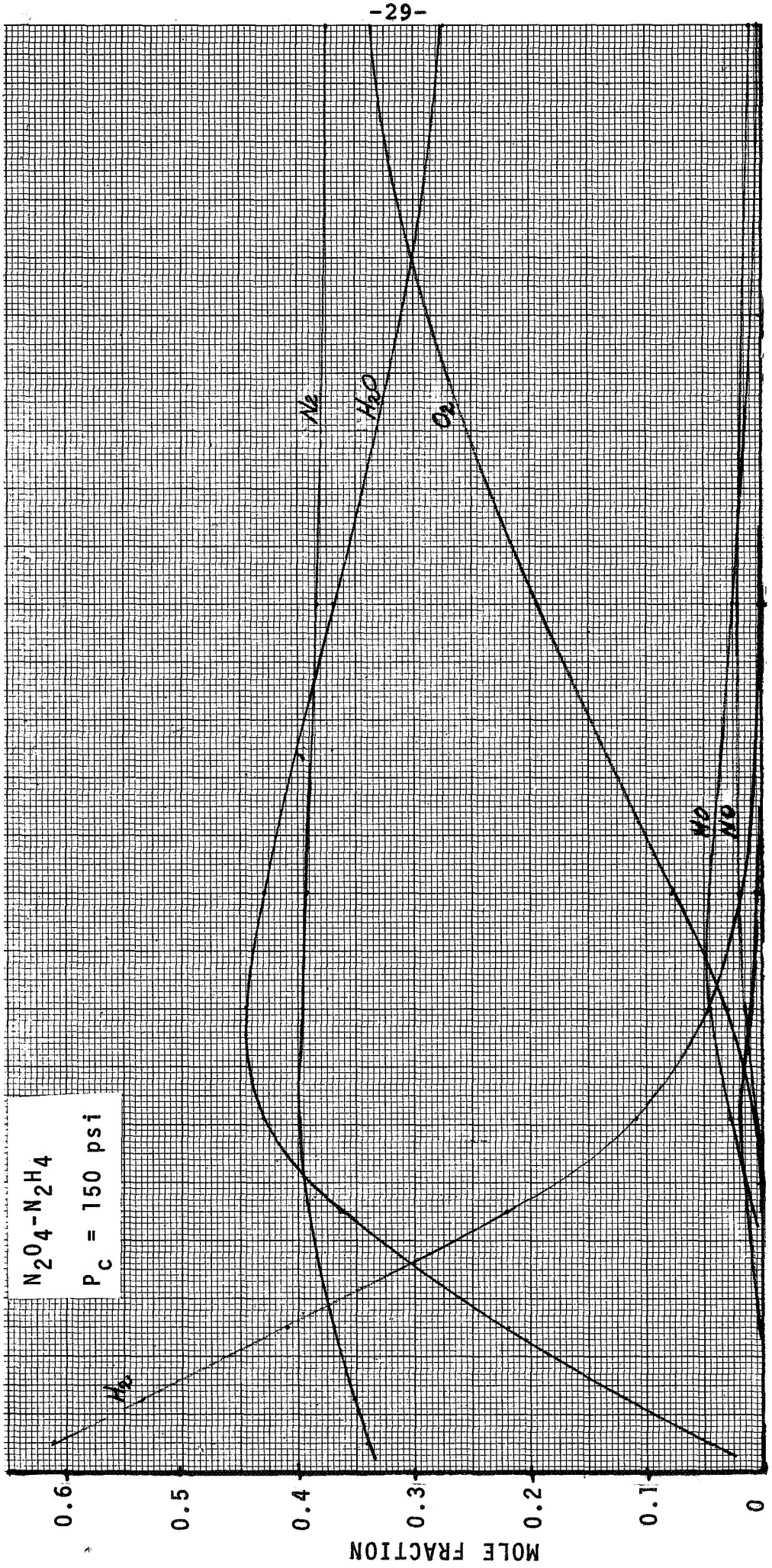

Figure 6. Concluded
b. Specie Composition

at such great odds with it. Consequently such a study was performed and is described in the following section.

4.1.2 Fuel Decomposition

The results for equilibrium fuel (hydrazine) composition were obtained as a function of temperature (again using the ACE program). The temperature range considered was between 300°K and 3000°K. These equilibrium results can be viewed as the decomposition of hydrazine to the vapor products presented when both are at the same temperature. Hydrazine decomposition is temperature dependent both as to products and to rate. At room temperature the decomposition rate is barely detectable and the products are known to be ammonia and nitrogen[6]. The decomposition rate increases gradually with temperature at first then becomes rapid near 430 °K and explosive above that[6]. Of course it is well known that in the presence of a catalyst, hydrazine is a respectable monopropellant; achieving flame temperatures on the order of 1000°K as shown in Figure 6-a.

The decomposition results are presented in Figure 7 where it is seen that for temperatures in excess of 800°K, hydrazine decomposes into nitrogen and hydrogen as per the previous calculations. At the highest temperatures some dissociation of hydrogen into hydrogen atoms is evident. Below the 800°K temperature ammonia becomes the predominant specie (almost 80 percent at room temperature) which, interestingly enough, is in agreement with the observation of Reference 6 and the experimental data of this program.

It is also interesting to contrast the behavior of hydrazine with that of the oxidizer--nitrogen tetroxide. Such a study is presented in the following subsection.

4.1.3 Oxidizer Decomposition

In contrast to the highly temperature dependent decomposition of hydrazine, nitrogen tetroxide decomposes into the same species independent of temperature although the rate of decomposition is still strongly temperature dependent. Figure 8 shows that for the temperature range considered, N_2O_4 decomposes into oxygen and nitrogen.

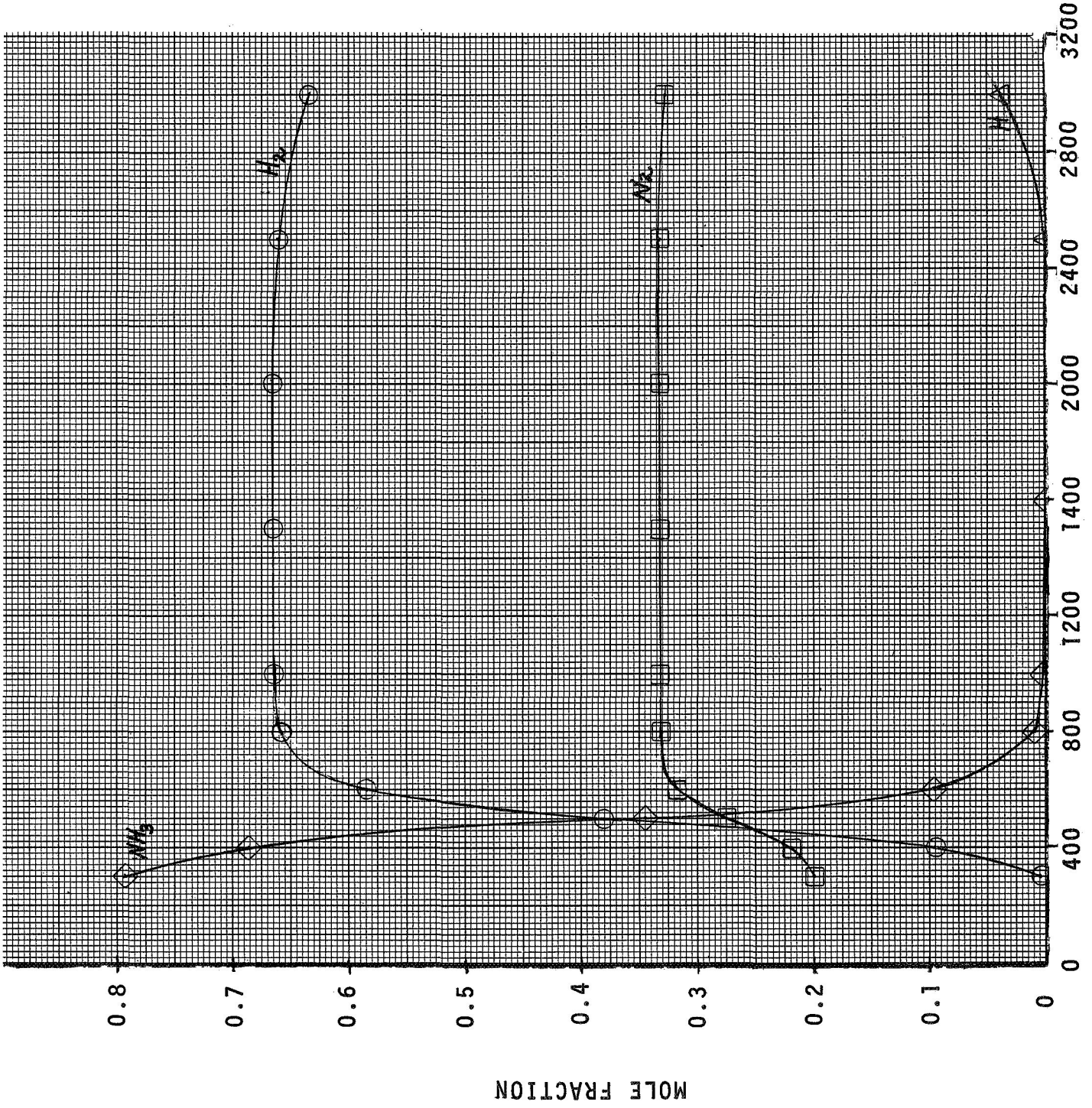

Figure 7. Equilibrium Products of Hydrazine Decomposition Versus Equilibrium Temperature

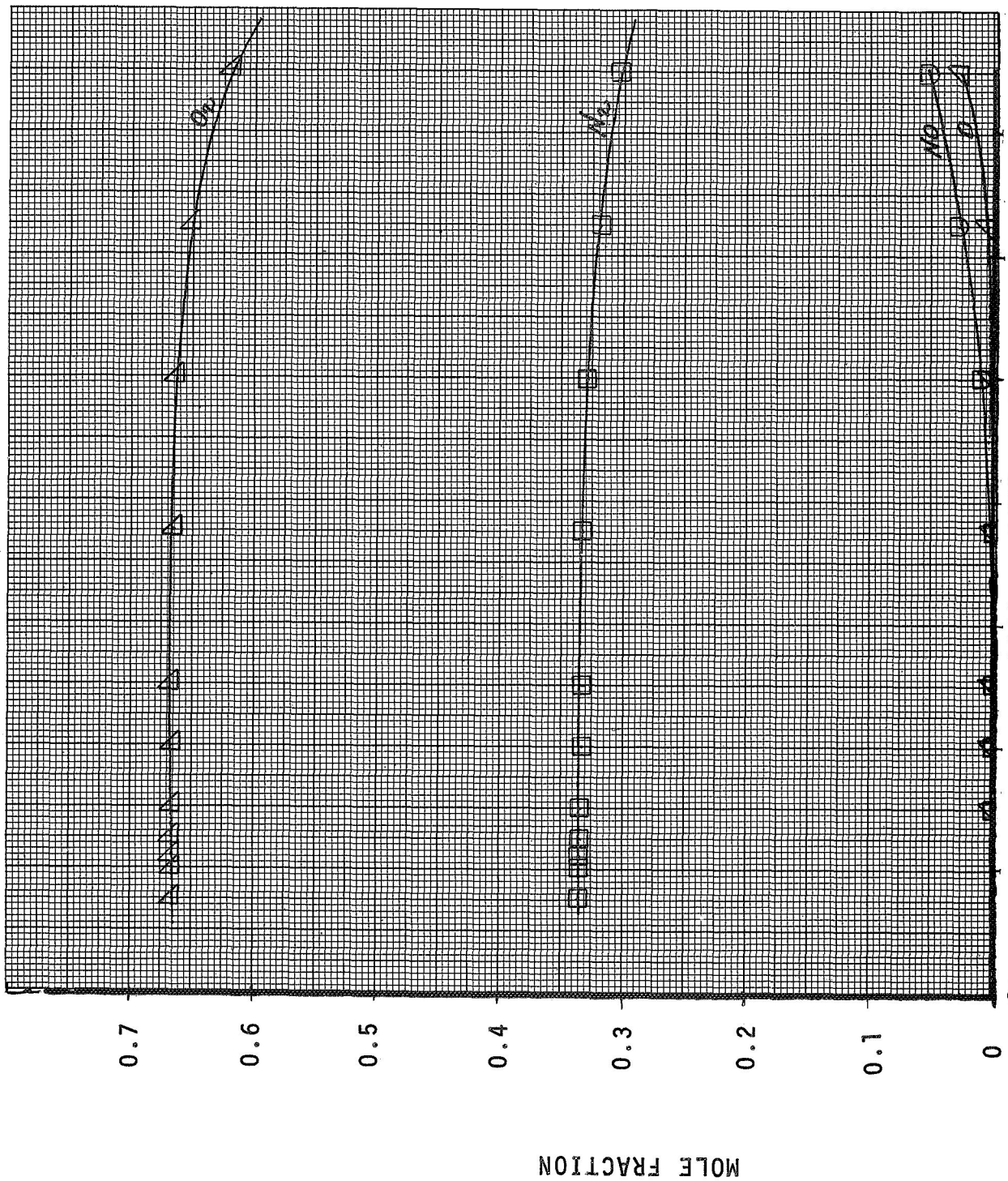

Figure 8. Equilibrium Products of Nitrogen Tetroxide Decomposition Versus Equilibrium Temperature

Again at the highest temperatures dissociation events occur and atomic oxygen and NO are found. In the oxidizer rich regions of the boundary flow small amounts of NO were detected by the mass spectrometer (see Part III).

These results prompted a study of similar temperature dependent equilibrium solutions--this time for a mixture of oxidizer and fuel characteristic of the bulk of the experimental data. The results of this study are presented next.

4.1.4 Temperature Dependent Oxidizer-Fuel Reaction Products (O/F=0.5)

While the hydrazine decomposition study showed that it was possible to theoretically demonstrate the existance of ammonia present in the boundary flow (if the reaction occurs at low temperature), the experimental data also indicate that a pure fuel situation does not exist in the boundary flow principally because of the significant quantity of water that is found even for the lowest value of local O/F. In order to improve upon the physical representation then, a mixture of oxidizer and fuel (O/F = 0.5) was chosen for further study (such a mixture ratio is representative of most of the fuel rich boundary flow data--see Figure 3). The equilibrium reaction products for such a mixture was predicted by the ACE program as a function of temperature and the results are presented in Figure 9. The most significant finding of this calculation is the low percentage of ammonia relative to the experimental data even for the lowest temperatures considered. At 450 K which is typical of the chamber wall temperatures during the sampling event, only 2 percent ammonia is predicted to be present.

Several conclusions about the physical state existing in the boundary flow can be drawn from these theoretical results in the light of the experimental data characteristics. First it is obvious that the fuel which is presumably sprayed onto the chamber walls is not reacting violently (i.e., as a monopropellant) even though the chamber wall temperature is quite close to the temperature at which hydrazine decomposition occurs rapidly. However the experimental data

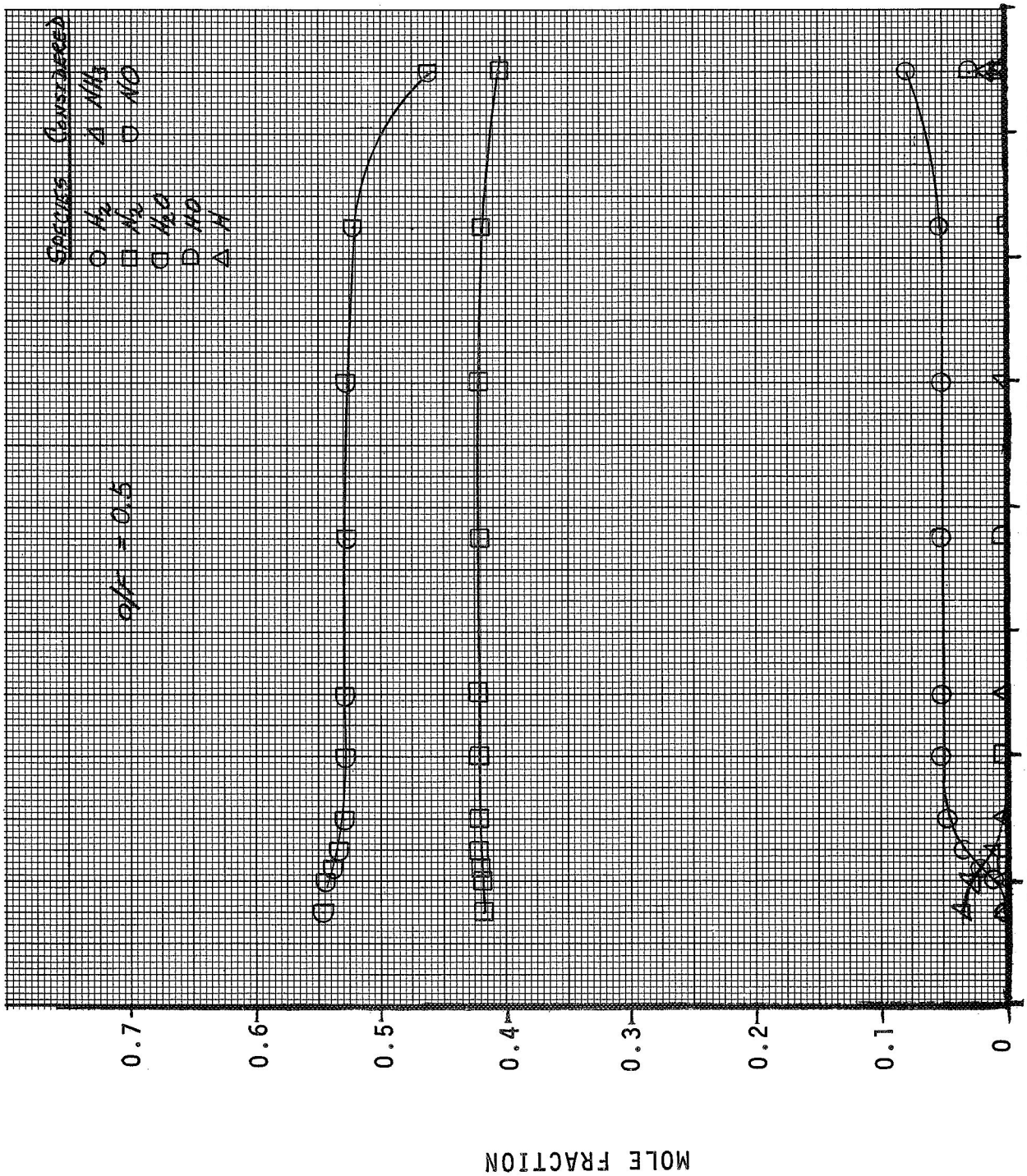

Figure 9. Temperature Dependent Equilibrium Products of Reaction of N_2H_4/N_2O_4

do show that the fuel is decomposing to ammonia and nitrogen.* Secondly, the water which is detected experimentally probably comes from further out in the boundary layer (i.e., a non-homogeneous boundary flow) and is characteristic of a mixture--i.e., the sample is drawn from hotter portions of the boundary flow away from the wall as well as the cooler wall portion). As shown by Figure 9, high water concentrations exist in such regions. The situation is compounded by unequal diffusion effects although these probably are of second order to the temperature and sample mixing effects.** These effects are treated further in Section 4.3, where, to explore the validity of the foregoing interpretation of the boundary physics, a theoretical boundary layer analysis was conducted using an existing turbulent boundary layer code.

4.2 EQUILIBRIUM GRAM-ATOM ANALYSIS

A study was made of the composition data from a randomly selected data set from the approximately 200 samples available from the test program. In this study the theoretical equilibrium species composition predicted by the ACE program was compared to the experimental species

*The experimental results are not free from ambiguity in this regard. As discussed in Part IV there exists the possibility that the ammonia determinations by the mass spectrometer may be a characteristic of the spectrometer itself (at elevated sample temperatures). This possibility is reinforced by the limited gas chromatography analysis which were performed in which little or no ammonia was detected but where an unknown component supposedly mixture of water, hydrazine and perhaps ammonia or nitric acid was obtained. Such a highly polar mixture is impossible to resolve on the gas chromatograph with current technology (or with other methods because water is present) so that definitive resolution of the "mixture" was not obtained. As a consequence in this program reliance had to be placed upon the mass spectrometer results where no composition presumptions of this kind needed to be made.

**As will be noted later there is some doubt that all the water present in the boundary flow was obtained in the sampling process. Increased water would of course make the experimental findings more like that of Figure 9 although the ammonia concentrations would still be significantly higher than the theoretical level.

composition. The predictions were based on the experimental atom-grams of the elements obtained from the experimental species data. To make the situation clear, the analysis procedure can be diagramed as follows:

a. Experimental species mole fraction - $\chi_i(e)$ - determined by mass spectrometer for a given sample

b. Element gram atom fraction - α_i - calculated from experimental $\chi_i(e)$

c. Theoretical specie mole fraction - $\chi_i(t)$ - calculated by ACE program as a function of temperature, T, from the α_i

For example, a sample containing 50 percent H_2O and 50 percent N_2 would have 40 percent atom-gram fraction of H and N and a 20 percent atom-gram fraction of atomic oxygen, O. The ACE program determines a theoretical equilibrium composition from these atom-gram fractions which is temperature dependent. For example, the foregoing atom-gram data would produce H_2O and N_2 at high temperatures.

For a complex mixture of species such as found in the experimental data where free hydrogen and oxygen are found with water and ammonia, it is not a priori evident that a unique temperature exists which will yield the measured specie composition. Several factors could cause such disparity: 1) invalid spectrometer data; 2) samples obtained from boundary flow gases which are not in equilibrium; 3) samples obtained from a mixture of gases frozen at their local temperature in the boundary flow in the sampling process.

Surprisingly, in the vast majority of the samples which have been so analyzed a unique temperature is found where species agreement exists and this temperature is usually not greatly different from the measured wall temperature.

4.2.1 Comparison of Experiment and Theory

In this section the species mole fractions determined by the mass spectrometer for individual boundary flow samples are

compared with the equilibrium mole fraction obtained for consistent atomic fractions from the ACE program. These calculations were performed for all the sample bottles obtained from runs 16, 24, and 26. These runs were chosen to represent the fuel rich (run 16) and oxidizer rich (run 24) regions. Run 26 was used mostly for the exploration of the effect on the composition due to the level of pressure assumed in the calculations.

4.2.1.1 Fuel Rich Results

Examination of Figures 10-a through 10-f for the fuel rich condition discloses that a consistent temperature is found at which the theoretical temperaure dependent composition curves cross the experimental composition data simultaneously. Significantly, this "cross-over temperature" is only some 20 to 40°K greater than the wall temperature measured during the sampling process. In Figure 10-a for example, which displays the results for sample bottle 1 from run 16, the dramatic change in composition predicted theoretically can be seen. As indicated previously, the composition change is due to the decomposition of ammonia, NH_3. Besides NH_3, the other species present are: hydrogen, H_2, nitrogen, N_2, oxygen, O_2, and water. For this particular sample the oxygen was present only in vanishingly small amounts. The theoretical results are shown by the lines marked by the appropriate symbols. Proceeding from left to right, ammonia is found to be the principal species; nitrogen is present at about 30 percent and water at somewhat less than 10 percent. On the right, at higher temperature, the ammonia has vanished and the principal species is hydrogen; the other species being relatively constant. The experimental composition is represented by the short horizontal line appropriately designated. The intersection of the short horizontal (experimental) line with the corresponding theoretical curve is shown by an arrow. For this particular plot the arrows occur at 475°K ± 10 percent. Alternately, at 475°K the agreement between theoretical and experimental concentration is within 2 percent (of full scale).

It is interesting to note that the equilibrium composition for bottle 5 of run 16 was first computed with atomic gram atom data

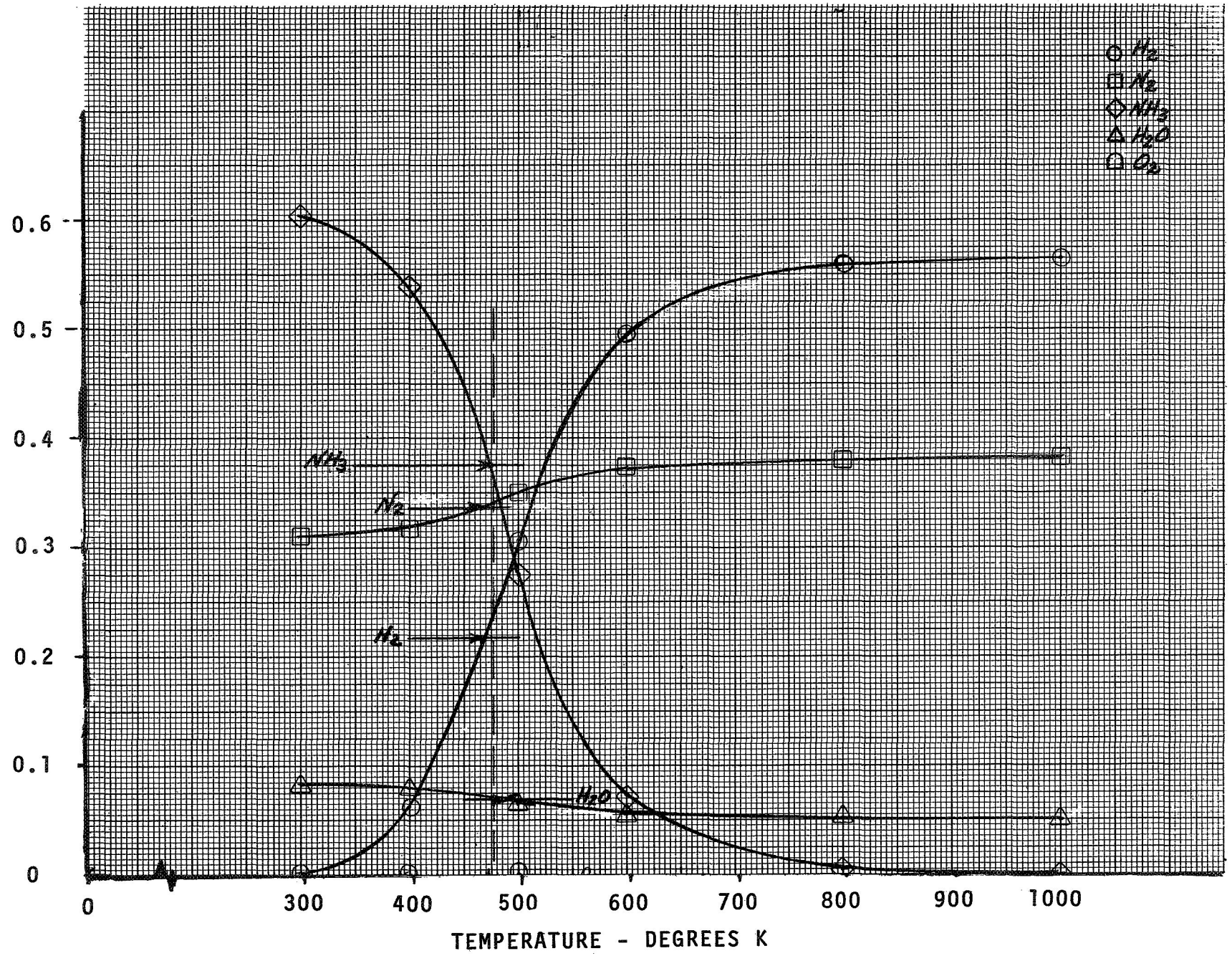

Figure 10. Fuel Rich Equilibrium Gram Atom Analysis
a. Run 16, Bottle 1

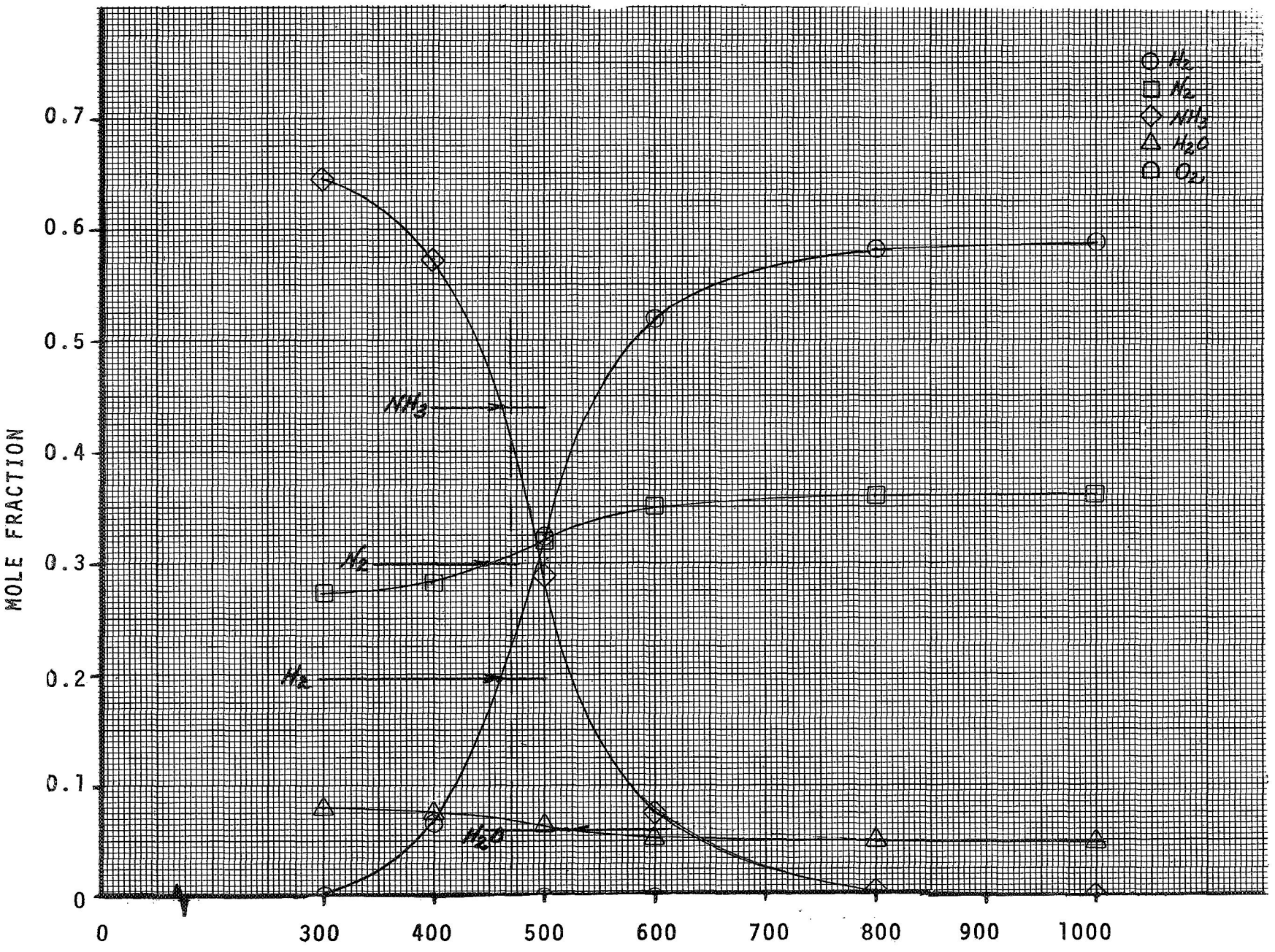

Figure 10. Continued

b. Run 16, Bottle 2

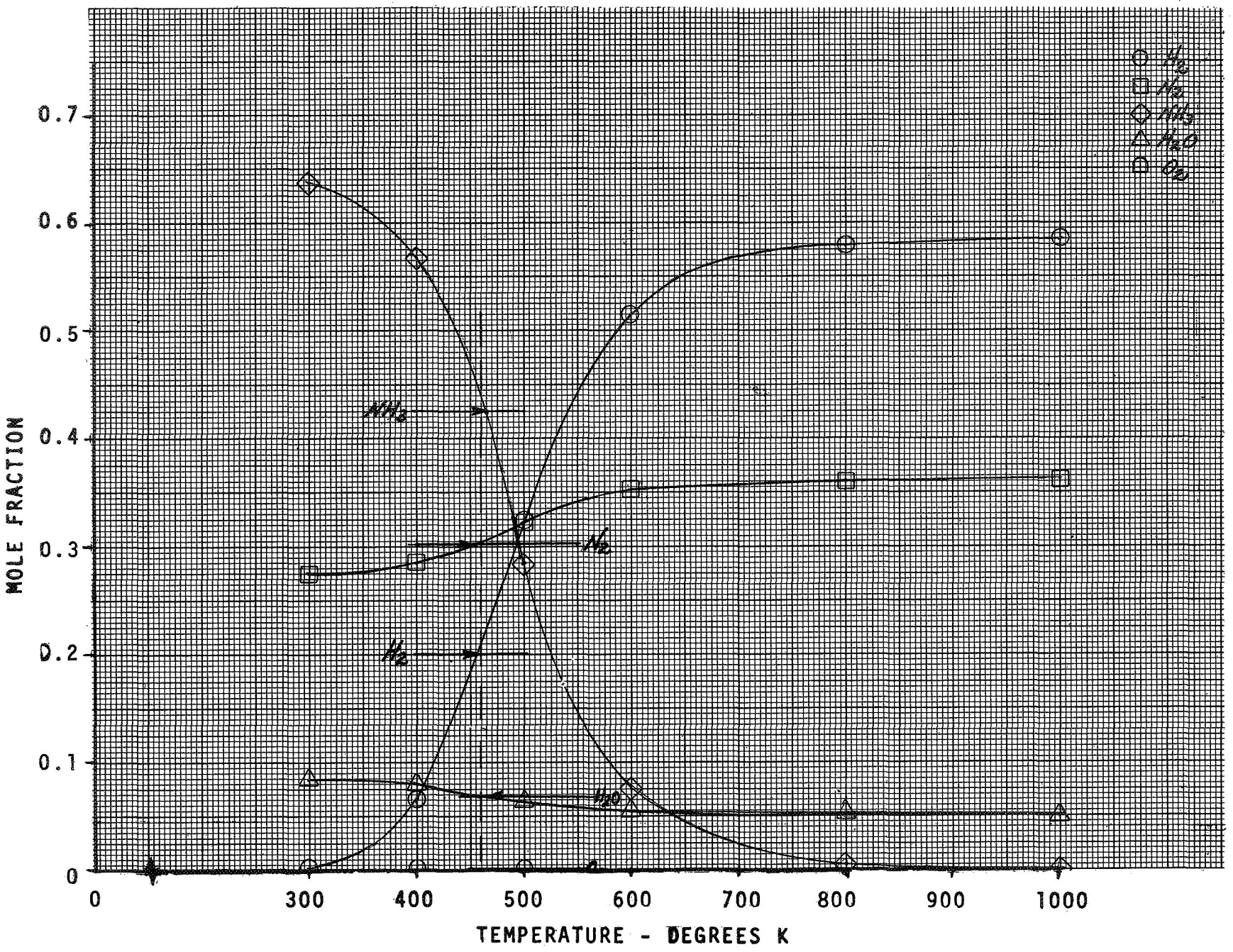

Figure 10. Continued
c. Run 16, Bottle 3

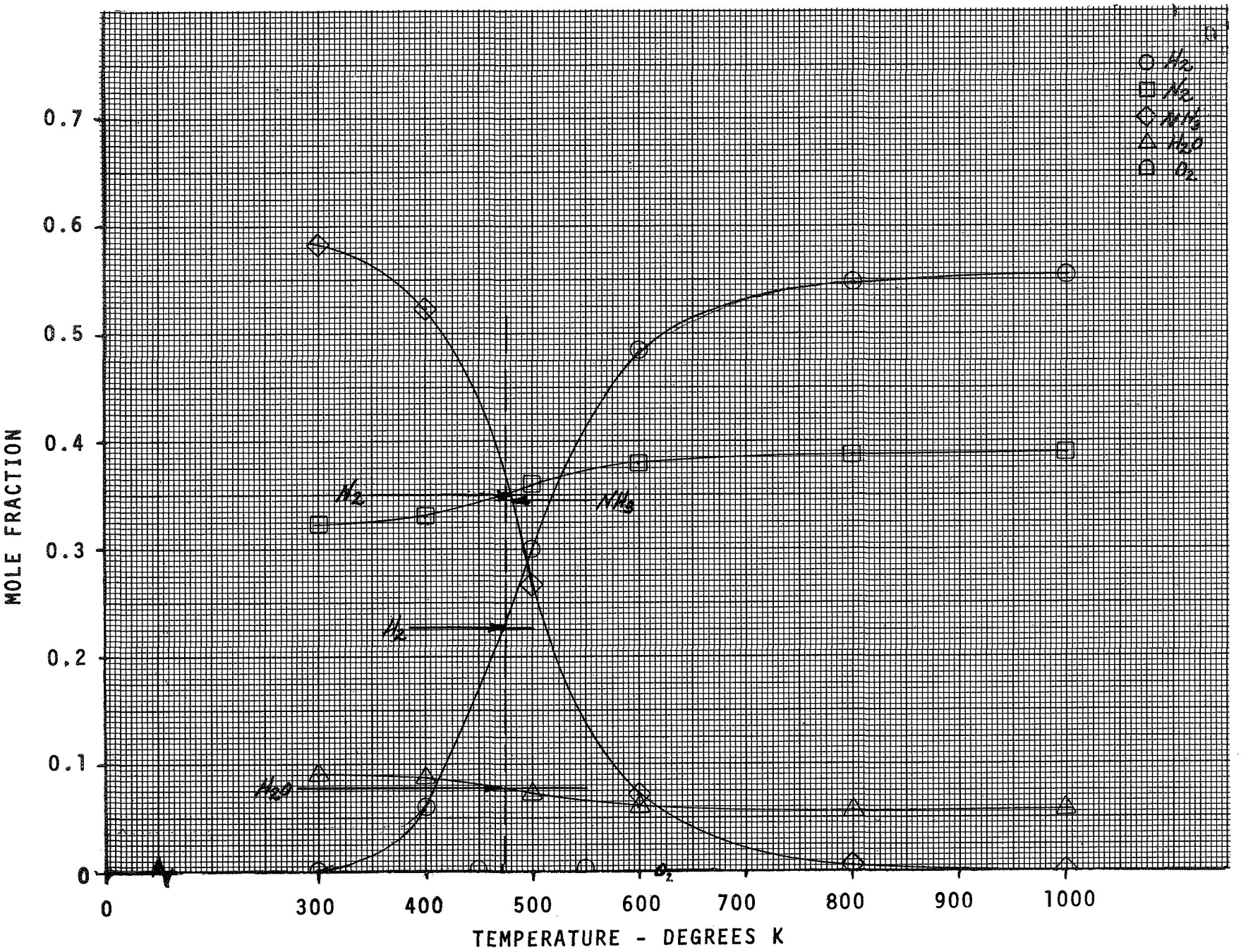

Figure 10. Continued
d. Run 16, Bottle 4

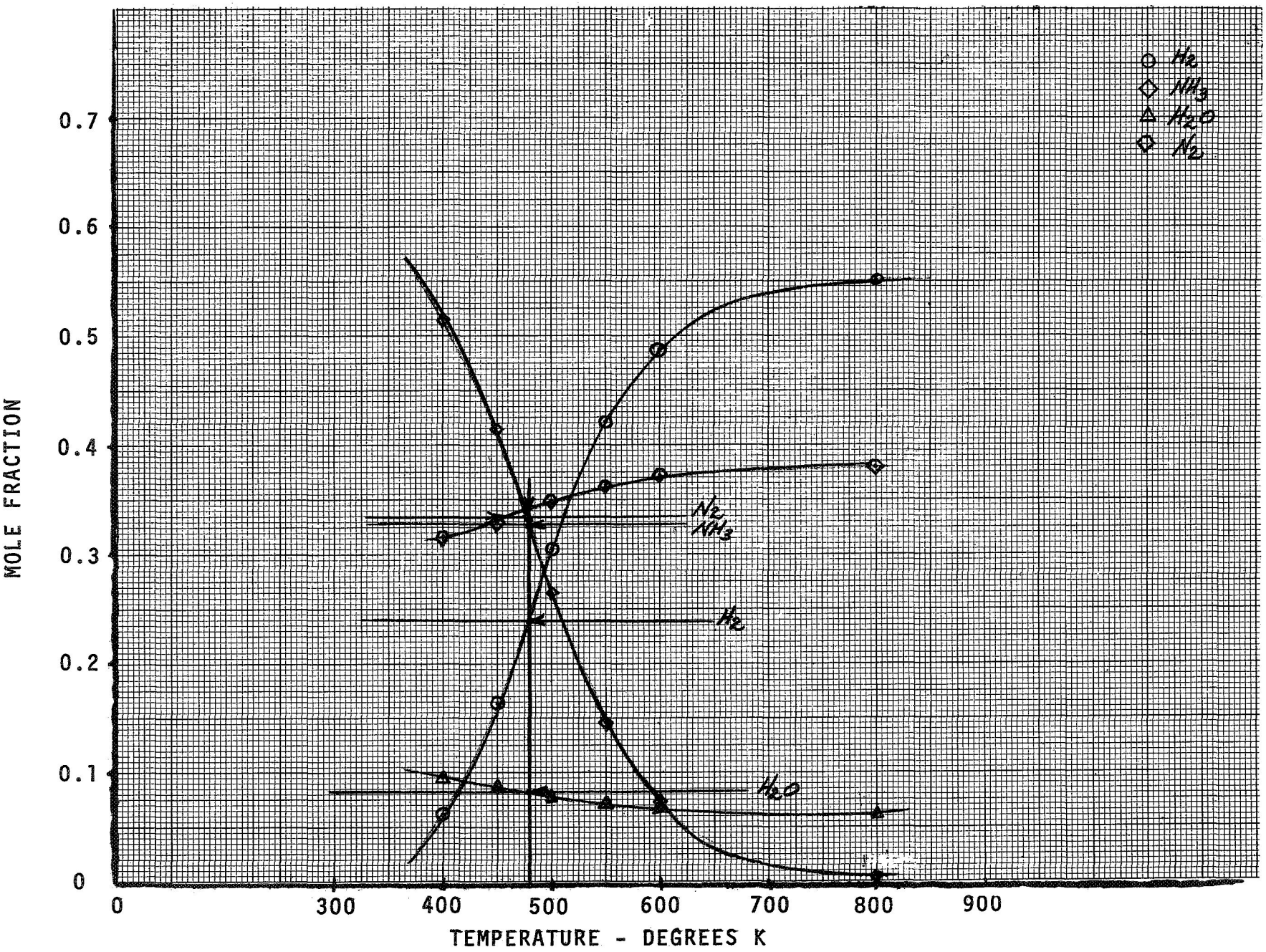

Figure 10, Continued

c. Run 16, Bottle 5

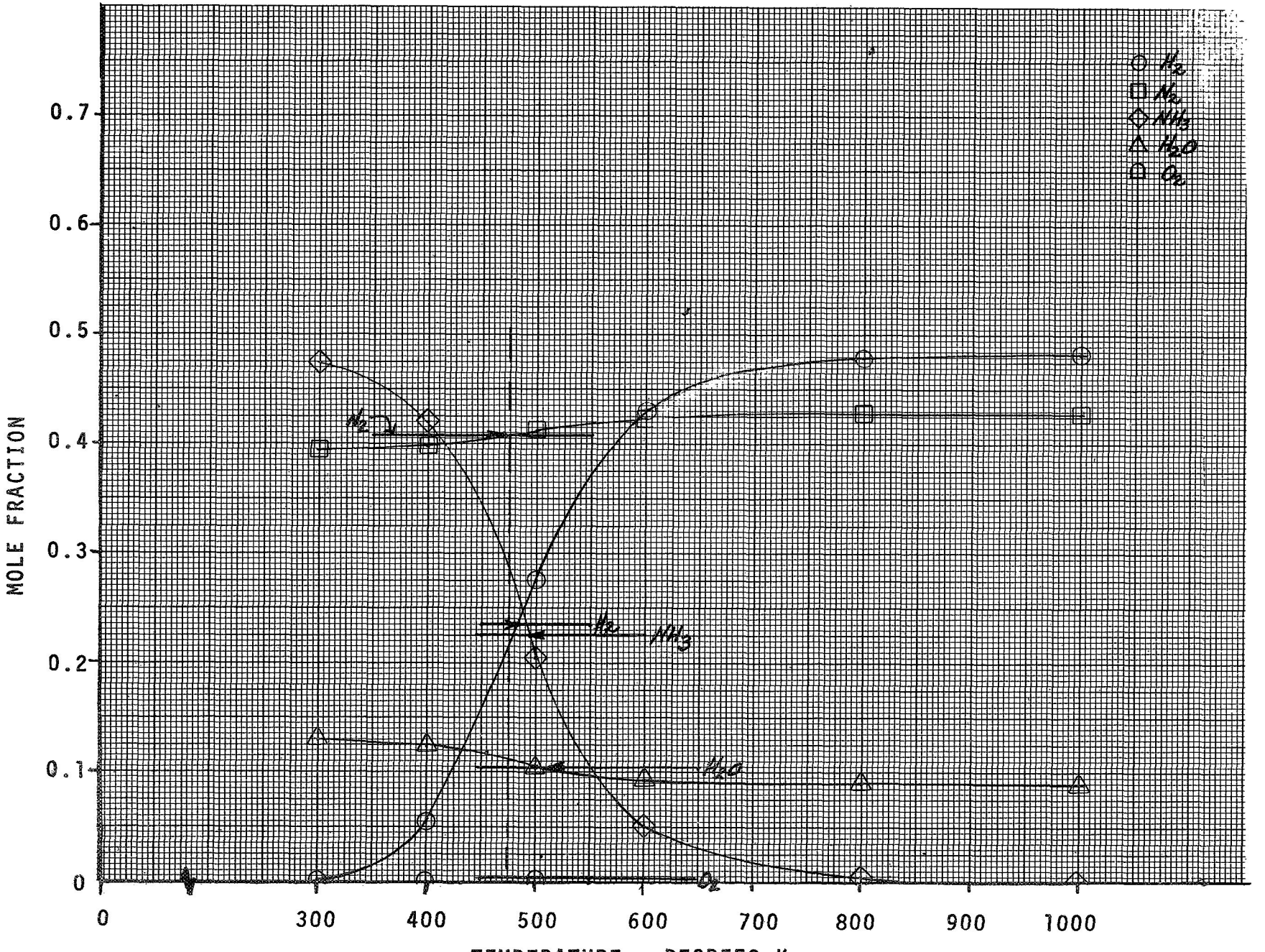

Figure 10. Concluded

f. Run 16, Bottle 6

from spurious mass spectrometer data (which was a consequence of an oscillograph trace reading error) and for such data a cross-over temperature was not obtained as shown in Figure 11. After suitable correction of the mass spectrometer data, an excellent cross-over was obtained (Figure 10-e). This suggests that such theoretical comparisons could be used as one of the criteria to use in checking the validity of the sample analysis results.

4.2.1.2 Oxidizer-Rich Results

While very good agreement is found for the fuel-rich data, the agreement is found to be not so consistently good for the oxidizer rich data (run 24). Good agreement is evident in the bottle 3 data of this series (presented in Figure 12-a through 12-f). Good agreement is also obtained from bottle 1 and 4 of run 26 (Figures 13-a and 13-b) which are also oxidizer rich--where a cross-over temperature of 1000°K and 550°K is found. In bottle 3 (Figure 12-c) a high temperature (near 600°K) is also found. In these cases it can be conjectured that the boundary layer sample is composed of gases frozen near the reaction temperature existing away from the wall. This could well be the situation if little or no fuel is being sprayed on the wall so that a liquid layer does not form.

There appears to be a definite trend in the run 24 data that the higher the concentration of O_2, the poorer the agreement between the experimental data and the theoretical equilibrium composition. Note also the constant theoretical composition over the temperature range considered.

Several possibilities for explaining the disparity between the experimental and theoretical data exist. First a high temperature dissociation of the water could occur which would produce H_2 and O_2 at the sacrifice of H_2O. Secondly, a nonequilibrium condition could exist at the lower temperature with the free hydrogen and oxygen resulting from the decomposition of the fuel and oxidizer respectively. The kinetics of the chemical processes involved in the description of the situation was not explored in this study. The ammonia evident in the experimental data in Figures 12-a, b, and c (bottles 1, 2, and 3, respectively) which cannot exist at high temperatures supports the

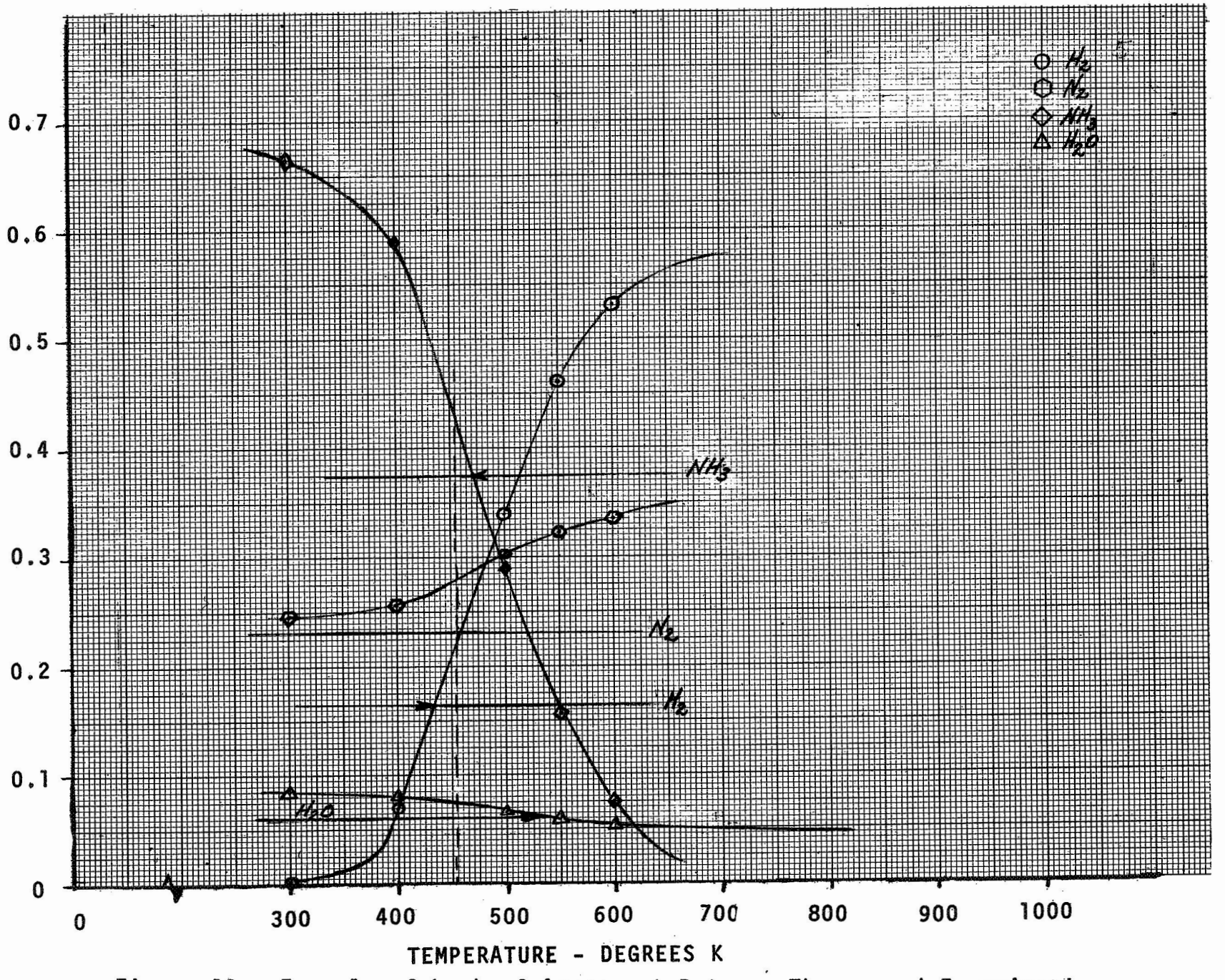

Figure 11. Example of Lack of Agreement Between Theory and Experiment Due to Improper Data Reduction

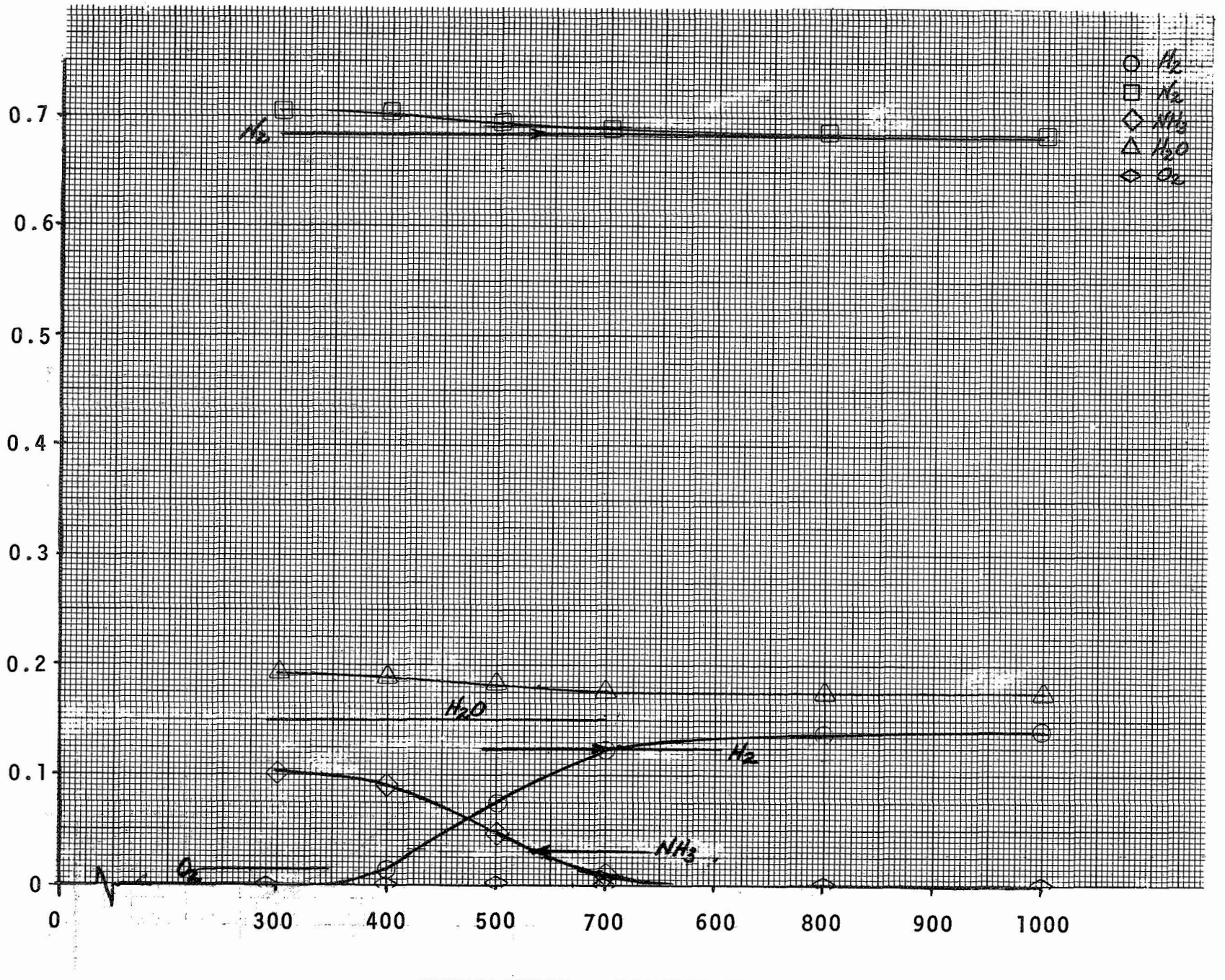

Figure 12. Oxidizer Rich Equilibrium Gram Atom Analysis

a. Run 24, Bottle 1

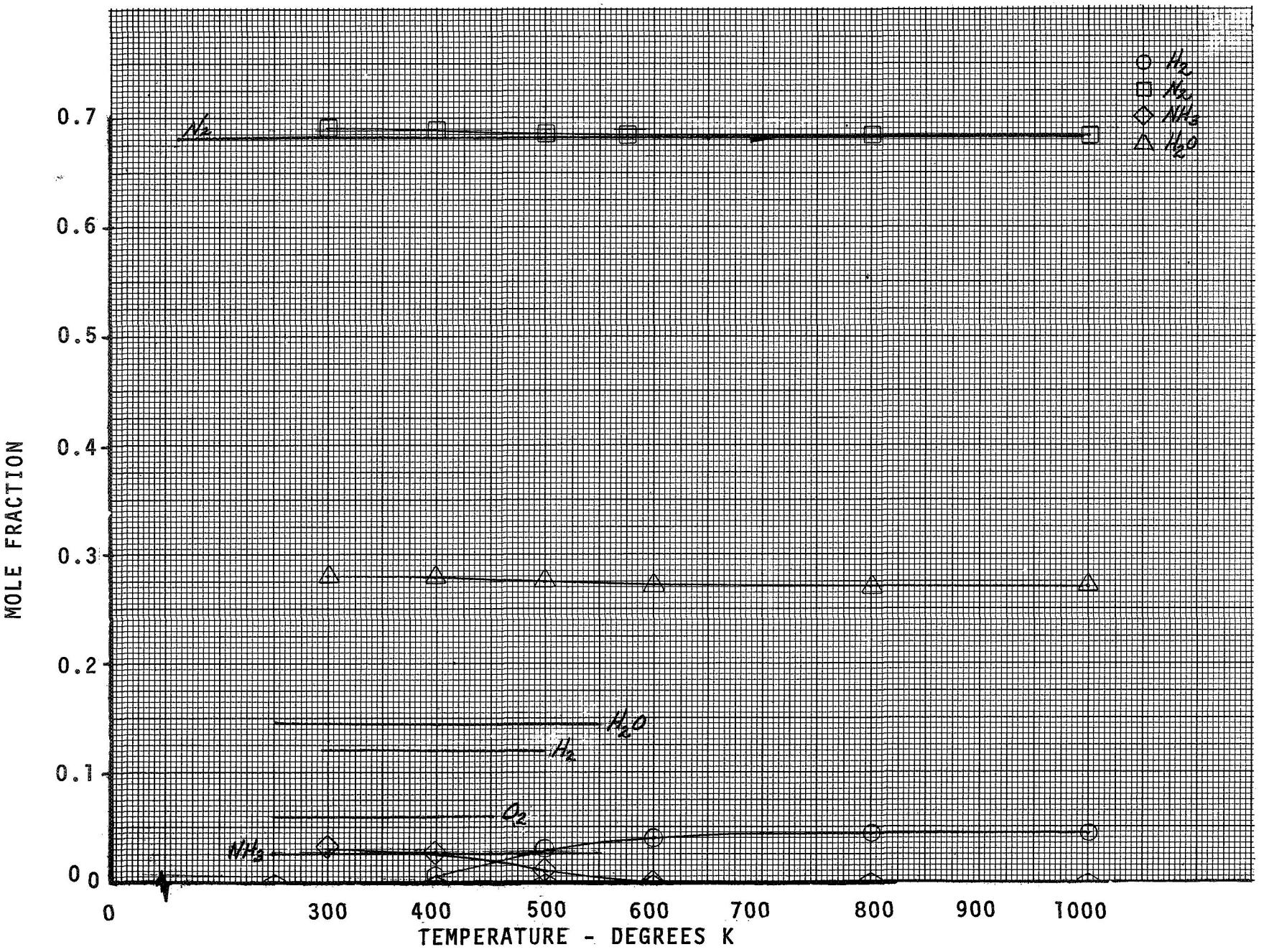

Figure 12. Continued

b. Run 24, Bottle 2

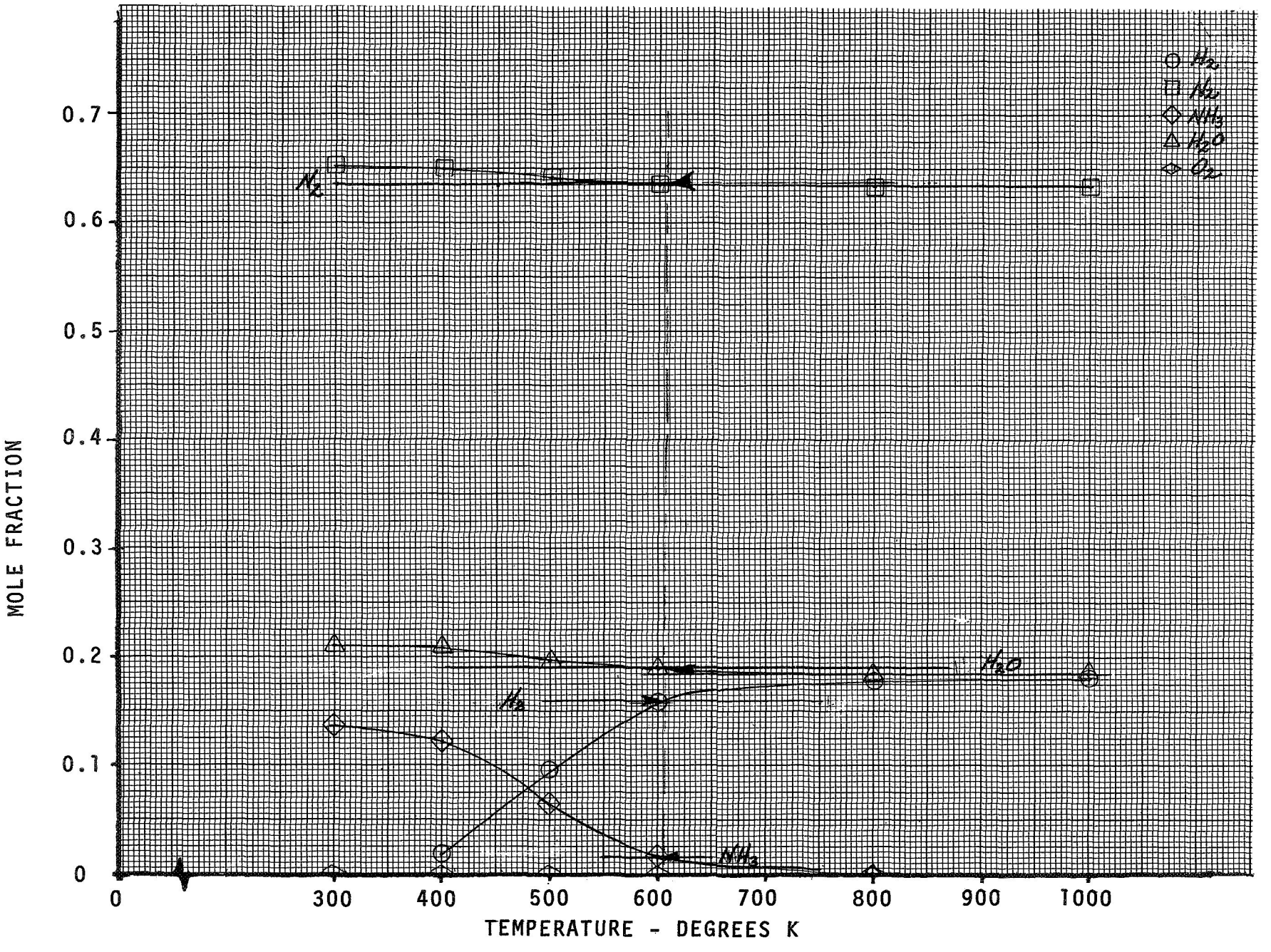

Figure 12. Continued

c. Run 24, Bottle 3

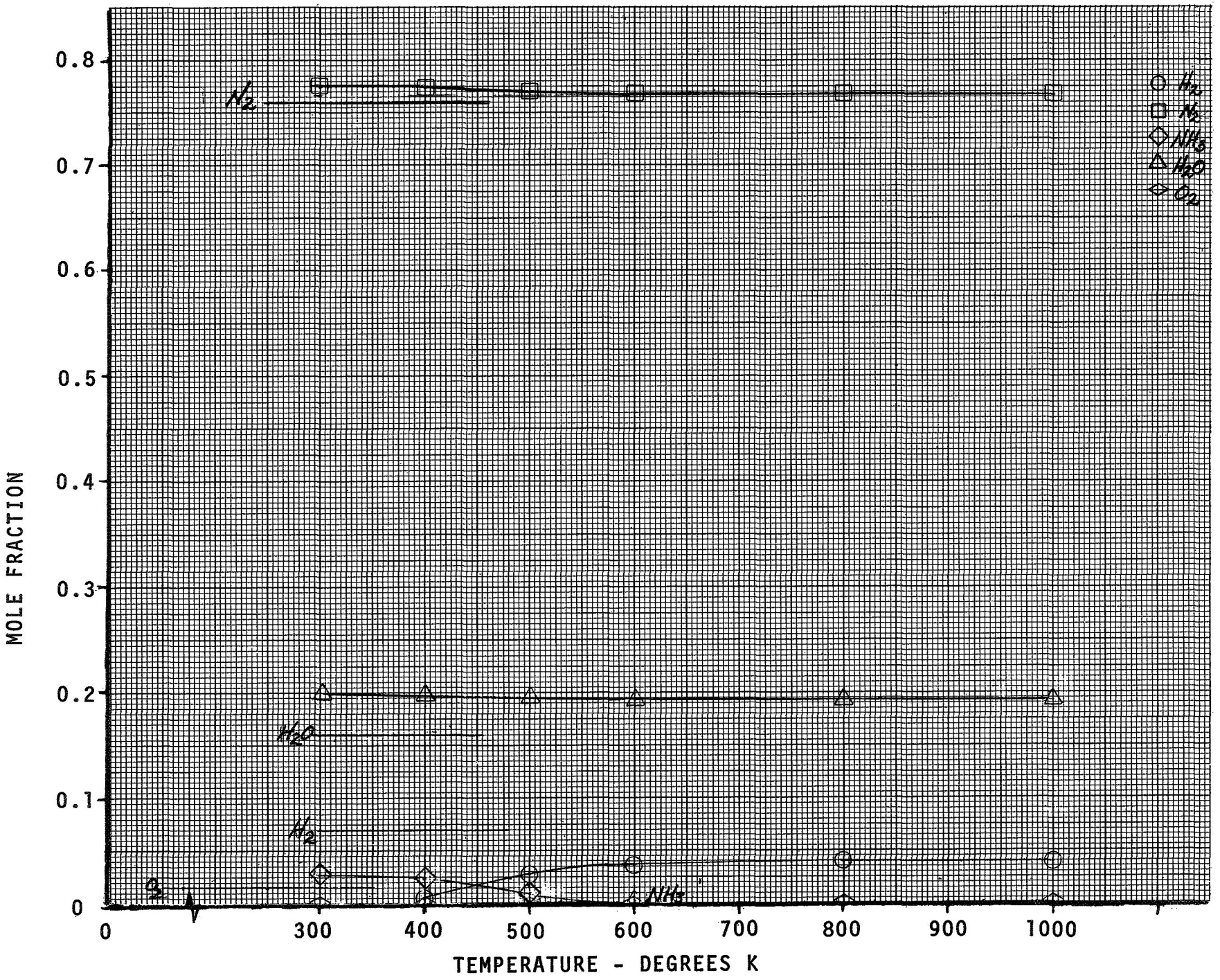

Figure 12. Continued

d. Run 24, Bottle 4

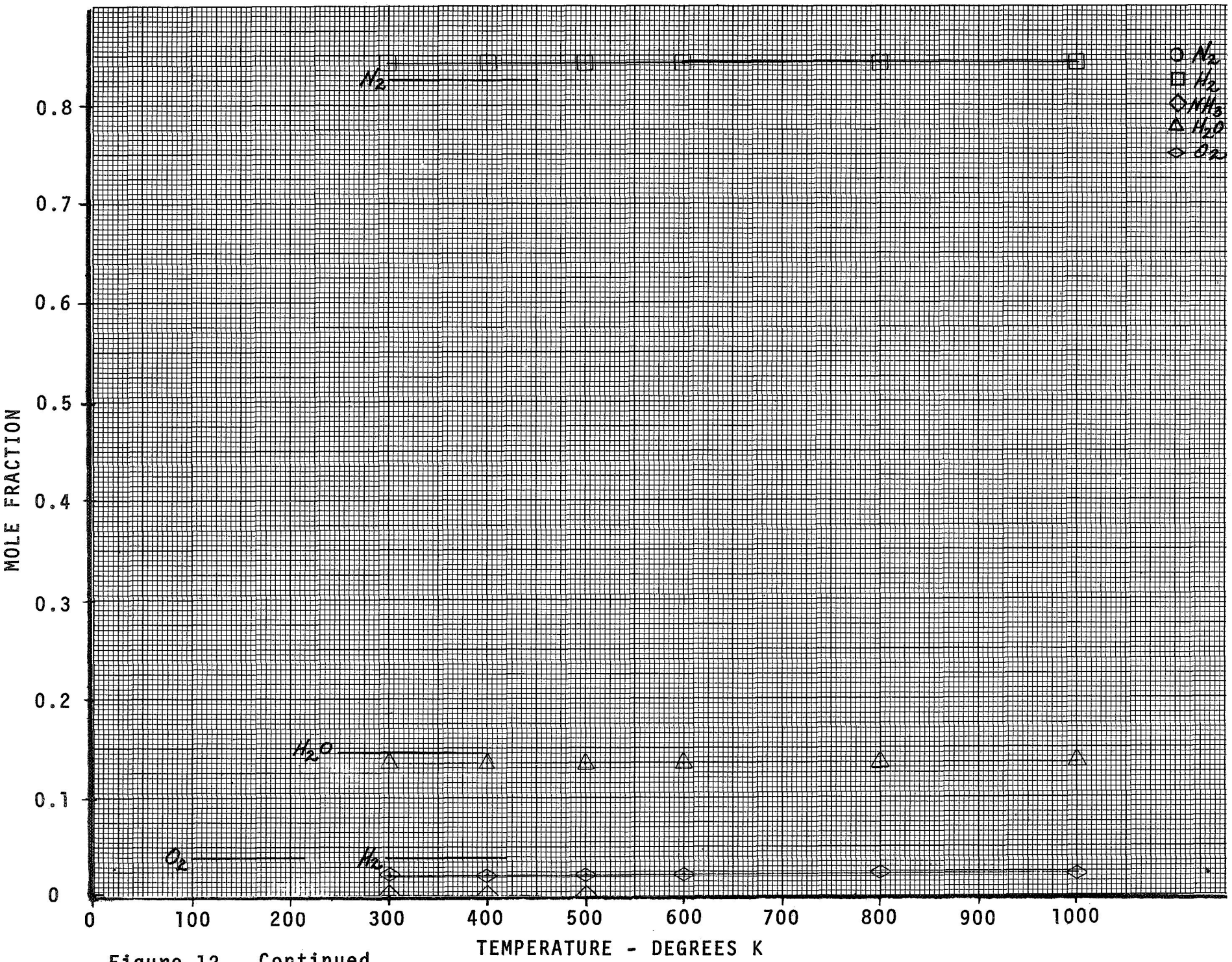

Figure 12. Continued

e. Run 24, Bottle 5

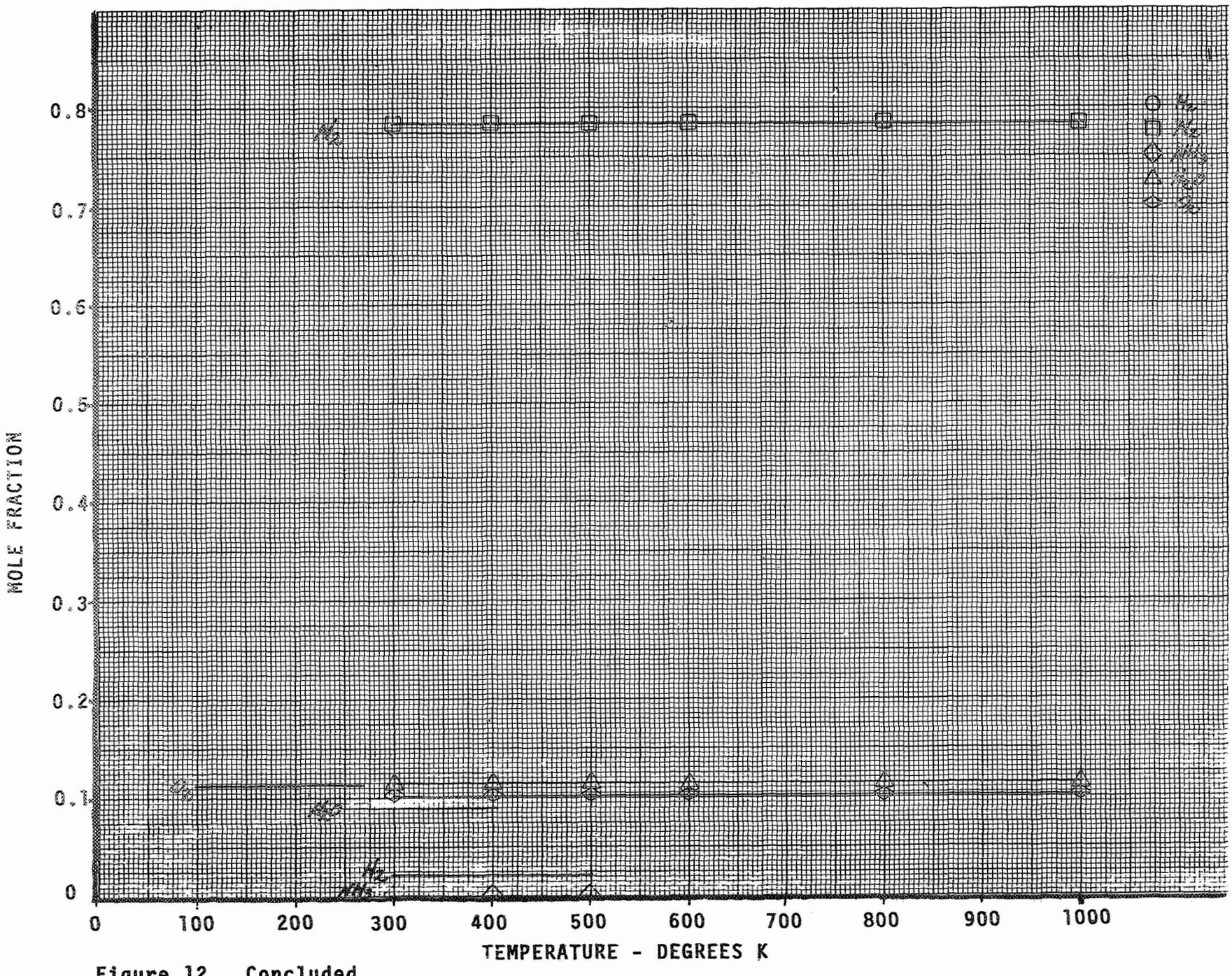

Figure 12. Concluded

f. Run 24, Bottle 6

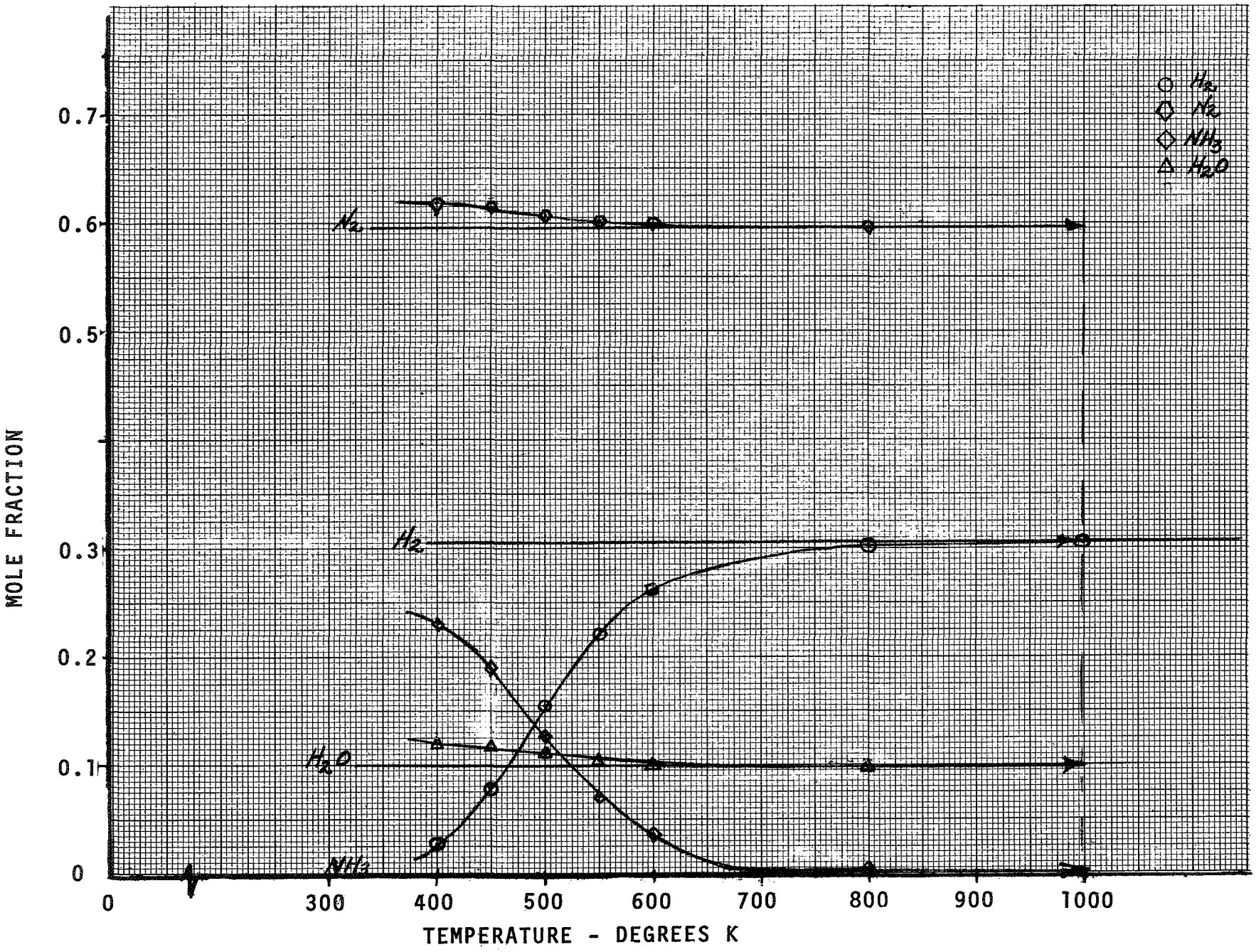

Figure 13. Oxidizer Rich Comparison Continued

a. Run 26, Bottle 1

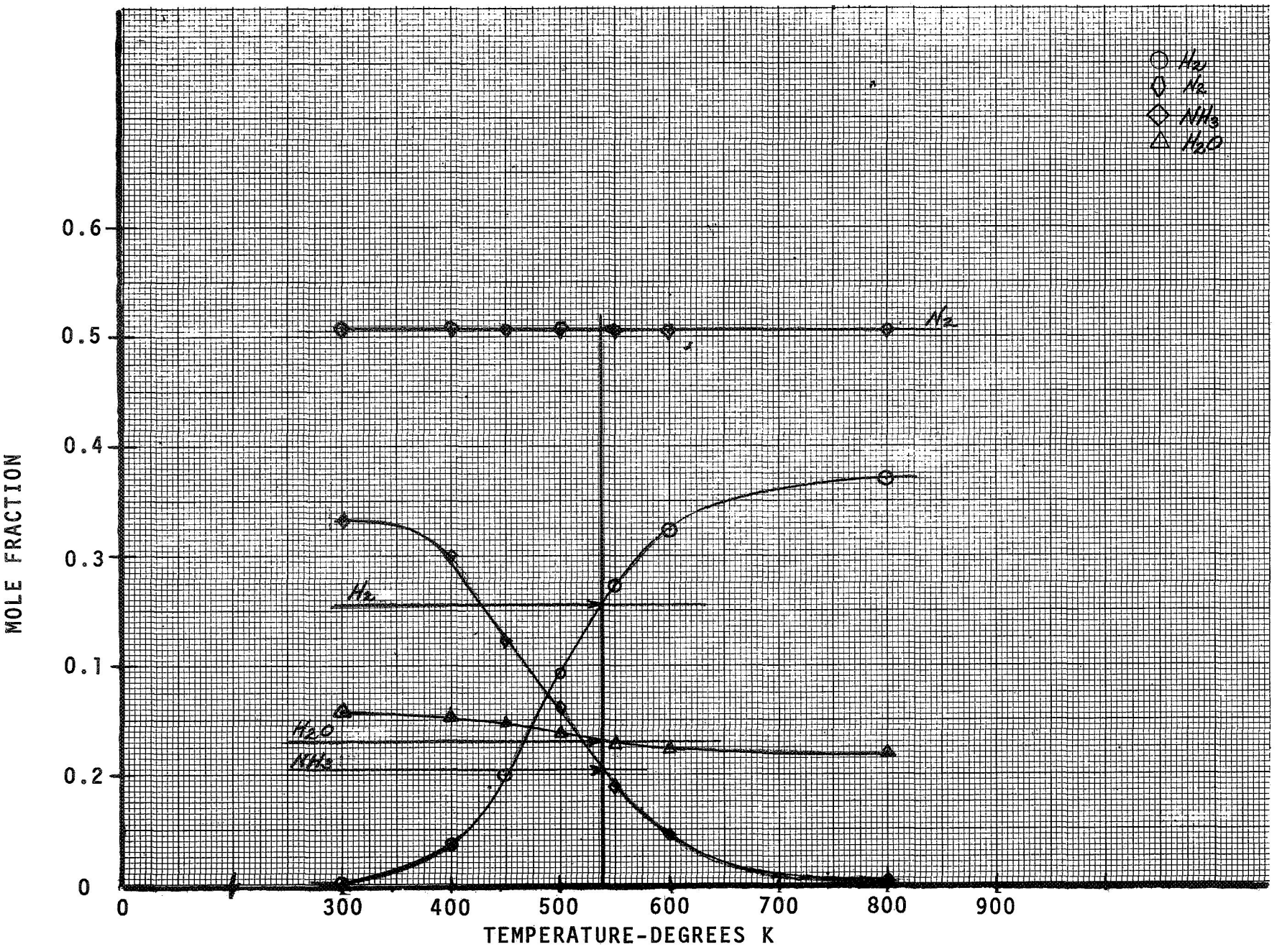

Figure 13. Concluded

b. Run 26, Bottle 4

latter view. A third possibility is that the water is decomposed in the mass spectrometer. Personal communications with physical chemists, mass spectroscopists, etc., and the fact that such results are limited to the oxidizer-rich region discourages this possibility.

4.2.2 Pressure Dependence

It is not a priori obvious which pressure to choose in performing the equilibrium calculations. Obviously the limiting pressures of chamber stagnation and absolute zero exist, but in the sampling and spectrometer analysis process the sample exists, at one time or another, over almost this entire range of pressure although admittedly only transiently for most of it. The pressures at which the sample is exposed for a significant period of time are the chamber pressure, the sample bottle pressure and the mass spectrometer pressure. Accordingly, these three pressures shown below (in atmospheres) were selected for comparison using the run 26, bottle 3 data:

10.9	-	chamber pressure
1.9	-	typical bottle pressure
0.00001	-	mass spectrometer leak chamber pressure

As shown in Figures 14-a and 14-b, the cross-overs are excellent for the two higher pressure cases--there not being too much difference between the two. However, for the 1.9 case, the cross-over temperature is 440^{0}K which is a little lower than the mean temperature of the laminar portion of the boundary layer (which is quite conservative based on the results of the next section) which must be above the measured wall temperature of 420^{0}K. Of the two, the higher pressure condition seems the more reasonable condition to choose. For the lowest pressure (Figure 14-c) no cross-over temperature in the range considered is evident (which is fairly conclusive evidence that the composition was frozen at the higher pressure during the sampling process).

4.2.3 Curve Fit Errors

At the conclusion of this phase of the analytical effort, it was ascertained that the specific heat curve fits for the species data

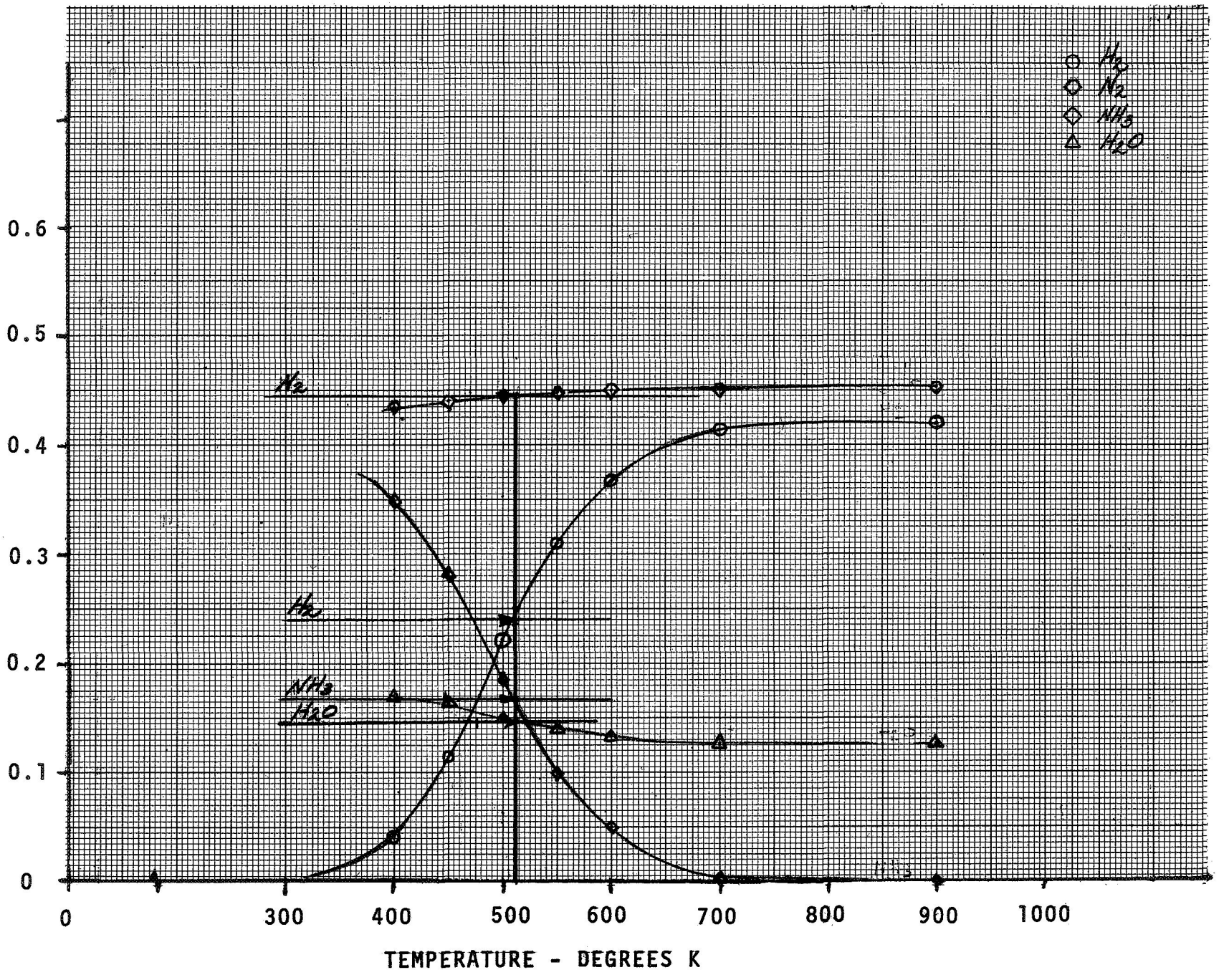

Figure 14. Effect of Pressure on Equilibrium Gram Atom Comparison

a. Pressure = 10.9 Atmospheres

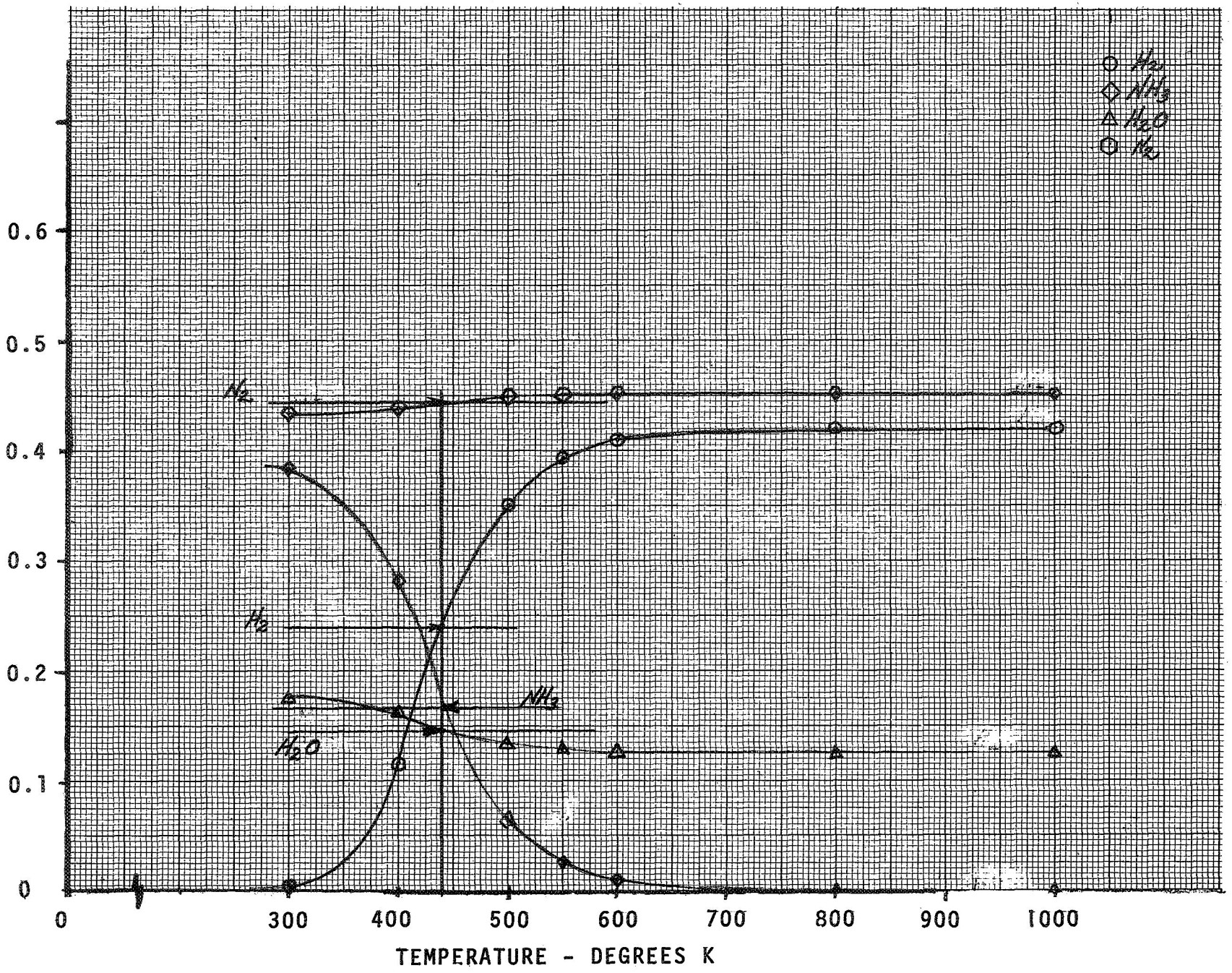

Figure 14. Continued

b. Pressure = 1.9 Atmospheres

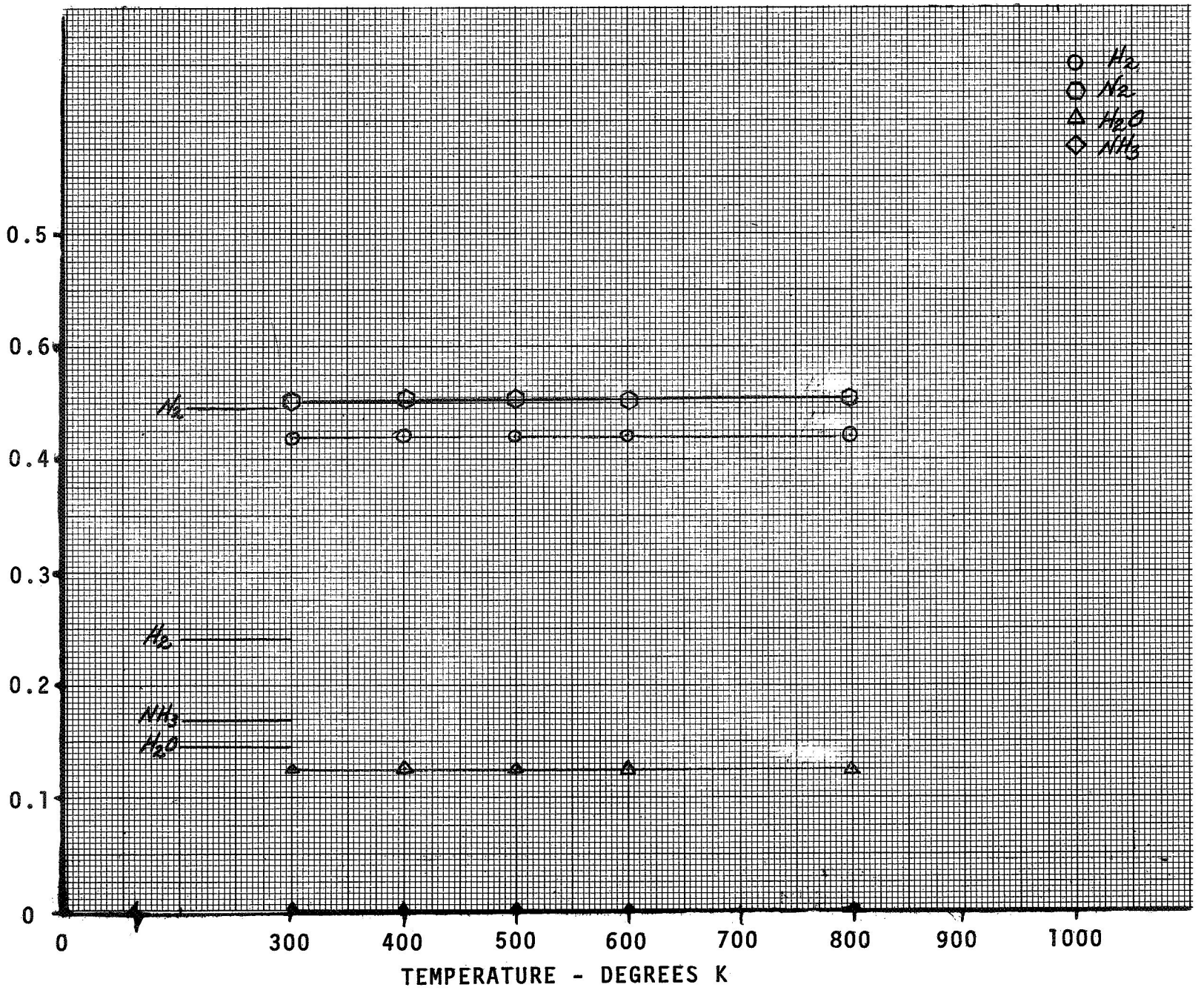

Figure 14. Concluded

c. Pressure = $1 \cdot 10^{-5}$ Atmospheres

(from JANAF) used in the ACE program were not as good as one might want at the lower temperatures. The effect of these errors on the results was not explored but they are believed to be small. The equilibrium data presented up to this point must therefore be regarded with some suspicion at the lowest temperatures as far as absolute level of accuracy is concerned.

New data (i.e., curve fits) were created for the species of interest (H_2O, NH_3, N_2, H_2, O_2) in the range 300°K to 4000°K for the boundary layer studies described in the next section.

4.3 BOUNDARY LAYER STUDY

One of the more important theoretical studies performed was the application of the newly developed turbulent boundary layer program BLIMP) to the study of the complex flow situation in the chamber. It is to be recognized that this study was exploratory in nature. Besides demonstrating the technique, the study had as its goals the following:

a. The equilibrium composition determination in the boundary flow as a function of the dimension normal to the chamber wall.

b. The effect of unequal diffusion on the local composition

c. The prediction of the experimental sample composition by modeling the sampling process in the theoretical boundary flow.

Of these, the last was the most crude since the lack of knowledge concerning the true nature of the boundary flow, evident in the preceding sections, prevented an accurate modeling of the boundary flow. Before launching into a detailed discussion of these three topics, a few abbreviated remarks concerning the more outstanding features of the computer code will be made to give an appreciation for the solution which was made. A detailed discussion of either the code or its theoretical foundation is outside the provence of this report and interested readers may consult References 7 and 8.

4.3.1 BLIMP Computer Code General Features

The BLIMP program applies a novel numerical solution procedure, termed an integral-matrix method, to solve with as much accuracy as desired a rather comprehensive set of laminar/turbulent boundary-layer equations. The equations apply to general chemical systems, performing a chemical equilibrium solution at each node in the boundary layer representation. Unequal diffusion and thermal diffusion effects are included by using a bifurcation approximation for the diffusion coefficients.

The procedure applies to arbitrary planar or axisymmetric blunt or sharp body geometries, the first of which was used for this study. The boundary-layer edge gas must be adiabatic but it may be nonisentropic. With regard to boundary-layer edge conditions, it is necessary to supply only composition of the edge gas, stagnation enthalpy and pressure, and distributions of pressure, entropy (if nonisentropic) and incident radiation flux in the streamwise direction.

At the wall it is possible to assign temperature and mass fluxes of various component gas mixtures into the boundary layer, to require the surface to be in equilibrium with whatever condensed species is predicted by the program to be the surface species, to permit rate-controlled surface reactions and to perform a steady-state energy balance at the wall (in which case the boundary layer is completely coupled to the wall response).

4.3.2 Boundary Layer Solution Details

In this section the results from the computer analysis of the boundary flow for two assumed wall conditions will be presented. The two conditions modeled (1) the typical fuel rich composition determined in the actual boundary flow sampling where on the average the oxidizer to fuel ratio was about 0.5; and (2) the "fuel on the wall" hypothesis where the composition at the wall was assumed to be pure fuel. The oxidizer rich situation was not treated.

The computer output is presented in Appendix A for a point in the chamber corresponding approximately to station 2 ($x = 1.75$ inches).

Although solutions were obtained for other points, the results did not show a strong x-dependence and therefore the output from these other stations has not been included in this report. Only output details germain to the discussion here will be considered. A complete description of the output from the BLIMP program is presented in Reference 9. The profiles of species temperature, velocity, etc., are of most interest here and only the most predominant of the 11 species utilized in the solutions will be presented.

4.3.2.1 Profiles

Figure 15-a presents the species profile through the boundary layer at the second station for O/F = 0 at the wall and Figure 15-b presents the profiles for O/F = 0.5 at the wall. In both cases the edge O/F is 1.3. Both cases demonstrate similar trends--high ammonia concentrations at the wall which rapidly disappear; high hydrogen and low water concentrations near the wall; and the opposite condition near the edge. The nitrogen concentration is relatively constant except at the wall where a sharp downward dip is evident. The most noticeable difference between the two cases is the much higher hydrogen and ammonia concentrations near the wall for the pure fuel situation (which is to be expected from the results of Section 4.1.2).

Special notice must be taken of the effect of diffusion on the results. The effect is especially apparent for the pure fuel condition. Note at the wall that significant quantities of water exist in addition to ammonia and nitrogen. Without diffusion there would be no water at the wall. Note also the increase in water concentration locally in the vicinity of the wall. The concentration variation is thermally induced by the high temperature gradients in this region.

A typical velocity profile through the boundary layer is shown in Figure 16 which, as can be seen, differs somewhat from the typical self-similar theoretical profile. The temperature profile presented in Figure 17 shows that a high temperature gradient exists near the wall in the laminar sublayer especially for the O/F = 0.5 condition and a somewhat lower gradient for the pure fuel condition. The

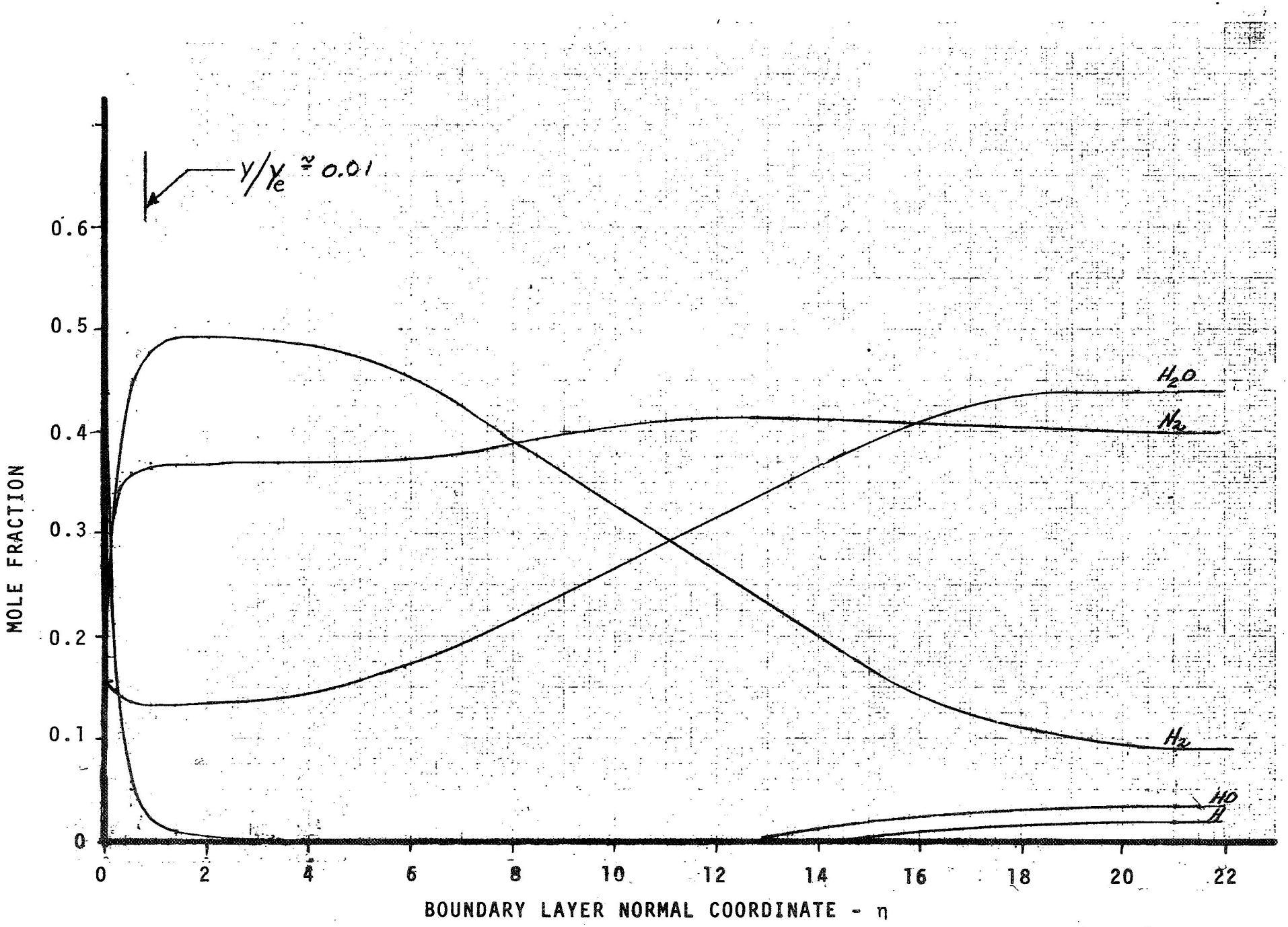

Figure 15. Species Composition Profile Through Theoretical Boundary Layer
a. O/F = 0 at the Wall

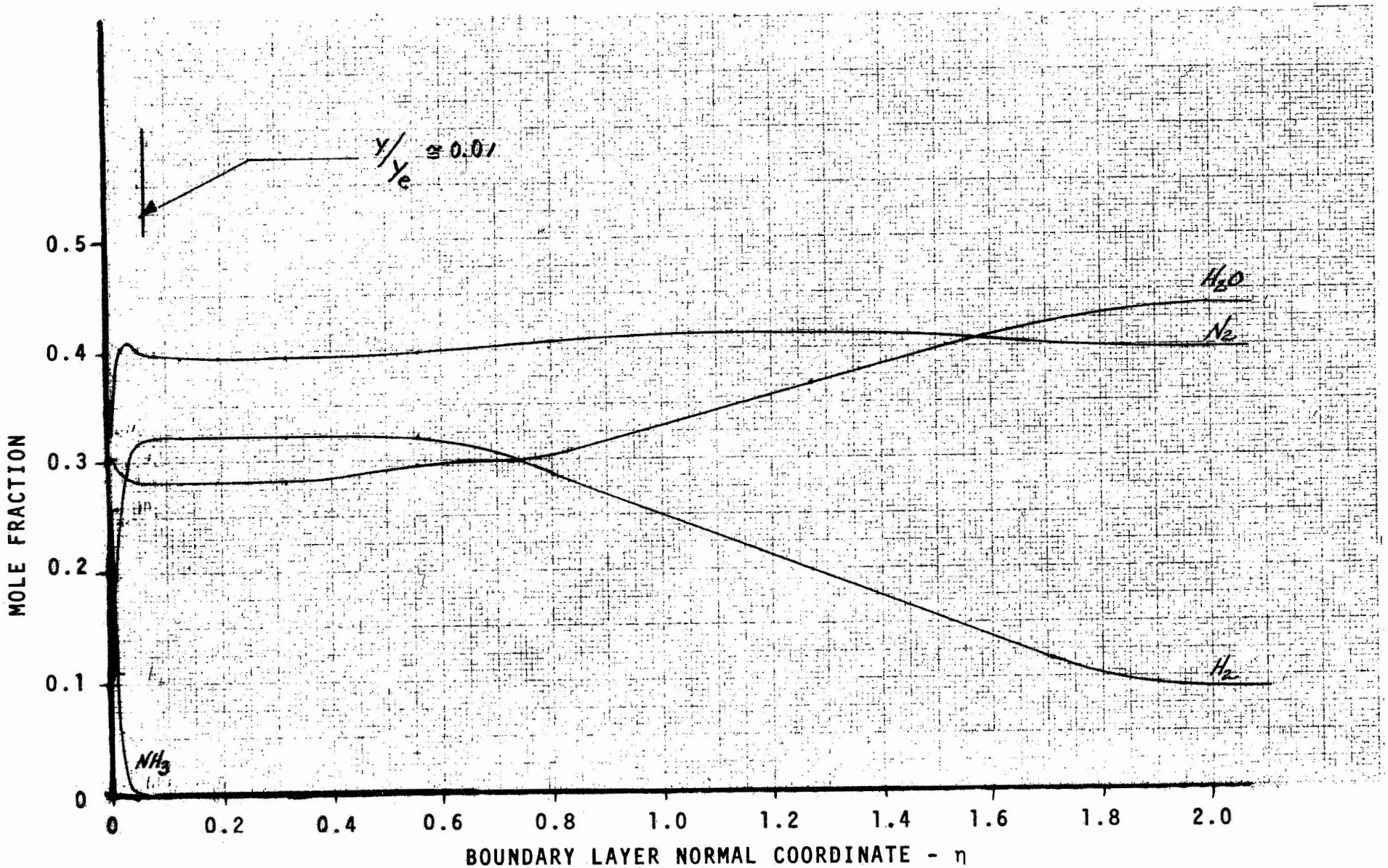

Figure 15. Concluded

b. O/F = 0.5 at the Wall

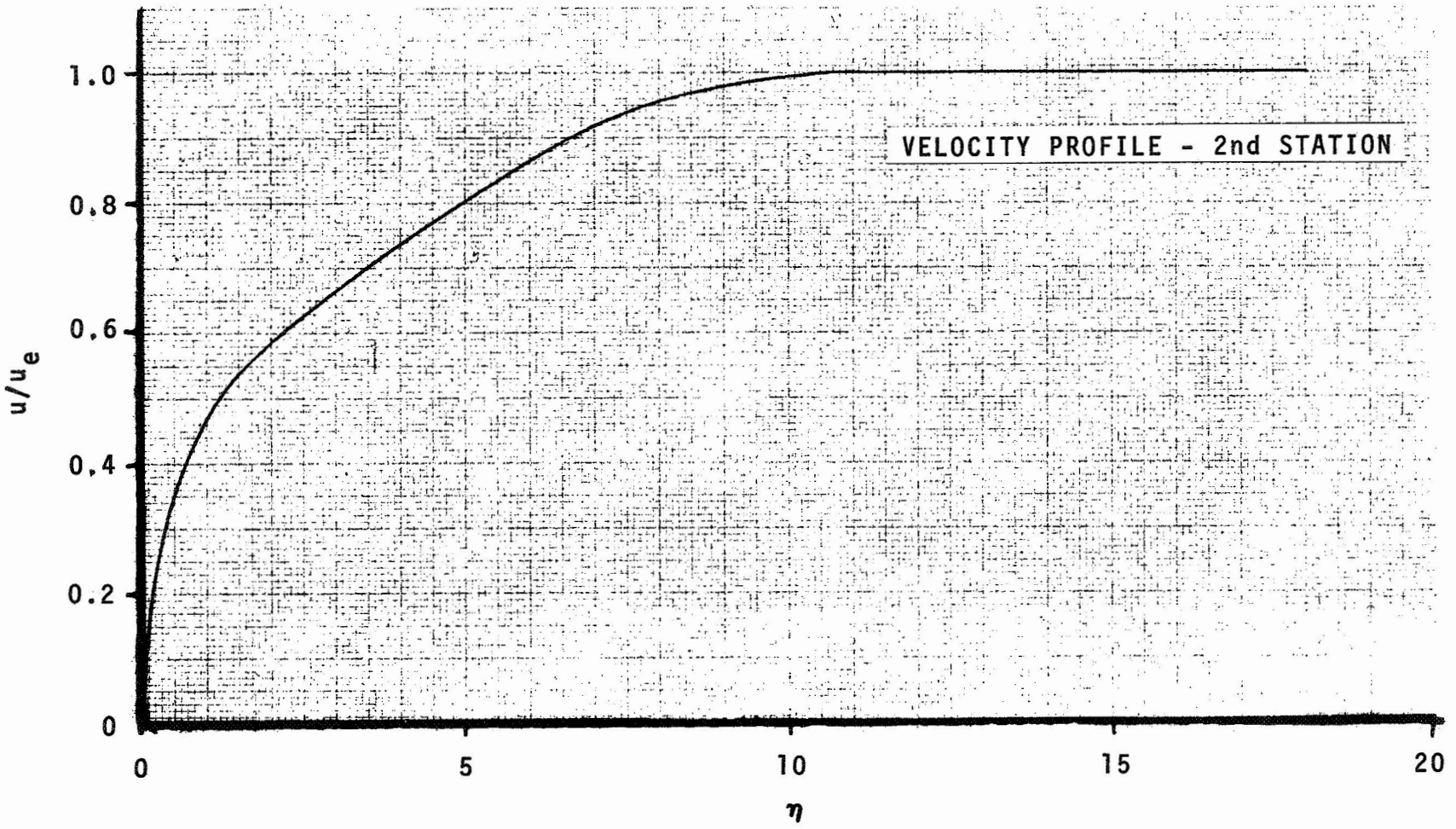

Figure 16. Velocity Profile in Boundary Layer

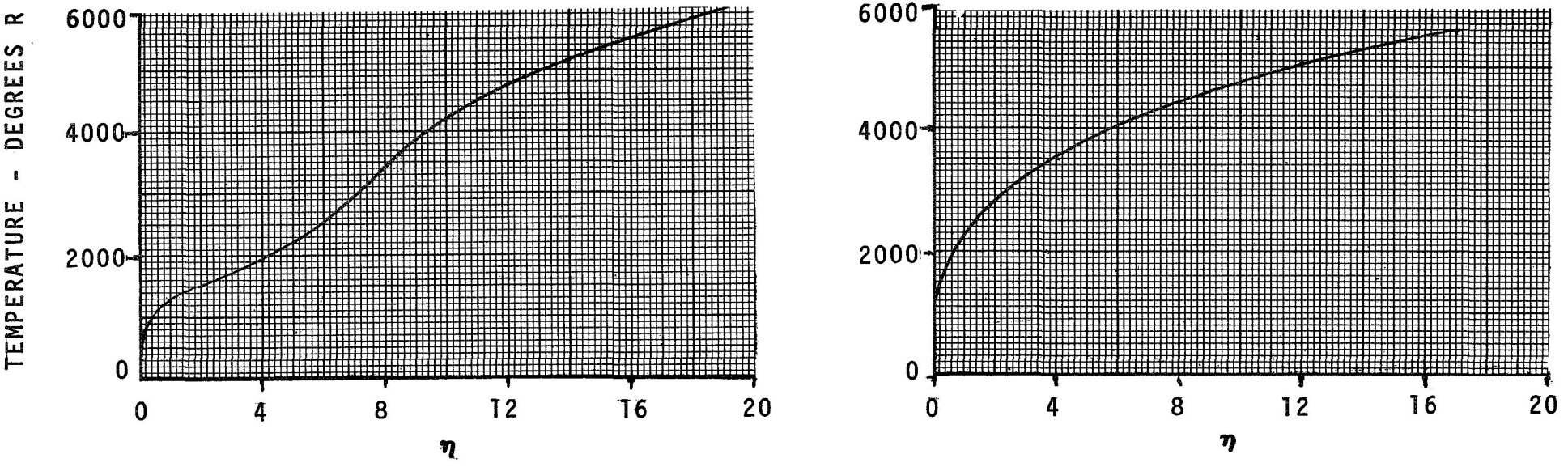

Figure 17. Temperature Through the Boundary Layer

density, enthalpy, and other thermodynamic property profiles across the boundary layer which have not been plotted here can be found in the BLIMP output presented in Appendix A.

As the reader has probably noted the profiles have been plotted as a function of a parameter, η, (ETA in Appendix A) rather than the physical y coordinate. Such a coordinate is tantamount to a logarithmic scale, the use of which is necessary if the details of the gradients existing in the laminar sublayer are to be displayed at all. Some idea of the expansion is demonstrated by the 0.01 y/y_e point in these figures. The functional y dependence of η is given by:

$$\eta = \frac{u_e}{\sqrt{2\xi}} \int_o^y \rho dy$$

where

$$\xi = \int_o^\lambda u_e \rho_e \mu_e d\lambda$$

is the transformed running coordinate.

Comment needs also to be made on the assumptions used to make the calculations. The assumptions are:

1. Steady state conditions
2. Edge static pressure equal to the average measured chamber static pressure
3. Adiabatic and isentropic edge condition
4. Transition momentum thickness Reynold's number = 250
5. Turbulent Clauser number = 0.019
6. Equilibrium chemistry
7. Edge thermodynamic state specified by the mean mixture ratio enthalpy
8. Edge velocity equal to bulk mean equilibrium mean velocity

9. Wall temperature equal to 800°R

10. Enthalpy of hydrazine (or of mixture) equal to that of the products at $T = T_{wall}$ $(x = 0)$

11. Error function type profiles of concentration, velocity, etc., at beginning of chamber $(x = 0)$.

The first six of these assumptions are conventionally applied in situations of this kind and need no further elaboration here. As mentioned at the beginning of Section 4, assumption 7 is a necessary fact of life at the present time. For the present chamber which has a large L* and contraction ratio, the mean mixture ratio state is probably fairly well representative of the actual situation near the chamber exit plane. Up near the injector end the thermodynamic state "driving" the boundary flow is certainly different than the mean condition. On the other hand, the gas dynamics are also uncertain because of reverse flow and other phenomena such that the application of conventional boundary layer theory to this region is questionable to begin with. Assumption 8 is thought to be quite a good one for the same reason as assumption 7 and the fact that the bulk gas dynamic velocity is not greatly different from the liquid jet velocity of the injector spray.

The 800°R wall temperature was arbitrarily chosen to represent the wall condition early in the sampling process. For most of the runs the wall temperature rose about 50°F from the initial temperature during the interval from ignition to sampling. Actually the wall temperature is neither constant with time nor axial position. These effects were not explored but are expected to be of second order importance.

Because little is currently known about the detailed distribution of thermodynamic, aerodynamic and chemical properties near the injector of a rocket motor, it was found necessary to arbitrarily establish the initial profiles of the major independent parameters at an initial upstream station. An approximate error function profile was chosen for the representation. Since the computer program employs a sophisticated nonsimilar profile computational procedure,

the initial arbitrary profile is "washed out" and replaced by a more "natural" profile a sufficient distance downstream. For the calculations of this study the "natural" profile was established at the second station.

4.3.2.2 Unequal Diffusion Effects and Comparison with Data

One of the principal motivations for performing the boundary layer analysis was to explore the major characteristic evident throughout the data--the atomic imbalance. Because of the simple chemical formulae relating the three elements of the hydrazine/nitrogen tetroxide propellant system, a highly useful and informative relationship involving atomic ratios can readily be formulated. As shown in Part IV the relationship is such, due to the 2:1 ratio of oxygen to nitrogen and hydrogen to nitrogen, that the sum of the two ratios must equal 2 independent of the mixture ratio, provided, and this is most important, provided that atoms in a given molecular "cloud" do not become vastly dissociated from their original partners. Thus, if all atoms move about with equal freedom one would expect the relationship

$$\frac{O}{N} + \frac{H}{N} = 2 \qquad (4)$$

to hold independent of the local mixture ratio. This is tantamount to assuming equal diffusion. It is readily apparent in the data that the foregoing relationship is not observed--in fact, great departures from it are calculated from the species data. The BLIMP boundary layer solution, by the fact that it includes both unequal and thermal diffusion effects, can shed some theoretical light on the situation. A study of the atomic ratios for the O/F = 0.0 at the wall case produced the results shown in Figure 18. Of particular interest is the summation curve which is to be compared with the equal diffusion dashed line. It is seen that the unequal diffusion of the species causes the ratio to depart from the theoretical 2 value by about 10 percent over the great majority of the boundary layer. In the region from which the bulk of the sample is drawn the difference is more like 5 percent. In this region the theoretical results show an H/N

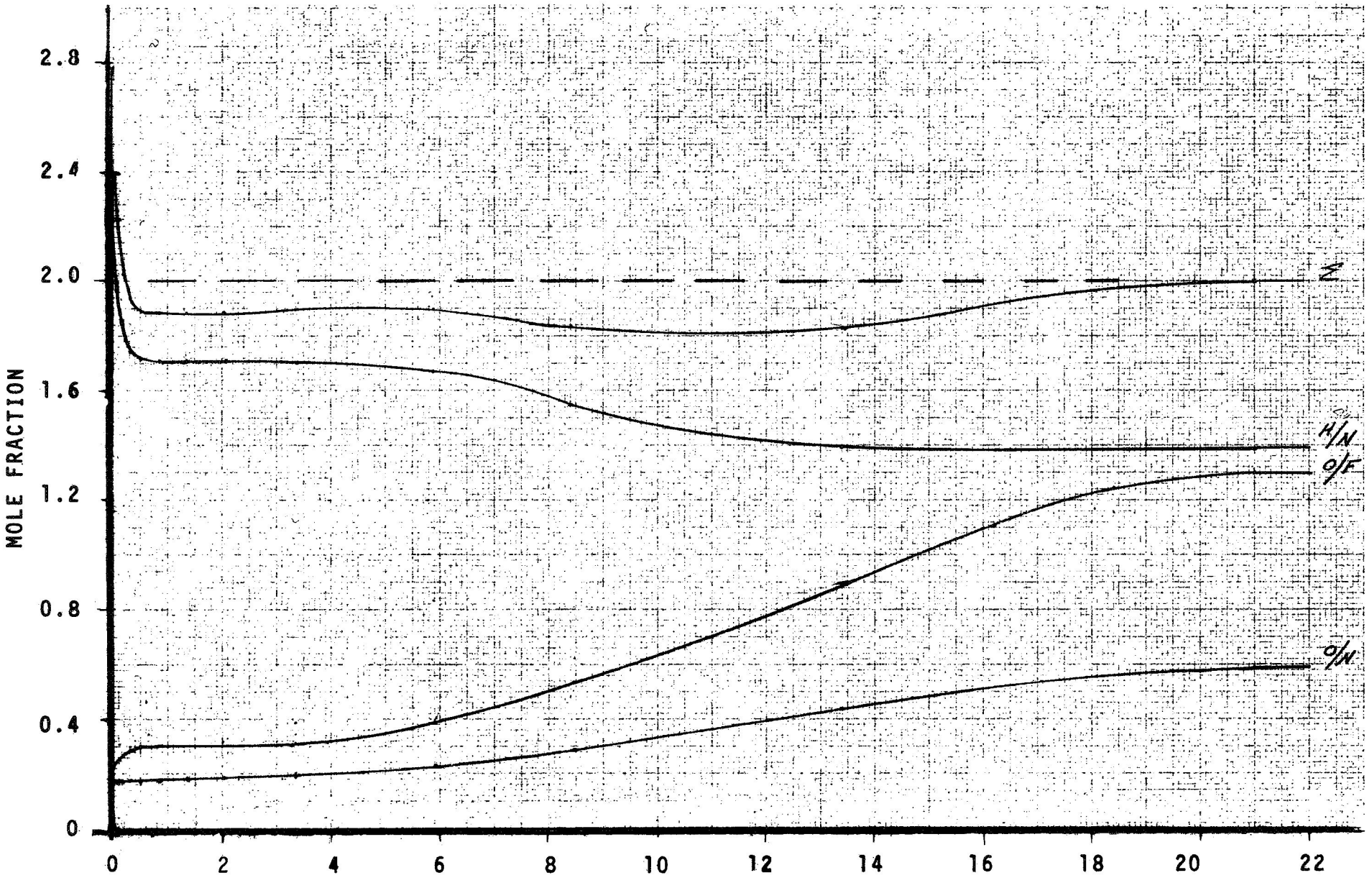

Figure 18. Atomic Ratio Variation Through the Boundary Layer

ratio of about 1.7 and an O/N ratio of about 0.2. The O/F ratio is about 0.3. Table 1 summarizes the bulk of the experimental atomic ratio data from the fuel rich region of the boundary flow (which can be compared withthe theoretical results). The theoretical atomic ratios appear to be, in general, the upper limit of the experimental values.

It can be seen in this data that the summation column, $\sum$, frequently contains entries where the summation is less than unity, however, the bulk of the data averages around 1.5 (compared to the theoretical boundary layer value of 1.90). It is also seen that the H/N ratio rarely gets above 1.70. Nor does the O/N ratio get above 0.2. (In the cases where it does--9-6 and 10-6--the data is suspect since the O/F ratios are so high.)

The column labeled "Theoretical Water" is the increment in water mole fraction required to achieve the theoretical balance (i.e., $\sum = 2.0$). In a large number of cases a significant increase in the water percentage would be required to affect such a balance--frequently more than the water actually determined. At this time it cannot be definitely established whether the results obtained reflect unequal diffusion phenomena or the loss of water vapor in the sampling gas through some separation or condensation phenomena. Further experimental research in this area is necessary to determine, with reasonable assurance, the physical processes involved.

4.3.3 Sample Bottle Predictions

The boundary layer solutions provided a means for simulating the sampling process taking place in the chamber. It was hoped that several characteristics of the process could be learned from the simulation. First of these is the degree of agreement between the theoretical and experimental composition. It is obvious from the previously presented profiles that the amount of ammonia present theoretically is insufficient to provide good agreement. The quantitative degree of the insufficiency is not apparent however. Second, the simulation provides a more accurate estimate of the disturbance penetration the sampling process produces in the boundary flow than that

TABLE 1

ATOMIC RATIO DATA

Sampling Time		O/N	H/N	$\sum$	O/F	Theoretical H_2O	Actual H_2O
Run/ Bottle	Sec						
9-1	1	0.17	1.63	1.80	0.3086	6.33	16.40
3		0.16	1.54	1.70	0.2995	9.70	14.90
4		0.18	1.01	1.19	0.5310	31.45	22.26
6		0.35	0.78	1.13	1.3200	34.09	18.96
10-1	1	0.17	0.99	1.16	0.4989	26.83	37.33
2		0.15	1.01	1.16	0.4477	29.67	23.70
3		0.22	1.43	1.65	0.4436	9.58	38.50
4		0.09	0.40	0.49	0.6679	71.98	8.70
6		0.35	0.67	1.02	1.5042	40.05	4.54
11-1	0.6	0.08	1.08	1.16	0.2243	30.85	24.02
2		0.15	1.49	1.64	0.2945	11.37	19.42
3		0.08	1.20	1.28	0.2105	25.66	23.33
4		0.04	0.71	0.75	0.1756	55.23	19.52
5		0.11	0.70	0.81	0.4586	47.82	23.78
6		0.06	0.62	0.68	0.2796	56.82	24.57
12-1	1.2	0.03	0.86	0.89	0.1055	48.92	15.13
2		0.06	1.51	1.57	0.1321	16.16	10.41
3		0.10	1.70	1.80	0.1812	7.00	8.61
4		0.17	1.56	1.73	0.3128	8.81	19.18
5		0.07	1.05	1.12	0.2057	31.80	29.86
13-1	1.7	0.11	1.12	1.23	0.2887	27.33	26.71
2		0.11	1.24	1.35	0.2736	21.85	26.41
4		0.09	0.86	0.95	0.3148	39.52	26.9
5		0.06	0.78	0.84	0.2279	44.75	30.89
6		0.05	0.57	0.62	0.2652	59.08	25.43
14-2	1.2	0.11	1.02	1.13	0.3154	31.40	26.21
3		0.04	1.04	1.08	0.1368	37.11	17.83
4		0.04	0.58	0.62	0.2225	59.10	26.23
5		0.12	0.76	0.88	0.4646	42.75	26.23
6		0.06	0.52	0.58	0.3754	61.83	22.40
15-1	1.1	0.07	1.42	1.49	0.1482	17.45	23.27
3		0.14	1.38	1.52	0.3007	15.58	21.21
4		0.17	0.68	0.85	0.7157	43.27	19.49
5		0.12	1.12	1.24	0.3326	25.60	27.44
6		0.16	1.05	1.21	0.4408	26.47	23.50
16-1	1.4	0.07	1.60	1.67	0.1275	10.99	20.64
2		0.06	1.76	1.82	0.1111	5.50	18.73
3		0.07	1.75	1.82	0.1194	5.78	19.19
4		0.07	1.56	1.63	0.1403	12.00	21.54
5		0.09	1.56	1.65	0.1824	10.90	23.56
6		0.10	1.33	1.43	0.2255	18.98	22.02

TABLE 1 (concluded)

Sampling Time		O/N	H/N	$\sum$	O/F	Theoretical H_2O	Actual H_2O
Run/ Bottle	Sec						
28-1	2	0.10	1.89	1.99	0.1621	-0.11	18.66
2		0.09	1.74	1.83	0.1596	5.42	19.70
3		0.10	1.39	1.49	0.2136	17.33	24.07
4		0.12	1.31	1.43	0.2644	18.86	26.48
6		0.17	1.24	1.43	0.4092	19.66	22.94
27-1	0.5	0.06	1.47	1.53	0.1282	16.59	19.00
2		0.11	0.57	0.66	0.5818	59.90	10.21
4		0.09	0.73	0.82	0.3576	47.12	20.82
5		0.14	0.44	0.58	0.9509	60.95	15.54
6		0.07	0.77	0.84	0.2789	40.11	29.92
29-2	0.9	0.09	1.46	1.55	0.1783	15.89	18.57
6		0.18	0.57	0.75	0.9239	47.28	23.40
30-3	0.92	0.11	1.54	1.65	0.2045	11.05	22.80

determined using the 1/7th power velocity profile method used in the preliminary study performed in the early stages of the program (and reported in Volume IV).

One of the major uncertainties in simulating the sampling process is the description of the streamlines in the disturbed flow field. In the preliminary study the "region of influence" was assumed to be described by a simple rectangle of width equal to the sampling port. The heighth of the disturbed region (i.e., the rectangle) was determined by an integration of the local mass flux over y until a matched condition was obtained.

$$\int_{o}^{y} eu \, dy = \dot{m}_s \tag{5}$$

In the procedure employed here, a potential flow solution was used to more accurately describe the flow field during the sampling event.

4.3.3.1 Potential Flow Solution

It was initially desired to obtain a theoretical solution for the stream lines resulting in the boundary flow from the sample removal process by application of potential flow theory (i.e., imposing a sink in a parallel flow having a velocity gradient appropriate to a boundary layer). This desire was quickly dashed by the complexities inherent in such a rotational flow field situation and the very restrictive assumption of uniform parallel flow had to be made. There is some justification for this simplification however: the thickness of the laminar sublayer in which the largest gradients of velocity and other parameters exists is negligible on a mass flux thickness basis compared to the boundary layer as a whole. For instance, across most of the boundary layer the velocity is within 10 percent of the edge value.

A sink in a uniform flow field is a classic problem for which the stream line and stream function have simple analytical formulation. The flow pattern produced by such a superposition is sketched below. In the problem at hand, where the chamber wall is taken to be a flat plate, interest is in the half space given by $y > 0$. The

solution for the streamlines is symmetric about the 0-x axis and a section of the separation streamline surface in a plane normal to this axis is a half-circle as shown in the sketches below.

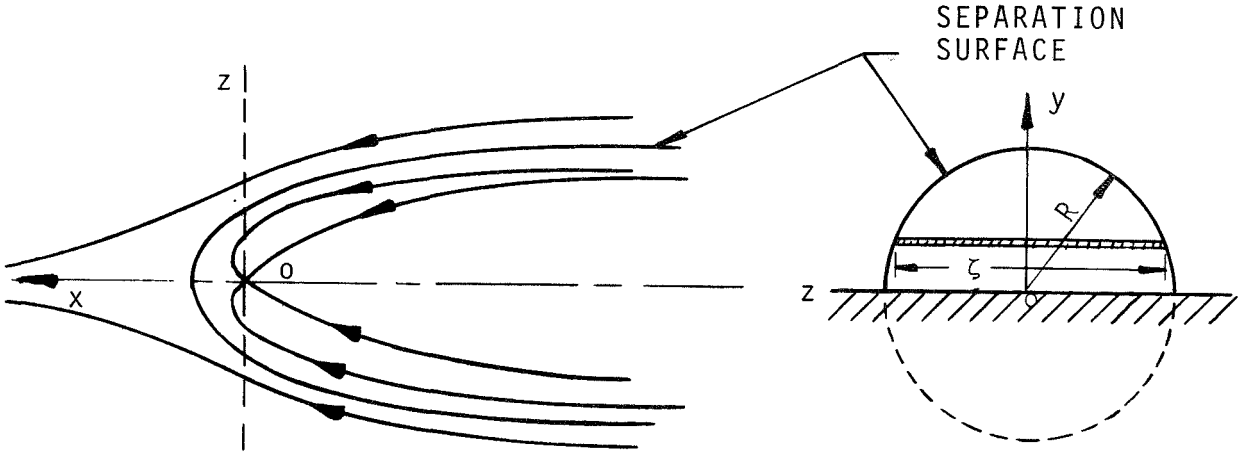

The radius R is a function of the distance from the sink, the strength of the flow fields and is given implicitly by the equation:

$$u_e \frac{R^2}{2} - \frac{Q}{4\pi}\left(1 + \frac{x}{\sqrt{R^2 + u^2}}\right) = 0 \qquad (6)$$

where u_e is the parallel velocity and Q is the sink intensity. Rather than evaluate the separation surface radius, R, from assumed approximate gas dynamic parameter levels, the circular arc boundary is accepted as a replacement for the reactangular region used in the preliminary solution procedure and the boundary layer properties are allowed to take their theoretical y-dependent values within this region. The circular boundary is then a variable limit of integration, the unique value for which, R*, is found when the integrated mass flux in the region equals that in the sample bottle being predicted. That is:

$$\left.\frac{dm}{d\tau}\right|_s = \int_0^{R^*} \rho(y)\ u(y)\ \xi(y)\ dy \qquad (7)$$

where $\zeta(y)$ is the local width of the integration interval at the y coordinate within the semi-circular region. The integration is performed using the following approximating formula:

$$\frac{dm}{d\tau} = \sum_{i=1}^{K} \frac{1}{2}(y_{i+1} - y_i)(\Pi_{i+1} + \Pi) \tag{8}$$

where

$$\Pi_i = \rho_i u_i \zeta(y_i) \tag{9}$$

and where K is the largest integer such that:

$$y_K \leq R \quad \text{and} \quad y_{K+1} > R \quad ; \quad (\Pi_{K+1} = 0 \text{ since } \zeta(R) = 0)$$

By plotting $\dot{m}/u_e$ versus R/δ where δ is the boundary layer thickness at the sampling station, a graphical solution for R* can be obtained. Typical plots are presented in Figures 19-a and 19-b. Now from the experimental data both the sampling interval, $\Delta\tau$, and the mass of sample gas obtained, m_s, are known from standard thermodynamic relations. By assuming choked sampling flow conditions it follows that:

$$\dot{m} = \frac{dm}{d\tau} \simeq \frac{m_s}{\Delta\tau} \tag{10}$$

and entering this value on the figure, the value for R* is obtained.

4.3.3.2 Specie Prediction and Comparison with Data

We are interested in comparing the experimental species and atomic fractions in the sample bottle with the content of the flow field which is theoretically taken in by the sampling process.

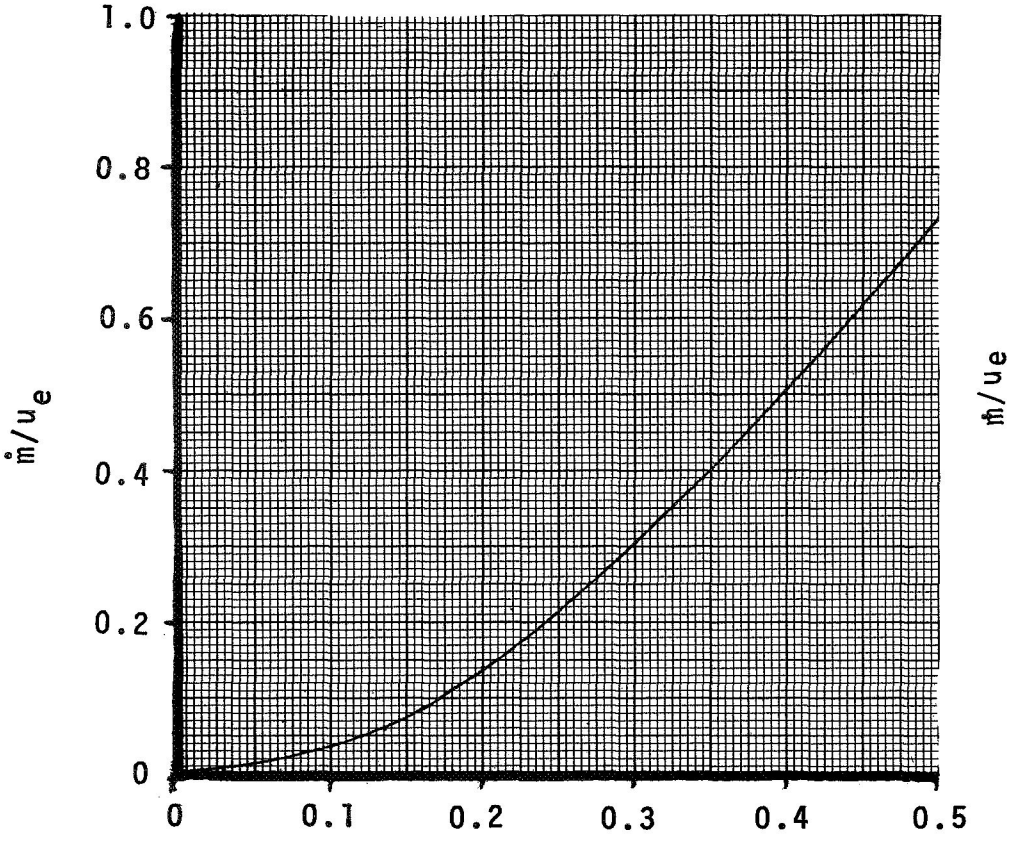

a. O/F = 0 at the Wall

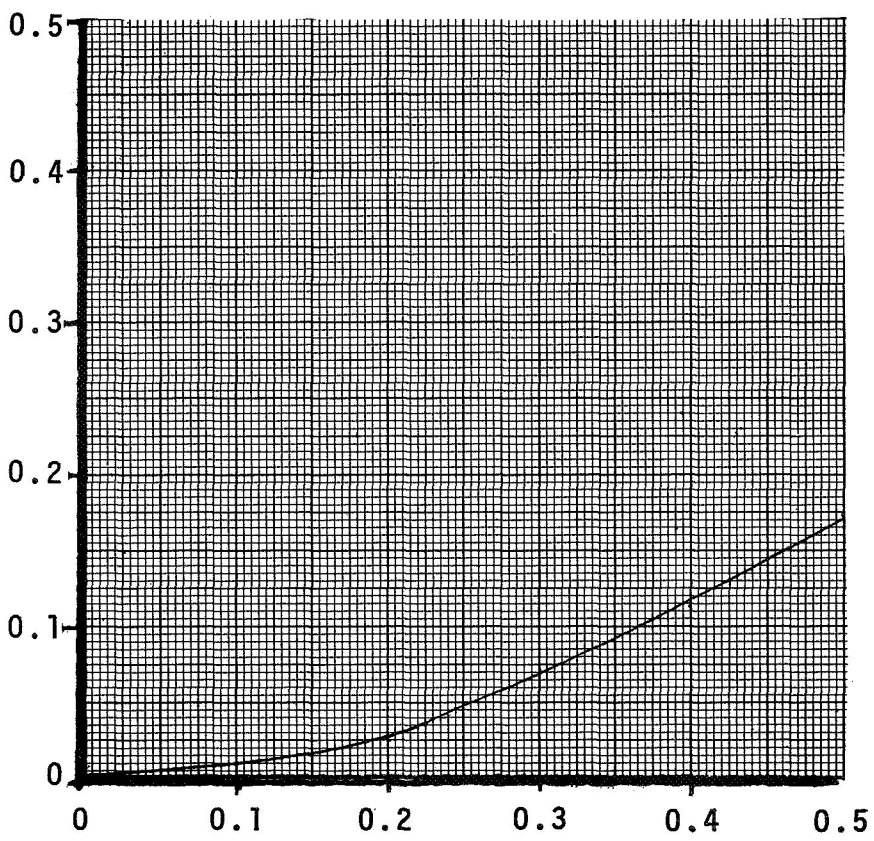

b. O/F = 0.5 at the Wall

Figure 19. Mass Flow Characteristic in the Boundary Layer

The mass of gas of element j, flowing through a stream tube area, $\zeta_i \Delta y$, (per second) is:

$$\dot{m}_{ji} = \chi_{ji} u_i \rho_i \zeta_i \Delta y_i = m' \Delta y_i \tag{11}$$

where

$$u_i \rho_i (\Delta y_i \zeta_i) \tag{12}$$

is the mass of mixture flowing through $\zeta_i \Delta y_i$ and where x_{ji} is the mass fraction of <u>element</u> j in the i^{th} strip.

The mass fraction of the element j flowing through the stream tube is:

$$\overline{\beta}_j = \frac{1}{2} \frac{\sum_{i=1}^{K} (y_{i+1} - y_i)(m'_{i+1,j} + m'_{i,j})}{\sum_{i=1}^{K} \frac{(u_{i+1} + u_i)}{2} \frac{(\rho_{i+1} + \rho_i)}{2} (\zeta_{i+1} + \zeta_i)(y_{i+1} - y_i)} \tag{13}$$

If it is assumed that the sampling does not change the molar composition, then with

$$V_i = \frac{T_i \overline{R}}{P_i M_i} \tag{14}$$

γ_{ij} (defined to be the number of moles of species j flowing per second at node i) is given by:

$$\gamma_{ij} \Delta y_i = \frac{\chi_{ij} u_i \zeta_i}{V_i} \Delta y_i \tag{15}$$

where χ_{ij} is the mole fraction of species j at node i. Similarly, the mole fraction of species j flowing per second:

$$\bar{\chi}_j = \frac{\sum_{i=1}^{K} (y_{i+1} - y_i)(\gamma_{i+1,j} + \gamma_{i,j})}{\sum_{i=1}^{K} \frac{(u_{i+1} + u_i)(\zeta_{i+1} + \zeta_i)}{(V_{i+1} + V_i)} (y_{i+1} - y_i)} \tag{16}$$

The results for the mole fraction calculations are plotted versus R/δ in Figures 20-a and 20-b for O/F = 0 and 0.5 (respectively) at the wall. It is found that the composition is constant except for the lowest values of R which, of course, correspond to low sampling rates. And again the changes at the low R values are due to the ammonia decomposition in the laminar sublayer.

Next these theoretical results are compared with typical experimental sample composition data selected at random from the array of test data available. Run 11, bottle 1 (station 1) was chosen for the first comparison for which the gas sample data is as follows (from Part III)

$$p = 15.47 \text{ psia}; \quad V = 75 \text{ cc}; \quad T = 325^0\text{F}; \quad \Delta\tau = 0.6 \text{ sec.}$$

where

$$T = \frac{T_s + T_{V1}}{2}$$

T_{V1} - pneumatic valve #1 temperature

T_s - helium heater gas supply temperature

The mole fractions are read from Part III, Section 3. From this data a mass, Δm, of 1.03×10^{-4} lb in the bottle is computed. Finally, for the theoretical bulk mean edge velocity, u_e, of 252 ft/sec

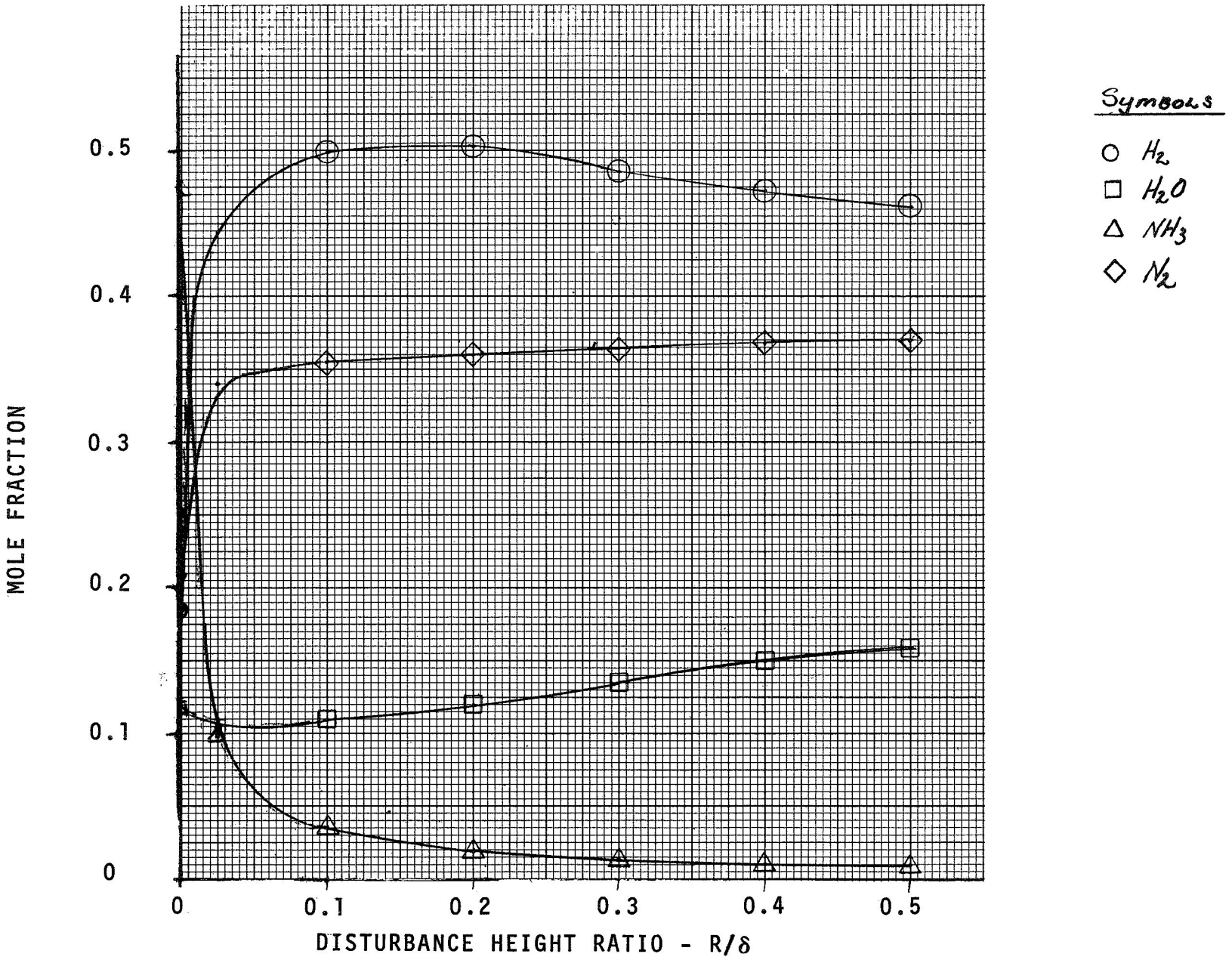

Figure 20. Theoretical Sample Composition as a Function of Disturbance Height (Sampling Rate)

a. O/F = 0 at the Wall

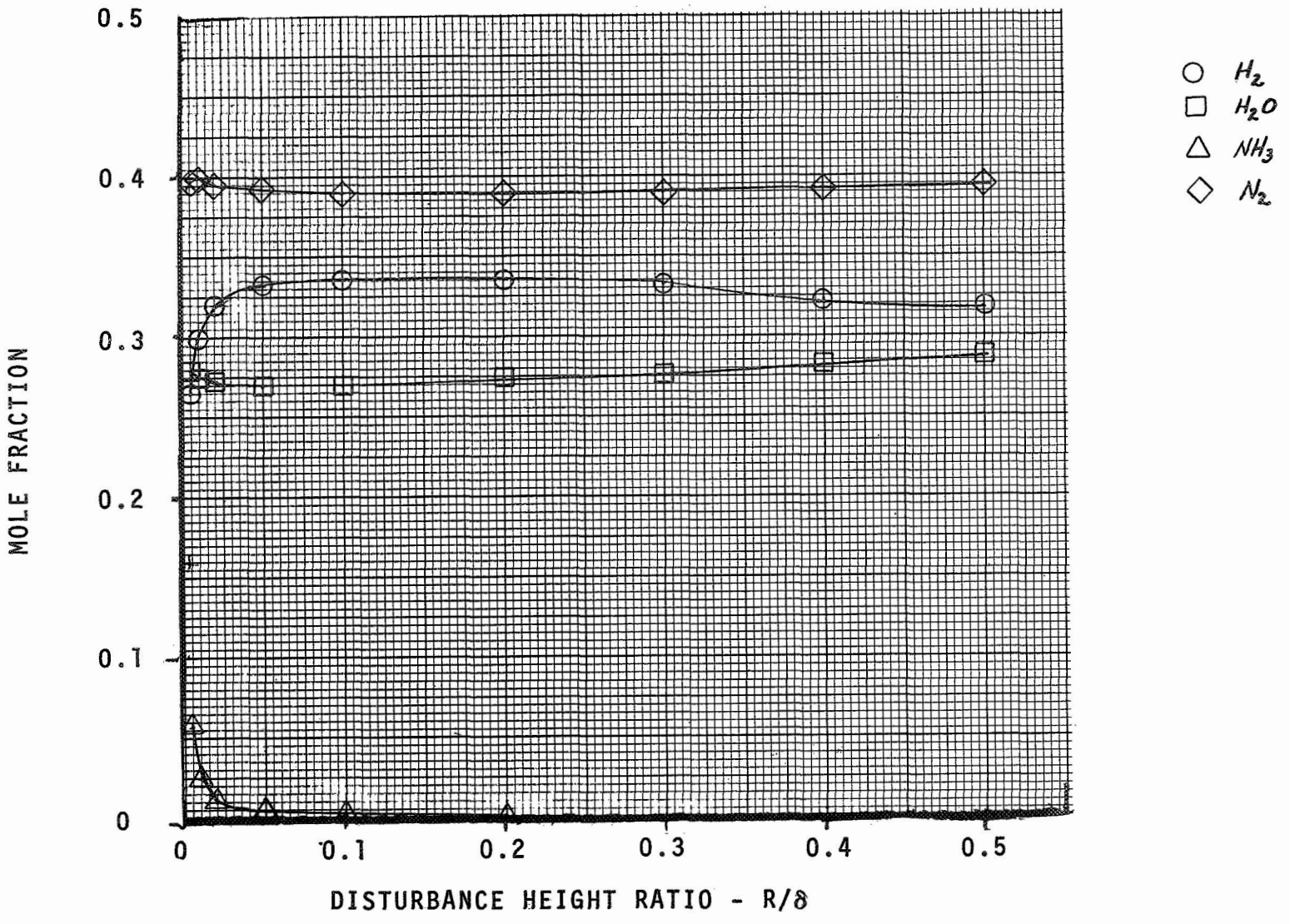

Figure 20. Concluded

b. O/F = 0.5 at the Wall

$$\frac{\dot{m}}{u_e} = \frac{\Delta m}{\Delta \tau} \frac{1}{u_e} = 0.68 \times 10^{-6}$$

The comparison for mole fractions obtained by experimental and theoretical results are presented in Table 2 below:

TABLE 2

COMPARISON OF THEORETICAL AND ACTUAL SAMPLE COMPOSITION – FUEL RICH

	Species	NH_3	H_2O	N_2	H_2	R/δ
	Data-Bottle 1, Run 11	0.18	0.09	0.466	0.24	
O/F = 1.3 at edge	O/F = 0 at wall	0.03	0.11	0.356	0.50	0.135
	O/F = 0.5 at wall	0.001	0.273	0.390	0.335	0.230

While the comparison between theory and experiment does not show good agreement it is possible that different assumptions for the edge and wall conditions could produce better agreement. In particular, it is obvious that a thicker ammonia layer and/or a thin liquid layer of ammonia (or hydrazine) would produce closer agreement with experimentally determined composition.

A liquid layer of ammonia or hydrazine at the wall can be treated by the BLIMP program: either by assigning the surface of the chamber as NH_3 liquid or by injecting ammonia through the surface in sufficient quantity to avoid total vaporization; however, such solutions could not be performed within the current scope of work.

Since the first comparison was relatively unsuccessful with the fuel rich situation, as less fuel rich condition was chosen: i.e., run 10, bottle 3, for which:

$$\frac{1}{u_e} \frac{\Delta m}{\Delta \tau} = 0.81 \times 10^{-6}$$

The results are compared in Table 3.

TABLE 3

COMPARISON OF THEORETICAL AND ACTUAL SAMPLE COMPOSITION – MODERATELY FUEL RICH

Species	NH_3	H_2O	N_2	H_2	R^*/δ from $\dot{m} = \frac{\Delta m}{\Delta \tau}$
Data Bottle 3, Run 10	0.043	0.172	0.40	0.388	
O/F = 0 at Wall	0.025	0.115	0.36	0.50	0.15
O/F = 0.5 at Wall	0.001	0.275	0.39	0.335	0.255

Much better agreement between the computed composition and that from the experiment determinations are found for this case as was expected. Note how the pure fuel condition (at the wall) produces the best agreement for NH_3 and H_2O while the 0.5 mixture condition produces the best agreement for N_2 and H_2. Note also for both examples that the sampling disturbance went no further than 1/4 of the boundary layer thickness (for the wall conditions assumed) in the limit (i.e., where the local flow properties within the region had their undisturbed values).

4.3.3.3 Gram Atom Comparison

Since the possibility exists that the collected sample represents a nonequilibrium chemical situation, more meaningful comparisons may result from atomic analysis rather than species analysis (i.e., comparing atomic mass fractions). Accordingly, the gram atom fractions were calculated from the theoretical species flux and the results are presented in Figures 21-a and 21-b. Note how much more constant the atomic fractions are as a function of R even for small values of R (equivalent to small sampling flow rates). The theoretical results are compared to the same samples as in the preceding section and are presented in Tables 4 and 5, respectively.

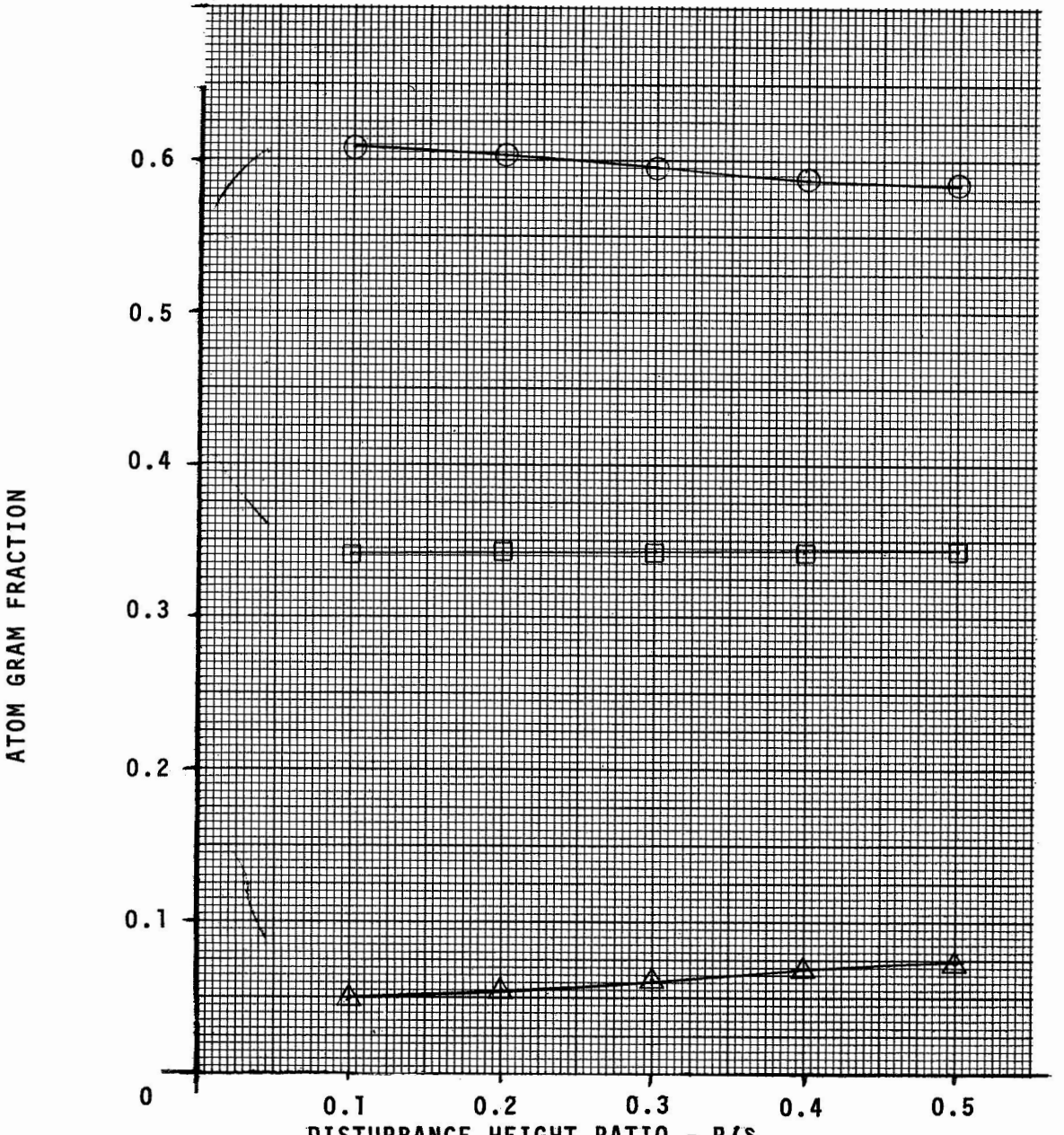

Figure 21. Theoretical Atomic Compositions of Sample as a Function of Disturbance Heights (Sampling Rate)

a. O/F = 0 at the Wall

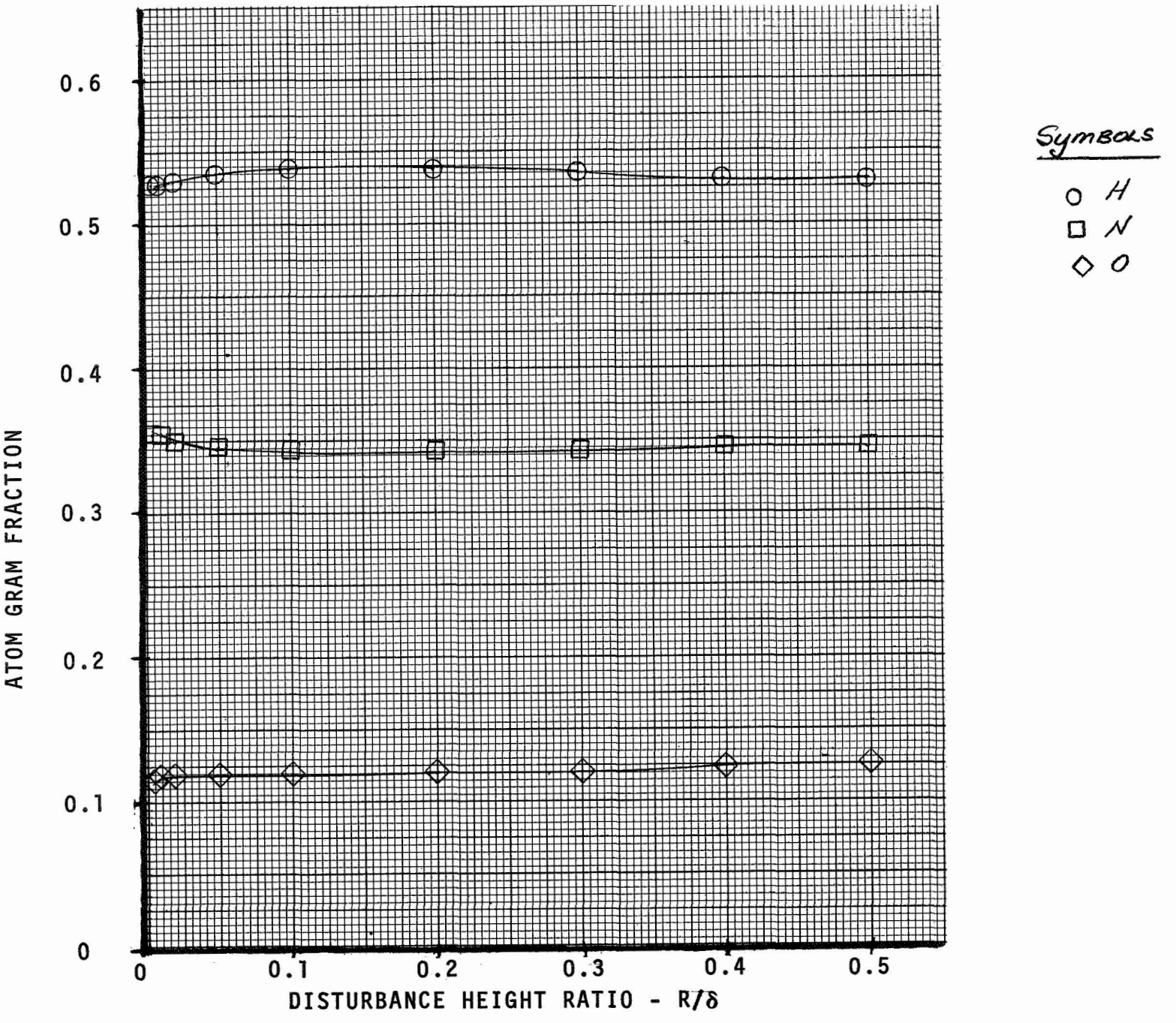

Figure 21. Concluded

b. O/F = 0.5 at the Wall

TABLE 4

REPEAT OF TABLE 2 WITH ATOMIC RATIOS

Atom Species	H	N	O	R/δ
Data Bottle 1, Run 11	0.50	0.45	0.04	
O/F = 0 at Wall	0.607	0.34	0.135	
O/F = 0.5 at Wall	0.54	0.34	0.12	0.230

TABLE 5

REPEAT OF TABLE 3 WITH ATOMIC RATIOS

Atom Species	H	N	O	R/δ
Data Bottle 3, Run 10	0.55	0.375	0.083	
O/F = 0 at Wall	0.605	0.342	0.05	0.15
O/F = 0.5 at Wall	0.54	0.342	0.12	0.255

Comparison of these tables with the respective tables of the preceding subsection show that a dramatic improvement occurs when the comparison is made on the atom gram basis. This result can be expected since the theoretical predictions could not allow enough NH_3 to exist because of the temperature gradient although the correct amount of hydrogen was present. Again this result reinforces

the conjecture that the experimental samples were drawn from a boundary flow in which a substantial portion of the flow was liquid. The agreement evident in Table 5 is impressively good where the maximum error in any of the elements is like 5 percent.

4.3.4 Mean Temperature in the Sample Flow

The foregoing boundary layer analysis can be used to analytically predict the magnitude of the cross-over temperature obtained in the equilibrium studies described in Section 4.2. Since $\overline{T}_{crossover}$ can be assumed to be an average temperature of the sample stream tube we can define it by the following formula

$$\overline{T} = \frac{U_e \int_0^R \rho \frac{u}{u_e} T\zeta dy}{U_e \int_0^R \rho \frac{u}{u_e} \zeta dy}$$

T representing the temperature at distance y from the wall and $\rho U\zeta dy$ the mass weighing function at that distance. The denominator is the total mass flux.

When $\overline{T}$ is computed for the case where O/F is 0.5 at the wall a very high temperature (of the order of 2300^0R) is obtained. This results from the high heat of reactions involved between oxidizer and fuel as explained previously.

For O/F = 0 condition (at the wall) the temperature profile is not so steep at the wall and $\overline{T}$ is lower, although $\overline{T}$ is still significantly higher than the crossover temperatures for the fuel rich data. Note that these high levels of temperature are consistent with the equilibrium crossover temperatures for those samples containing little fuel and where, presumably, there did not exist a liquid layer on the wall.

SECTION 5

PREDICTIONS OF NONABLATING THRUST CHAMBER CONVECTIVE HEAT TRANSFER RATES

Predictions of heat transfer to the combustion chamber and nozzle walls of the Jet Propulsion Laboratory nonablative rocket motor were performed utilizing the Aerotherm Real Gas Energy Integral Boundary Layer computer program (ARGEIBL). Various developments of this prediction technique are described in References 10 through 12. Briefly, the boundary layer heat transfer quantities are evaluated from the integral form of the quasisteady-state boundary layer energy equation, in which a convective transfer coefficient model is utilized to relate the wall heating rate to the enthalpy potential between the boundary layer edge and the surface gases. The essential assumption utilized in the solution of the energy equation is that the flat plate dependence of heat transfer coefficient on energy thickness is also valid for flows with a streamwise pressure gradient. This assumption is supported by the work of References 13 and 14. The resulting first order differential equation in terms of energy thickness is numerically integrated in the ARGEIBL computer program as a function of boundary layer running length. The exact formulation currently utilized in the ARGEIBL code is presented in Reference 14.

In Section 5.1, the input requirements of the ARGEIBL code are defined and values utilized in the predictions of the nonablative rocket motor heat flux are presented. In addition, several assumptions used to obtained the input data are discussed. The heat flux predictions are then presented in Section 5.2 and compared to the heat flux experimentally obtained in this program.

5.1 COMPUTER CODE INPUT

The ARGEIBL computer code requires as input the following data:

1. Free stream properties as a function of boundary layer running length

a. Velocity

b. Static enthalpy

c. Prandtl number

d. Pressure

2. Nonablative surface quantities as a function of boundary layer running length

   a. Static enthalpy of gases adjacent to the wall

   b. Chamber radius

3. Boundary layer gas properties input parametrically as a function of pressure and enthalpy

   a. Temperature

   b. Molecular weight

   c. Specific heat

   d. Viscosity

4. Transition criterion

5.2 DISCUSSION OF ASSUMPTIONS

For a liquid layer rocket motor the foregoing input data can not be defined rigorously (see Section 4). The primary source of difficulty is the uncertainty in the local chemical composition of the gases throughout the boundary layer and at the edge of the boundary layer.* Measurements of the chemical composition of the gases adjacent to the surface provide valuable information on surface gas phase properties, but since the heat transfer was, and generally is, strongly dependent on the conditions at the edge of the boundary layer, accurate knowledge of the edge gas composition and temperature are needed to adequately predict the boundary layer heat transfer with the

*The collected samples represent an average over some boundary layer distance — y = 0 to y'. Presumably y' is not too large compared to δ.

ARGEIBL code. Obviously, if complete mixing of the injected propellant takes place, the edge chemical composition would be defined and the ACE program could be utilized to evaluate the thermochemical state. As suggested earlier in this report, however, various complicating phenomena caused by dominant mechanical mixing within the injector sprays (at the injector end of the chamber especially) which produce substantial property gradients in the flow field away from the boundary flow, make the evaluation of the local boundary layer edge properties nebulous. Additional phenomena such as condensate (liquid NH_3) in the boundary layer, mass addition to the boundary layer edge (due to spray having a large radial component), and kinetic effects probably occur in the combustion chamber environment and hence the modeling of the physical situation by the present theoretical procedure is certainly tenuous.

In order to formulate a thermodynamically consistent set of input data applicable to the ARGEIBL prediction technique, several assumptions about the nature of the thrust chamber boundary layer were made. Some of the assumptions may be questionable, but they are reasonable and do reduce the known information to a usable set of data. The assumptions are as follows:

1. The measured molecular compositions of bottle samples represent the composition of the entire boundary layer at the sampling locations (hence all boundary layer and surface gas property terms are defined for this composition).

2. The composition of the boundary layer at a given location is invariant with time.

3. The composition of the free stream flow is equal to the equilibrium mixture of the injected propellants at the optimum flame temperature and measured chamber pressure.

4. The velocity and static enthalpy at the edge of the boundary layer are defined from an isentropic expansion of the free stream gases.

5. The properties of the boundary layer between sampling stations are defined by interpolations based on the

isentropic expansion pressures. (An artificially small pressure variation is input for interpolation between combustion chamber locations.)

6. The composition of the boundary layer in the nozzle throat region is identical to the measured bottle composition of the 6th sampling location.

7. The surface temperature at a given time is adequately defined from a one-dimensional transient heat conduction analysis of the rocket motor wall.

8. A laminar boundary layer is initiated adjacent to the injector face and transition occurs at $Re_\theta = 250$.

The assumption that the edge static enthalpy be based on the composition of the free stream gas at the local static temperature is, at first glance, inconsistent with the assumption that the average composition of gases in the boundary layer be the same as the measured bottle composition. Indeed, these assumptions would be consistent only if the mathematical model being utilized in the computer code could treat correctly the extreme variations of composition within the boundary layer. The mathematical model, however, permits only one composition and, in this case, the measured wall composition was used because it would logically have the most direct influence on the heat transfer to the surface. Hence the thermodynamic and transport properties of the measured compositions were input to the prediction technique. The selection of the free stream composition to define the edge enthalpy was based on the belief that because of the rapid changes of composition in the boundary layer, the energy at the edge of the boundary would more directly influence the heat transfer then would the temperature (at least in the formulation of the energy thickness integral equation). In addition, experience by the authors with the BLIMP prediction technique* has shown that with large changes

*As explained earlier in this report, the BLIMP program allows continuous variation of chemical composition across the boundary layer.

in composition, enthalpy profiles tend to remain more uniform than do the temperature profiles. This is indicated schematically in Figure 22 as it would apply to the hypothesized boundary layer in the nonablative rocket motor.

5.3 INPUT CALCULATION DETAILS

Based on the above assumptions, all of the input data required by the ARGEIBL code to calculate the convective heat flux to the combustion chamber and nozzle walls were defined. The ACE computer code described earlier in this report was utilized to compute the properties of the isentropically free stream combustion products. The velocity, static enthalpy, Prandtl number and pressure were evaluated as a function of flow area ratio. Then, based on the combustion chamber and nozzle geometry shown in Figure 2, the expansion properties were related to boundary layer running length (λ). Figure 23-a shows the variation of area ratio with boundary layer running length (λ). Also, in Figure 23-b the body radius is presented as a function of λ. Since expansion properties were calculated in terms of area ratio, Figure 23-c was utilized to evaluate their relationship to λ. The variations of edge velocity, static enthalpy, and pressure with λ are presented in Figures 23-c through 23-e for both Run 16 and Run 24, respectively. The slight differences in properties between Runs 16 and 24 were due to the slightly different oxidizer to fuel ratios metered in the two tests.

The evaluation of surface temperature at each input location was performed utilizing the graphical one-dimensional transient heat conduction solutions of Reference 15. An iterative procedure was required, however, since the conduction solution is a function of the wall heating rate boundary condition. First guesses of the local surface temperatures were made and the ARGEIBL solution was found. Using the new heat transfer coefficient values, surface temperatures were recalculated. For both cases predicted, only one run was necessary to obtain the surface temperatures for 0.4, 1.4, and 2.4 seconds from initiation of firing.

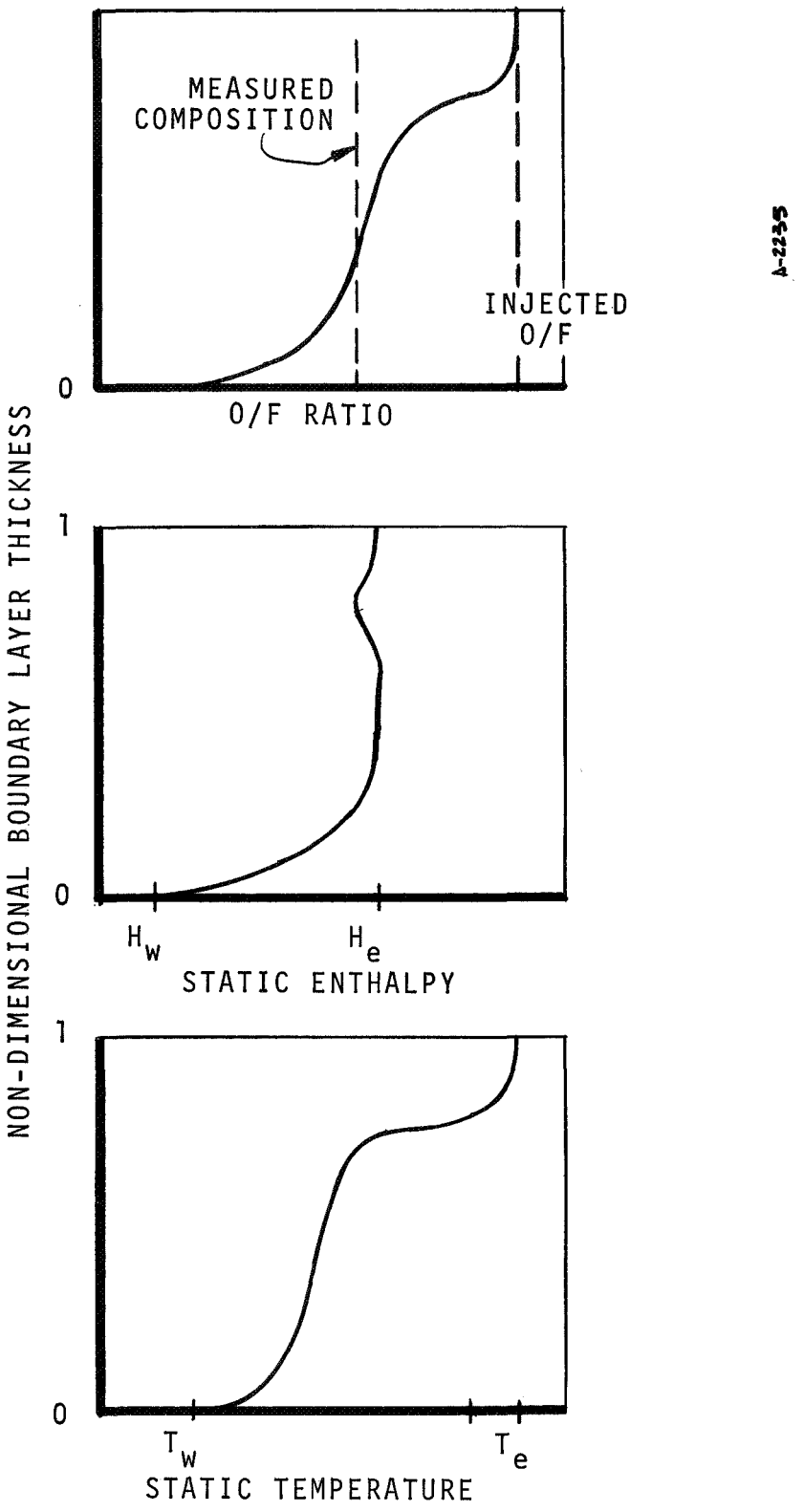

Figure 22. Schematic Representations of Composition, Enthalpy, and Temperature Profiles in the Nonablative Rocket Motor

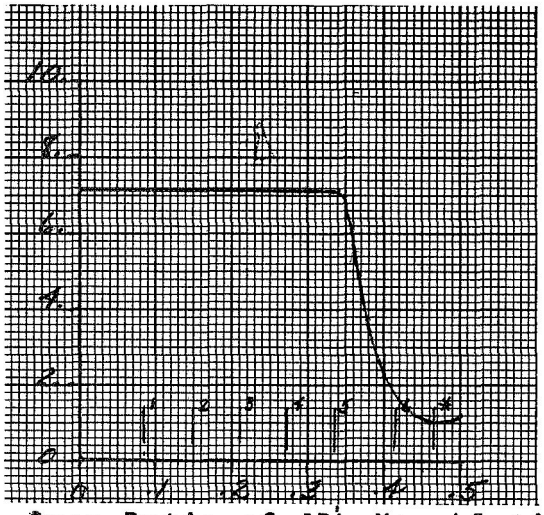

a. Area Ratio of JPL Nonablative Rocket Motor as a Function of Boundary Layer Length (λ)

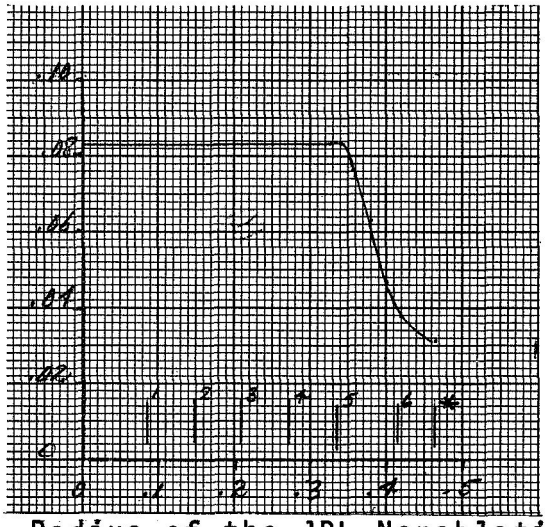

b. Radius of the JPL Nonablative Rocket Motor as a Function of λ

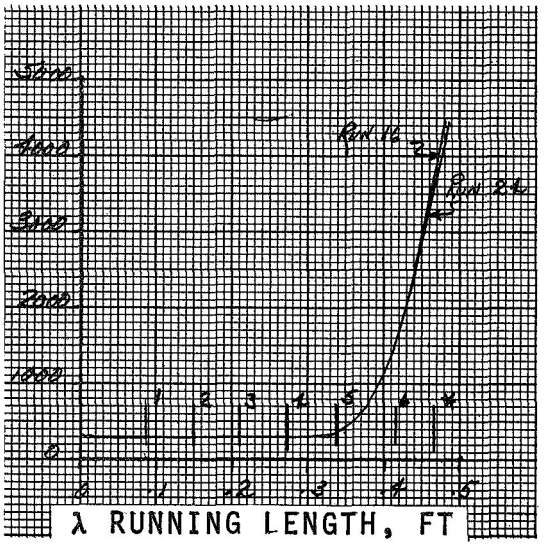

c. Edge Velocity Based on Overall Mixture Ratio

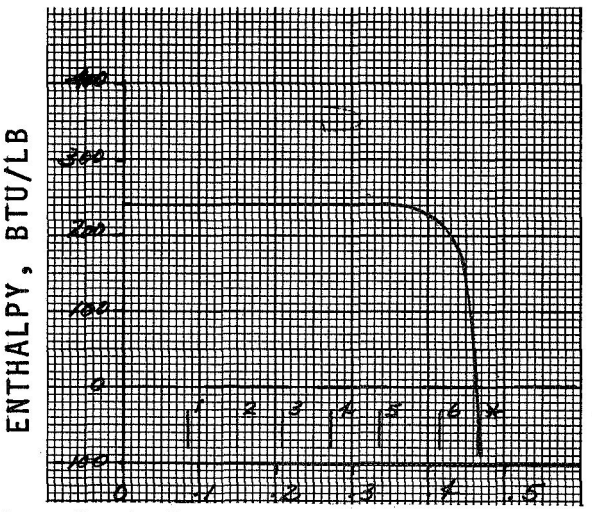

d. Enthalpy Boundary Condition

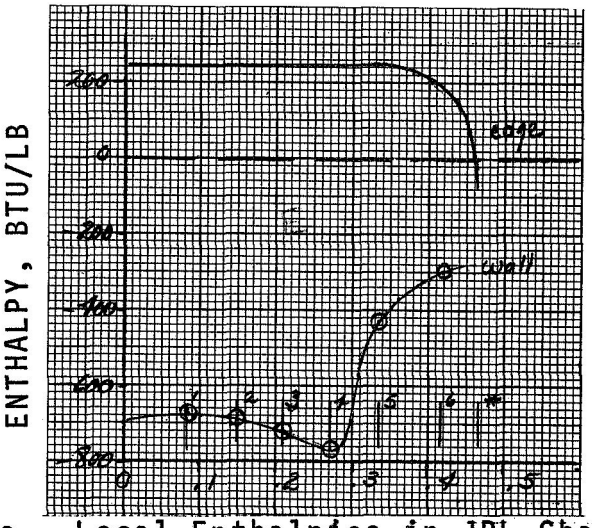

e. Local Enthalpies in JPL Chamber and Nozzle

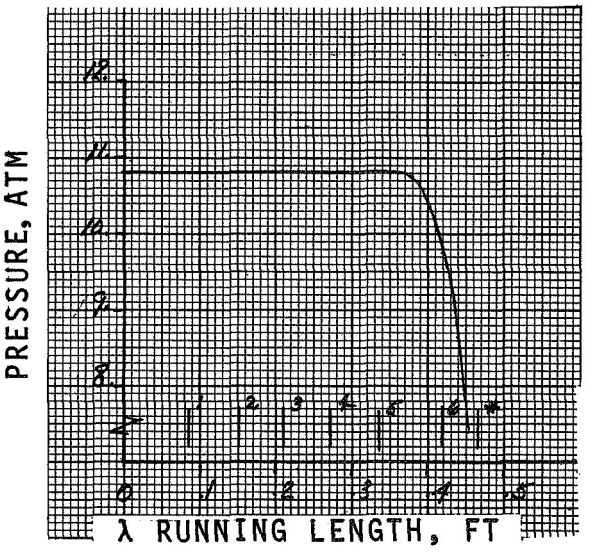

f. Pressure Profile

Figure 23. Boundary Conditions for Heat Transfer Study

Based on the assumption that the gases adjacent to the wall were at wall temperature, the wall enthalpy was defined from the thermodynamic property tables computer by the ACE computer code for the local measured compositions. Figure 23-e shows a typical variation of static wall enthalpy with running length input to the ARGEIBL program. It should be noted that, although the ACE program typically calculates the equilibrium molecular composition of the elemental quantities input to it, this was not done for data from locations 2 and 3 of run 24, since the measured compositions were thought not to be in chemical equilibrium. Instead, these systems were "frozen" at their measured (nonequilibrium) molecular compositions to evaluate their system properties. A complete set of thermodynamic and transport property variations were input to the ARGEIBL code at nine locations in the combustion chamber and nozzle.

5.4 PREDICTION RESULTS

Based on the input assumption presented above, the ARGEIBL code was utilized to predict the boundary layer heat transfer characteristics for the JPL nonablative rocket motor. Predictions were performed at 0.4, 1.4 and 2.4 seconds after ignition for both run 16 and run 24. These runs corresponded to heat flux gage data at the 0 and 90 degree locations. The predictions are presented graphically in Figure 24-a and b. In addition, heat flux gage results corresponding to the prediction locations and time are plotted for the measurement locations. In Figures 25-a and b, the heat transfer coefficient values (based on enthalpy potential) are presented. The transfer coefficient history at the throat must be input to the ablation prediction technique (following section). Notice that both the heat flux and the heat transfer coefficients at the throat decrease with time. This, of course, is due to the increasing surface temperature and the resulting decreases in the energy driving potential and changes in the boundary layer transport properties.

Attention is drawn to two significant characteristics of these figures ; first--the excellent agreement with the experimental data exhibited by the theoretical predictions. In similiar problems the theoretical heat fluxes have had to be factored by at least 0.7 to

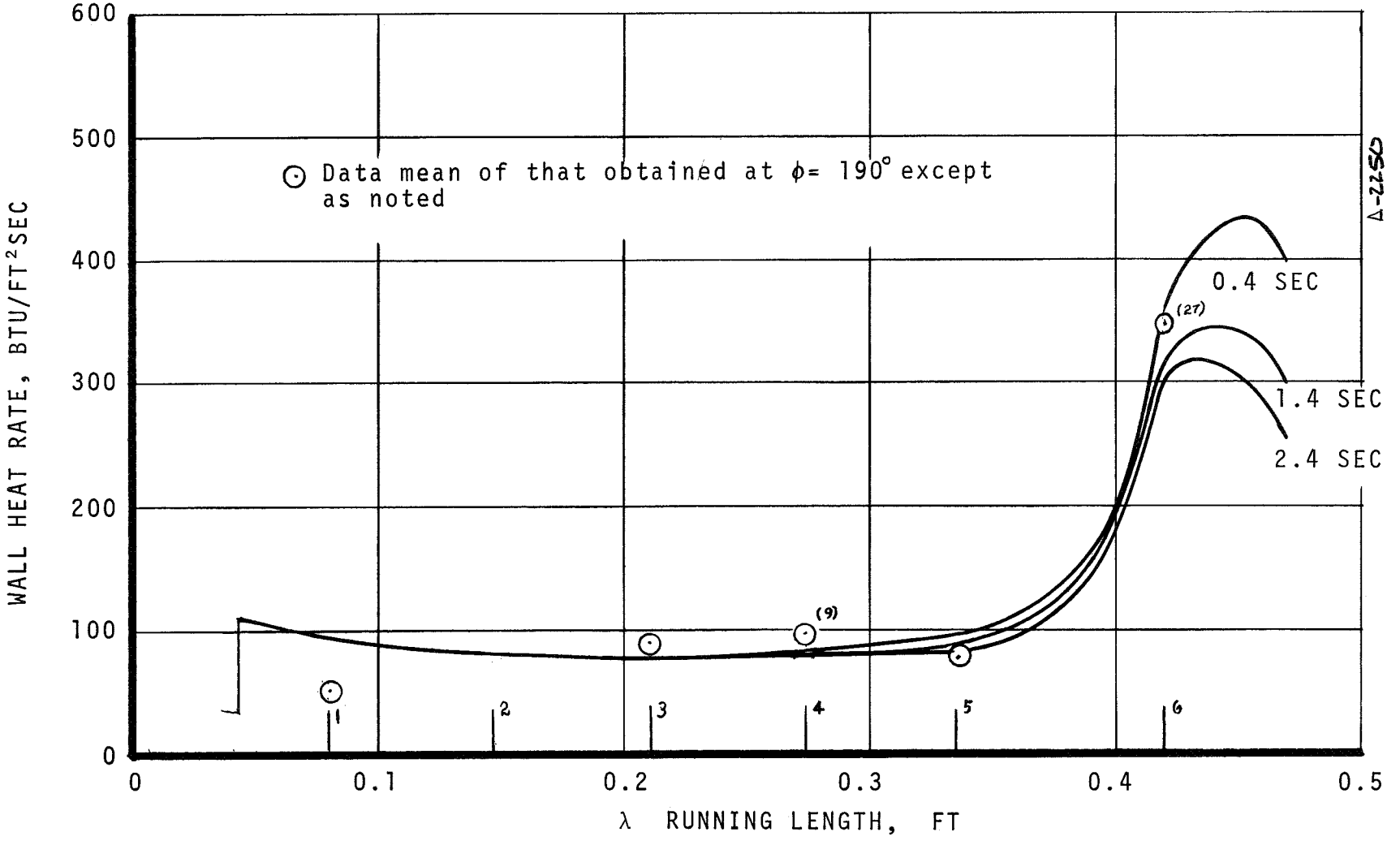

Figure 24. Heat Flux Prediction Comparison with Data
a. Fuel Rich Position, ϕ = 190°

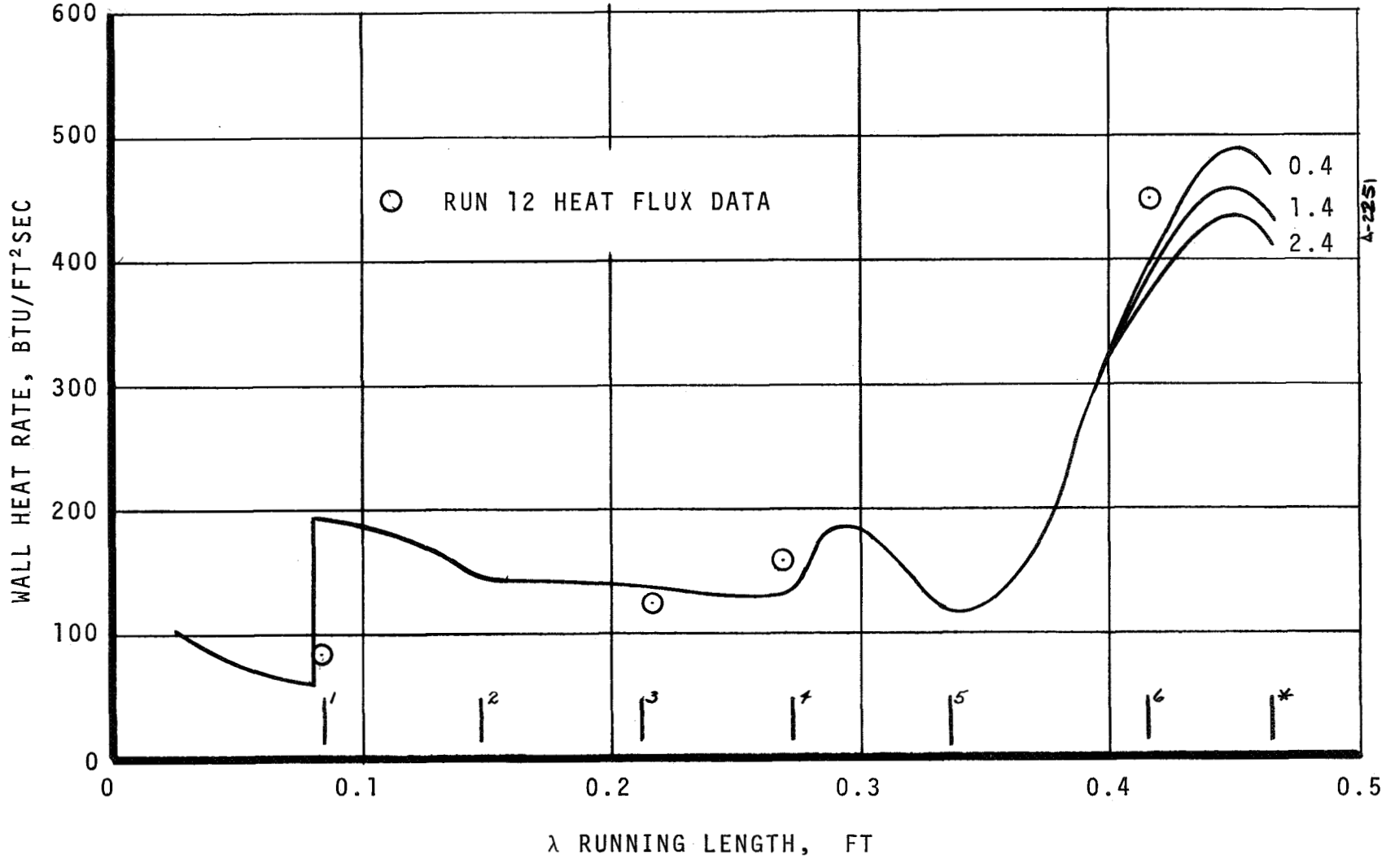

Figure 24. Concluded
b. Oxidizer Rich Position, ϕ = 270°

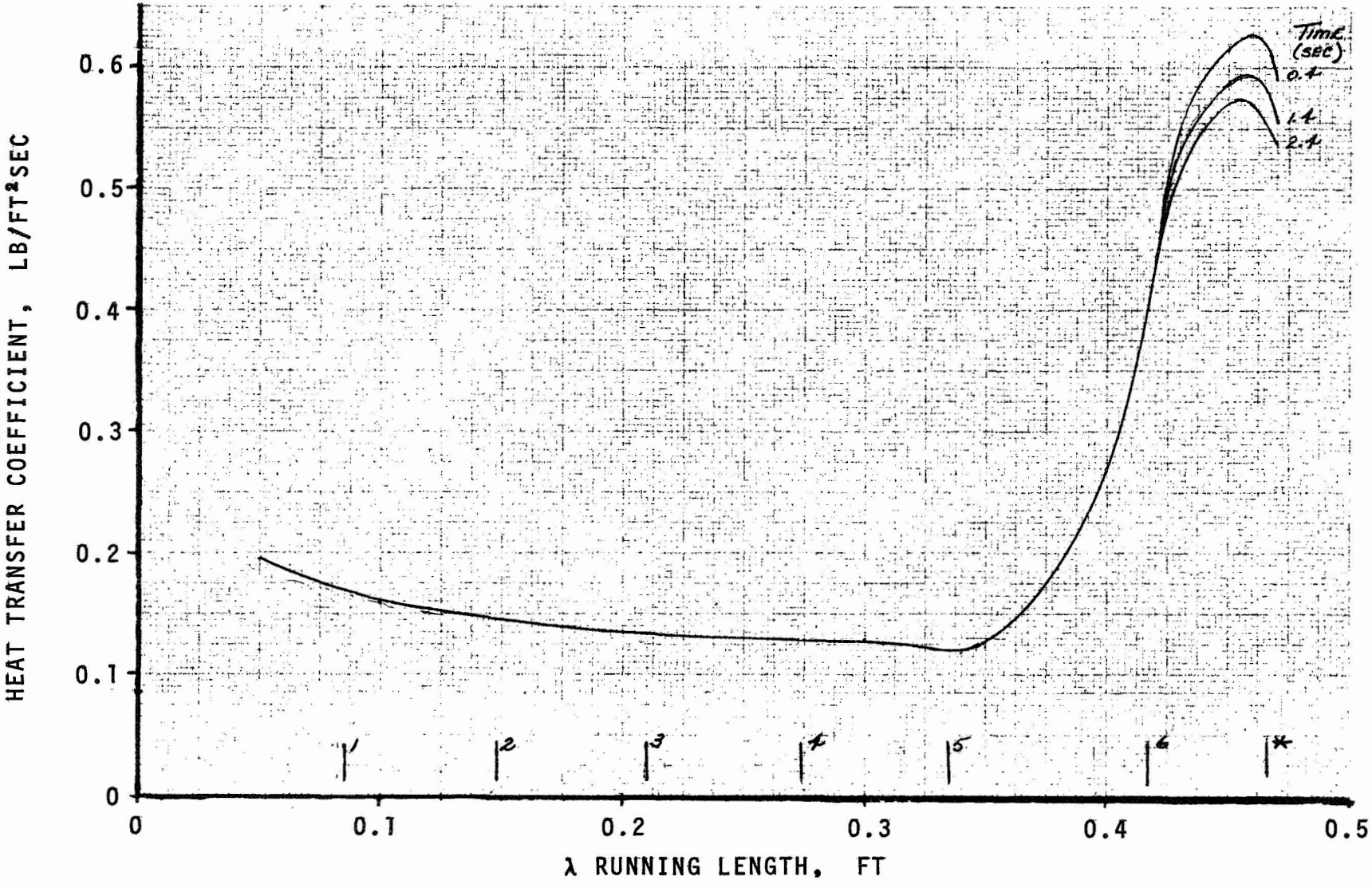

Figure 25. Predicted Heat Transfer Coefficient Variations in the Nonablative Rocket Engine

a. Fuel Rich Position, $\phi = 190^0$

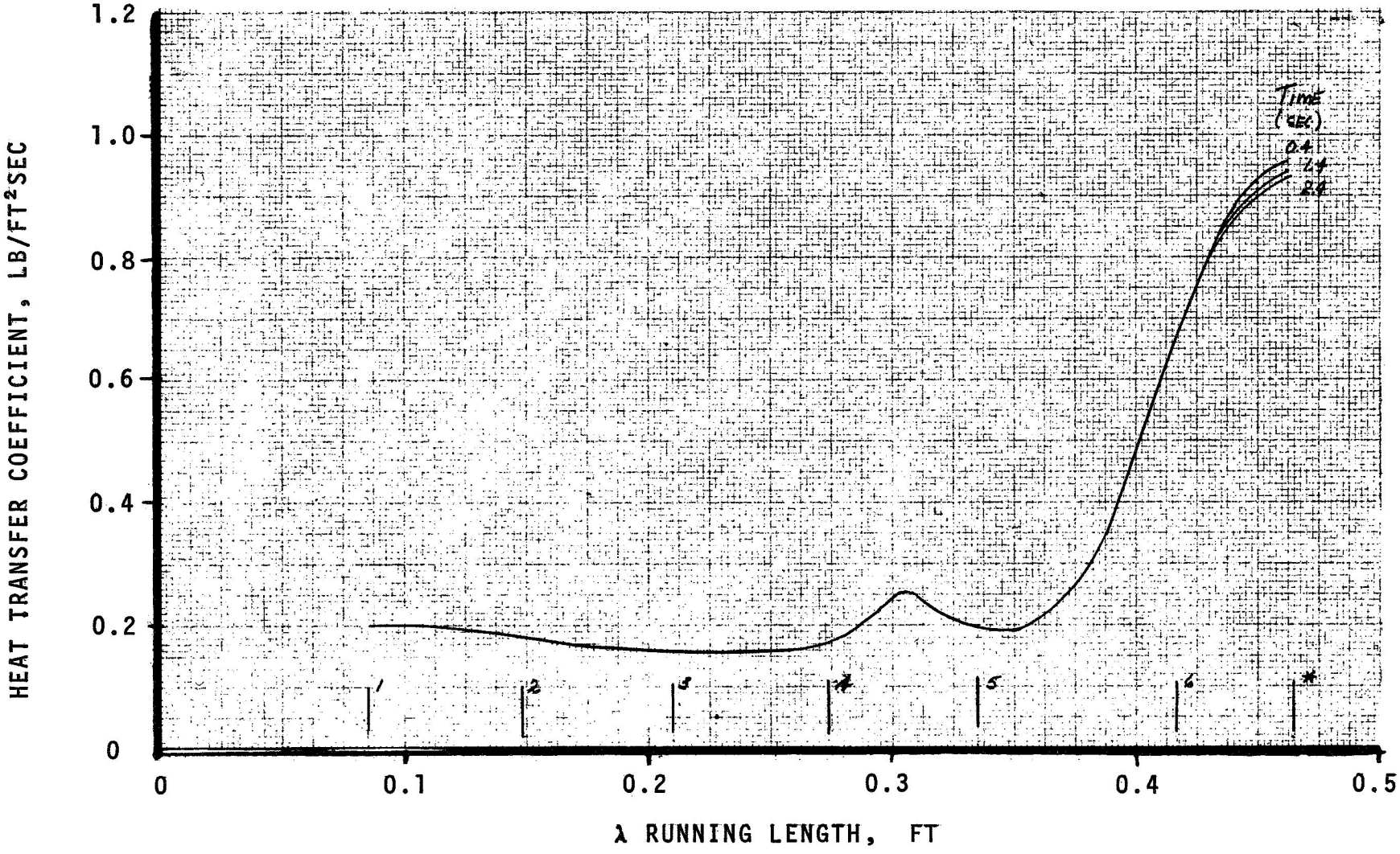

Figure 25. Concluded
b. Oxidizer Rich Position, ϕ = 270°

obtain agreement with experimental data. The agreement obtained here was determined without any iterating or factoring of the data once the edge condition philosphy was chosen. This improvement is,at this time, attributed to the benefit of having composition data.

The second characteristic is the change of level between the two injector positions. Note that the 50% increase (approximately) in heat flux at the oxidizer rich position over the fuel rich position is substantiated by the theoretical predictions. It is also significant to note that this change is far less than the chemistry changes and (as will be shown in the next section) less than the ablation response for the same two positions--a trend also substantiated by the theoretical ablation predictions.

SECTION 6

PREDICTIONS OF THE ABLATIVE RESPONSE OF THE REFRASIL PHENOLIC NOZZLE THROAT

The ablative response of the Jet Propulsion Laboratory Refrasil-phenolic nozzle was predicted for two angular locations in the throat section. Predictions were performed by the Aerotherm Charring Material Ablation (CMA) computer program. The prediction technique considers, among other phenomena, transient heat conduction, material degradation, pyrolyses gas generation, and surface recession. In addition, the CMA program couples the in-depth response of the ablative material to a parametrically input set of thermochemical data points. More complete descriptions of the CMA code are presented in References 16 and 17. The ACE computer code was utilized to evaluate the required surface thermochemistry data for use in the ablation predictions. In the code, a convective coefficient model which considers the effects of unequal species diffusion, surface melt removal, and surface chemical equilibrium, is built into this particular program option. The heat transfer coefficient values required to relate the surface thermochemistry calculations to the surface energy balance calculations performed in the CMA code were computed by the ARGEIBL program described in the preceding section. Some changes in the ARGEIBL input were required to obtain the heat transfer coefficient values for the higher surface temperatures of the ablative materials.

The input to the CMA program including descriptions of the ACE program output and ARGEIBL "hot wall" predictions are presented in Section 6.1.1, and the CMA predictions of the throat response are presented and compared to the data in Section 6.1.2. A portion of the computer output for the fuel rich case is presented in Appendix B.

6.1 COMPUTER CODE INPUT AND ASSUMPTIONS

6.1.1 Input Quantities

The input data required to predict ablative materials response with the CMA code are as follows:

1. Geometrical Constraints
   a. Material geometry (e.g., flat plate or axisymmetric)
   b. Thickness of material
   c. Back wall boundary condition
2. Material Properties as a Function of Temperature
   a. Material decomposition kinetics
   b. Heats of formation of virgin material, char, and pyrolysis gases
   c. Specific heats of virgin material and char
   d. Sensible enthalpy of pyrolysis gases
   e. Thermal conductivity of virgin material and char in the direction normal to the ablating surface
   f. Surface emissivity
3. Surface Boundary Conditions
   a. Boundary layer edge gas recovery enthalpy
   b. Boundary layer edge gas heat transfer coefficient
   c. Ratio of mass to heat transfer coefficients
   d. Incident radiation heat flux
   e. Parametric input of the surface thermochemical response

6.1.2 Discussion of Assumptions and Details of Input Calculations

The geometrical constraints for the problem were defined from drawings of the ablative rocket motor. Figure 2 shows the rocket nozzle contour and Figure 26 schematically presents the nodal network utilized in the CMA predictions. The backwall of the ablative material was assumed to be insulated since, for the firing duration studied here, the heat soak did not reach the back surface.

Since the material properties for Refrasil-phenolic were not available, the properties of a very similar material (MX 2600-96, silica-phenolic) were utilized to perform the predictions. Note that

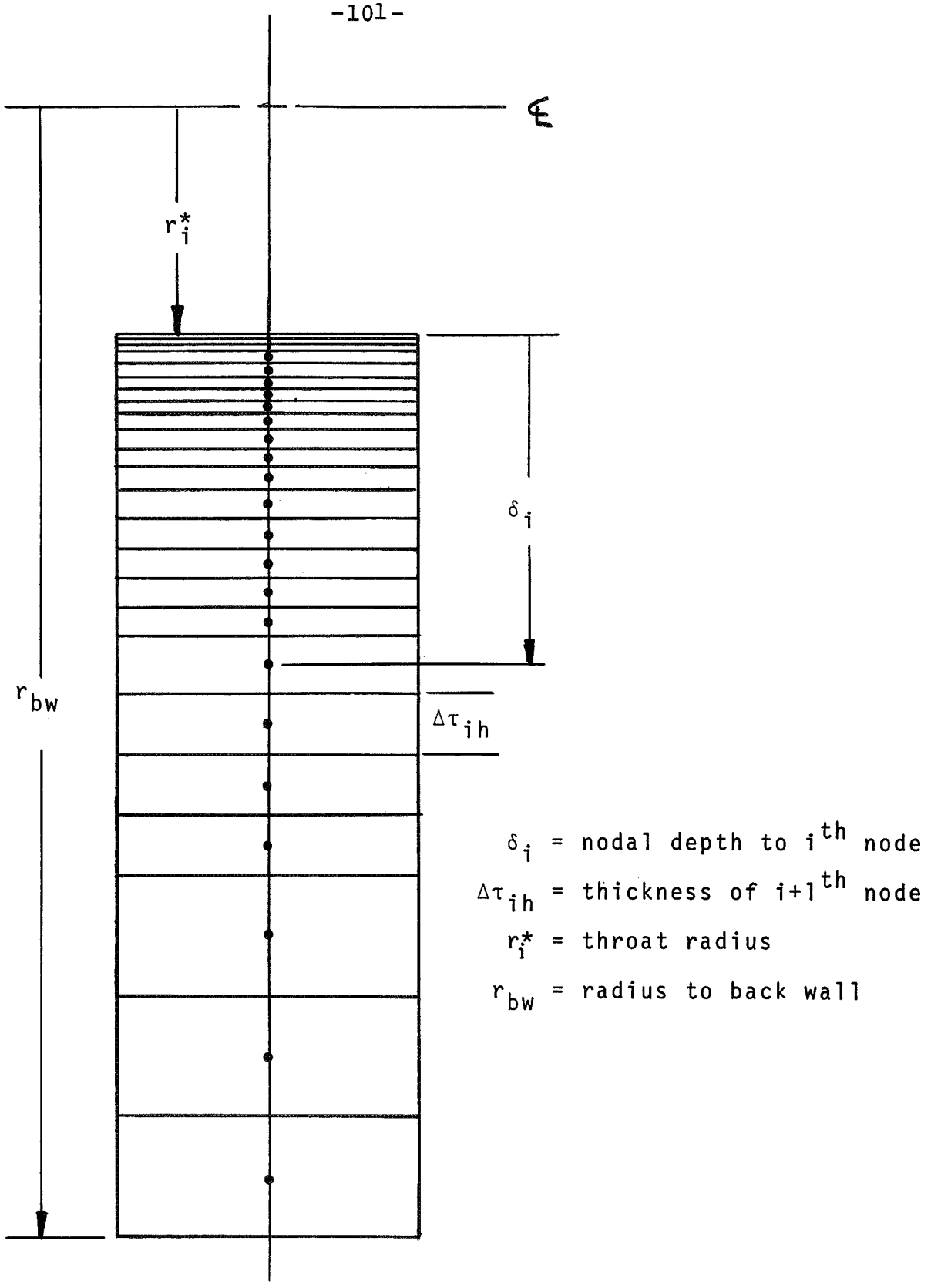

Figure 26. Schematic of CMA Nodal Geometry

both Refrasil-phenolic and MX 2600-96 are silica tape reinforced phenolics with roughly 30 percent resin fraction by mass. The properties of MX 2600-96 utilized in the predictions of the JPL ablative nozzle are given in Reference 18 and are not repeated here. The thermal conductivity was input for the 90 degree lay-up angle direction.

The time dependent surface boundary conditions were basically defined consistent with the assumptions made to predict the nonablative rocket motor heat flux data (Section 5). The principal exception was that the boundary layer gases (assumed to have the same atomic composition as that measured in bottle 6 of the appropriate run) were necessarily at a much higher temperature than in the corresponding cold wall boundary layer. Higher surface temperatures mean, of course, that at the boundary layer edge, the enthalpy would be higher for the bottle composition gases than for the overall mixture ratio gas composition (neglecting products of ablation). In the "hot wall" case, then, the temperature profile through the boundary layer was assumed to be reasonably uniform (i.e., temperature constant with y) and the edge static enthalpy was defined for the bottle composition at a temperature slightly below the temperature for sonic flow of the overall mixture ratio composition. Also the edge velocities were taken as the sonic velocity of the overall mixture for each case considered. The recovery enthalpy was therefore defined.

To obtain the heat transfer coefficient value corresponding to the "hot wall" nozzle, the ARGEIBL program was run for a wall temperature of 4200^{o}R and an edge static condition as defined above. These predictions of heat transfer coefficient applied to all times after the initial temperature rise of the surface and the adjacent boundary layer gases. The transfer coefficients calculated for the nonablative rocket are accurate for any cold wall (as are the "cold wall" edge enthalpies) so that they were applicable to the early times of the phenolic nozzle ablative response predictions. The variations of heat transfer coefficient with time are presented in Figure 27 for the bottle 6 composition of runs 16 and 24.

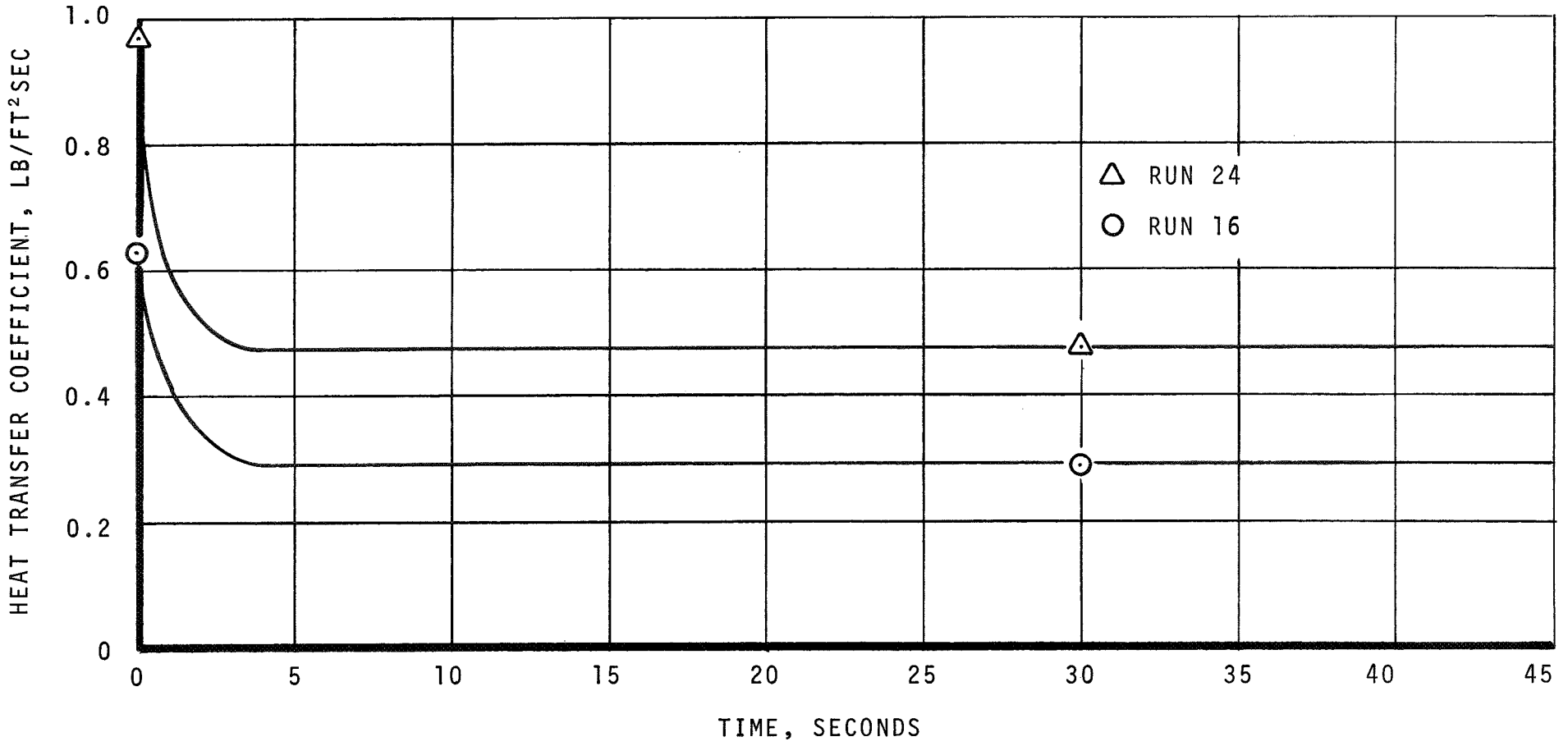

Figure 27. Heat Transfer Coefficient Histories at the Throat of the JPL Ablative Nozzle

The radiative heat transfer from the throat surface was defined as that radiation which leaves the nozzle exit. The remainder of the radiation was re-radiated back from an equal temperature surface through a nonparticipating medium. The radiation view factor from the throat to the exit was taken as 0.05.

The parametric calculations of surface thermochemistry was performed with the ACE computer program. The composition of the edge gases was assumed to be the same as the bottle 6 composition. The surface char material, composed primarily of silica [SiO_2 (liquid)] was assumed to be characterized by a melt temperature of 4200°R. That is, if the surface temperature reached the melt temperature, then the thermochemically controlled surface species could be removed as a liquid. A more complete description of the ACE melt removal ablation model is presented in the references cited earlier. Typical ACE results for the run 16 edge gas condition are presented in Figure 28 in the form of nondimensional ablation rate versus temperature curves for various nondimensional pyrolysis gas rates.

6.2 RESULTS OF ABLATIVE RESPONSE PREDICTIONS

Ablative response predictions were performed for two locations in the JPL Refrasil-phenolic nozzle. The two predictions corresponded to the locations of minimum and maximum measured ablation (i.e., the 190 and 270 degree positions respectively measured from the vertical – refer to Figure 2). The predicted recession rates averaged over a 64 second firing were 3.8 mils/second and 6.9 mils/second for the two positions respectively. These are comparable to the firing data results in Table 6 where the agreement with maximum ablation data is seen to be excellent and that with the minimum – fair. Considering the uncertainties in the measurements and the assumptions required for the analysis, the agreement is amazing.

Figure 29 presents a plot of surface recession rate versus time for runs 16 and 27. In addition, surface temperature versus time is presented in Figure 30 for the two positions.

It is apparent that many physical phenomena are occurring in the combustion chamber and nozzle which were not fully accounted for

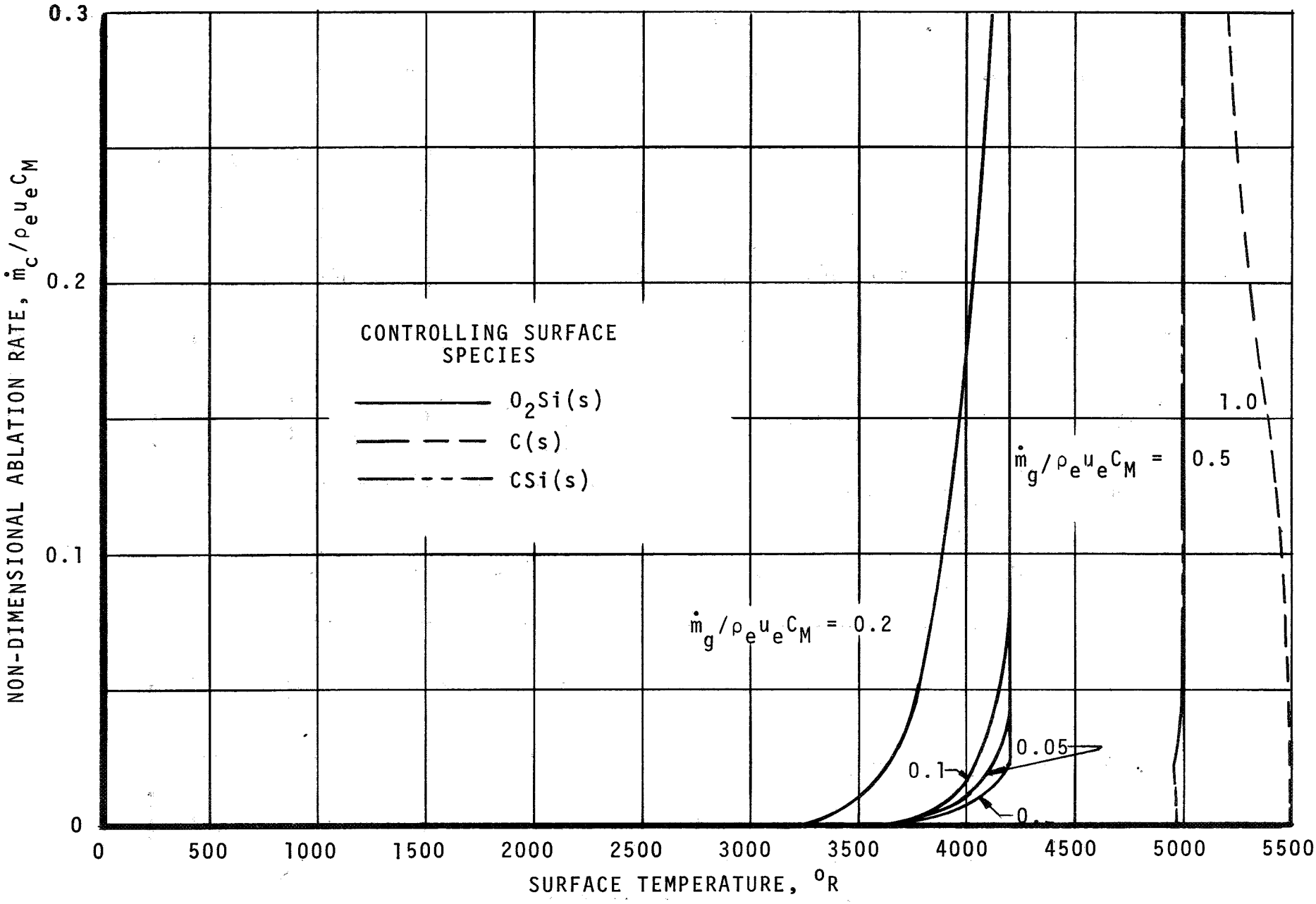

Figure 28. Surface Thermochemistry Data for Refrasil Phenolic Response to Bottle 6, Run 16 Boundary Layer Composition

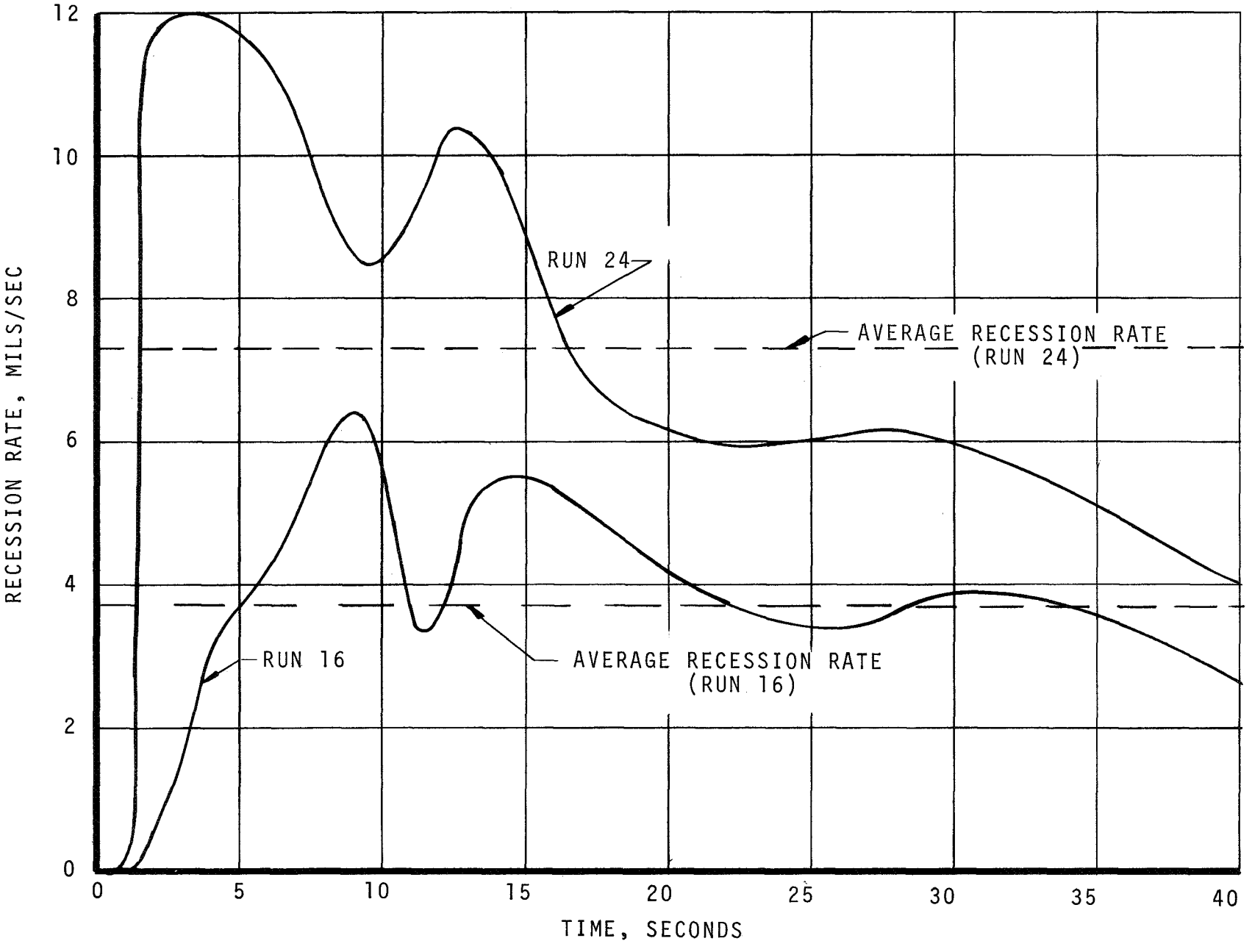

Figure 29. Average Instantaneous Recession Rate Versus Time

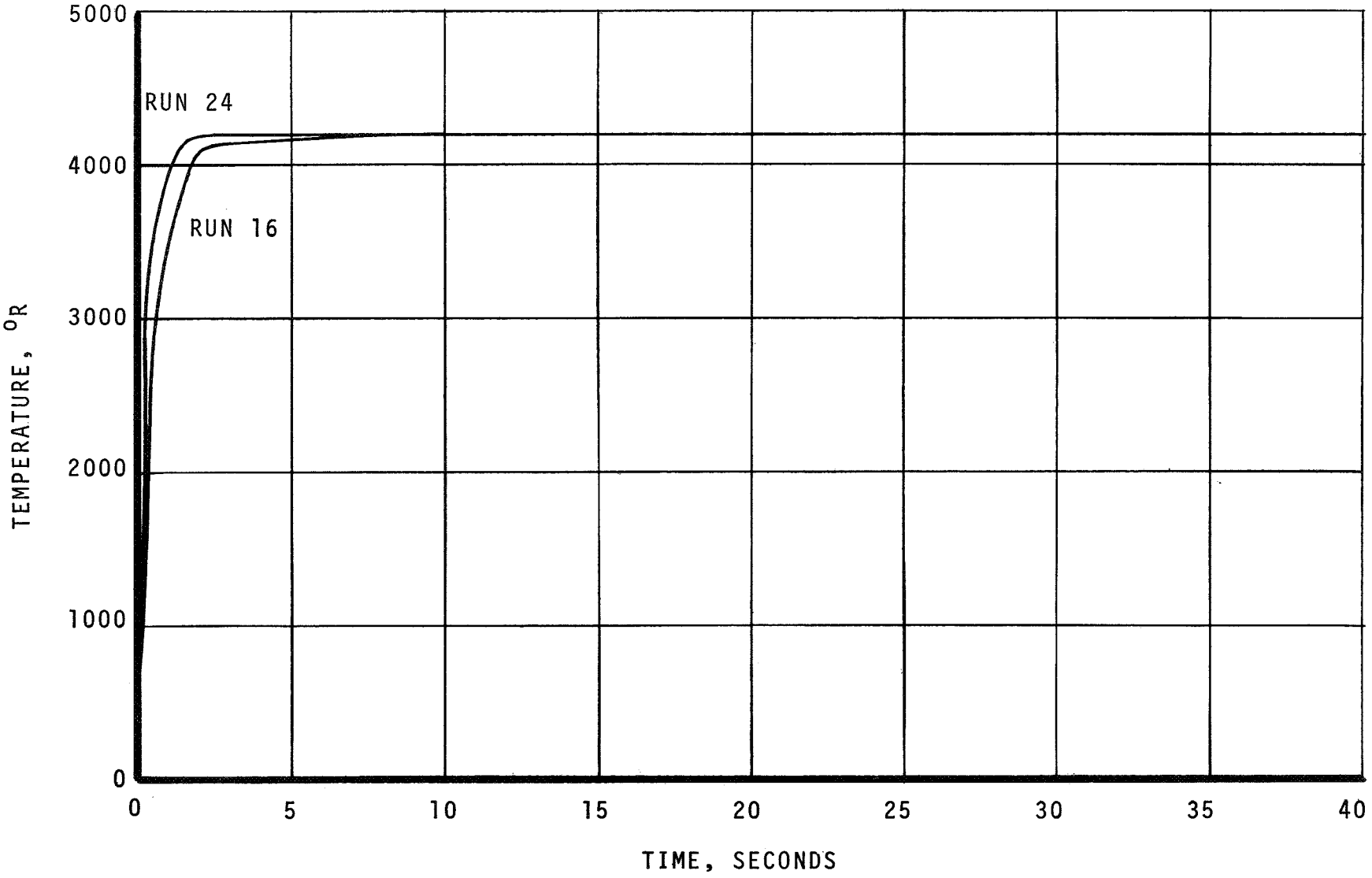

Figure 30. Comparison of Predicted Surface Temperature for Runs 16 and 24 (Ablation Chamber)

by the mathematical models employed in these analyses. An example is the melt removal model which allows the surface to be removed mechanically only at a fixed temperature. Although the temperature chosen is representative of the silica failing temperature, the material actually flows for a wide range of temperatures. The model, moreover, does not consider the melt flow from the upstream surface to the prediction station (which apparently did occur). In addition, since the surface and in-depth solutions are one-dimensional, the effect of nonaxisymmetric heat conduction and ablation are not considered. The differences between the two predictions are, therefore, due only to variations in the surface boundary condition (i.e., composition related differences). It should be noted that all of the effects described above are of secondary importance to the accuracy of the predictions as the results attest. Indeed, since the predictions agree with the data, it is expected that further predictions would be valuable additions to the ablative rocket nozzle analysis literature.

TABLE 6

COMPARISON OF PREDICTED AND MEASURED ABLATION

	Recession Inches	
Azimuth-ϕ	Actual	Predicted
270°*	0.4	0.44
160°	~.0	0.24

Firing Time = 64 seconds

*Maximum ablation point

REFERENCES

1. Rowley, R. W.: An Experimental Investigation of Uncooled Thrust Chamber Materials for Use in Storable Liquid Propellant Rocket Engines. Jet Propulsion Laboratory, California Institute of Technology, Pasadena, California, JPL-TR-32-561, February 15, 1964.

2. Rowley, R. W. and Tyler, W. H.: The Effect of Injector Design on Thrust-Chamber Erosion. AIAA Paper No. 65-586, presented at AIAA Propulsion Joint Specialist Conference, Colorado Springs, Colorado, June 14-18, 1965.

3. Personal communication with Donald Bond.

4. Johnson, B. H.: An Experimental Investigation of the Effects of Combustion on the Mixing of Highly Reactive Liquid Propellants. Jet Propulsion Laboratory, California Instititute of Technology, JPL-TR-32-689, July 15, 1965.

5. Rupe, J. H. and Jaivin, G. I.: The Effects of Injection Mass Flux Distributions and Resonant Combustion on Local Heat Transfer in a Liquid-Propellant Rocket Engine. Jet Propulsion Laboratory, California Institute of Technology, Pasadena, California, JPL-TR-32-648, October 1, 1964.

6. Kit, Boris and Evered, D. S.: Rocket Propellant Handbook. The MacMillan Company, New York, 1960.

7. Kendall, R. M. and Bartlett, E. P.: Nonsimilar Solution of the Multicomponent Laminar Boundary Layer by an Integral Matrix Method, AIAA Journal, Vol. 6, No. 6, June 1968, pp. 1089-1097.

8. Bartlett, E. P., Kendall, R. M., and Rindal, R. A.: A Unified Approximation for Mixture Transport Properties for Multicomponent Boundary Layer Applications. Aerotherm Corporation, Mountain View, California, Final Report No. 66-7, Part IV, March 14, 1967 (also NASA CR -1063).

9. Anderson, L. W.: User's Manual, Boundary Layer Integral Matrix Procedure (BLIMP). Aerotherm Corporation, Mountain View, California (to be published).

10. Vidya Staff: Effects of Supersonic Aircraft Speed upon Aerial Photography. Vidya Division, Itek Corporation, Palo Alto, California, Vidya Report No. 37, 1961.

11. Ambrok, G. S.: Approximate Solution of Equations, Thermal Boundary Layer with Variations in Boundary Layer Structure. Soviet Physics. Tech. Physics, Vol. 2, No. 9, 1957, pp. 1979.

12. Mayer, E.: Analysis of Convective Heat Transfer in Rocket Nozzles. ARS Jour., July 1961.

REFERENCES (concluded)

13. Massier, P. F., Gier, H.L., Witte, A. B., and Harper, E. Y.: Jet Propulsion Labortory Research Summary No. 36-11, for the period August 1, 1961 to October 1, 1961, pp. 80-89.

14. McCuen, P. A., Schaefer, J. W., Lundberg, R. E. and Kendall, R.M.: A Study of Solid-Propellant Rocket Motor Exposed Materials Behavior. AFRPL-TR-65-33. Vidya Report No. 149, Vidya Division of Itek Corporation., February 26, 1965.

15. Schneider, P. J.: Temperature Response Charts. John Wiley & Sons, Inc., New York, 1963.

16. Moyer, C. B. and Rindal, R. A.: Finite Difference Solution for the In-Depth Response of Charring Materials Considering Surface Chemical and Energy Balances. NASA CR-1061 (Aerotherm Report No. 66-7, Part II), March 14, 1967.

17. User's Manual, Charring Ablation (CMA) Computer Program, Version 2, Aerotherm Corporation, January 1969.

18. Schaefer, J. W., Dahm, T. J., Rodriguez, D. A., Reese, J. J., Jr., and Wool, M. R.: Studies of Ablative Material Performance for Solid Rocket Nozzle Applications. NASA CR-72429 (Aerotherm Report No. 68-30), March 1, 1968.

APPENDIX A

BLIMP SOLUTION EXAMPLES

Run 1-O/F=.5 at wall

```
BOUNDARY LAYER INTEGRAL MATRIX PROGRAM (BLIMP)

AEROTHERM CORPORATION,PALO ALTO,CALIF (RMK,EPB)      IDENTIFICATION

CASE 7009 FLAT PLATE, O/F=1,3 AT EDGE AND .5 AT WALL, UNEQ, DIFF,

CONTROL NUMBERS  1  2  3  4  5  6  7  8  9 10 11 12 13 14 15 16 17 18 19 20

                 1  3  2  0  4  3  2  0  2  0  0  2  0  0  0  0  0  1  0  0


  U/UE TO       NODAL PT,                       ETA VALUES
 NORM, ETA      AT WHICH
                ETA NORM,
 .9,500-01         11         0.000     2,400-02  4,000-02  7,200-02  1,200-01  2,000-01  3,200-01  4,800-01  8,000-01
                              1,400+00  2,000+00  3,200+00  5,000+00

CASE                       1,00000+00

TOTAL ENTHALPY,BTU/LB      2.43000+02

TOTAL PRESSURE,ATM         1,09000+01

INCIDENT RAD FLUX,B/SF2 -0,00000

   MIXING LENGTH CONSTANT   =  4,4000-01
   SUBLAYER CONSTANT, YA+   =  1,1823+01
   CLAUSER NUMBER           =  1,9000-02
   TURBULENT SCHMIDT NUMBER=  7,5000-01
   TURBULENT PRANDTL NUMBER=  7,5000-01
   TRANSITION MOM,THICK,RE =  2,5000+02


   CASE    ,10000+01 - - - - - - - - - - - - - - - - - - - - - - - - - - 23 APR 69 17:44:56
                NUMBER OF ELEMENTS= 3     DIFFUSION EXPONENT=  ,4310     CURVE FIT MOL, WT,=23,400

                                               REFERENCE PROPERTIES

                            MOLECULAR WEIGHT=32,000      SIGMA=3,4670     EPSILON/K= 106,70


RELATIVE ELEMENTAL COMPOSITIONS, ATOMIC WTS/UNIT MASS
     AT,NO.   ELEMENT     ATOMIC WT     EDGE GAS      PYRO,GAS 1     CHAR 1       PYRO,GAS 2     CHAR 2       PYRO,GAS 3     CHAR 3
       1     HYDROGEN      1,00797      ,0540712      -,0000000     -,0000000     -,0000000     -,0000000     -,0000000     -,0000000
       7     NITROGEN     14,00800      ,0393138      -,0000000     -,0000000     -,0000000     -,0000000     -,0000000     -,0000000
       8      OXYGEN      16,00000      ,0246744      -,0000000     -,0000000     -,0000000     -,0000000     -,0000000     -,0000000
4,  1 2,  7 0,  0 0,  0 0,  0 0,  0 0,  0                           H4N2
   ,22790+05     ,68536+05    .22986+02    ,24193-02   -,19593+07    ,10810+03 3000,0000 1
   ,22790+05     ,68536+05    ,31432+02    ,48794-04   -,13970+08    ,10810+03 5000,0000 1 1,1452
2,  7 4,  8 0,  0 0,  0 0,  0 0,  0 0,  0                           N2O4
   ,21700+04     ,78597+05    ,29773+02    ,59443-03   -,17883+07    ,13491+03 3000,0000 1
   ,21700+04     ,78597+05    ,31781+02    ,17563-05   -,38597+07    ,13491+03 5000,0000 1 1,8042
1,  8 0,  0 0,  0 0,  0 0,  0 0,  0 0,  0                           O
   ,59559+05     ,13522+05    ,49723+01    ,38077-05    ,15475+05    ,50096+02 3000,0000 1
   ,59559+05     ,13522+05    ,65749+01  -,22427-03   -,89178+07    ,50096+02 5000,0000 1   ,7397
2,  1 0,  0 0,  0 0,  0 0-  0 0,  0 0,  0                           H2
   ,00000        ,21321+05    ,62748+01    ,95547-03    ,37158+05    ,48506+02 2000,0000 1
   ,00000        ,21208+05    ,79548+01    ,37918-03   -,20717+07    ,48464+02 4000,0000 1   ,3893
2,  1 1,  8 0,  0 0,  0 0,  0 0,  0 0,  0                           H2O
  -,57798+05     ,30769+05    ,75011+01    ,23601-02   -,29281+05    ,68634+02 2000,0000 1
  -,57798+05     ,30209+05    ,13230+02    ,25103-03   -,61512+07    ,68422+02 4000,0000 1   ,7749
3,  1 1,  7 0,  0 0,  0 0,  0 0,  0 0,  0                           H3N
  -,10970+05     ,42561+05    ,98741+01    ,37069-02   -,27151+06    ,77258+02 2000,0000 1
  -,10970+05     ,41634+05    ,17390+02    ,78927-03   -,71540+07    ,76908+02 4000,0000 1   ,8721
2,  7 0,  0 0,  0 0,  0 0,  0 0,  0 0,  0                           N2
   ,00000        ,22430+05    ,69778+01    ,81617-03   -,36596+05    ,63865+02 2000,0000 1
   ,00000        ,22165+05    ,88319+01    ,59748-04   -,14065+07    ,63765+02 4000,0000 1 1,0262
1,  1 0,  0 0,  0 0,  0 0,  0 0,  0 0,  0                           H
   ,52102+05     ,13423+05    ,48022+01    ,55547-04    ,17309+06    ,38862+02 3000,0000 1
   ,52102+05     ,13423+05    ,30875+01    ,31502-03    ,92974+07    ,38862+02 5000,0000 1   ,3018
1,  1 1,  8 0,  0 0,  0 0,  0 0,  0 0,  0                           HO
   ,93300+04     ,21404+05    ,77319+01    ,39439-03   -,97356+06    ,61382+02 3000,0000 1
   ,93300+04     ,21404+05    ,96514+01  -,44353-04   -,68611+07    ,61382+02 5000,0000 1   ,8715
1,  7 1,  8 0,  0 0,  0 0,  0 0,  0 0,  0                           NO
   ,21580+05     ,22700+05    ,87762+01    ,89903-04   -,78966+06    ,68849+02 3000,0000 1
   ,21580+05     ,22700+05    ,91626+01    ,65788-05   -,21252+07    ,68849+02 5000,0000 1   ,9981
2,  8 0,  0 0,  0 0,  0 0,  0 0,  0 0,  0                           O2
   ,00000        ,23540+05    ,76310+01    ,71015-03   -,89282+05    ,68008+02 2000,0000 1
   ,00000        ,23455+05    ,88335+01    ,30128-03   -,17061+07    ,67975+02 4000,0000 1 1,0000
```

CP-FROZEN	CP-EQUIL	DLNM/DLNT	DLNM/DLNP	GAMMA
,52593-00	,13928+01	-,43093-00	,21124-01	,11384+01

TEMP = 3094,1519 DEG-K PRES = 10,8673 ATM MOL WT = 20,4691120
RELATIVE MASSES OF COMPONENTS 1,2 AND 3 ,00000 ,00000 ,00000
ENTHALPY = ,1340974+03 CAL/GM ENTROPY = ,30291+01 CAL/GM-DEG K
DENSITY = ,546872-01 LB/CUFT
VEL = ,285+03 FT/SEC MACH = ,727-01 AREA = ,641-01 SQFT/LB/SEC

SPECIES	MOLE FR,	SPECIES	MOLE FR,	SPECIES	MOLE FR,
H4N2	,14677-13	N2O4	,38607-17	O	,44164-02
H2	,87003-01	H2O	,43960-00	H3N	,11523-05
N2	,39829-00	H	,18613-01	HO	,34971-01
NO	,81443-02	O2	,89667-02		

CP-FROZEN	CP-EQUIL	DLNM/DLNT	DLNM/DLNP	GAMMA
,52593-00	,13928+01	-,43093-00	,21124-01	,11384+01

TEMP = 3094,1519 DEG-K PRES = 10,8673 ATM MOL WT = 20,4691110
RELATIVE MASSES OF COMPONENTS 1,2 AND 3 ,00000 ,00000 ,00000
ENTHALPY = ,1340974+03 CAL/GM ENTROPY = ,30291+01 CAL/GM-DEG K
DENSITY = ,546872-01 LB/CUFT
VEL = ,285+03 FT/SEC MACH = ,727-01 AREA = ,641-01 SQFT/LB/SEC

SPECIES	MOLE FR,	SPECIES	MOLE FR,	SPECIES	MOLE FR,
H4N2	,14677-13	N2O4	,38607-17	O	,44164-02
H2	,87003-01	H2O	,43960-00	H3N	,11523-05
N2	,39829-00	H	,18613-01	HO	,34971-01
NO	,81443-02	O2	,89667-02		

CP-FROZEN	CP-EQUIL	DLNM/DLNT	DLNM/DLNP	GAMMA
,52593-00	,13928+01	-,43093-00	,21124-01	,11384+01

TEMP = 3094,1519 DEG-K PRES = 10,8673 ATM MOL WT = 20,4691110
RELATIVE MASSES OF COMPONENTS 1,2 AND 3 ,00000 ,00000 ,00000
ENTHALPY = ,1340974+03 CAL/GM ENTROPY = ,30291+01 CAL/GM-DEG K
DENSITY = ,546872-01 LB/CUFT
VEL = ,285+03 FT/SEC MACH = ,727-01 AREA = ,641-01 SQFT/LB/SEC

SPECIES	MOLE FR,	SPECIES	MOLE FR,	SPECIES	MOLE FR,
H4N2	,14677-13	N2O4	,38607-17	O	,44164-02
H2	,87003-01	H2O	,43960-00	H3N	,11523-05
N2	,39829-00	H	,18613-01	HO	,34971-01
NO	,81443-02	O2	,89667-02		

DISTANCE,FT	,10000-01	,85000-01	,14820-00	,21070-00	,27300-00	,33580-00	,41290-00
ROKAP	,10000+01	,10000+01	,10000+01	,10000+01	,10000+01	,10000+01	,10000+01
XI,(LB/SEC)**2	,87114-05	,74047-04	,12910-03	,18355-03	,23782-03	,29253-03	,35969-03
PRESSURE RATIO	,99700-00	,99700-00	,99700-00	,99700-00	,99700-00	,99700-00	,99700-00
STATIC PRESSURE,ATM	,10867+02	,10867+02	,10867+02	,10867+02	,10867+02	,10867+02	,10867+02
EDGE VELOCITY,FT/SEC	,28519+03	,28519+03	,28519+03	,28519+03	,28519+03	,28519+03	,28519+03
BETA	,21102-05	,43750-05	,55266-05	-,10631-04	-,38634-05	,79052-06	-,17320-04
INCIDENT RADIATION FLUX	,00000	,00000	,00000	,00000	,00000	,00000	,00000
ENTROPY DROP,BTU/LB R	,00000	,00000	,00000	,00000	,00000	,00000	,00000
WALL TEMPERATURE,DEG R	,80000+03	,80000+03	,80000+03	,80000+03	,80000+03	,80000+03	,80000+03
COMP FLUX,LB/SEC FT**2	-,00000	-,00000	-,00000	-,00000	-,00000	-,00000	-,00000
COMP FLUX,LB/SEC FT**2	-,00000	-,00000	-,00000	-,00000	-,00000	-,00000	-,00000
COMP FLUX,LB/SEC FT**2	-,00000	-,00000	-,00000	-,00000	-,00000	-,00000	-,00000

CASE ,10000+01 - - - - - - - STREAMWISE DIMENSION ,10000+01FEET * * *, 23 APR 69 17144156

ITERATED VALUES

ITS	TIME	ALPH	FPPW	DAMP	MAX,LIN ERROR	MAX,ERRORS IN CONSERVATION EQS, MOMENTUM	ENERGY	H4N2	N2O4
1	3,010	5,000	,7500	,3333	2,-01	5 3,0+00 12	-1,2+03 12	9,2=01 12	-8,9-01 0

ALPHA	XI (LB /SEC)**2	ROKAP (FT)	PRESSURE (ATM)	EDGE VELOCITY (FT/SEC)	BETA	FLUX NORMALIZING PARAMETER	DIFFUSIONAL TOT ENTH (BTU/SEC SQ FT)	HEAT FLUXES RERAD
5,000+00	8,711-06	1,000+00	1,087+01	2,852+02	0,000	2,087+01	=0,000 =0,000	0,000

WALL SHEAR (LB/SQ FT)	MECH REM	MASS FLUXES PYROL GAS (LB/SEC SQ FT)	CHAR	TOTAL GAS	ELEMENTAL MASS DIFFUSIVE FLUXES (LB/SEC SQ FT) FOR HYDROGEN	NITROGEN	OXYGEN
1,120+00	0,000	0,000	0,000	0,000	=0,000	=0,000	=0,000

MOM TRANS COEFF, RHO*UE*CF/2	HEAT TRANS COEFF, RHO*UE*CH	BLOWING PARAMETERS (BASED ON CH) FOR PYROL GAS	CHAR	TOTAL GAS	ELEMENTAL MASS TRANSFER COEFFICIENTS, RHOE*UE*CM (LB/SEC SQ FT) FOR HYDROGEN	NITROGEN	OXYGEN
1,264-01	0,000	0,000	0,000	0,000	0,000	0,000	0,000

MOMENTUM THICKNESS, THETA (FT)	DISPLACE, THICKNESS, DELSTAR (FT)	SHAPE FACTOR, DELSTAR /THETA	ENTHALPY THICKNESS, LAMBDA (FT)	REYNOLDS NUMBER PER FOOT	MASS THICKNESSES (FT) FOR HYDROGEN	NITROGEN	OXYGEN
4,669-04	6,225-04	1,333+00	1,073-03	2,792+05	4,290-03	6,899-03	6,427-03

NODAL INFORMATION

DISTANCE FROM WALL (FT)	ETA	F	FP (#U/UE)	FPP	FPPP	TOTAL ENTHALPY,G (BTU/LB)	GP (BTU/LB)	GPP (BTU/LB)	STATIC ENTHALPY (BTU/LB)	TEMP (DEG R)
0,000	0,000	0,000	0,000	7,500-01	=1,797+01	=1,380+02	0,000	1,628-02	=1,380+02	3,115+03
2,427-05	1,200-01	1,916-03	1,700-02	3,411+03	5,530+00	=1,380+02	=1,104-03	=3,257-02	=1,380+02	3,115+03
4,045-05	2,000-01	3,619-03	2,800-02	1,845+01	=1,004+00	=1,380+02	3,600-03	1,479-01	=1,380+02	3,114+03
7,280-05	3,600-01	9,989-03	5,000-02	1,239+01	2,470-01	=1,380+02	=1,893-02	=4,302-01	=1,380+02	3,115+03
1,213-04	6,000-01	2,595-02	8,400-02	1,476+01	=4,976-02	=1,380+02	8,951-02	1,334+00	=1,380+02	3,115+03
2,022-04	1,000+00	7,092-02	1,400-01	1,348+01	=1,396-02	=1,380+02	=4,458-01	=4,010+00	=1,380+02	3,114+03
3,236-04	1,600+00	1,789-01	2,200-01	1,345+01	1,304-02	=1,380+02	2,095+00	1,248+01	=1,381+02	3,114+03
4,855-04	2,400+00	3,987-01	3,300-01	1,382+01	=3,936-03	=1,330+02	9,570+00	6,211+00	=1,332+02	3,123+03
8,133-04	4,000+00	1,099+00	5,400-01	1,205+01	=1,815-02	=1,120+02	1,527+01	9,098-01	=1,125+02	3,223+03
1,456-03	7,000+00	3,179+00	8,200-01	6,619-02	=1,807-02	=5,500+01	2,510+01	5,648+00	=5,609+01	3,569+03
2,160-03	1,000+01	5,865+00	9,500-01	2,473-02	=9,569-03	4,000+01	3,632+01	1,833+00	3,853+01	4,184+03
3,723-03	1,600+01	1,176+01	9,900-01	=7,522-04	1,075-03	1,950+02	=6,471-01	=1,416+01	1,934+02	5,343+03
6,166-03	2,500+01	2,071+01	1,000+00	0,000	=9,079-04	2,430+02	0,000	1,430+01	2,414+02	5,565+03

DISTANCE FROM WALL (FT)	DENSITY, RHO (LB/CU FT)	VISCOSITY, MU LB/SEC FT	RHO*MU /RHOE*MUE, C	SPECIFIC HEAT (BTU/LB R)	THERMAL COND (BTU /SEC FT R)	PRANDTL NUMBER	MODIFIED SCHMIDT NUMBER	MOLECULAR WEIGHT	RHOSQ*EPS /RHOE*MUE	MACH NUMBER
0,000	7,237-02	3,408-05	8,073+01	5,876+01	4,057-05	4,936+01	7,283+01	1,515+01	0,000	0,000
2,427-05	7,237-02	3,408-05	8,073+01	5,876+01	4,057-05	4,936+01	7,283+01	1,515+01	0,000	1,337-03
4,045-05	7,238-02	3,407-05	8,073+01	5,876+01	4,056-05	4,936+01	7,283+01	1,515+01	0,000	2,202-03
7,280-05	7,237-02	3,408-05	8,073+01	5,876+01	4,057-05	4,936+01	7,283+01	1,515+01	0,000	3,931-03
1,213-04	7,237-02	3,408-05	8,073+01	5,876+01	4,057-05	4,936+01	7,283+01	1,515+01	0,000	6,604-03
2,022-04	7,237-02	3,408-05	8,073+01	5,876+01	4,057-05	4,936+01	7,283+01	1,515+01	0,000	1,101-02
3,236-04	7,237-02	3,408-05	8,073+01	5,876+01	4,056-05	4,936+01	7,283+01	1,515+01	0,000	1,730-02
4,855-04	7,218-02	3,414-05	8,066+01	5,880+01	4,066-05	4,936+01	7,283+01	1,515+01	0,000	2,591-02
8,133-04	7,051-02	3,497-05	8,074+01	5,891+01	4,150-05	4,964+01	7,283+01	1,527+01	0,000	4,198-02
1,456-03	6,575-02	3,790-05	8,159+01	5,917+01	4,419-05	5,075+01	7,283+01	1,577+01	0,000	6,191-02
2,160-03	5,953-02	4,313-05	8,405+01	5,857+01	4,780-05	5,285+01	7,284+01	1,674+01	0,000	6,897-02
3,723-03	5,380-02	5,346-05	9,415+01	5,493+01	4,968-05	5,911+01	7,286+01	1,932+01	0,000	7,071-02
6,166-03	5,462-02	5,579-05	9,977+01	5,267+01	4,748-05	6,189+01	7,284+01	2,043+01	0,000	7,261-02

DISTANCE FROM WALL,FT

0,000 2,427-05 4,045-05 7,280-05 1,213-04 2,022-04 3,236-04 4,855-04 8,133-04 1,456-03
2,160-03 3,723-03 6,166-03

ELEMENTAL FRACTIONS AND THEIR FIRST AND SECOND DERIVATIVES WITH RESPECT TO ETA

H4N2	6,666-01	6,666-01	6,667-01	6,666-01	6,666-01	6,666-01	6,666-01	6,666-01	6,600-01	6,350-01
	5,900-01	4,820-01	4,348-01							
	0,000	5,341-04	4,700-04	-5,151-04	1,821-04	=1,127-04	2,904-04	=1,205-03	=5,727-03	=1,301-02
	=1,222-02	=4,467-02	0,000							
	=8,890-03	1,778-02	=1,938-02	7,067-03	=1,257-03	=2,167-04	1,560-03	=5,298-03	=3,547-04	=4,503-03
	5,034-03	=1,585-02	2,578-02							
N2O4	3,333-01	3,333-01	3,333-01	3,333-01	3,333-01	3,333-01	3,333-01	3,333-01	3,400-01	3,649-01
	4,099-01	5,179-01	5,652-01							
	0,000	2,598-07	=6,339-07	2,242-06	=1,083-05	5,391-05	=2,532-04	1,110-03	6,391-03	9,603-03
	2,511-02	=2,586-02	0,000							
	1,786-06	=1,131-06	=1,521-05	5,234-05	=1,612-04	4,848-04	=1,509-03	4,917-03	1,684-03	4,572-04
	9,880-03	=2,687-02	3,262-02							
O	1,000-04	1,000-04	4,001-05	1,000-04	1,000-04	1,000-04	1,000-04	1,000-04	1,001-05	1,000-04
	1,000-04	1,000-04	1,001-05							
	=0,000	=5,344-04	=4,694-04	5,129-04	=1,713-04	5,876-05	=3,711-05	9,480-05	=6,636-04	3,411-03
	=1,289-02	7,053-02	=0,000							
	8,888-03	=1,778-02	1,939-02	=7,120-03	1,419-03	=2,681-04	=5,158-05	3,814-04	=1,329-03	4,046-03
	=1,491-02	4,272-02	=5,839-02							

MOLE FRACTIONS

H4N2	1,284-14	1,284-14	1,282-14	1,284-14	1,284-14	1,284-14	1,284-14	1,307-14	1,561-14	2,591-14
	4,687-14	3,685-14	1,534-14							
N2O4	5,301-36	5,301-36	5,192-36	5,300-36	5,299-36	5,294-36	5,285-36	6,399-36	7,145-35	1,258-31
	5,563-27	5,777-20	3,393-18							
O	8,147-11	8,147-11	8,069-11	8,147-11	8,146-11	8,142-11	8,135-11	8,934-11	2,781-10	8,976-09
	1,167-06	1,034-03	4,245-03							
H2	4,105-01	4,105-01	4,105-01	4,105-01	4,105-01	4,105-01	4,105-01	4,105-01	4,032-01	3,745-01
	3,171-01	1,512-01	8,904-02							
H2O	2,196-01	2,196-01	2,195-01	2,196-01	2,196-01	2,196-01	2,196-01	2,196-01	2,257-01	2,502-01
	2,980-01	4,137-01	4,388-01							
H3N	5,975-05	5,975-05	5,982-05	5,975-05	5,975-05	5,975-05	5,976-05	5,914-05	5,116-05	3,209-05
	1,550-05	2,871-06	1,195-06							
N2	3,699-01	3,699-01	3,699-01	3,699-01	3,699-01	3,699-01	3,699-01	3,699-01	3,709-01	3,750-01
	3,827-01	3,980-01	3,987-01							
H	3,766-05	3,766-05	3,751-05	3,766-05	3,765-05	3,765-05	3,763-05	3,924-05	6,329-05	2,665-04
	1,863-03	1,682-02	1,871-02							
HO	1,167-06	1,167-06	1,160-06	1,167-06	1,167-06	1,166-06	1,166-06	1,230-06	2,373-06	1,783-05
	3,624-04	1,554-02	3,422-02							
NO	2,302-08	2,302-08	2,287-08	2,302-08	2,302-08	2,301-08	2,300-08	2,450-08	5,359-08	5,956-07
	1,794-05	2,507-03	7,870-03							
O2	1,957-11	1,957-11	1,937-11	1,957-11	1,957-11	1,956-11	1,954-11	2,144-11	6,929-11	2,606-09
	4,414-07	1,143-03	8,408-03							

CASE ,10000+01 - - - - - - - STREAMWISE DIMENSION ,85000-01FEET - - -, 23 APR 69 17:45:00

ALPHA	XI (LB/SEC)**2	ROKAP (FT)	PRESSURE (ATM)	EDGE VELOCITY (FT/SEC)	BETA	FLUX NORMALIZING PARAMETER	HEAT FLUXES DIFFUSIONAL (BTU/SEC SQ FT)	TOT ENTH (BTU/SEC SQ FT)	RERAD (BTU/SEC SQ FT)
4,015+00	7,405-05	1,000+00	1,087+01	2,852+02	0,000	7,158-02	2,814+02	2,814+02	0,000

WALL SHEAR (LB/SQ FT)	MECH REM	MASS FLUXES PYROL GAS (LB/SEC SQ FT)	CHAR	TOTAL GAS	ELEMENTAL MASS DIFFUSIVE FLUXES (LB/SEC SQ FT) FOR HYDROGEN	NITROGEN	OXYGEN
6,671-01	0,000	0,000	0,000	0,000	3,111-06	-2,172-06	-9,385-07

MOM TRANS COEFF, RHO*UE*CF/2	HEAT TRANS COEFF, RHO*UE*CH	BLOWING PARAMETERS (BASED ON CH) FOR PYROL GAS	CHAR	TOTAL GAS	ELEMENTAL MASS TRANSFER COEFFICIENTS, RHOE*UE*CM (LB/SEC SQ FT) FOR HYDROGEN	NITROGEN	OXYGEN
7,526-02	1,408-01	0,000	0,000	0,000	-1,019-04	1,858-05	-6,385-06

MOMENTUM THICKNESS, THETA (FT)	DISPLACE. THICKNESS, DELSTAR (FT)	SHAPE FACTOR, DELSTAR /THETA	ENTHALPY THICKNESS, LAMBDA (FT)	REYNOLDS NUMBER PER FOOT	MASS THICKNESSES (FT) FOR HYDROGEN	NITROGEN	OXYGEN
1,143-03	-6,407-05	-5,605-02	1,042-03	2,792+05	5,313-03	1,000-02	9,033-03

NODAL INFORMATION

DISTANCE FROM WALL (FT)	ETA	F	FP (=U/UE)	FPP	FPPP	TOTAL ENTHALPY, G (BTU/LB)	GP (BTU/LB)	GPP (BTU/LB)	STATIC ENTHALPY (BTU/LB)	TEMP (DEG R)
0,000	0,000	0,000	0,000	6,183-01	7,007-01	-1,755+03	1,392+03	-1,134+02	-1,755+03	8,000+02
1,245-05	9,637-02	2,958-03	6,211-02	6,632-01	2,310-01	-1,620+03	1,422+03	7,432+02	-1,620+03	8,954+02
2,186-05	1,606-01	8,324-03	1,050-01	6,692-01	-4,553-02	-1,530+03	1,342+03	-3,234+03	-1,530+03	9,718+02
4,452-05	2,891-01	2,723-02	1,877-01	5,963-01	-1,088+00	-1,377+03	1,092+03	-6,580+02	-1,378+03	1,210+03
9,126-05	4,018-01	7,328-02	2,842-01	4,140-01	-8,032-01	-1,184+03	8,939+02	-1,398+03	-1,184+03	1,641+03
1,965-04	8,031-01	1,822-01	3,847-01	2,396-01	-2,828-01	-9,563+02	5,613+02	-6,723+02	-9,566+02	2,110+03
3,922-04	1,285+00	3,908-01	4,730-01	1,387-01	-1,360-01	-7,514+02	3,150+02	-3,500+02	-7,518+02	2,515+03
6,915-04	1,927+00	7,186-01	5,418-01	8,738-02	-2,370-02	-6,019+02	1,808+02	-6,801+01	-6,023+02	2,799+03
1,364-03	3,212+00	1,481+00	6,438-01	7,857-02	9,981-03	-4,072+02	1,366+02	-6,629-01	-4,079+02	3,207+03
2,821-03	5,621+00	3,267+00	8,343-01	6,815-02	-1,883-02	-9,970+01	1,104+02	-2,109+01	-1,008+02	3,793+03
4,489-03	8,031+00	5,435+00	9,500-01	3,018-02	-1,289-02	1,105+02	6,627+01	-1,559+01	1,090+02	4,408+03
3,014-03	1,285+01	1,018+01	9,971-01	-2,149-05	3,506-04	2,765+02	8,338+00	-8,458+00	2,748+02	4,405+03
,351-02	2,008+01	1,740+01	1,000+00	0,000	-3,447-04	2,430+02	0,000	6,150+00	2,414+02	5,565+03

DISTANCE FROM WALL (FT)	DENSITY, RHO (LB/CU FT)	VISCOSITY, MU LB/SEC FT	RHO*MU /RHOE*MUE, C	SPECIFIC HEAT (BTU/LB R)	THERMAL COND (BTU /SEC FT R)	PRANDTL NUMBER	MODIFIED SCHMIDT NUMBER	MOLECULAR WEIGHT	RHOSQ*EPS /RHOE*MUE	MACH NUMBER
0,000	3,562-01	1,456-05	1,700+00	4,329+01	1,012-05	6,239+01	7,269+01	1,915+01	0,000	0,000
1,245-05	3,065-01	1,569-05	1,574+00	4,373+01	1,180-05	5,816+01	7,273+01	1,844+01	1,108+02	1,035+02
2,186-05	2,765-01	1,656-05	1,499+00	4,377+01	1,300-05	5,577+01	7,278+01	1,806+01	7,233+02	1,647+02
4,452-05	2,115-01	1,903-05	1,317+00	4,535+01	1,637-05	5,271+01	7,284+01	1,720+01	4,460+01	2,500+02
9,126-05	1,520-01	2,313-05	1,151+00	4,805+01	2,140-05	5,196+01	7,285+01	1,676+01	1,394+00	3,190+02
1,965-04	1,165-01	2,721-05	1,038+00	5,072+01	2,667-05	5,175+01	7,284+01	1,652+01	3,401+00	3,802+02
3,922-04	9,732-02	3,053-05	9,726+01	5,268+01	3,107-05	5,176+01	7,284+01	1,645+01	6,870+00	4,295+02
6,915-04	8,740-02	3,275-05	9,371+01	5,395+01	3,411-05	5,180+01	7,284+01	1,644+01	1,192+01	4,678+02
1,364-03	7,676-02	3,592-05	9,028+01	5,549+01	3,825-05	5,212+01	7,284+01	1,655+01	1,329+01	5,236+02
2,821-03	6,562-02	4,027-05	8,650+01	5,724+01	4,393-05	5,247+01	7,284+01	1,673+01	9,713+00	6,320+02
4,489-03	5,878-02	4,513-05	8,684+01	5,707+01	4,781-05	5,387+01	7,285+01	1,741+01	7,793+00	6,884+02
8,014-03	5,842-02	4,473-05	8,554+01	5,670+01	4,788-05	5,297+01	7,287+01	1,729+01	7,698+00	7,191+02
1,351-02	5,462-02	5,579-05	9,977-01	5,267+01	4,748-05	6,189+01	7,284+01	2,043+01	6,730+00	7,261+02

DISTANCE FROM WALL,FT

0,000 1,245-05 2,186-05 4,452-05 9,126-05 1,965-04 3,922-04 6,915-04 1,364-03 2,821-03
4,489-03 8,014-03 1,351-02

ELEMENTAL FRACTIONS AND THEIR FIRST AND SECOND DERIVATIVES WITH RESPECT TO ETA

H4N2	6,774-01	6,158-01	5,754-01	5,585-01	5,756-01	5,907-01	5,957-01	5,966-01	5,920-01	5,816-01
	5,494-01	5,396-01	4,348-01							
	7,091-01	-6,624-01	-4,849-01	6,324+02	8,573-02	2,217+02	3,578-03	-1,006-03	-3,675-03	-9,884-03
	-9,139-03	-7,581-03	0,000							
	3,416+00	-2,447+00	7,973+00	5,585-01	-3,251-01	-7,065+02	-6,526-03	-7,744-03	3,589-03	-8,743-03
	8,781-03	-7,843-03	9,941-03							
N2O4	2,527-01	4,464-01	5,730-01	6,114-01	5,406-01	4,839-01	4,635-01	4,593-01	4,624-01	4,896-01
	5,420-01	6,621-01	5,652-01							
	2,250+00	2,086+00	1,480+00	-3,309-01	-3,245-01	-8,358-02	-1,652-02	-7,483-04	5,649-03	1,644-02
	2,772-02	6,077-03	0,000							
	-1,155+01	8,127+00	-2,699+01	-1,199+00	1,266+00	2,341+01	4,424-02	4,857-03	5,101-03	3,857-03
	5,612-03	-1,450-02	1,281-02							
O	6,991-02	-6,225-02	-1,484-01	-1,699+01	-1,162-01	-7,464-02	-5,916-02	-5,584-02	-5,438-02	-7,123-02
	-9,139-02	-2,017-01	1,001-05							
	-1,541+00	-1,423+00	-9,950-01	2,677-01	2,388-01	6,141-02	1,294-02	1,754-03	-1,974-03	-6,555-03
	-1,769-02	1,503-03	-0,000							
	8,131+00	-5,680+00	1,901+01	6,406-01	-9,408-01	-1,635+01	-3,771-02	2,887-03	-8,690-03	4,887-03
	-1,429-02	2,234-02	-2,276-02							

MOLE FRACTIONS

H4N2	7,332+24	3,519-22	3,351-21	3,184-19	2,600-17	4,023-16	1,902-15	4,363-15	1,092-14	2,936-14
	5,216-14	6,027-14	1,534-14							
N2O4	1,000+30	1,000-30	1,000-30	1,000-30	1,000-30	1,000-30	1,000-30	8,379-39	2,513-34	1,562-29
	1,659-25	8,783-26	3,393-18							
O	1,000+30	1,000-30	1,000-30	2,421-34	3,054-24	7,041-18	2,826-14	2,304-12	3,469-10	7,182-08
	5,151-06	4,327-06	4,245-03							
H2	1,153-01	1,935-01	2,385-01	3,044-01	3,278-01	3,381-01	3,407-01	3,411-01	3,348-01	3,253-01
	2,850-01	3,013-01	8,904-02							
H2O	2,940-01	2,862-01	2,823-01	2,746-01	2,721-01	2,704-01	2,706-01	2,708-01	2,763-01	2,815-01
	3,100-01	2,791-01	4,388-01							
H3N	2,667-01	1,528-01	8,506-02	1,378-02	1,333-03	2,855-04	1,162-04	7,167-05	4,037-05	2,181-05
	1,172-05	1,300-05	1,195-06							
N2	3,239-01	3,675-01	3,941-01	4,072-01	3,987-01	3,912-01	3,885-01	3,880-01	3,887-01	3,926-01
	4,010-01	4,156-01	3,987-01							
H	1,012-24	7,163-22	5,101-20	8,874-16	2,914-11	2,031-08	8,231-07	5,859-06	5,353-05	5,610-04
	3,220-03	3,291-03	1,871-02							
HO	3,557-31	9,912-28	1,971-25	4,519-20	2,743-14	1,181-10	1,344-08	1,653-07	2,898-06	6,064-05
	7,094-04	6,163-04	3,422-02							
NO	4,294-37	4,122-33	1,977-30	3,730-24	2,380-17	4,592-13	1,237-10	2,413-09	7,225-08	2,698-06
	5,242-05	4,502-05	7,870-03							
O2	1,000+30	1,000-30	1,000-30	1,727-34	1,521-24	2,910-18	1,077-14	8,468-13	1,276-10	2,666-08
	2,335-06	1,670-06	8,408-03							

CASE ,10000+01 - - - - - - - STREAMWISE DIMENSION ,14820-00FEET - - -, 23 APR 69 17:46:42

ALPHA	X1 (LB /SEC)**2	ROKAP (FT)	PRESSURE (ATM)	EDGE VELOCITY (FT/SEC)	BETA	FLUX NORMALIZING PARAMETER	HEAT FLUXES DIFFUSIONAL (BTU/SEC SQ FT)	TOT ENTH	RERAD
3,981+00	1,291-04	1,000+00	1,087+01	2,852+02	0,000	5,421-02	2,498+02	2,498+02	0,000

WALL SHEAR (LB/SQ FT)	MASS FLUXES MECH REM	PYROL GAS	CHAR	TOTAL GAS (LB/SEC SQ FT)	ELEMENTAL MASS DIFFUSIVE FLUXES (LB/SEC SQ FT) FOR HYDROGEN	NITROGEN	OXYGEN
6,955-01	0,000	0,000	0,000	0,000	2,003-06	3,825-06	-5,828-06

MOM TRANS COEFF, RHO*UE*CF/2	HEAT TRANS COEFF, RHO*UE*CH	BLOWING PARAMETERS (BASED ON CH) FOR PYROL GAS	CHAR	TOTAL GAS	ELEMENTAL MASS TRANSFER COEFFICIENTS, RHOE*UE*CM (LB/SEC SQ FT) FOR HYDROGEN	NITROGEN	OXYGEN
7,847-02	1,226-01	0,000	0,000	0,000	-6,812-05	-3,467-05	-4,171-05

MOMENTUM THICKNESS, THETA (FT)	DISPLACE, THICKNESS, DELSTAR (FT)	SHAPE FACTOR, DELSTAR /THETA	ENTHALPY THICKNESS, LAMBDA (FT)	REYNOLDS NUMBER PER FOOT	MASS THICKNESSES (FT) FOR HYDROGEN	NITROGEN	OXYGEN
1,490-03	5,967-05	4,005-02	1,556-03	2,792+05	5,645-05	1,085-02	9,757-03

NODAL INFORMATION

DISTANCE FROM WALL (FT)	ETA	F	FP (=U/UE)	FPP	FPPP	TOTAL ENTHALPY,G (BTU/LB)	GP (BTU/LB)	GPP (BTU/LB)	STATIC ENTHALPY (BTU/LB)	TEMP (DEG R)
0,000	0,000	0,000	0,000	8,444-01	6,988-01	-1,795+03	1,609+03	2,260+03	-1,795+03	8,000+02
1,641-05	9,555-02	3,948-03	8,353-02	9,003-01	4,705-01	-1,638+03	1,611+03	-2,219+03	-1,638+03	9,137+02
2,911-05	1,592-01	1,109-02	1,404-01	8,651-01	-1,575+00	-1,540+03	1,435+03	-3,312+03	-1,540+03	1,013+03
6,075-05	2,866-01	3,544-02	2,373-01	6,500-01	-1,803+00	-1,380+03	1,114+03	-1,724+03	-1,380+03	1,310+03
1,253-04	4,777-01	9,083-02	3,344-01	3,968-01	-8,475-01	-1,197+03	8,078+02	-1,485+03	-1,197+03	1,716+03
2,639-04	7,962-01	2,137-01	4,275-01	2,183-01	-2,730-01	-9,997+02	4,817+02	-5,623+02	-1,000+03	2,126+03
5,135-04	1,274+00	4,385-01	5,065-01	1,249-01	-1,180-01	-8,228+02	2,813+02	-2,767+02	-8,233+02	2,474+03
8,905-04	1,911+00	7,824-01	5,683-01	7,856-02	-2,762-02	-6,850+02	1,747+02	-5,768+01	-6,856+02	2,748+03
1,734-03	3,185+00	1,564+00	6,573-01	7,011-02	1,436-02	-4,897+02	1,471+02	1,422+01	-4,905+02	3,109+03
3,599-03	5,574+00	3,349+00	8,357-01	6,670-02	-1,721-02	-1,342+02	1,355+02	-2,392+01	-1,353+02	3,873+03
5,766-03	7,962+00	5,499+00	9,500-01	3,069-02	-1,294-02	1,185+02	7,492+01	-2,679+01	1,170+02	4,346+03
1,052-02	1,274+01	1,021+01	9,986-01	6,704-05	1,242-04	2,595+02	2,706+00	-3,439+00	2,579+02	5,110+03
1,796-02	1,991+01	1,737+01	1,000+00	0,000	-1,430-04	2,430+02	0,000	2,684+00	2,414+02	5,565+03

DISTANCE FROM WALL (FT)	DENSITY, RHO (LB/CU FT)	VISCOSITY, MU LB/SEC FT	RHO*MU /RHOE*MUE, C	SPECIFIC HEAT (BTU/LB R)	THERMAL COND (BTU /SEC FT R)	PRANDTL NUMBER	MODIFIED SCHMIDT NUMBER	MOLECULAR WEIGHT	RHOSQ*EPS /RHOE*MUE	MACH NUMBER
0,000	3,577-01	1,464-05	1,714+00	4,303-01	1,007-05	6,251-01	7,269-01	1,923+01	0,000	0,000
1,641-05	3,012-01	1,597-05	1,575+00	4,334-01	1,198-05	5,780-01	7,274-01	1,849+01	3,279-02	1,376-02
2,911-05	2,646-01	1,709-05	1,480+00	4,360-01	1,349-05	5,523-01	7,280-01	1,802+01	1,926-01	2,142-02
6,075-05	1,966-01	2,013-05	1,295+00	4,548-01	1,729-05	5,292-01	7,285-01	1,730+01	9,315-01	3,030-02
1,253-04	1,472-01	2,395-05	1,155+00	4,791-01	2,187-05	5,247-01	7,285-01	1,698+01	2,492+00	3,699-02
2,639-04	1,178-01	2,753-05	1,062+00	5,006-01	2,632-05	5,237-01	7,285-01	1,683+01	5,548+00	4,252-02
5,135-04	1,009-01	3,040-05	1,004+00	5,170-01	3,002-05	5,237-01	7,285-01	1,678+01	1,044+01	4,683-02
8,905-04	9,087-02	3,259-05	9,695-01	5,289-01	3,287-05	5,244-01	7,285-01	1,678+01	1,693+01	5,003-02
1,734-03	8,037-02	3,536-05	9,303-01	5,440-01	3,663-05	5,252-01	7,285-01	1,679+01	1,788+01	5,466-02
3,599-03	6,571-02	4,116-05	8,854-01	5,657-01	4,373-05	5,324-01	7,285-01	1,710+01	1,195+01	6,346-02
5,766-03	5,959-02	4,462-05	8,706-01	5,677-01	4,720-05	5,366-01	7,286-01	1,741+01	9,828+00	6,921-02
1,052-02	5,458-02	5,111-05	9,132-01	5,530-01	4,959-05	5,699-01	7,286-01	1,874+01	8,243+00	7,113-02
1,796-02	5,462-02	5,579-05	9,977-01	5,267-01	4,748-05	6,189-01	7,284-01	2,043+01	8,256+00	7,261-02

DISTANCE FROM WALL,FT

0,000 1,641-05 2,911-05 6,075-05 1,253-04 2,639-04 5,135-04 8,905-04 1,734-03 3,599-03
5,766-03 1,052-02 1,796-02

ELEMENTAL FRACTIONS AND THEIR FIRST AND SECOND DERIVATIVES WITH RESPECT TO ETA

H4N2	6,685-01	5,939-01	5,570-01	5,509-01	5,660-01	5,752-01	5,785-01	5,788-01	5,778-01	5,638-01
	5,451-01	4,926-01	4,348-01							
	-8,179-01	-7,116-01	-3,653-01	1,095-01	5,375-02	1,340-02	2,580-03	-4,216-04	-2,398-03	-7,454-03
	-8,818-03	-1,209-02	0,000							
	1,079-01	2,116+00	3,131+00	-3,641-01	-2,189-01	-3,452-02	-1,077-02	1,345-03	-4,448-03	2,153-04
	-1,358-03	-1,124-05	3,385-03							
N2O4	2,564-01	4,924-01	6,052-01	6,092-01	5,495-01	5,148-01	5,022-01	4,985-01	5,029-01	5,215-01
	5,818-01	6,135-01	5,652-01							
	2,590+00	2,221+00	1,122+00	-4,556-01	-2,024-01	-5,083-02	-1,159-02	-9,677-04	4,646-03	1,775-02
	2,353-02	-5,131-03	0,000							
	1,878-01	-7,906+00	-2,661+01	1,841+00	8,093-01	1,428-01	2,145-02	1,189-02	-3,080-03	1,405-02
	-9,217-03	-2,780-03	4,212-03							
O	7,505-02	-8,636-02	-1,622-01	-1,601-01	-1,155-01	-8,993-02	-8,069-02	-7,730-02	-8,065-02	-8,527-02
	-1,269-01	-1,061-01	1,001-05							
	-1,772+00	-1,510+00	-7,367-01	3,462-01	1,487-01	3,743-02	9,007-03	1,389-03	-2,248-03	-1,030-02
	-1,471-02	1,722-02	-0,000							
	-2,957-01	5,789+00	1,848+01	-1,477+00	-5,904-01	-1,083-01	-1,068-02	-1,324-02	7,528-03	-1,427-02
	1,057-02	2,791-03	-7,596-03							

MOLE FRACTIONS

H4N2	6,993-24	5,984-22	8,565-21	1,066-18	4,098-17	3,959-16	1,525-15	3,471-15	8,377-15	2,945-14
	5,050-14	5,414-14	1,534-14							
N2O4	1,000-30	1,000-30	1,000-30	1,000-30	1,000-30	1,000-30	1,000-30	2,845-39	3,545-35	8,618-29
	6,866-26	1,721-21	3,393-18							
O	1,000-30	1,000-30	1,000-30	2,151-31	5,894-23	1,134-17	1,513-14	1,227-12	1,250-10	1,466-07
	3,473-06	2,705-04	4,245-03							
H2	1,122-01	1,986-01	2,479-01	2,996-01	3,153-01	3,217-01	3,239-01	3,235-01	3,230-01	3,049-01
	2,889-01	1,995-01	8,904-02							
H2O	3,046-01	2,961-01	2,914-01	2,851-01	2,830-01	2,820-01	2,816-01	2,825-01	2,824-01	2,964-01
	3,016-01	3,669-01	4,388-01							
H3N	2,570-01	1,272-01	5,803-02	6,730-03	9,280-04	2,557-04	1,174-04	7,224-05	4,337-05	1,868-05
	1,250-05	4,872-06	1,195-06							
N2	3,262-01	3,781-01	4,027-01	4,086-01	4,008-01	3,961-01	3,944-01	3,939-01	3,945-01	3,978-01
	4,061-01	4,126-01	3,987-01							
H	9,981-25	2,090-21	3,819-19	1,749-14	1,029-10	2,351-08	5,834-07	4,128-06	3,247-05	7,098-04
	2,767-03	1,262-02	1,871-02							
HO	3,735-31	4,009-27	2,655-24	2,246-18	1,510-13	1,572-10	9,537-09	1,171-07	1,632-06	9,264-05
	5,610-04	7,034-03	3,422-02							
NO	4,586-37	2,125-32	4,167-29	3,732-22	1,804-16	6,567-13	8,416-11	1,639-09	3,723-08	4,566-06
	3,990-05	9,097-04	7,870-03							
O2	1,000-30	1,000-30	1,000-30	1,489-31	3,076-23	5,117-18	6,348-15	4,989-13	4,909-11	6,089-08
	1,514-06	2,024-04	8,408-03							

Run 2 - O/F = 0 at wall

```
            BOUNDARY LAYER INTEGRAL MATRIX PROGRAM (BLIMP)

        AEROTHERM CORPORATION,PALO ALTO,CALIF (RMK,EPB)      IDENTIFICATION

CASE 7009   UNEQUAL          DIFF, ON B,L, COMPOSITION  RUN 2

        CONTROL NUMBERS  1  2  3  4  5  6  7  8  9 10 11 12 13 14 15 16 17 18 19 20

                         1  3  2  0  4  3  2  0  2  0  0  2  0  0  0  0  0  1  0  0

    U/UE TO        NODAL PT,                             ETA VALUES
   NORM, ETA       AT WHICH
                   ETA NORM,
    9,500-01          11         0,000     2,400-02  4,000-02  7,200-02  1,200-01  2,000-01  3,200-01  4,800-01  8,000-01
                                 1,400+00  2,000+00  3,200+00  5,000+00

CASE                     1,00000+00

TOTAL ENTHALPY,BTU/LB    2,43000+02

TOTAL PRESSURE,ATM       1,09000+01

INCIDENT RAD FLUX,B/SF2 -0,00000

    MIXING LENGTH CONSTANT  =  4,4000-01
    SUBLAYER CONSTANT, YA+  =  1,1823+01
    CLAUSER NUMBER          =  1,9000-02
    TURBULENT SCHMIDT NUMBER=  7,5000-01
    TURBULENT PRANDTL NUMBER=  7,5000-01
    TRANSITION MOM,THICK,RE =  2,5000+02



        CASE    ,10000+01 - - - - - - - - - - - - - - - - - - - - - - - - - - 21 APR 69 15:15:50
                    NUMBER OF ELEMENTS= 3     DIFFUSION EXPONENT=  ,4310     CURVE FIT MOL, WT,=23,400

                                                  REFERENCE PROPERTIES

                           MOLECULAR WEIGHT=32,000     SIGMA=3,4670     EPSILON/K= 106,70


RELATIVE ELEMENTAL COMPOSITIONS, ATOMIC WTS/UNIT MASS
     AT,NO,   ELEMENT     ATOMIC WT     EDGE GAS    PYRO,GAS 1     CHAR 1     PYRO,GAS 2     CHAR 2     PYRO,GAS 3     CHAR 3
        1    HYDROGEN      1,00797      ,0263733    -,0000000    -,0000000    -,0000000    -,0000000    -,0000000    -,0000000
        7    NITROGEN     14,00800      ,0303293    -,0000000    -,0000000    -,0000000    -,0000000    -,0000000    -,0000000
        8     OXYGEN      16,00000      ,0342853    -,0000000    -,0000000    -,0000000    -,0000000    -,0000000    -,0000000
4,  1 2,  7 0,  0 0,  0 0,  0 0,  0 0,  0                             H4N2
   ,22790+05    ,68536+05    ,22986+02    ,24193-02   -,19593+07    ,10810+03 3000,0000 1
   ,22790+05    ,68536+05    ,31432+02    ,48794-04   -,13970+08    ,10810+03 5000,0000 1 1,1452
2,  7 4,  8 0,  0 0,  0 0,  0 0,  0 0,  0                             N204
   ,21700+04    ,78597+05    ,29773+02    ,59443-03   -,17883+07    ,13491+03 3000,0000 1
   ,21700+04    ,78597+05    ,31781+02    ,17563-05   -,38597+07    ,13491+03 5000,0000 1 1,8042
1,  8 0,  0 0,  0 0,  0 0,  0 0,  0 0,  0                             O
   ,59559+05    ,13522+05    ,49723+01    ,38077-05    ,15475+05    ,50096+02 3000,0000 1
   ,59559+05    ,13522+05    ,65749+01   -,22427-03   -,89178+07    ,50096+02 5000,0000 1  ,7397
2,  1 0,  0 0,  0 0,  0 0,  0 0,  0 0,  0                             H2
   ,00000       ,21321+05    ,62748+01    ,95547-03    ,37158+05    ,48506+02 2000,0000 1
   ,00000       ,21208+05    ,79548+01    ,37918-03   -,20717+07    ,48464+02 4000,0000 1  ,3893
2,  1 1,  8 0,  0 0,  0 0,  0 0,  0 0,  0                             H2O
  -,57798+05    ,30769+05    ,75011+01    ,23601-02   -,29281+05    ,68634+02 2000,0000 1
  -,57798+05    ,30209+05    ,13230+02    ,25103-03   -,61512+07    ,68422+02 4000,0000 1  ,7749
3,  1 1,  7 0,  0 0,  0 0,  0 0,  0 0,  0                             H3N
  -,10970+05    ,42561+05    ,98741+01    ,37069-02   -,27151+06    ,77258+02 2000,0000 1
  -,10970+05    ,41634+05    ,17390+02    ,78927-03   -,71540+07    ,76908+02 4000,0000 1  ,8721
2,  7 0,  0 0,  0 0,  0 0,  0 0,  0 0,  0                             N2
   ,00000       ,22430+05    ,69778+01    ,81617-03   -,36596+05    ,63865+02 2000,0000 1
   ,00000       ,22165+05    ,88319+01    ,59748-04   -,14065+07    ,63765+02 4000,0000 1 1,0262
1,  1 0,  0 0,  0 0,  0 0,  0 0,  0 0,  0                             H
   ,52102+05    ,13423+05    ,48022+01    ,55547-04    ,17309+06    ,38862+02 3000,0000 1
   ,52102+05    ,13423+05    ,30875+01    ,31502-03    ,92974+07    ,38862+02 5000,0000 1  ,3018
1,  1 1,  8 0,  0 0,  0 0,  0 0,  0 0,  0                             HO
   ,93300+04    ,21404+05    ,77319+01    ,39439-03   -,97356+06    ,61382+02 3000,0000 1
   ,93300+04    ,21404+05    ,96514+01   -,44353-04   -,68611+07    ,61382+02 5000,0000 1  ,8715
1,  7 1,  8 0,  0 0,  0 0,  0 0,  0 0,  0                             NO
   ,21580+05    ,22700+05    ,87762+01    ,89903-04   -,78966+06    ,68849+02 3000,0000 1
   ,21580+05    ,22700+05    ,91626+01    ,65788-05   -,21252+07    ,68849+02 5000,0000 1  ,9981
2,  8 0,  0 0,  0 0,  0 0,  0 0,  0 0,  0                             O2
   ,00000       ,23540+05    ,76310+01    ,71015-03   -,89282+05    ,68008+02 2000,0000 1
   ,00000       ,23455+05    ,88335+01    ,30128-03   -,17061+07    ,67975+02 4000,0000 1 1,0000

    ELEMENT   HYDROGEN    NITROGEN    OXYGEN
    BASE SP     H4N2        N204        O
```

DISTANCE,FT	,10000-01	,85000-01	,14820-00	,21070-00	,27300-00	,33580-00	,41290-00
ROKAP	,10000+01	,10000+01	,10000+01	,10000+01	,10000+01	,10000+01	,10000+01
XI,(LB/SEC)**2	,10025-04	,85210-04	,14857-03	,21122-03	,27367-03	,33663-03	,41392-03
PRESSURE RATIO	,99700-00	,99700-00	,99700-00	,99700-00	,99700-00	,99700-00	,99700-00
STATIC PRESSURE,ATM	,10867+02	,10867+02	,10867+02	,10867+02	,10867+02	,10867+02	,10867+02
EDGE VELOCITY,FT/SEC	,23532+03	,23532+03	,23532+03	,23532+03	,23532+03	,23532+03	,23532+03
BETA	-,13941-05	-,98768-05	-,10479-04	-,92152-05	-,13843-04	-,15765-04	-,14565-04
INCIDENT RADIATION FLUX	,00000	,00000	,00000	,00000	,00000	,00000	,00000
ENTROPY DROP,BTU/LB R	,00000	,00000	,00000	,00000	,00000	,00000	,00000
WALL TEMPERATURE,DEG R	,80000+03	,80000+03	,80000+03	,80000+03	,80000+03	,80000+03	,80000+03
COMP FLUX,LB/SEC FT**2	-,00000	-,00000	-,00000	-,00000	-,00000	-,00000	-,00000
COMP FLUX,LB/SEC FT**2	-,00000	-,00000	-,00000	-,00000	-,00000	-,00000	-,00000
COMP FLUX,LB/SEC FT**2)	-,00000	-,00000	-,00000	-,00000	-,00000	-,00000	-,00000

CASE ,10000+01 - - - - - - - STREAMWISE DIMENSION ,10000-01FEET - - -, 21 APR 69 15:15:50

ITERATED VALUES

ITS	TIME	ALPH	FPPW	DAMP	MAX,LIN ERROR	MAX,ERRORS IN CONSERVATION EQS, MOMENTUM	ENERGY	H4N2	N2O4
1	3,414 6,000	,7500	,3333	2,-01	5	4,4+00 12	-3,6+03 12	2,5+00 12	-2,4+00 0

ALPHA	XI (LB/SEC)**2	ROKAP (FT)	PRESSURE (ATM)	EDGE VELOCITY (FT/SEC)	BETA	FLUX NORMALIZING PARAMETER	HEAT FLUXES DIFFUSIONAL	TOT ENTH	RERAD (BTU/SEC SQ FT)
0,000+00	1,002-05	1,000+00	1,087+01	2,353+02	0,000	2,239-01	-0,000	-0,000	0,000

WALL SHEAR (LB/SQ FT)	MECH REM	MASS FLUXES PYROL GAS (LB/SEC SQ FT)	CHAR	TOTAL GAS	ELEMENTAL MASS DIFFUSIVE FLUXES (LB/SEC SQ FT) FOR HYDROGEN	NITROGEN	OXYGEN
1,153+00	0,000	0,000	0,000	0,000	-0,000	-0,000	-0,000

MOM TRANS COEFF, RHO*UE*CF/2	HEAT TRANS COEFF, RHO*UE*CH	BLOWING PARAMETERS (BASED ON CH) FOR PYROL GAS	CHAR	TOTAL GAS	ELEMENTAL MASS TRANSFER COEFFICIENTS, RHOE*UE*CM (LB/SEC SQ FT) FOR HYDROGEN	NITROGEN	OXYGEN
1,577-01	0,000	0,000	0,000	0,000	0,000	0,000	0,000

MOMENTUM THICKNESS, THETA (FT)	DISPLACE, THICKNESS, DELSTAR (FT)	SHAPE FACTOR, DELSTAR /THETA	ENTHALPY THICKNESS, LAMBDA (FT)	REYNOLDS NUMBER PER FOOT	MASS THICKNESSES (FT) FOR HYDROGEN	NITROGEN	OXYGEN
4,959-04	1,187-03	2,394+00	1,577-03	3,565+05	2,841-03	3,977-03	3,772-03

NODAL INFORMATION

DISTANCE FROM WALL (FT)	ETA	F	FP (=U/UE)	FPP	FPPP	TOTAL ENTHALPY,G (BTU/LB)	GP (BTU/LB)	GPP (BTU/LB)	STATIC ENTHALPY (BTU/LB)	TEMP (DEG R)
0,000	0,000	0,000	0,000	7,500-01	-1,557+01	-5,130+02	0,000	-2,682-02	-5,130+02	8,009+02
8,905-06	1,440-01	2,563-03	1,700-02	-2,511-02	4,800+00	-5,130+02	1,576-03	5,537-02	-5,130+02	8,009+02
1,484-05	2,400-01	4,578-03	2,800-02	1,636-01	-8,694-01	-5,130+02	-5,497-03	-2,062-01	-5,130+02	8,009+02
2,671-05	4,320-01	1,226-02	5,000-02	1,001-01	2,082-01	-5,130+02	3,108-02	5,855-01	-5,130+02	8,009+02
4,452-05	7,200-01	3,139-02	8,400-02	1,240-01	-4,192-02	-5,130+02	-1,464-01	-1,818+00	-5,130+02	8,009+02
7,420-05	1,200+00	8,538-02	1,400-01	1,120-01	-8,116-03	-5,130+02	7,293-01	5,468+00	-5,130+02	8,009+02
1,188-04	1,920+00	2,150-01	2,200-01	1,122-01	8,702-03	-5,100+02	9,073+00	1,771+01	-5,101+02	8,023+02
1,787-04	2,880+00	4,788-01	3,300-01	1,151-01	-2,670-03	-4,970+02	1,398+01	-7,488+00	-4,971+02	8,083+02
3,049-04	4,800+00	1,318+00	5,400-01	1,004-01	-1,262-02	-4,750+02	1,361+01	7,100+00	-4,753+02	8,481+02
5,915-04	8,400+00	3,815+00	8,200-01	5,515-02	-1,255-02	-3,800+02	3,917+01	7,103+00	-3,807+02	1,006+03
1,117-03	1,200+01	7,039+00	9,500-01	2,061-02	-6,646-03	-2,000+02	5,887+01	3,837+00	-2,010+02	2,216+03
3,236-03	1,920+01	1,411+01	9,900-01	-6,272-04	7,467-04	1,600+02	1,845+01	-1,506+01	1,589+02	5,258+03
7,074-03	3,000+01	2,485+01	1,000+00	0,000	-6,305-04	2,430+02	0,000	1,165+01	2,419+02	5,566+03

DISTANCE FROM WALL (FT)	DENSITY, RHO (LB/CU FT)	VISCOSITY, MU LB/SEC FT	RHO*MU /RHOE*MUE, C	SPECIFIC HEAT (BTU/LB R)	THERMAL COND (BTU SEC FT R)	PRANDTL NUMBER	MODIFIED SCHMIDT NUMBER	MOLECULAR WEIGHT	RHOSQ*EPS /RHOE*MUE	MACH NUMBER
0,000	3,077-01	1,300-05	9,389-01	5,283+01	1,171-05	5,862-01	7,291-01	1,656+01	0,000	0,000
8,905-06	3,077-01	1,300-05	9,389-01	5,283+01	1,171-05	5,862-01	7,291-01	1,656+01	0,000	2,375-03
1,484-05	3,077-01	1,300-05	9,389-01	5,283+01	1,171-05	5,862-01	7,291-01	1,656+01	0,000	3,912-03
2,671-05	3,077-01	1,300-05	9,389-01	5,283+01	1,171-05	5,862-01	7,291-01	1,656+01	0,000	6,985-03
4,452-05	3,077-01	1,300-05	9,389-01	5,283+01	1,171-05	5,862-01	7,291-01	1,656+01	0,000	1,173-02
7,420-05	3,077-01	1,300-05	9,389-01	5,283+01	1,171-05	5,863-01	7,291-01	1,656+01	0,000	1,956-02
1,188-04	3,066-01	1,301-05	9,364-01	5,289+01	1,176-05	5,852-01	7,291-01	1,653+01	0,000	3,068-02
1,787-04	3,020-01	1,305-05	9,254-01	5,319+01	1,195-05	5,809+01	7,289-01	1,640+01	0,000	4,567-02
3,049-04	2,749-01	1,342-05	8,659+01	5,450+01	1,320-05	5,538+01	7,281-01	1,567+01	0,000	7,118-02
5,915-04	1,982-01	1,483-05	6,898-01	5,798+01	1,813-05	4,741+01	7,274-01	1,340+01	0,000	9,035-02
1,117-03	9,212-02	2,610-05	5,643-01	5,894+01	3,319-05	4,635+01	7,284-01	1,372+01	0,000	6,850-02
3,236-03	5,417-02	5,275-05	6,708-01	5,524+01	4,968-05	5,866+01	7,286-01	1,914+01	0,000	5,837-02
7,074-03	5,462-02	5,580-05	7,153-01	5,267+01	4,749-05	6,189+01	7,284-01	2,043+01	0,000	5,991-02

DISTANCE FROM WALL,FT

0,000 8,905-06 1,484-05 2,671-05 4,452-05 7,420-05 1,188-04 1,787-04 3,049-04 5,915-04
1,117-03 3,236-03 7,074-03

ELEMENTAL FRACTIONS AND THEIR FIRST AND SECOND DERIVATIVES WITH RESPECT TO ETA

H4N2	1,000+00	1,000+00	1,000+00	1,000+00	1,000+00	1,000+00	1,000+00	1,000+00	9,800-01	9,050-01
	7,501-01	4,900-01	4,348-01							
	0,000	-4,560-08	7,349-07	-6,569-06	3,008-05	-1,497-04	7,032-04	-3,082-03	-1,416-02	-3,387-02
	-4,194-02	-4,715-02	0,000							
	1,215-05	-2,091-05	4,596-05	-1,193-04	3,726-04	-1,122-03	3,491-03	-1,138-02	-1,677-04	-1,078-02
	6,294-03	-7,741-03	1,647-02							
N2O4	1,000-05	1,000-05	1,000-05	1,000-05	1,000-05	1,000-05	1,000-05	1,000-05	2,001-02	9,501-02
	2,499-01	5,100-01	5,652-01							
	0,000	3,417-07	-1,144-06	6,172-06	-2,913-05	1,451-04	-6,818-04	2,988-03	1,468-02	3,106-02
	5,268-02	-1,162-02	0,000							
	-4,766-06	9,533-06	-4,042-05	1,166-04	-3,618-04	1,088-03	-3,385-03	1,103-02	1,153-03	7,942-03
	4,069-03	-2,193-02	2,408-02							
O	1,001-05	1,001-05	1,001-05	1,001-05	1,001-05	1,001-05	1,001-05	1,001-05	1,001-05	1,001-05
	1,001-05	1,001-05	1,001-05							
	-0,000	-2,961-07	4,094-07	3,970-07	-9,445-07	4,575-06	-2,138-05	9,374-05	-5,199-04	2,813-03
	-1,073-02	5,878-02	-0,000							
	-7,385-06	1,138-05	-5,538-06	2,714-06	-1,082-05	3,434-05	-1,062-04	3,462-04	-9,854-04	2,837-03
	-1,036-02	2,967-02	-4,056-02							

MOLE FRACTIONS

H4N2	1,834-23	1,833-23	1,833-23	1,833-23	1,833-23	1,833-23	1,962-23	2,620-23	1,519-22	2,182-20
	1,231-15	3,996-14	1,535-14							
N2O4	1,000-30	1,000-30	1,000-30	1,000-30	1,000-30	1,000-30	1,000-30	1,000-30	1,000-30	1,000-30
	1,000-30	2,004-20	3,398-18							
O	1,000-30	1,000-30	1,000-30	1,000-30	1,000-30	1,000-30	1,000-30	1,000-30	1,000-30	1,000-30
	3,107-17	6,756-04	4,249-03							
H2	2,081-01	2,081-01	2,081-01	2,081-01	2,081-01	2,080-01	2,104-01	2,203-01	2,833-01	4,780-01
	4,925-01	1,634-01	8,906-02							
H2O	1,756-05	1,744-05	1,755-05	1,756-05	1,756-05	1,756-05	1,753-05	1,740-05	1,364-02	5,535-02
	1,490-01	4,083-01	4,388-01							
H3N	5,503-01	5,503-01	5,503-01	5,503-01	5,503-01	5,503-01	5,476-01	5,356-01	4,409-01	1,490-01
	3,676-04	3,334-06	1,196-06							
N2	2,416-01	2,416-01	2,416-01	2,416-01	2,416-01	2,416-01	2,421-01	2,441-01	2,621-01	3,177-01
	3,581-01	3,979-01	3,987-01							
H	1,454-24	1,453-24	1,453-24	1,453-24	1,453-24	1,452-24	1,618-24	2,557-24	4,519-23	3,789-19
	7,315-08	1,503-02	1,872-02							
HO	1,726-35	1,715-35	1,726-35	1,726-35	1,726-35	1,725-35	1,957-35	3,348-35	8,327-31	2,348-25
	2,190-10	1,221-02	3,424-02							
NO	1,000-30	1,000-30	1,000-30	1,000-30	1,000-30	1,000-30	1,000-30	1,000-30	1,234-36	2,182-30
	8,728-13	1,828-03	7,874-03							
O2	1,000-30	1,000-30	1,000-30	1,000-30	1,000-30	1,000-30	1,000-30	1,000-30	1,000-30	1,000-30
	4,748-18	6,839-04	8,413-03							

CASE ,10000*01 - - - - - - - STREAMWISE DIMENSION ,85000*01FEET - - -, 21 APR 69 15:15:54

ALPHA	XI (LB /SEC)**2	ROKAP (FT)	PRESSURE (ATM)	EDGE VELOCITY (FT/SEC)	BETA	FLUX NORMALIZING PARAMETER	HEAT FLUXES DIFFUSIONAL (BTU/SEC SQ FT)	TOT ENTH (BTU/SEC SQ FT)	RERAD
4,413*00	8,521*-05	1,000*00	1,087*01	2,353*02	0,000	7,679*02	1,513*02	1,513*02	0,000

WALL SHEAR (LB/SQ FT)	MECH REM	MASS FLUXES PYROL GAS (LB/SEC SQ FT)	CHAR	TOTAL GAS	ELEMENTAL MASS DIFFUSIVE FLUXES (LB/SEC SQ FT) FOR HYDROGEN	NITROGEN	OXYGEN
5,514*-01	0,000	0,000	0,000	0,000	1,525*-05	*-1,195*-05	*-3,303*-06

MOM TRANS COEFF, RHO*UE*CF/2	HEAT TRANS COEFF, RHO*UE*CH	BLOWING PARAMETERS (BASED ON CH) FOR PYROL GAS	CHAR	TOTAL GAS	ELEMENTAL MASS TRANSFER COEFFICIENTS, RHOE*UE*CM (LB/SEC SQ FT) FOR HYDROGEN	NITROGEN	OXYGEN
7,539*-02	1,053*-01	0,000	0,000	0,000	*-2,211*-04	5,843*-05	*-1,208*-05

MOMENTUM THICKNESS, THETA (FT)	DISPLACE. THICKNESS, DELSTAR (FT)	SHAPE FACTOR, DELSTAR /THETA	ENTHALPY THICKNESS, LAMBDA (FT)	REYNOLDS NUMBER PER FOOT	MASS THICKNESSES (FT) FOR HYDROGEN	NITROGEN	OXYGEN
1,142*-03	3,594*-03	3,147*00	1,557*-03	3,565*05	3,726*-03	7,896*-03	6,844*-03

NODAL INFORMATION

DISTANCE FROM WALL (FT)	ETA	F	FP (=U/UE)	FPP	FPPP	TOTAL ENTHALPY, G (BTU/LB)	GP (BTU/LB)	GPP (BTU/LB)	STATIC ENTHALPY (BTU/LB)	TEMP (DEG R)
0,000	0,000	0,000	0,000	1,007*00	6,050*-01	*-1,194*03	1,339*03	5,925*02	*-1,194*03	8,000*02
1,994*-05	1,059*-01	5,725*-03	1,085*-01	1,027*00	*-2,194*-01	*-1,051*03	1,327*03	*-8,157*02	*-1,051*03	8,538*02
3,432*-05	1,765*-01	1,589*-02	1,782*-01	9,150*-01	*-2,956*00	*-9,619*02	1,167*03	*-3,714*03	*-9,619*02	8,890*02
6,568*-05	3,177*-01	4,892*-02	2,816*-01	5,759*-01	*-1,847*00	*-8,293*02	7,450*02	*-2,263*03	*-8,294*02	9,484*02
1,183*-04	5,296*-01	1,190*-01	3,710*-01	3,106*-01	*-6,577*-01	*-7,120*02	4,104*02	*-8,965*02	*-7,122*02	1,013*03
2,165*-04	8,826*-01	2,654*-01	4,496*-01	1,624*-01	*-1,823*-01	*-6,094*02	2,097*02	*-2,401*02	*-6,096*02	1,086*03
3,803*-04	1,412*00	5,224*-01	5,151*-01	9,453*-02	*-7,388*-02	*-5,265*02	1,135*02	*-1,233*02	*-5,268*02	1,176*03
6,200*-04	2,118*00	9,062*-01	5,681*-01	6,215*-02	*-1,785*-02	*-4,673*02	6,814*01	*-5,178*00	*-4,676*02	1,260*03
1,165*-03	3,530*00	1,765*00	6,473*-01	5,666*-02	1,008*-02	*-3,784*02	5,617*01	*-1,178*01	*-3,789*02	1,506*03
2,420*-03	6,178*00	3,697*00	8,145*-01	6,277*-02	*-5,463*-03	*-2,231*02	7,923*01	2,919*01	*-2,238*02	2,010*03
4,241*-03	8,826*00	6,049*00	9,500*-01	3,520*-02	*-1,536*-02	3,117*01	9,098*01	*-2,031*01	3,017*01	3,459*03
9,041*-03	1,412*01	1,130*01	9,986*-01	*-2,196*-03	1,240*-03	2,788*02	1,208*01	*-9,485*00	2,777*02	4,283*03
1,687*-02	2,207*01	1,922*01	1,000*00	0,000	*-6,874*-04	2,430*02	0,000	6,442*00	2,419*02	5,566*03

DISTANCE FROM WALL (FT)	DENSITY, RHO (LB/CU FT)	VISCOSITY, MU LB/SEC FT	RHO*MU /RHOE*MUE, C	SPECIFIC HEAT (BTU/LB R)	THERMAL COND (BTU /SEC FT R)	PRANDTL NUMBER	MODIFIED SCHMIDT NUMBER	MOLECULAR WEIGHT	RHOSQ*EPS /RHOE*MUE	MACH NUMBER
0,000	3,091*-01	1,344*-05	9,752*-01	5,211*01	1,172*-05	5,975*-01	7,275*-01	1,662*01	0,000	0,000
1,994*-05	2,812*-01	1,400*-05	9,242*-01	5,224*01	1,296*-05	5,643*-01	7,269*-01	1,613*01	3,167*-02	1,443*-02
3,432*-05	2,642*-01	1,436*-05	8,905*-01	5,230*01	1,381*-05	5,436*-01	7,267*-01	1,579*01	1,830*-01	2,292*-02
6,568*-05	2,373*-01	1,491*-05	8,304*-01	5,283*01	1,535*-05	5,131*-01	7,269*-01	1,513*01	8,806*-01	3,413*-02
1,183*-04	2,121*-01	1,546*-05	7,695*-01	5,380*01	1,704*-05	4,881*-01	7,274*-01	1,444*01	2,440*00	4,218*-02
2,165*-04	1,899*-01	1,608*-05	7,167*-01	5,487*01	1,877*-05	4,700*-01	7,279*-01	1,387*01	5,625*00	4,784*-02
3,803*-04	1,708*-01	1,686*-05	6,759*-01	5,574*01	2,049*-05	4,587*-01	7,283*-01	1,349*01	1,085*01	5,125*-02
6,200*-04	1,574*-01	1,762*-05	6,508*-01	5,630*01	2,186*-05	4,538*-01	7,285*-01	1,332*01	1,810*01	5,370*-02
1,165*-03	1,319*-01	1,990*-05	6,160*-01	5,692*01	2,502*-05	4,527*-01	7,287*-01	1,334*01	2,077*01	5,541*-02
2,420*-03	1,015*-01	2,438*-05	5,812*-01	5,780*01	3,064*-05	4,600*-01	7,286*-01	1,371*01	1,231*01	6,147*-02
4,241*-03	6,733*-02	3,684*-05	5,822*-01	5,855*01	4,312*-05	5,001*-01	7,284*-01	1,565*01	5,414*00	5,972*-02
9,041*-03	5,934*-02	4,366*-05	6,082*-01	5,683*01	4,734*-05	5,241*-01	7,287*-01	1,708*01	4,206*00	5,973*-02
1,687*-02	5,462*-02	5,580*-05	7,153*-01	5,267*01	4,749*-05	6,189*-01	7,284*-01	2,043*01	3,563*00	5,991*-02

DISTANCE FROM WALL,FT

0,000 1,994*-05 3,432*-05 6,568*-05 1,183*-04 2,165*-04 3,803*-04 6,200*-04 1,165*-03 2,420*-03
4,241*-03 9,041*-03 1,687*-02

ELEMENTAL FRACTIONS AND THEIR FIRST AND SECOND DERIVATIVES WITH RESPECT TO ETA

H4N2 9,832*-01 9,096*-01 8,674*-01 8,217*-01 8,000*-01 7,918*-01 7,872*-01 7,846*-01 7,697*-01 7,412*-01
6,291*-01 5,465*-01 4,348*-01
-7,021-01 *-6,618*-01 *-5,063*-01 *-1,917*-01 *-4,708*-02 *-1,092*-02 *-5,436*-03 *-5,617*-03 *-9,290*-03 *-2,774*-02
-3,908-02 *-1,076*-02 0,000
-3,514-01 1,113*00 3,291*00 1,166*00 1,993*-01 5,510*-03 1,522*-02 *-1,573*-02 1,053*-02 *-2,446*-02
1,590*-02 *-5,204*-03 7,912*-03

N2O4 *-3,377*-01 *-9,783*-02 3,884*-02 1,857*-01 2,528*-01 2,758*-01 2,824*-01 2,847*-01 2,986*-01 3,299*-01
4,608*-01 6,716*-01 5,652*-01
2,288*00 2,152*00 1,637*00 6,073*-01 1,394*-01 2,309*-02 5,101*-03 4,955*-03 9,104*-03 2,922*-02
5,787*-02 1,043*-02 0,000
1,224*00 *-3,802*00 *-1,078*01 *-3,811*00 *-6,064*-01 *-5,268*-02 *-1,528*-02 1,487*-02 *-8,990*-03 2,419*-02
-2,548-03 *-1,537*-02 1,275*-02

O 3,545*-01 1,882*-01 9,371*-02 *-7,438*-03 *-5,287*-02 *-6,758*-02 *-6,961*-02 *-6,930*-02 *-6,830*-02 *-7,107*-02
-8,995-02 *-2,181*-01 1,001*-05
*-1,586*00 *-1,490*00 *-1,131*00 *-4,156*-01 *-9,235*-02 *-1,217*-02 3,358*-04 6,620*-04 1,854*-04 *-1,480*-03
-1,879-02 3,307*-04 *0,000
-8,729-01 2,689*00 7,484*00 2,645*00 4,071*-01 4,717*-02 6,229*-05 8,618*-04 *-1,537*-03 2,785*-04
-1,335-02 2,057*-02 *-2,066*-02

MOLE FRACTIONS

H4N2	1,355-23	1,501-22	5,761-22	3,941-21	2,156-20	1,022-19	4,673-19	1,525-18	1,999-17	5,078-16
	2,368-14	5,720-14	1,535-14							
N2O4	1,000-30	1,000-30	1,000-30	1,000-30	1,000-30	1,000-30	1,000-30	1,000-30	1,000-30	1,000-30
	9,876-33	1,375-26	3,398-18							
O	1,000-30	1,000-30	1,000-30	1,000-30	1,000-30	2,483-39	4,191-36	1,849-33	2,266-27	1,845-19
	2,929-09	1,929-06	4,249-03							
H2	1,926-01	2,598-01	3,026-01	3,694-01	4,283-01	4,734-01	5,024-01	5,135-01	5,177-01	4,976-01
	3,887-01	3,157-01	8,906-02							
H2O	1,242-01	1,212-01	1,191-01	1,151-01	1,110-01	1,077-01	1,069-01	1,072-01	1,162-01	1,358-01
	2,255-01	2,655-01	4,388-01							
H3N	4,686-01	3,566-01	2,886-01	1,941-01	1,211-01	6,944-02	3,567-02	1,985-02	4,700-03	6,513-04
	3,829-05	1,503-05	1,196-06							
N2	2,146-01	2,625-01	2,897-01	3,213-01	3,396-01	3,495-01	3,550-01	3,575-01	3,614-01	3,660-01
	3,855-01	4,160-01	3,987-01							
H	1,308-24	6,285-23	6,117-22	1,907-20	5,015-19	1,249-17	3,578-16	5,456-15	2,665-12	7,864-09
	1,752-04	2,447-03	1,872-02							
HO	1,163-31	1,257-29	2,009-28	1,353-26	7,684-25	4,294-23	3,062-21	1,008-19	3,196-16	1,129-11
	9,037-06	3,825-04	3,424-02							
NO	8,842-38	2,119-35	5,438-34	7,481-32	8,424-30	9,385-28	1,406-25	8,574-24	1,142-19	2,680-14
	2,709-07	2,532-05	7,874-03							
O2	1,000-30	1,000-30	1,000-30	1,000-30	1,000-30	1,000-30	7,291-37	2,910-34	3,260-28	2,665-20
	7,436-10	6,795-07	8,413-03							

CASE ,10000+01 - - - - - - - STREAMWISE DIMENSION ,14820-00FEET - - -, 21 APR 69 15:17:50

ALPHA	XI (LB /SEC)**2	ROKAP (FT)	PRESSURE (ATM)	EDGE VELOCITY (FT/SEC)	BETA	FLUX NORMALIZING PARAMETER	HEAT FLUXES DIFFUSIONAL (BTU/SEC SQ FT)	TOT ENTH (BTU/SEC SQ FT)	RERAD
4,205+00	1,486-04	1,000+00	1,087+01	2,353+02	0,000	5,816+02	1,606+02	1,606+02	0,000

WALL SHEAR (LB/SQ FT)	MECH REM	MASS FLUXES PYROL GAS (LB/SEC SQ FT)	CHAR	TOTAL GAS	ELEMENTAL MASS DIFFUSIVE FLUXES (LB/SEC SQ FT) FOR HYDROGEN	NITROGEN	OXYGEN
5,486-01	0,000	0,000	0,000	0,000	1,330-05	-1,061-05	-2,693-06

MOM TRANS COEFF, RHO*UE*CF/2	HEAT TRANS COEFF, RHO*UE*CH	BLOWING PARAMETERS (BASED ON CH) FOR PYROL GAS	CHAR	TOTAL GAS	ELEMENTAL MASS TRANSFER COEFFICIENTS, RHOE*UE*CM (LB/SEC SQ FT) FOR HYDROGEN	NITROGEN	OXYGEN
7,500-02	1,021-01	0,000	0,000	0,000	-2,111-04	5,810-05	-1,096-05

MOMENTUM THICKNESS, THETA (FT)	DISPLACE, THICKNESS, DELSTAR (FT)	SHAPE FACTOR, DELSTAR /THETA	ENTHALPY THICKNESS, LAMBDA (FT)	REYNOLDS NUMBER PER FOOT	MASS THICKNESSES (FT) FOR HYDROGEN	NITROGEN	OXYGEN
1,421-03	5,648-03	3,974+00	1,797-03	3,565+05	4,152-03	9,000-03	7,756-03

NODAL INFORMATION

DISTANCE FROM WALL (FT)	ETA		FP (=U/UE)	FPP	FPPP	TOTAL ENTHALPY,G (BTU/LB)	GP (BTU/LB)	GPP (BTU/LB)	STATIC ENTHALPY (BTU/LB)	TEMP (DEG R)
0,000	0,000	0,000	0,000	1,277+00	2,401+00	-1,330+03	1,793+03	2,591+03	-1,330+03	8,000+02
2,499-05	1,009-01	6,707-03	1,330-01	1,279+00	-2,350+00	-1,146+03	1,729+03	-3,856+03	-1,146+03	8,748+02
4,349-05	1,682-01	1,840-02	2,120-01	1,043+00	-4,666+00	-1,040+03	1,401+03	-5,889+03	-1,040+03	9,231+02
8,491-05	3,027-01	5,473-02	3,178-01	5,878+01	-2,101+00	-8,955+02	8,222+02	-2,721+03	-8,956+02	1,004+03
1,561-04	5,046-01	1,285-01	4,034-01	3,084+01	-6,672-01	-7,730+02	4,502+02	-9,657+02	-7,732+02	1,099+03
2,923-04	8,409-01	2,781-01	4,782-01	1,626+01	-1,997-01	-6,632+02	2,416+02	-2,741+02	-6,635+02	1,225+03
5,253-04	1,346+00	5,365-01	5,403-01	9,456+02	-7,006-02	-5,700+02	1,400+02	-1,289+02	-5,703+02	1,373+03
8,733-04	2,018+00	9,184-01	5,912-01	6,122+02	-2,903-02	-4,970+02	8,910+01	-2,233+01	-4,974+02	1,521+03
1,659-03	3,364+00	1,762+00	6,605-01	5,160+02	1,473-02	-3,916+02	7,183+01	-3,342+00	-3,920+02	1,760+03
3,480-03	5,887+00	3,619+00	8,167-01	6,396+02	-4,925-03	-1,908+02	9,930+01	2,512+01	-1,915+02	2,461+03
5,940-03	8,409+00	5,861+00	9,500-01	3,684+02	-1,658-02	8,027+01	9,205+01	-3,087+01	7,928+01	3,564+03
1,224-02	1,346+01	1,086+01	1,000+00	-2,134-03	1,128+03	2,650+02	3,588+00	-4,197+00	2,639+02	5,016+03
2,245-02	2,102+01	1,842+01	1,000+00	0,000	-5,639-04	2,430+02	0,000	3,249+00	2,419+02	5,566+03

DISTANCE FROM WALL (FT)	DENSITY, RHO (LB/CU FT)	VISCOSITY, MU LB/SEC FT	RHO*MU /RHOE*MUE,	SPECIFIC HEAT C (BTU/LB R)	THERMAL COND (BTU /SEC FT R)	PRANDTL NUMBER	MODIFIED SCHMIDT NUMBER	MOLECULAR WEIGHT	RHOSQ*EPS /RHOE*MUE	MACH NUMBER
0,000	3,157-01	1,363-05	1,010+00	5,071+01	1,149-05	6,019+01	7,271+01	1,697+01	0,000	0,000
2,499-05	2,777-01	1,443-05	9,409-01	5,080+01	1,314-05	5,579+01	7,267+01	1,633+01	6,729-02	1,754-02
4,349-05	2,557-01	1,492-05	8,954-01	5,097+01	1,427-05	5,326+01	7,268+01	1,586+01	3,408+01	2,671-02
8,491-05	2,234-01	1,567-05	8,216-01	5,177+01	1,622-05	5,001+01	7,273+01	1,508+01	1,370+00	3,709-02
1,561-04	1,953-01	1,650-05	7,564-01	5,289+01	1,826-05	4,781+01	7,279+01	1,442+01	3,410+00	4,339-02
2,923-04	1,700-01	1,763-05	7,036-01	5,398+01	2,045-05	4,655+01	7,283+01	1,399+01	7,147+00	4,715-02
5,253-04	1,498-01	1,898-05	6,674-01	5,482+01	2,257-05	4,610+01	7,285+01	1,382+01	1,267+01	4,947-02
8,733-04	1,350-01	2,031-05	6,436-01	5,543+01	2,446-05	4,603+01	7,286+01	1,380+01	1,958+01	5,123-02
1,659-03	1,174-01	2,244-05	6,182-01	5,611+01	2,725-05	4,619+01	7,286+01	1,389+01	2,228+01	5,345-02
3,480-03	8,742-02	2,849-05	5,847-01	5,744+01	3,449-05	4,745+01	7,285+01	1,446+01	1,236+01	5,762-02
5,940-03	6,633-02	3,772-05	5,874-01	5,819+01	4,363-05	5,031+01	7,285+01	1,589+01	7,116+00	5,937-02
1,224-02	5,493-02	5,022-05	6,475-01	5,555+01	4,953-05	5,632+01	7,286+01	1,851+01	4,880+00	5,875-02
2,245-02	5,462-02	5,580-05	7,153-01	5,267+01	4,749-05	6,189+01	7,284+01	2,043+01	4,825+00	5,991-02

DISTANCE FROM WALL,FT

0,000 2,499-05 4,349-05 8,491-05 1,561-04 2,923-04 5,253-04 8,733-04 1,659-03 3,480-03
5,940-03 1,224-02 2,245-02

ELEMENTAL FRACTIONS AND THEIR FIRST AND SECOND DERIVATIVES WITH RESPECT TO ETA

H4N2	9,357-01	8,411-01	7,958-01	7,569-01	7,437-01	7,406-01	7,392-01	7,369-01	7,282-01	6,935-01
	6,117-01	4,997-01	4,348-01							
	-9,394-01	-8,251-01	-5,202-01	-1,390-01	-2,255-02	-2,486-03	-2,819-03	-4,458-03	-7,820-03	-2,448-02
	-3,281-02	-1,528-02	0,000							
	-2,165+00	4,431+00	4,633+00	1,034+00	1,198-01	-5,154-04	-8,074-04	-4,064-03	-9,334-04	-1,227-02
	5,674-03	1,274-03	2,763-03							
N2O4	-2,733-01	3,402-02	1,800-01	3,035-01	3,434-01	3,496-01	3,494-01	3,493-01	3,637-01	3,911-01
	5,225-01	6,229-01	5,652-01							
	3,053+00	2,670+00	1,667+00	4,319-01	6,110-02	-1,779-03	-7,333-04	3,911-03	9,314-03	3,193-02
	5,177-02	-2,193-03	0,000							
	7,141+00	-1,474+01	-1,507+01	-3,288+00	-3,865-01	1,268-02	-8,534-03	2,234-02	-1,431-02	3,224-02
	-1,651-02	-4,884-03	5,464-03							
O	3,376-01	1,249-01	2,420-02	-6,032-02	-8,702-02	-9,016-02	-8,864-02	-8,622-02	-9,192-02	-8,452-02
	-1,342-01	-1,226-01	1,001-05							
	-2,114+00	-1,845+00	-1,147+00	-2,930-01	-3,854-02	4,265-03	3,553-03	5,469-04	-1,493-03	-7,446-03
	-1,896-02	1,747-02	-0,000							
	-4,976+00	1,031+01	1,044+01	2,254+00	2,667-01	-1,217-02	9,341-03	-1,828-02	1,524-02	-1,996-02

1,083-02 3,611-03 -8,227-03

MOLE FRACTIONS

H4N2	1,255-23	3,110-22	1,645-21	1,558-20	1,147-19	8,531-19	5,144-18	2,102-17	1,220-16	2,750-15
	2,757-14	5,835-14	1,535-14							
N2O4	1,000-30	1,000-30	1,000-30	1,000-30	1,000-30	1,000-30	1,000-30	1,000-30	1,000-30	1,000-30
	7,940-32	4,635-22	3,398-18							
O	1,000-30	1,000-30	1,000-30	1,000-30	1,017-38	2,132-34	2,716-30	5,637-27	9,362-23	5,146-19
	7,748-09	1,602-04	4,249-03							
H2	1,802-01	2,681-01	3,206-01	3,930-01	4,460-01	4,782-01	4,908-01	4,932-01	4,891-01	4,561-01
	3,787-01	2,160-01	8,906-02							
H2O	1,565-01	1,516-01	1,481-01	1,421-01	1,368-01	1,338-01	1,334-01	1,351-01	1,398-01	1,694-01
	2,276-01	3,533-01	4,388-01							
H3N	4,363-01	2,916-01	2,126-01	1,181-01	5,755-02	2,308-02	9,019-03	4,089-03	1,450-03	1,959-04
	3,357-05	5,731-06	1,196-06							
N2	2,270-01	2,888-01	3,186-01	3,468-01	3,596-01	3,649-01	3,668-01	3,676-01	3,697-01	3,743-01
	3,934-01	4,137-01	3,987-01							
H	1,265-24	2,416-22	4,507-21	3,179-19	1,985-17	1,767-15	1,203-13	3,570-12	2,617-10	6,254-07
	2,630-04	1,094-02	1,872-02							
HO	1,514-31	8,768-29	3,142-27	6,009-25	1,064-22	3,195-20	7,191-18	5,723-16	1,500-13	4,246-09
	1,575-05	5,170-03	3,424-02							
NO	1,224-37	2,066-34	1,357-32	6,322-30	2,722-27	2,216-24	1,305-21	2,275-19	1,633-16	3,004-11
	5,338-07	6,160-04	7,874-03							
O2	1,000-30	1,000-30	1,000-30	1,000-30	2,771-39	4,654-35	5,129-31	9,820-28	1,530-23	9,247-16
	2,024-09	1,069-04	8,413-03							

APPENDIX B

ABLATION PREDICTION (CMA) PRINTOUT

Fuel Rich- Low Ablation Case

PREDICTION AT THROAT OF JPL CHAMBER, UN 16, EDGE AND RECOVERY ENTHALPIES BASED ON OVERALL O/F, MATERIAL IS REFRASIL PHENOLIC(MXS89/MX2600)
COMPOSITION AT EDGE IS BOTTLE 6 MEASURED ELEMENTS R~~2~~,7009=1

---REACTION KINETIC EQUATION---

```
DRHO/DTIME = GAMMA ( BA*EXP(-EA/T)RHOOA((RHOA-RHORA)/RHOOA)**PSIA )
           + GAMMA ( BB*EXP(-EB/T)RHOOB((RHOB-RHORB)/RHOOB)**PSIB )
          +(1-GAMMA)( BC*EXP(-EC/T)RHOOC((RHOC-RHORC)/RHOOC)**PSIC )
```

---REACTION KINETIC CONSTANTS---

REACTION	RHOO (LB/CU FT)	RHOR	B (1/SEC)	PSI	E (DEG R)	T REAC (DEG R)
A	60,75	32,40	,4480+10	3,00	,3680+05	600,
B	20,24	,00	,1400+05	3,00	,1540+05	1000,
C	120,30	120,30	-,0000	-,00	-,0000	90000,

RESIN VOLUME FRACTION, GAMMA = ,395(MASS FRACTION = ,305)

---TIME INCREMENT INFORMATION---

INITIAL TIME (SEC) =,000 FINAL TIME (SEC) 45,00

OUTPUT INTERVAL = ,200 SEC FROM INITIAL TIME UNTIL 3,000 SEC
OUTPUT INTERVAL = 1,000 SEC FROM 3,000 SEC UNTIL 15,000 SEC
OUTPUT INTERVAL = 5,000 SEC FROM 15,000 SEC UNTIL FINAL TIME

MAXIMUM TIME STEP =1,00 SECONDS

---NODAL DATA---

NODE NO.	MATL NO.	TEMPERATURE (DEG,RANKINE)	RELATIVE AREA	THICKNESS (INCHES)	NODAL DEPTH (INCHES)	CONT,RESISTANCE (SQFT-S-DEG/BTU)
1	1	530,00	,3750-00	,00500	,000000*	-,0000
2	1	530,00	,3850-00	,01000	,010000	-,0000
3	1	530,00	,3950-00	,01000	,020000	-,0000
4	1	530,00	,4100-00	,02000	,035000	-,0000
5	1	530,00	,4300-00	,02000	,055000	-,0000
6	1	530,00	,4500-00	,02000	,075000	-,0000
7	1	530,00	,4700-00	,02000	,095000	-,0000
8	1	530,00	,4900-00	,02000	,115000	-,0000
9	1	530,00	,5125-00	,02500	,137500	-,0000
10	1	530,00	,5400-00	,03000	,165000	-,0000
11	1	530,00	,5700-00	,03000	,195000	-,0000
12	1	530,00	,6050-00	,04000	,230000	-,0000
13	1	530,00	,6500-00	,05000	,275000	-,0000
14	1	530,00	,7000-00	,05000	,325000	-,0000
15	1	530,00	,7500-00	,05000	,375000	-,0000
16	1	530,00	,8000-00	,05000	,425000	-,0000
17	1	530,00	,8500-00	,05000	,475000	-,0000
18	1	530,00	,9250-00	,10000	,550000	-,0000
19	1	530,00	,1025+01	,10000	,650000	-,0000
20	1	530,00	,1125+01	,10000	,750000	-,0000
21	1	530,00	,1225+01	,10000	,850000	-,0000
22	1	530,00	,1375+01	,20000	1,000000	-,0000
23	1	530,00	,1575+01	,20000	1,200000	-,0000
24	1	530,00	,1775+01	,20000	1,400000	-,0000

*INITIAL INTERNAL RADIUS ,375 AREA PROP,TO RADIUS**1,00
MINIMUM THICKNESS OF LAST ABLATOR NODE (INCHES) ,0100
THERE ARE 10 NODELETS ASSIGNED TO EACH ABLATING NODE

BACK WALL CONVECTION COEF BTU/FTSQ-SEC-DEG R	BACK WALL EMISSIVITY	RESERVOIR TEMPERATURE
-,0000	-,000	-,00

---HEAT OF FORMATION OF MATERIAL CONSTITUENTS---
(BTU/LB)

PLASTIC	CHAR	GAS
-4656,00	-5540,00	,00

ENTHALPY DATUM TEMPERATURE = 536,000 DEG RANKINE

---MATERIAL THERMAL PROPERTY DATA---

MATERIAL NO, 1 VIRGIN PLASTIC | MATERIAL NO, 2 CHAR | MATERIAL NOS, 3 THROUGH 10 BACK-UP

MATERIAL NO, 1 — DENSITY = 104,773 LB/CU FT

TEMPERATURE (DEG R)	SPECIFIC HEAT (BTU/LB-DEG)	CONDUCTIVITY (BTU/FT-SEC-DEG)	SENSIBLE ENTHALPY (BTU/LB)	EMISSIVITY
530,00	,2600	,0001070	-1,60	,8500
800,00	,2750	,0001090	70,62	,8500
1160,00	,3100	,0001100	175,92	,8500
1500,00	,4720	,0001100	308,86	,8500
2000,00	,4840	,0001100	547,86	,8500
3000,00	,4930	,0001100	1036,36	,8500
4000,00	,4980	,0001100	1531,86	,8500
5000,00	,5000	,0001100	2030,86	,8500

MATERIAL NO, 2 — DENSITY = 85,579 LB/CU FT

TEMPERATURE (DEG R)	SPECIFIC HEAT (BTU/LB-DEG)	CONDUCTIVITY (BTU/FT-SEC-DEG)	SENSIBLE ENTHALPY (BTU/LB)	EMISSIVITY
530,00	,2100	,0003200	-1,92	,8500
1000,00	,4300	,0003320	148,48	,8500
1500,00	,4720	,0003480	373,98	,8500
2000,00	,4840	,0003600	612,98	,8500
3000,00	,4930	,0003880	1101,48	,8500
3500,00	,4950	,0004000	1348,48	,8500
4000,00	,4980	,0004300	1596,73	,8500
5000,00	,5000	,0005920	2095,73	,8500

TABLE OF OPTIONAL MASS-FRACTION FUNCTIONS FOR THERMAL CONDUCTIVITY
K = F1(X)*KP + F2(X)*KC

X	F1(X)	F2(X)
1,0000	1,0000	,0000
,8000	,5000	-,0000
,5500	,5000	-,0000
,2500	-,0000	1,0000
-,0000	-,0000	1,0000

---RESIN DECOMPOSITION GAS SENSIBLE ENTHALPY---

TEMPERATURE (DEG R)	900,00	1800,00	2700,00	3600,00	4500,00
ENTHALPY (BTU/LB)	-1780,00	-890,00	460,00	2640,00	3750,00
TEMPERATURE (DEG R)	5400,00	6300,00			
ENTHALPY (BTU/LB)	5050,00	7100,00			

---TIME DEPENDENT BOUNDARY CONDITIONS---

TIME (SEC)	PROB OPTN	RECOVERY ENTHALPY (BTU/LB)	RADIATION HEAT RATE (BTU/SQ FT-SECOND)	HEAT COEFF (LB/SQ FT-SECOND)	PRESSURE (ATM)	BLOWING REDUCTION PARAMETER
,00	1	222,00	-,00	,6300	-,00000	,400
1,00	1	2000,00	-,00	,3900	-,00000	,400
4,00	1	2550,00	-,00	,2850	-,00000	,400
45,00	1	2550,00	-,00	,2850	-,00000	,400

CH/CHO = PHI/(EXP(PHI)-1,) WHERE PHI = 2,*BRP*M DOT/CHO, BRP IN TABLE

---SURFACE EQUILIBRIUM DATA---

RATIO OF MASS TO HEAT TRANSFER COEFFICIENTS = ,730
UNEQUAL DIFFUSION EXPONENT = ,431
NOMINAL SURFACE VIEW FACTOR = ,050 (OPTION 1)
FISSURE MODEL NOT USED FOR GAS TERMS
HEAT TRANSFER COEFFICIENT MULTIPLIED BY (R INITIAL/R CURRENT)**EX,
WHERE EX = (1,8-,2N)/(1,-N) AND N IS THE BURNING RATE EXPONENT,
IN THIS PROBLEM N HAS BEEN SET EQUAL TO -,00000

P = 6,2000 ATM

TEMPERATURE (DEG R)	EDGE ENTH AT T-WALL	TEMPERATURE (DEG R)	EDGE ENTH AT T-WALL	TEMPERATURE (DEG R)	EDGE ENTH AT T-WALL
5400,00	2224,22	3600,00	1108,20	1800,00	90,76
4500,00	1658,27	2700,00	583,80	900,00	-371,01

M-DOT-GAS/CM = 3.0000 PRESSURE = 6.2000 ATM

TEMP (DEG R)	M-DOT-CHAR/CM	CHEM,PROD (BTU/LB)	SURFACE SPECIES	TEMP (DEG R)	M-DOT-CHAR/CM	CHEM,PROD (BTU/LB)	SURFACE SPECIES
900,00	,0001	1652,43		5789,32	,0200	-482,14	C*
1800,00	,0001	974,08		5785,94	,0500	-612,06	C*
2700,00	,0001	-29,64		5780,33	,1000	-827,83	C*
3600,00	,0001	-359,22		5769,18	,2000	-1256,66	C*
4500,00	,0001	26,86		5758,13	,3000	-1682,05	C*
5400,00	,0001	-290,17		5736,35	,5000	-2523,25	C*
5791,56	,0001	-395,77	C*	5614,26	1,0000	-2711,48	C*
5790,45	,0100	-438,76	C*	4998,60	3,0000	-5079,52	CSI*

M-DOT-GAS/CM = ,0500 PRESSURE = 6,2000 ATM

TEMP (DEG R)	M-DOT-CHAR/CM	CHEM,PROD (BTU/LB)	SURFACE SPECIES	TEMP (DEG R)	M-DOT-CHAR/CM	CHEM,PROD (BTU/LB)	SURFACE SPECIES
900,00	,0001	484,48		4199,40	,1000	-38,61	O2SI
1800,00	,0001	183,95		4199,40	,2000	-106,73	O2SI
2700,00	,0001	67,33		4199,40	,3000	-203,31	O2SI
3442,09	,0001	127,06	O2SI	4199,40	,5000	-527,66	O2SI
4010,22	,0100	93,68	O2SI	4199,40	1,0000	-1810,20	O2SI
4112,75	,0200	53,53	O2SI	4199,40	3,0000	-7560.04	O2SI
4199,40	,0500	-11,46	O2SI				

M-DOT-GAS/CM = ,0100 PRESSURE = 6,2000 ATM

TEMP (DEG R)	M-DOT-CHAR/CM	CHEM,PROD (BTU/LB)	SURFACE SPECIES	TEMP (DEG R)	M-DOT-CHAR/CM	CHEM,PROD (BTU/LB)	SURFACE SPECIES
900,00	,0001	445,42		4199,40	,1000	12,68	O2SI
1800,00	,0001	171,38		4199,40	,2000	-35,95	O2SI
2700,00	,0001	148,76		4199,40	,3000	-100,63	O2SI
3481,06	,0001	159,12	O2SI	4199,40	,5000	-327,42	O2SI
4063,89	,0100	103,78	O2SI	4199,40	1,0000	-1518,56	O2SI
4169,18	,0200	60,51	O2SI	4199,40	3,0000	-7259.20	O2SI
4199,40	,0500	33,20	O2SI				

M-DOT-GAS/CM = .0001 PRESSURE = 6,2000 ATM

TEMP (DEG R)	M-DOT-CHAR/CM	CHEM,PROD (BTU/LB)	SURFACE SPECIES	TEMP (DEG R)	M-DOT-CHAR/CM	CHEM,PROD (BTU/LB)	SURFACE SPECIES
900,00	,0001	435,77		4199,40	,1000	22,94	O2SI
1800,00	,0001	168,32		4199,40	,2000	-22,35	O2SI
2700,00	,0001	168,80		4199,40	,3000	-81,42	O2SI
3490,20	,0001	166,19	O2SI	4199,40	,5000	-286,24	O2SI
4076,51	,0100	105,94	O2SI	4199,40	1,0000	-1446,92	O2SI
4182,45	,0200	61,88	O2SI	4199,40	3,0000	-7184,74	O2SI
4199,40	,0500	42,31	O2SI				

---OUTPUT---

-,0000 SECONDS

TIME STEP	SURF ITER	PROB OPTN	SURFACE RAD (IN)	H WALL (BTU/LB)	H EDGE (BTU/LB)	HEAT COEFF (LB/SQ FT-SEC)	CH/CHO
1	0	1	,3750	,00	222,00	,6300	,00000

---ABLATION RATES---

B PRIME	B PRIME G	M DOT CHAR (LB/SQ FT-SEC)	M DOT GAS (LB/SQ FT-SEC)	M CHAR (LB/ORIG SQ FT)	M GAS (LB/ORIG SQ FT)
,00000	,00000	,000000	,000000	,000000	,000000

---RECESSIONS/RECESSION RATES---

SURFACE (IN) / (IN/SEC)	CHAR (,02) (IN) / (IN/SEC)	PYROLYSIS (,98) (IN) / (IN/SEC)
,0000000/ ,0000000	,0000000/ ,0000000	,0000000/ ,0000000

---SURFACE ENERGY FLUX TERMS---
CURRENT RATES (BTU/SQ FT SURFACE-SEC)
AND INTEGRATED VALUES (BTU/ORIG SQ FT)

	CONVECTED IN	RADIATED IN	RADIATED OUT	CHEMICAL GENERATION	CONDUCTION AWAY
RATE	,000	,000	,000	,000	,000
TOTAL	,000	,000	,000	,000	,000

---INTERIOR ENERGY TERMS---
CURRENT RATES (BTU/SQ FT SURFACE-SEC)
AND INTEGRATED VALUES (BTU/ORIG SQ FT)

	PYROL GAS PICK UP	DECOMP ABSORPTION	CONVECTION WITH SOLIDS	STORAGE IN SOLID	LOSS AT REAR FACE
RATE	,000	,000	,000	,000	,106-04
TOTAL	,000	,000	,000	,000	,106-06

NODE	MAT	TEMP (DEG R)	DENSITY (LB/CU FT)	ENTHALPY (BTU/LB)	NODE	MAT	TEMP (DEG R)	DENSITY (LB/CU FT)	ENTHALPY (BTU/LB)
1	1	530,00	104,773	-4857,60	13	1	530,00	104,773	-4857,60
2	1	530,00	104,773	-4857,60	14	1	530,00	104,773	-4857,60
3	1	530,00	104,773	-4857,60	15	1	530,00	104,773	-4857,60
4	1	530,00	104,773	-4857,60	16	1	530,00	104,773	-4857,60
5	1	530,00	104,773	-4857,60	17	1	530,00	104,773	-4857,60
6	1	530,00	104,773	-4857,60	18	1	530,00	104,773	-4857,60
7	1	530,00	104,773	-4857,60	19	1	530,00	104,773	-4857,60
8	1	530,00	104,773	-4857,60	20	1	530,00	104,773	-4857,60
9	1	530,00	104,773	-4857,60	21	1	530,00	104,773	-4857,60
10	1	530,00	104,773	-4857,60	22	1	530,00	104,773	-4857,60
11	1	530,00	104,773	-4857,60	23	1	530,00	104,773	-4857,60
12	1	530,00	104,773	-4857,60	24	1	530,00	104,773	-4857,60

1,0000 SECONDS

TIME STEP	SURF ITER	PROB OPTN	SURFACE RAD (IN)	H WALL (BTU/LB)	H EDGE (BTU/LB)	HEAT COEFF (LB/SQ FT-SEC)	CH/CHO
67	3	1	,3750	980,39	2000,00	,3743	,95984

---ABLATION RATES---

B PRIME	B PRIME G	M DOT CHAR (LB/SQ FT-SEC)	M DOT GAS (LB/SQ FT-SEC)	M CHAR (LB/ORIG SQ FT)	M GAS (LB/ORIG SQ FT)
,14528	,14496	,000088	,039611	,000007	,024730

---RECESSIONS/RECESSION RATES---

SURFACE (IN) / (IN/SEC)	CHAR (,02) (IN) / (IN/SEC)	PYROLYSIS (,98) (IN) / (IN/SEC)
,0000010/ ,0000124	,0000010/ ,0000112	,0247508/ ,0247119

---SURFACE ENERGY FLUX TERMS---
CURRENT RATES (BTU/SQ FT SURFACE-SEC)
AND INTEGRATED VALUES (BTU/ORIG SQ FT)

	CONVECTED IN	RADIATED IN	RADIATED OUT	CHEMICAL GENERATION	CONDUCTION AWAY
RATE	,382+03	,000	,268+01	,162+01	,381+03
TOTAL	,238+03	,000	,147+01	,329+02	,270+03

---INTERIOR ENERGY TERMS---
CURRENT RATES (BTU/SQ FT SURFACE-SEC)
AND INTEGRATED VALUES (BTU/ORIG SQ FT)

	PYROL GAS PICK UP	DECOMP ABSORPTION	CONVECTION WITH SOLIDS	STORAGE IN SOLID	LOSS AT REAR FACE
RATE	,959+02	,427+02	,113+00	,237+03	,106-04
TOTAL	,372+02	,273+02	,984-02	,204+03	,107-04

NODE	MAT	TEMP (DEG R)	DENSITY (LB/CU FT)	ENTHALPY (BTU/LB)	NODE	MAT	TEMP (DEG R)	DENSITY (LB/CU FT)	ENTHALPY (BTU/LB)
1	0	3385,26	86,596	-4208,49	13	1	530,00	104,773	-4857,61
2	0	2775,70	88,749	-4427,45	14	1	530,00	104,773	-4857,61
3	0	1794,83	100,939	-4511,03	15	1	530,00	104,773	-4857,61
4	0	1007,99	104,729	-4725,79	16	1	530,00	104,773	-4857,61
5	1	677,90	104,773	-4818,04	17	1	530,00	104,773	-4857,61
6	1	569,83	104,773	-4846,95	18	1	530,00	104,773	-4857,61
7	1	539,39	104,773	-4855,09	19	1	530,00	104,773	-4857,61
8	1	531,98	104,773	-4857,08	20	1	530,00	104,773	-4857,61
9	1	530,29	104,773	-4857,53	21	1	530,00	104,773	-4857,61
10	1	530,02	104,773	-4857,60	22	1	530,00	104,773	-4857,61
11	1	530,00	104,773	-4857,61	23	1	530,00	104,773	-4857,61
12	1	530,00	104.773	-4857,61	24	1	530,00	104,773	-4857,61

5,0000 SECONDS

TIME STEP	SURF ITER	PROB OPTN	SURFACE RAD (IN)	H WALL (BTU/LB)	H EDGE (BTU/LB)	HEAT COEFF (LB/SQ FT-SEC)	CH/CHO
112	3	1	,3855	1472,19	2550,00	,2546	,93887

---ABLATION RATES---

B PRIME	B PRIME G	M DOT CHAR (LB/SQ FT-SEC)	M DOT GAS	M CHAR (LB/ORIG SQ FT)	M GAS
,34088	,09137	,046367	,016979	,076272	,112999

---RECESSIONS/RECESSION RATES---

SURFACE (IN)	/ (IN/SEC)	CHAR (,02) (IN)	/ (IN/SEC)	PYROLYSIS (,98) (IN)	/ (IN/SEC)
,0105380	/ ,0065015	,0264454	/ ,0075843	,0823494	/ ,0104603

---SURFACE ENERGY FLUX TERMS---
CURRENT RATES (BTU/SQ FT SURFACE-SEC)
AND INTEGRATED VALUES (BTU/ORIG SQ FT)

	CONVECTED IN	RADIATED IN	RADIATED OUT	CHEMICAL GENERATION	CONDUCTION AWAY
RATE	,274+03	,000	,636+01	-,563+02	,212+03
TOTAL	,139+04	,000	,247+02	-,651+02	,130+04

---INTERIOR ENERGY TERMS---
CURRENT RATES (BTU/SQ FT SURFACE-SEC)
AND INTEGRATED VALUES (BTU/ORIG SQ FT)

	PYROL GAS PICK UP	DECOMP ABSORPTION	CONVECTION WITH SOLIDS	STORAGE IN SOLID	LOSS AT REAR FACE
RATE	,662+02	,173+02	,926+02	,355+02	,106-04
TOTAL	,363+03	,117+03	,145+03	,669+03	,535-04

NODE	MAT	TEMP (DEG R)	DENSITY (LB/CU FT)	ENTHALPY (BTU/LB)	NODE	MAT	TEMP (DEG R)	DENSITY (LB/CU FT)	ENTHALPY (BTU/LB)
1	0	4199,40	85,911	-3830,73	13	1	530,70	104,773	-4857,42
2	0	3835,22	95,867	-4013,74	14	1	530,09	104,773	-4857,58
3	0	3488,86	96,019	-4179,74	15	1	530,01	104,773	-4857,60
4	0	3050,86	86,604	-4373,43	16	1	529,99	104,773	-4857,61
5	0	1940,02	94,064	-4625,04	17	1	529,99	104,773	-4857,61
6	0	1243,98	104,279	-4660,63	18	1	529,99	104,773	-4857,61
7	1	945,56	104,773	-4742,80	19	1	529,99	104,773	-4857,61
8	1	766,40	104,773	-4794,37	20	1	529,99	104,773	-4857,61
9	1	647,50	104,773	-4826,17	21	1	529,99	104,773	-4857,61
10	1	576,65	104,773	-4845,13	22	1	529,99	104,773	-4857,61
11	1	546,19	104,773	-4853,27	23	1	529,99	104,773	-4857,61
12	1	534,19	104,773	-4856,48	24	1	529,99	104,773	-4857,61

10,0000 SECONDS

TIME STEP	SURF ITER	PROB OPTN	SURFACE RAD (IN)	H WALL (BTU/LB)	H EDGE (BTU/LB)	HEAT COEFF (LB/SQ FT-SEC)	CH/CHO
143	3	1	,4119	1472,19	2550,00	,2257	,93750

---ABLATION RATES---

B PRIME	B PRIME G	M DOT CHAR (LB/SQ FT-SEC)	M DOT GAS (LB/SQ FT-SEC)	M CHAR (LB/ORIG SQ FT)	M GAS (LB/ORIG SQ FT)
,33678	,09592	,039677	,015801	,276381	,205095

---RECESSIONS/RECESSION RATES---
(IN) / (IN/SEC)

SURFACE	CHAR (,02)	PYROLYSIS (,98)
,0368998/ ,0055635	,0651056/ ,0094052	,1352501/ ,0105127

---SURFACE ENERGY FLUX TERMS---
CURRENT RATES (BTU/SQ FT SURFACE-SEC)
AND INTEGRATED VALUES (BTU/ORIG SQ FT)

	CONVECTED IN	RADIATED IN	RADIATED OUT	CHEMICAL GENERATION	CONDUCTION AWAY
RATE	,243+03	,000	,636+01	-,504+02	,186+03
TOTAL	,277+04	,000	,579+02	-,322+03	,239+04

---INTERIOR ENERGY TERMS---
CURRENT RATES (BTU/SQ FT SURFACE-SEC)
AND INTEGRATED VALUES (BTU/ORIG SQ FT)

	PYROL GAS PICK UP	DECOMP ABSORPTION	CONVECTION WITH SOLIDS	STORAGE IN SOLID	LOSS AT REAR FACE
RATE	,632+02	,149+02	,841+02	,243+02	,106-04
TOTAL	,726+03	,207+03	,539+03	,910+03	,110-03

NODE	MAT	TEMP (DEG R)	DENSITY (LB/CU FT)	ENTHALPY (BTU/LB)	NODE	MAT	TEMP (DEG R)	DENSITY (LB/CU FT)	ENTHALPY (BTU/LB)
1	0	4199,40	85,877	-3832,07	13	1	541,12	104,773	-4854,63
2	0	3876,96	85,815	-3995,10	14	1	532,79	104,773	-4856,86
3	0	3565,98	85,887	-4146,66	15	1	530,64	104,773	-4857,43
4	0	3164,76	86,044	-4338,90	16	1	530,13	104,773	-4857,57
5	0	2726,67	86,854	-4522,46	17	1	530,02	104,773	-4857,60
6	0	1926,22	94,516	-4642,87	18	1	529,99	104,773	-4857,61
7	0	1332,64	103,792	-4639,08	19	1	529,99	104,773	-4857,61
8	0	1048,14	104,735	-4713,85	20	1	529,99	104,773	-4857,61
9	1	853,45	104,773	-4769,74	21	1	529,99	104,773	-4857,61
10	1	707,83	104,773	-4810,04	22	1	529,99	104,773	-4857,61
11	1	618,96	104,773	-4833,81	23	1	529,99	104,773	-4857,61
12	1	566,84	104,773	-4847,75	24	1	529,99	104,773	-4857,61

20,0000 SECONDS

TIME STEP	SURF ITER	PROB OPTN	SURFACE RAD (IN)	H WALL (BTU/LB)	H EDGE (BTU/LB)	HEAT COEFF (LB/SQ FT-SEC)	CH/CHO
193	4	1	,4564	1472,19	2550,00	,1890	,94451

---ABLATION RATES---

B PRIME	B PRIME G	M DOT CHAR (LB/SQ FT-SEC)	M DOT GAS	M CHAR (LB/ORIG SQ FT)	M GAS
,31758	,09575	,030603	,013209	,644505	,380255

---RECESSIONS/RECESSION RATES---

(IN) / (IN/SEC)			
SURFACE	CHAR (,02)		PYROLYSIS (,98)
,0814375/ ,0042911	,1282869/ ,0052895		,2207654/ ,0084817

---SURFACE ENERGY FLUX TERMS---
CURRENT RATES (BTU/SQ FT SURFACE-SEC)
AND INTEGRATED VALUES (BTU/ORIG SQ FT)

	CONVECTED IN	RADIATED IN	RADIATED OUT	CHEMICAL GENERATION	CONDUCTION AWAY
RATE	,204+03	,000	,636+01	-,379+02	,159+03
TOTAL	,533+04	,000	,131+03	-,808+03	,438+04

---INTERIOR ENERGY TERMS---
CURRENT RATES (BTU/SQ FT SURFACE-SEC)
AND INTEGRATED VALUES (BTU/ORIG SQ FT)

	PYROL GAS PICK UP	DECOMP ABSORPTION	CONVECTION WITH SOLIDS	STORAGE IN SOLID	LOSS AT REAR FACE
RATE	,542+02	,116+02	,544+02	,392+02	,106-04
TOTAL	,143+04	,366+03	,128+04	,130+04	,233-03

NODE	MAT	TEMP (DEG R)	DENSITY (LB/CU FT)	ENTHALPY (BTU/LB)	NODE	MAT	TEMP (DEG R)	DENSITY (LB/CU FT)	ENTHALPY (BTU/LB)
1	0	4199,40	85,804	-3834,92	13	1	598,40	104,773	-4839,31
2	0	3918,57	85,748	-3977,06	14	1	557,20	104,773	-4850,33
3	0	3643,52	85,786	-4112,11	15	1	540,21	104,773	-4854,88
4	0	3277,13	85,865	-4290,39	16	1	533,62	104,773	-4856,64
5	0	2877,08	86,070	-4479,33	17	1	531,23	104,773	-4857,27
6	0	2551,30	86,596	-4618,04	18	1	530,20	104,773	-4857,55
7	0	2287,68	88,367	-4679,92	19	1	530,01	104,773	-4857,60
8	0	1693,16	97,697	-4646,23	20	1	529,99	104,773	-4857,61
9	0	1237,16	104,007	-4670,73	21	1	529,99	104,773	-4857,61
10	0	982,03	104,753	-4732,70	22	1	529,99	104,773	-4857,61
11	1	808,16	104,773	-4782,99	23	1	529,99	104,773	-4857,61
12	1	682,61	104,773	-4816,78	24	1	529,99	104,773	-4857,61

30,0000 SECONDS

TIME STEP	SURF ITER	PROB OPTN	SURFACE RAD (IN)	H WALL (BTU/LB)	H EDGE (BTU/LB)	HEAT COEFF (LB/SQ FT-SEC)	CH/CHO
234	2	1	,4954	1472,19	2550,00	,1624	,94075

---ABLATION RATES---

B PRIME	B PRIME G	M DOT CHAR (LB/SQ FT-SEC)	M DOT GAS (LB/SQ FT-SEC)	M CHAR (LB/ORIG SQ FT)	M GAS (LB/ORIG SQ FT)
,32979	,09144	,028260	,010842	,997638	,538198

---RECESSIONS/RECESSION RATES---

SURFACE (IN) / (IN/SEC)	CHAR (,02) (IN) / (IN/SEC)	PYROLYSIS (,98) (IN) / (IN/SEC)
,1204144/ ,0039626	,1812352/ ,0049576	,2890853/ ,0063059

---SURFACE ENERGY FLUX TERMS---

CURRENT RATES (BTU/SQ FT SURFACE-SEC)
AND INTEGRATED VALUES (BTU/ORIG SQ FT)

	CONVECTED IN	RADIATED IN	RADIATED OUT	CHEMICAL GENERATION	CONDUCTION AWAY
RATE	,175+03	,000	,636+01	-,337+02	,135+03
TOTAL	,770+04	,000	,211+03	-,126+04	,622+04

---INTERIOR ENERGY TERMS---

CURRENT RATES (BTU/SQ FT SURFACE-SEC)
AND INTEGRATED VALUES (BTU/ORIG SQ FT)

	PYROL GAS PICK UP	DECOMP ABSORPTION	CONVECTION WITH SOLIDS	STORAGE IN SOLID	LOSS AT REAR FACE
RATE	,453+02	,901+01	,580+02	,223+02	,106-04
TOTAL	,209+04	,500+03	,200+04	,163+04	,368-03

NODE	MAT	TEMP (DEG R)	DENSITY (LB/CU FT)	ENTHALPY (BTU/LB)	NODE	MAT	TEMP (DEG R)	DENSITY (LB/CU FT)	ENTHALPY (BTU/LB)
1	0	4199,40	85,785	-3835,67	13	1	679,84	104,773	-4817,52
2	0	3961,80	85,720	-3956,68	14	1	601,83	104,773	-4838,39
3	0	3728,43	85,748	-4071,45	15	1	563,03	104,773	-4848,77
4	0	3408,06	85,801	-4228,20	16	1	544,60	104,773	-4853,70
5	0	3045,62	85,912	-4402,90	17	1	536.25	104,773	-4855,93
6	0	2743,49	86,129	-4542,28	18	1	531,53	104,773	-4857,20
7	0	2487,15	86,534	-4651,79	19	1	530.25	104,773	-4857,54
8	0	2271,55	87,998	-4701,51	20	1	530,03	104,773	-4857,60
9	0	1677,19	97,241	-4676,18	21	1	529.99	104,773	-4857,61
10	0	1216,66	103,914	-4681,36	22	1	529,98	104,773	-4857,61
11	0	985,44	104,750	-4731,78	23	1	529,98	104,773	-4857,61
12	1	813,03	104,773	-4781,57	24	1	529,98	104,773	-4857,61

45,0000 SECONDS

TIME STEP	SURF ITER	PROB OPTN	SURFACE RAD (IN)	H WALL (BTU/LB)	H EDGE (BTU/LB)	HEAT COEFF (LB/SQ FT-SEC)	CH/CHO
280	2	1	,5448	1472,19	2550,00	,1369	,94122

---ABLATION RATES---

B PRIME	B PRIME G	M DOT CHAR (LB/SQ FT-SEC)	M DOT GAS (LB/SQ FT-SEC)	M CHAR (LB/ORIG SQ FT)	M GAS (LB/ORIG SQ FT)
,32611	,09142	,023462	,009139	1,486665	,759150

---RECESSIONS/RECESSION RATES---
(IN) / (IN/SEC)

SURFACE	CHAR (,02)	PYROLYSIS (,98)
,1698092/ ,0032899	,2504281/ ,0043575	,3750948/ ,0051780

---SURFACE ENERGY FLUX TERMS---
CURRENT RATES (BTU/SQ FT SURFACE-SEC)
AND INTEGRATED VALUES (BTU/ORIG SQ FT)

	CONVECTED IN	RADIATED IN	RADIATED OUT	CHEMICAL GENERATION	CONDUCTION AWAY
RATE	,148+03	,000	,636+01	-,280+02	,113+03
TOTAL	,110+05	,000	,343+03	-,189+04	,879+04

---INTERIOR ENERGY TERMS---
CURRENT RATES (BTU/SQ FT SURFACE-SEC)
AND INTEGRATED VALUES (BTU/ORIG SQ FT)

	PYROL GAS PICK UP	DECOMP ABSORPTION	CONVECTION WITH SOLIDS	STORAGE IN SOLID	LOSS AT REAR FACE
RATE	,387+02	,725+01	,489+02	,183+02	,106-04
TOTAL	,301+04	,678+03	,301+04	,208+04	,589-03

NODE	MAT	TEMP (DEG R)	DENSITY (LB/CU FT)	ENTHALPY (BTU/LB)	NODE	MAT	TEMP (DEG R)	DENSITY (LB/CU FT)	ENTHALPY (BTU/LB)
1	0	4199,40	85,755	-3836,83	13	1	812,02	104,773	-4781,86
2	0	3998,56	85,695	-3939,43	14	1	687,65	104,773	-4815,43
3	0	3800,18	85,713	-4037,20	15	1	615,35	104,773	-4834,77
4	0	3520,31	85,747	-4174,84	16	1	574,87	104,773	-4845,60
5	0	3194,15	85,811	-4333,48	17	1	552,96	104,773	-4851,46
6	0	2913,87	85,917	-4467,31	18	1	537,69	104,773	-4855,55
7	0	2673,62	86,101	-4577,50	19	1	531,88	104,773	-4857,10
8	0	2464,04	86,398	-4668,32	20	1	530,41	104,773	-4857,49
9	0	2262,86	87,616	-4720,07	21	1	530,07	104,773	-4857,58
10	0	1669,08	96,597	-4699,88	22	1	529,99	104,773	-4857,61
11	0	1229,29	103,637	-4684,01	23	1	529,98	104,773	-4857,61
12	0	996,74	104,720	-4729,33	24	1	529,98	104,773	-4857,61

DISTRIBUTION LIST FOR FINAL REPORT

CONTRACT NAS7-463

Copies		Designee
	NASA PASADENA OFFICE 4800 OAK GROVE DRIVE PASADENA, CALIFORNIA 91103	
1	PATENTS AND CONTRACTS MANAGEMENT	(x)
	JET PROPULSION LABORATORY 4800 OAK GROVE DRIVE PASADENA, CALIFORNIA 91103	
2	DONALD BOND	(x)
	CHIEF, LIQUID PROPULSION TECHNOLOGY RPL OFFICE OF ADVANCED RESEARCH AND TECHNOLOGY NASA HEADQUARTERS WASHINGTON, D. C., 20546	(x)
1	DIRECTOR, TECHNOLOGY UTILIZATION DIVISION OFFICE OF TECHNOLOGY UTILIZATION NASA HEADQUARTERS WASHINGTON, D.C., 20546	(x)
25	NASA SCIENTIFIC AND TECHNICAL INFORMATION FACILITY P. O. BOX 33 COLLEGE PARK, MARYLAND 20740	(x)
1	DIRECTOR, LAUNCH VEHICLES AND PROPULSION, SV OFFICE OF SPACE SCIENCE AND APPLICATIONS NASA HEADWUARTERS WASHINGTON, D.C., 20546	(x)
1	DIRECTOR, ADVANCED MANNED MISSION, MT OFFICE OF MANNED SPACE FLIGHT NASA HEADQUARTERS WASHINGTON, D.C., 20546	(x)
1	MISSION ANALYSIS DIVISION NASA AMES RESEARCH CENTER MOFFETT FIELD, CALIFORNIA 24035	(x)

NASA FIELD CENTERS

2	AMES RESEARCH CENTER MOFFETT FIELD, CALIFORNIA 94035	HANS M. MARK
1	GODDARD SPACE FLIGHT CENTER GREENBELT, MARYLAND 20771	MERLAND L. MOSESON CODE 620
2	JET PROPULSION LABORATORY CALIFORNIA INSTITUTE OF TECHNOLOGY 4800 OAK GROVE DRIVE PASADENA, CALIFORNIA 91103	HENRY BURLAGE, JR PROPULSION DIV. 38
2	LANGLEY RESEARCH CENTER LANGLEY STATION HAMPTON, VIRGINIA 23365	ED CORTWRIGHT DIRECTOR
2	LEWIS RESEARCH CENTER 21000 BROOKPARK ROAD CLEVELAND, OHIO 44135	DR. ABE SILVERSTEIN DIRECTOR
2	MARSHALL SPACE FLIGHT CENTER HUNTSVILLE, ALABAMA 35812	HANS G. PAUL CODE R-P+VED
2	MANNED SPACECRAFT CENTER HOUSTON, TEXAS 77001	J.G. THIBODAUX, JR. CHIEF, PROP. + POWER DIV.
2	JOHN F. KENNEDY SPACE CENTER, NASA COCOA BEACH, FLORIDA 32931	DR. KURT H. DEBUS

GOVERNMENT INSTALLATIONS

1	AERONAUTICAL SYSTEMS DIVISION AIR FORCE SYSTEMS COMMAND WRIGHT-PATTERSON AIR FORCE BASE DAYTON, OHIO 45433	D.L. SCHMIDT CODE ASRCNC-2
1	AIR FORCE MISSILE DEVELOPMENT CENTER HOLLOMAN AIR FORCE BASE NEW MEXICO 88330	MAJ. R.E. BRACKEN
1	AIR FORCE MISSILE TEST CENTER PATRICK AIR FORCE BASE, FLORIDA	L.J. ULLIAN
1	SPACE AND MISSILE SYSTEMS ORGANIZATION AIR FORCE UNIT POST OFFICE LOS ANGELES 45, CALIFORNIA 90045	COL. CLARK TECHNICAL DATA CENTER
1	ARNOLD ENGINEERING DEVELOPMENT CENTER ARNOLD AIR FORCE STATION TULLAHOMA, TENNESSEE 37388	DR. H.K. DOETSCH

1	BUREAU OF NAVAL WEAPONS DEPARTMENT OF THE NAVY WASHINGTON , D. C. 20546	J. KAY RTMS-41
1	DEFENSE DOCUMENTATION CENTER HEADQUARTERS CAMERON STATION, BUILDING 5 5010 DUKE STREET ALEXANDRIA, VIRGINIA 22314 ATTN' TISIA	
1	HEADQUARTERS, U.S. AIR FORCE WASHINGTON 25, D.C. 20546	COL.C.K. STAMBAUGH AFRST
1	PICATINNY ARSENAL DOVER, NEW JERSEY 07801	I. FORSTEN, CHIEF LIQUID PROPULSION LABORATORY,
2	AIR FORCE ROCKET PROPULSION LABORATORY RESEARCH AND TECHNOLOGY DIVISION AIR FORCE SYSTEMS COMMAND EDWARDS, CALIFORNIA 93523	RPRPD/MR. H. MAIN
1	U.S. ARMY MISSILE COMMAND REDSTONE ARSENAL ALABAMA 35809	MR. WALTER WHARTON
1	U.S. NAVAL ORDNANCE TEST STATION CHINA LAKE CALIFORNIA 93557	CODE 4562 CHIEF, MISSILE PROPULSION DIV.
	CPIA	
1	CHEMICAL PROPULSION INFORMATION AGENCY APPLIED PHYSICS LABORATORY 8621 GEORGIA AVENUE SILVER SPRING, MARYLAND 20910	TOM REEDY
	INDUSTRY CONTRACTORS	
1	AEROJET-GENERAL CORPORATION P. O. BOX 296 AZUSA, CALIFORNIA 91703	W. L. ROGERS
1	AEROJET-GENERAL CORPORATION P. O. BOX 1947 TECHNICAL LIBRARY, BLDG 2015, DEPT. 2410 SACRAMENTO, CALIFORNIA 95809	R. STIFF

1	SPACE DIVISION AEROJET-GENERAL CORPORATION 9200 EAST FLAIR DR. EL MONTE, CALIFORNIA 91734	S. MACHLAWSKI
1	AEROSPACE CORPORATION 2400 EAST EL SEGUNDO BOULEVARD P. O. BOX 95085 LOS ANGELES, CALIFORNIA 90045	JOHN G. WILDER MS-2293
1	ASTROSYSTEMS INTERNATIONAL, INC. 1275 BLOOMFIELD AVENUE FAIRFIELD, NEW JERSY 07007	A. MENDENHALL
1	ATLANTIC RESEARCH CORPORATION EDSALL ROAD AND SHIRLEY HIGHWAY ALEXANDRIA, VIRGINIA 22314	DR. RAY FRIEDMAN
1	AVCO SYSTEMS DIVISION WILMINGTON, MASSACHUSETTS	HOWARD B. WINKLER
1	BEECH AIRCRAFT CORPORATION BOULDER DIVISION BOX 631 BOULDER , COLORADO	J. H. RODGERS
1	BELL AEROSYSTEMS COMPANY P.O. BOX 1 BUFFALO, NEW YORK 14240	W. M. SMITH
1	BELLCOMM 955 L'ENFANT PLAZA, S. W. WASHINGTON, D. C.	H. S. LONDON
1	BENDIX SYSTEMS DIVISION BENDIX CORPORATION 3300 PLYMOUTH ROAD ANN ARBOR, MICHIGAN 48105	JOHN M. BRUEGER
1	BOEING COMPANY P. O. BOX 3707 SEATTLE, WASHINGTON 98124	J. D. ALEXANDER
1	BOEING COMPANY 1625 K STREET, N. W. WASHINGTON, D. C. 20006	LIBRARY

1	BOEING COMPANY P. O. BOX 1680 HUNTSVILLE, ALABAMA 35801	TED SNOW
1	MISSILE DIVISION CHRYSLER CORPORATION P. O. BOX 2628 DETROIT, MICHIGAN 48231	MR. JOHN GATES
1	WRIGHT AERONAUTICAL DIVISION CURTISS-WRIGHT CORPORATION WOOD-RIDGE, NEW JERSEY 07075	G. KELLEY
1	RESEARCH CENTER FAIRCHILD HILLER CORPORATION GERMANTOWN, MARYLAND	RALPH HALL
1	REPUBLIC AVIATION CORPORATION FAIRCHILD HILLER CORPORATION FARMINGDALE, LONG ISLAND, NEW YORK	LIBRARY
1	GENERAL DYNAMICS, CONVAIR DIVISION LIBRARY + INFORMATION SERVICES (128-00) P. O. BOX 1128	FRANK DORE
1	MISSILE AND SPACE SYSTEMS CENTER GENERAL ELECTRIC COMPANY VALLEY FORGE SPACE TECHNOLOGY CENTER P.O. BOX 8555 PHILADELPHIA, PA.	F. MEZGER F. E. SCHULTZ
1	GRUMMAN AIRCRAFT ENGINEERING CORP. BETHPAGE, LONG ISLAND NEW YORK 11714	JOSEPH GAVIN
1	HONEYWELL, INC. AEROSPACE DIV. 2600 RIDGWAY RD MINNEAPOLIS, MINN.	MR. GORDON HARMS
1	HUGHES AIRCRAFT CO. AEROSPACE GROUP CENTINELA AND TEALE STREETS CULVER CITY, CALIF. 90230	E. H. MEIER V.P.AND DIV. MGR., RESEARCH + DEV. DIV.
1	WALTER KIDDE AND COMPANY, INC. AEROSPACE OPERATIONS 567 MAIN STREET BELLEVILLE, NEW JERSEY	R. J. HANVILLE DIR. OF RESEARCH ENGR.
1	LING-TEMCO-VOUGHT CORPORATION P. O. BOX 5907 DALLAS, TEXAS 75222	WARREN G. TRENT

1	ARTHUR D. LITTLE, INC. 20 ACORN PARK CAMBRIDGE, MASSACHUSETTS 02140	LIBRARY
1	LOCKHEED MISSILES AND SPACE CO. ATTN-TECHNICAL INFORMATION CENTER P.O. BOX 504 SUNNYVALE, CALIFORNIA 94088	J. GUILL
1	LOCKHEED PROPULSION COMPANY P. O. BOX 111 REDLANDS, CALIFORNIA 92374	H. L. THACKWELL
1	THE MARQUARDT CORPORATION 16555 SATICOY STREET VAN NUYS ,CALIF. 91409	HOWARD MC FARLAND
1	BALTIMORE DIVISION MARTIN MARIETTA CORPORATION BALTIMORE, MARYLAND 21203	MR. JOHN CALATHES (3214)
1	DENVER DIVISION MARTIN MARIETTA CORPORATION P. O. BOX 179 DENVER, COLORADO 80201	DR MORGANTHALER A. J. KULLAS
1	ORLANDO DIVISION MARTIN MARIETTA CORP. BOX 5837 ORLANDO, FLORIDA	J. FERM
1	ASTROPOWER LABORATORY MC DONNELL-DOUGLAS AIRCRAFT COMPANY 2121 PAULARINO NEWPORT BEACH, CALIFORNIA 92663	DR. GEORGE MOC DIRECTOR, RESEARCH
1	MCDONNEL-DOUGLAS AIRCRAFT CORP. P. O. BOX 516 MUNICIPAL AIRPORT ST. LOUIS, MISSOURI 63166	R. A. HERZMARK
1	MISSILE AND SPACE SYSTEMS DIVISION MC DONNELL-DOUGLAS AIRCRAFT COMPANY 3000 OCEAN PARK BOULEVARD SANTA MONICA, CALIF. 90406	MR. R. W. HALLET CHIEF ENGINEER ADV. SPACE TECH.
1	SPACE+INFORMATION SYSTEMA DIVISION NORTH AMERICAN ROCKWELL 12214 LAKEWOOD BOULEVARD DOWNEY, CALIFORNIA 90241	LIBRARY
1	ROCKETDYNE (LIBRARY 586-306) 6633 CANOGA AVENUE CANOGA PARK, CALIF. 91304	DR. R. J. THOMPSON S. F. IACOBELLIS

1	NORTHROP SPACE LABORATORIES 3401 WEST BROADWAY HAWTHORNE, CALIFORNIA 90250	DR. WILLIAM HOWARD
1	AERONUTRONIC DIVISION PHILCO CORPORATION FORD ROAD NEWPORT BEACH, CALIFORNIA 92663	D. A. GARRISON
1	ASTRO-ELECTRONICS DIVISION RADIO CORPORATION OF AMERICA PRINCETON, NEW JERSEY 08540	Y. BRILL
1	ROCKET RESEARCH CORPORATION 520 SOUTH PORTLAND STREET SEATTLE, WASHINGTON 98108	FOY MCCULLOUGH, JR.
1	SUNSTRAND AVIATION 2421 11TH STREET ROCKFORD, ILLINOIS 61101	R. W. REYNOLDS
1	STANFORD RESEARCH INSTITUTE 333 RAVENSWOOD AVENUE MENLO PARK, CALIFORNIA 94025	DR. GERALD MARKSMAN
1	TRW SYSTEMS GROUP TRW INCORPORATED ONE SPACE PARK REDONDO BEACH, CALIF. 90278	G. W. ELVERUM
1	TAPCO DIVISION TRW, INCORPORATED 23555 EUCLID AVENUE CLEVELAND, OHIO 44117	P. T. ANGELL
1	REACTION MOTORS DIVISION THIOKOL CHEMICAL CORPORATION DENVILLE, NEW JERSEY 07832	DWIGHT S. SMITH
1	THIOKOL CHEMICAL CORPORATION HUNTSVILLE DIVISION HUNTSVILLE, ALABAMA 35807	JOHN GOODLOE
1	RESEARCH LABORATORIES UNITED AIRCRAFT CORP. 400 MAIN ST. EAST HARTFORD, CONN. 06108	ERLE MARTIN
1	HAMILTON STANDARD DIVISON UNITED AIRCRAFT CORP. WINDSOR LOCKS, CONN. 06096	MR. R. HATCH

1	UNITED TECHNOLOGY CENTER 587 METHILDA AVENUE P. O. BOX 358 SUNNYVALE, CALIFORNIA 94088	DR. DAVID ALTMAN
1	FLORIDA RESEARCH AND DEVELOPMENT PRATT AND WHITNEY AIRCRAFT UNITED AIRCRAFT CORPORATION P. O. BOX 2691 WEST PALM BEACH, FLORIDA 33402	R.J. COAR
1	VICKERS, INC. BOX 302 TROY, MICHIGAN	

485 CLYDE AVENUE, MOUNTAIN VIEW, CALIFORNIA 94040

TELEPHONE: (415) 964-3200, TELEX: 34-8355